HIGH-RESOLUTION STABLE ISOTOPE RECORDS AS INDICATORS OF LATE MIDDLE EOCENE CLIMATE CHANGE

BRIDGET WADE

Thesis submitted for the degree of Doctor of Philosophy
University of Edinburgh
2001

Declaration

I certify that all the data, their interpretations and conclusions presented in this thesis are my own, except where otherwise stated and acknowledged. This thesis has not been previously submitted as a degree at this, or any other University.

Bridget Wade
2001

ACKNOWLEDGEMENTS

I would like to thank my supervisor Dick Kroon for all his help and wisdom. His constant enthusiasm throughout my PhD made it all the more enjoyable. I really appreciate the assistance and endless patience of Colin Chilcott whose help with the mass spectrometer made this PhD possible. I am very grateful to Paul Pearson for teaching me Eocene planktonic foraminifer taxonomy and discussions thereafter about problematic taxa and results. This work also benefited from discussions with Karen Bice, Richard Norris, Lisa Sloan, Paul Wilson, Rachel Oxburgh and Matt Huber about the Eocene climate. Special thanks to Heiko Pälike for time-scale data and discussion on the cyclicity. The Ocean Drilling Program provided the samples examined in this thesis. This research was supported by UK Natural Environment Research Council reference number GT 04/97/93/ES.

I would also like to thank my fellow postgraduate students at the University of Edinburgh, for making the last four years such fun. Thanks to Steve for his assistance and encouragement. Special thanks to my parents and Uncle Kennie for all their love and support.

Finally I would like to thank Rich for the immeasurable amount of love and help over the last five years. Thank you for all the things you've done to make PhD life so much easier and making me happy.

ABSTRACT

High-resolution (3 kyr) stable isotope analyses ($\delta^{18}O$, $\delta^{13}C$) have been conducted on late middle Eocene planktonic foraminifera from the western North Atlantic (Ocean Drilling Program, Leg 171B, Site 1052). The data indicate significant (>1‰) and abrupt changes in mixed layer planktonic foraminifera $\delta^{18}O$. These variations probably result from large oscillations in sea surface temperatures. The variability is greater than that seen in open ocean Pleistocene records and indicates that the middle Eocene climatic system was not consistently warm or stable. There were intervals when annual sea surface temperatures were up to 5°C greater than modern mean values. These temperatures are similar to those recorded in the early Eocene, suggesting increased carbon dioxide or other greenhouse gases may have forced warm intervals.

New and existing planktonic foraminiferal biostratigraphic events of the late middle Eocene have been examined with a sampling resolution of 3 kyr. These have been calibrated to the astronomical time-scale to accurately define the timing of key biostratigraphic events, particularly the extinction of *Morozovella spinulosa*, which is a distinct biomarker for late middle Eocene sediments.

Fourier analysis reveals Milankovitch frequencies within the stable isotopic record. The long-period eccentricity signal (400 kyr) governs the large fluctuations in middle Eocene $\delta^{18}O$ and produced significant changes in water column stability and thermal stratification. Large oscillations in sea surface temperatures occurred with surface water temperatures periodically reduced for 100 kyr. A possible explanation is that these abrupt shifts in $\delta^{18}O$ represent orbitally forced variations in upwelling intensity, which greatly reduced sea surface temperatures. The direct effects of eccentricity on insolation are small. Therefore the prominent eccentricity variations were probably generated by nonlinear response to precessional forcing within the climatic system, rather than directly from eccentricity variations in solar insolation. Feedback effects within the oceanic – atmospheric system, possibly related to atmospheric transport, must have been important. The generally reduced surface to bottom temperature gradient in the Eocene may have facilitated the upwelling of deep water to the surface ocean.

It is concluded that the oscillations in the stable isotopic profiles in the western North Atlantic are due to climatic controls on the intensity of upwelling. The prominence of the eccentricity frequencies in middle Eocene climate records indicates that orbital modulation of solar insolation was an important parameter of climatic variability at this time.

TABLE OF CONTENTS

ABBREVIATIONS

A.	= *Acarinina*
C.	= *Chiasmolithus*
DSDP	= Deep Sea Drilling Project
$\delta^{18}O_{sw}$	= oxygen isotope composition of sea water
FAD	= first appearance datum
FO	= first occurrence
Foram	= foraminifera
G.	= *Globigerinatheka*
Ka	= thousand years ago
kyr	= thousand years
LAD	= last appearance datum
LO	= last occurrence
M.	= *Morozovella*
Ma	= million years ago
mbsf	= metres below sea floor
mbsl	= metres below sea level
mcd	= metres composite depth
myr	= million years
N.	= *Nuttalides*
Nanno	= nannofossil
O.	= *Orbulinoides*
ODP	= Ocean Drilling Program
PDB	= Pee Dee Belemnite
R.	= *Reticulofenestra*
S.	= *Subbotina*
SEM	= Scanning Electron Microscope
SMOW	= Standard Mean Ocean Water
SSTs	= Sea Surface Temperatures
XRF	= X-ray fluorescence

1. INTRODUCTION

1.1 Background and rationale

During the Eocene (54.7 to 33.7 million years ago) the climate was extremely different from that of today. The early Eocene was a "greenhouse" world, with carbon dioxide levels possibly much greater than modern (Pearson and Palmer, 2000). Polar temperatures were elevated, with palm trees as far north as the Arctic circle and no permanent ice-sheets anywhere on Earth (Zachos *et al.*, 1994). Climatic cooling occurred through the middle and late Eocene with large-scale Antarctic glaciation in the early Oligocene. The middle and late Eocene can therefore be considered as the transitional period between hot-house and ice-house states. But what were the tropics like and how stable was the climate at this time? These questions can be addressed by analysing the stable isotope composition of microfossils from cored marine sediments. Using this method many aspects of the Eocene climate can be deduced, such as the temperature of the sea surface and global ice volume.

Whilst the climatic shifts during the Eocene are understood in general terms, the middle Eocene climate has not been adequately documented in terms of its variability, timing of cooling and effect on vertical temperature gradients. This is because high-resolution Palaeogene records are scarce and most previously acquired Eocene records are incomplete, intermittently cored or disturbed by drilling through Eocene chert (Stott and Zachos, 1991). Complete records either lack the necessary resolution, or their microfossils are not sufficiently well preserved to record the rapid palaeoceanographic changes that are associated with the transition period from a non-glacial to glacial climate. The Ocean Drilling Program (ODP) Leg 171B, drilled five sites at the Blake Nose (western North Atlantic) (figure 1.1). The stable isotopic composition of planktonic foraminifera at this subtropical site enables the high-resolution documentation of the oceanic changes in the middle Eocene Atlantic Ocean.

1.2 Foraminifera and stable isotopes

Foraminifera are a major group within the marine benthos and zooplankton. They are single-celled protists that commonly shield their cytoplasm within a secreted calcareous ($CaCO_3$) skeleton (the test) (Banner, 1982). The preservation and accumulation of foraminifera tests within marine sediments yields a long and valuable fossil record, which micropalaeontologists have extensively exploited to infer palaeoceanographical and palaeoclimatological information.

A well established tool utilised in the study of palaeoclimatology and palaeoceanography is the stable isotopic signal recorded in the calcareous tests of fossil foraminifera. The ratio between the oxygen isotopes ^{16}O and ^{18}O of the ambient seawater is recorded in the tests of foraminifera during the biomineralization of calcite (Emiliani, 1954, 1955) and can be revealed by mass spectrometry. The ratio, expressed as $\delta^{18}O$ ‰ is dependent on temperature (Urey, 1947; O'Neil *et al.*, 1969) and on the oxygen isotope ratio of the ambient seawater, which is governed by the amount of evaporation, precipitation and global ice volume (Shackleton and Kennett, 1975). The δ notation defines the deviation in parts per thousand (‰) or per mil of the sample analysed from the Pee Dee Belemnite (PDB) standard (Craig, 1965). This is expressed below:

$$\delta^{18}O = \left[\frac{(^{18}O/^{16}O)\ \text{sample} - (^{18}O/^{16}O)\ \text{standard}}{(^{18}O/^{16}O)\ \text{standard}}\right] \times 1000$$

At higher temperatures, there is less fractionation of ^{18}O relative to ^{16}O, so foraminifera inhabiting warmer waters will be depleted in ^{18}O, whilst those species living in colder waters will be enriched in ^{18}O (Urey, 1947; Shackleton and Opdyke, 1973). The effect of temperature has been quantified as ~0.25‰/1°C (Epstein *et al.*, 1953).

Evaporation and atmospheric vapour transport influence the isotopic composition of seawater. During evaporation, the lighter ^{16}O isotope is preferentially removed into

the atmosphere and is returned to the oceans via precipitation. Therefore areas of extensive evaporation will have surface waters that are enriched in ^{18}O in comparison to areas of high precipitation. However, during cold climatic periods the ^{16}O becomes locked up in ice, making the oceanic water increasingly enriched in ^{18}O as ice volume increases. The full glacial to full interglacial shift in the marine oxygen isotope composition is approximately 1.2‰ (Shackleton and Kennett, 1975; Berger, 1979). The fluctuations in enrichment can be utilised to indicate global ice volume and the temperature of surface and deep ocean waters through time.

There are some uncertainties that present limitations to the oxygen isotope approach of palaeotemperature calculation. These include the modification of the $\delta^{18}O$ values in carbonate fossils by diagenesis, the unknown oxygen isotope composition of ancient oceans, salinity related effects (Craig and Gordon, 1965) and the fractionation of organically precipitated calcite that is not in equilibrium with the ambient ocean water (Shackleton *et al.*, 1973; Pearson *et al.*, 1993). Examination of extant foraminifera species, clearly indicate that "vital effects" can alter the environmental signal. This is particularly true of carbon isotopes (Shackleton *et al.*, 1973).

1.3 Geological setting

Blake Nose, or Blake Spur, is a salient in the western North Atlantic, located due east of northern Florida, on the eastern margin of the Blake Plateau (figure 1.1). Blake Nose forms a gentle ramp at the Blake Escarpment where water depths reach a maximum of 2700 metres. Strata of Cretaceous and Palaeogene age are present at shallow burial depths and have never been deeply buried by younger sediments. They are thus little affected by diagenesis. A thin veneer of manganese-rich sand and nodules shields these sediments from modern day erosional processes (Norris, Kroon *et al.*, 1998). Five sites (1049 - 1053) were drilled along a transect of Blake Nose by the ODP Leg 171B (figure 1.2).

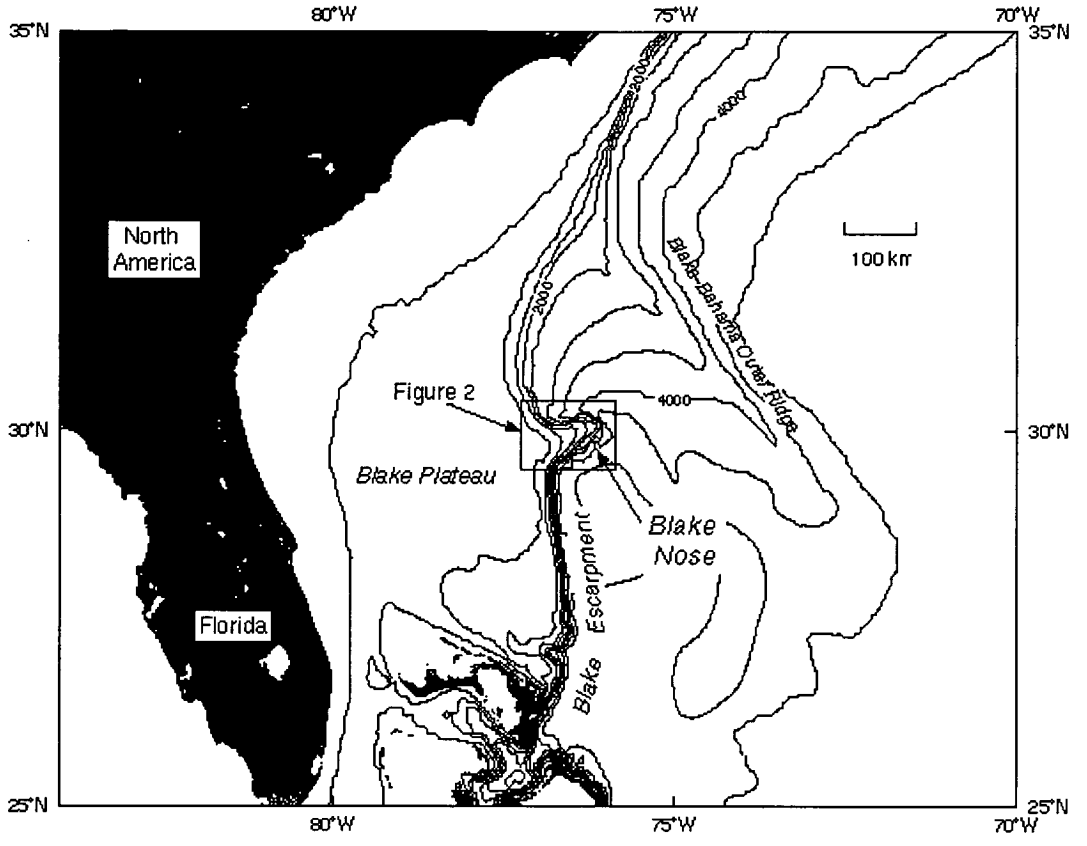

Figure 1.1. Location map of Blake Nose and Blake Plateau, ODP Leg 171B (Norris, Kroon *et al.*, 1998).

The primary objective of ODP Leg 171B was to drill shallow sites in a transect from the edge of the Blake Escarpment to the margin of the Blake Plateau. The main interest in these sites was to allow the vertical structure of the Palaeogene oceans to be interpreted and to provide subtropical sea surface temperatures by utilising moderately well preserved calcareous microfossils. These results are necessary to document major steps in climate evolution. Documentation of the oceanic changes associated with the transition from the warm to cool Eocene world in the subtropical Atlantic ocean is enabled by the completeness of the middle and upper Eocene section at Blake Nose. The ocean plays a very important part in climate change and this study allowed an examination of sea surface temperatures and the thermal gradient response at this time. The focus of this study is Site 1052 where middle Eocene sediments display rhythmic colour variations and relatively well preserved microfossils.

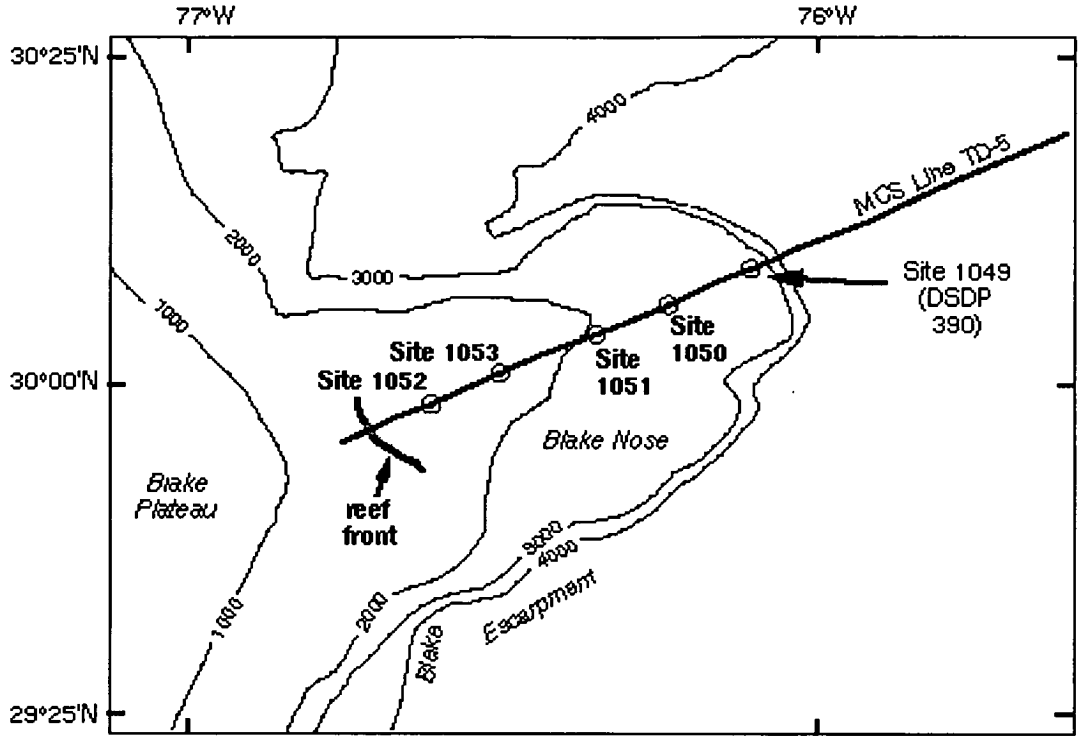

Figure 1.2. ODP Leg 171B drill locations, bathymetry (metres) and existing seismic lines (Norris, Kroon *et al.*, 1998).

1.3.1 Site 1052

Site 1052 is located on the upper part of the Blake Nose and is the shallowest site of the depth transect (figure 1.3). The bio-magnetostratigraphy indicates that the record spans the late Albian and late Eocene. The site is at present in the depth range of modern intermediate waters at ~ 1345 metres below sea level (mbsl). *Nuttalides truempyi* and *Aragonia* spp. are present but rare indicating a middle bathyal palaeodepth (600 - 1000 m) during the middle Eocene. The sediments consist of a pale yellow siliceous nannofossil ooze (Norris, Kroon *et al.*, 1998). Diatoms, radiolarians and sponge spicules make up the siliceous component.

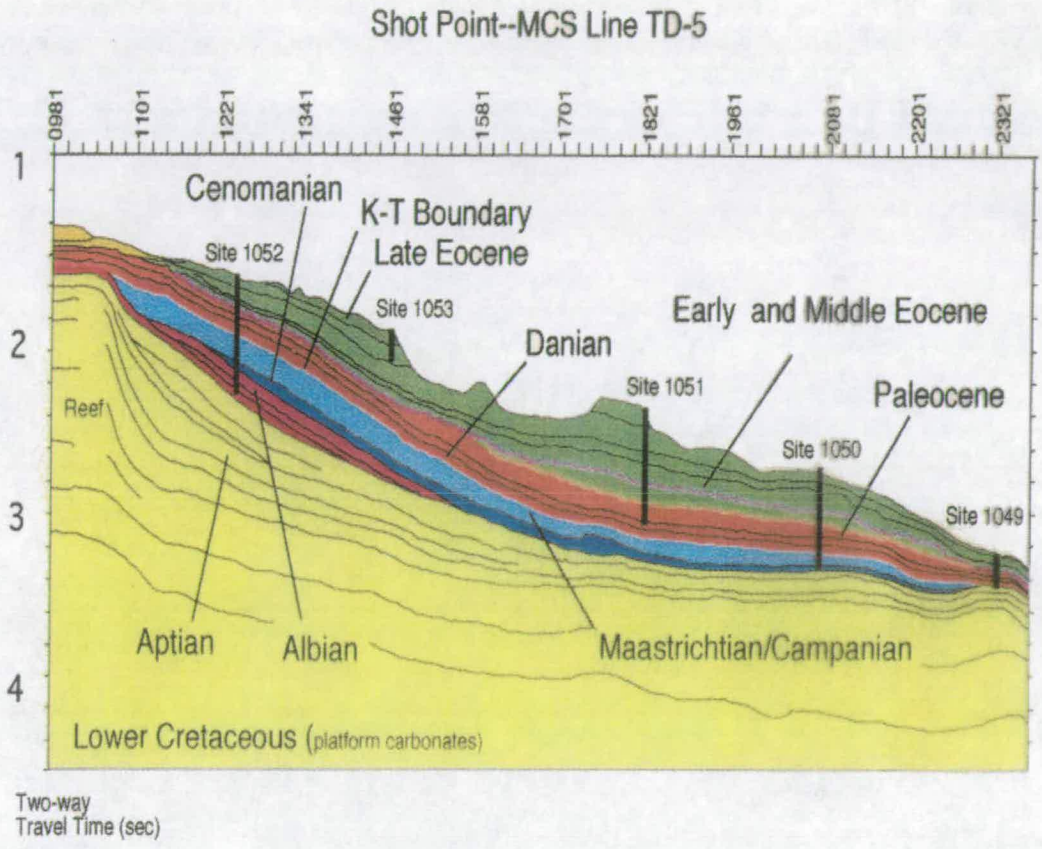

Figure 1.3. Seismic interpretation across Blake Nose showing the drill sites, major reflectors and their ages (Norris, Kroon *et al.*, 1998).

The magnetostratigraphy of Holes 1052B and 1052F are shown in figures 1.4 and 1.5 respectively, whilst a composite is shown in figure 1.6. The clear magnetic polarity stratigraphy (figures 1.4 and 1.5) and excellent record of cyclic variations in magnetic susceptibility and colour (see chapter 2) make this site ideal to study middle Eocene climate change at a high temporal resolution.

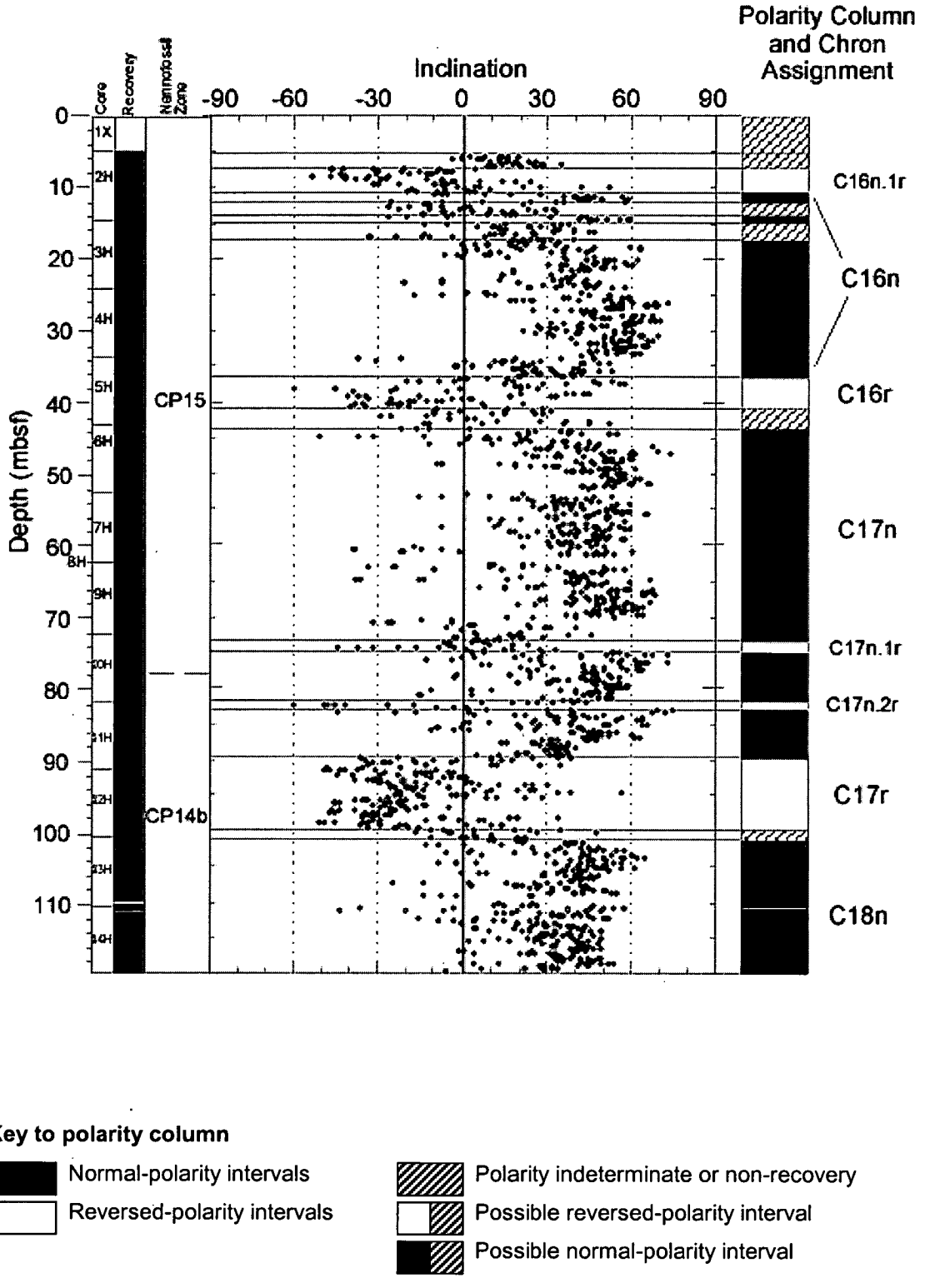

Figure 1.4. Magnetostratigraphy and polarity chron assignments at Hole 1052B (after Norris, Kroon *et al.*, 1998).

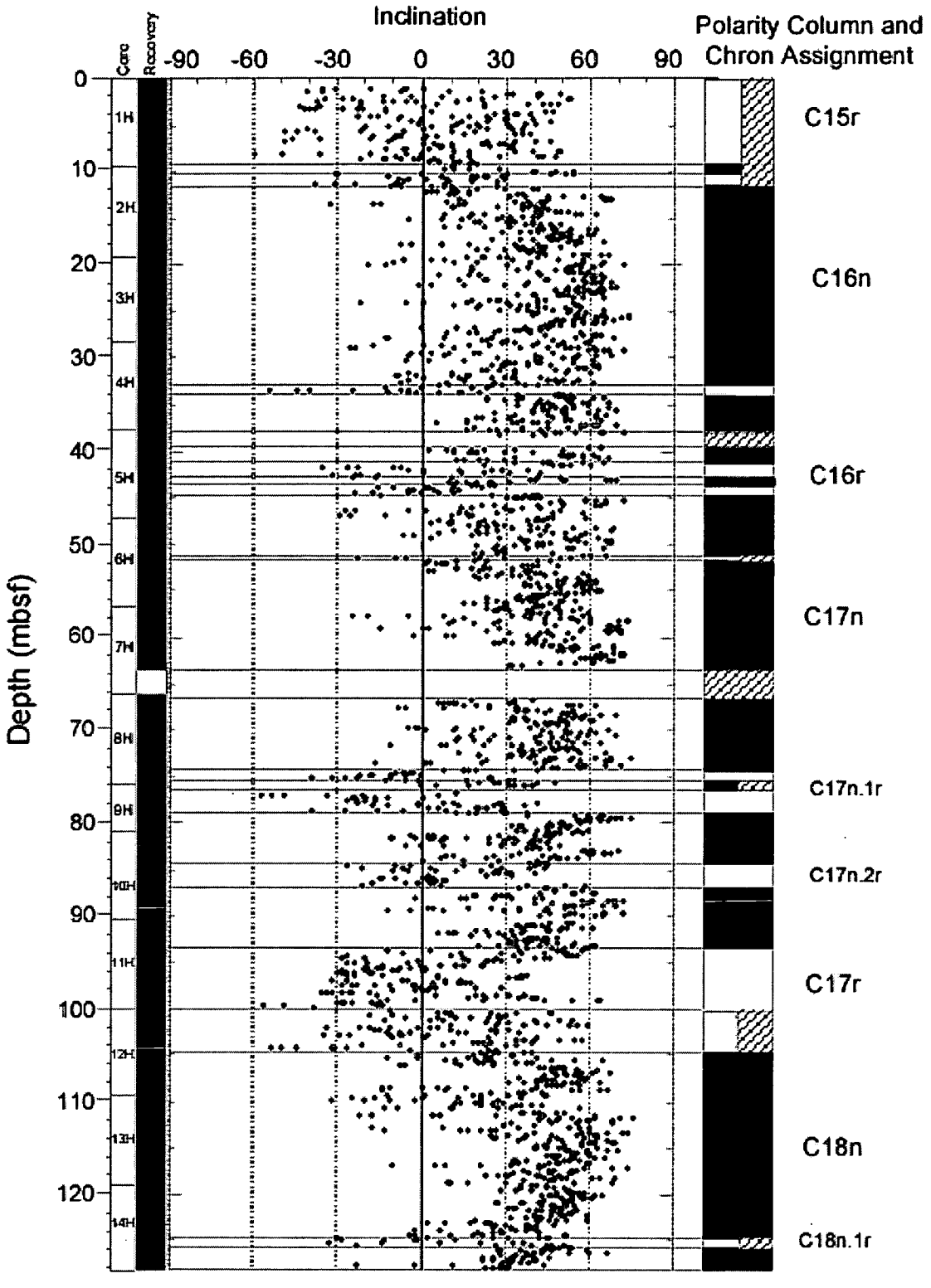

Figure 1.5. Magnetostratigraphy and polarity chron assignments at Hole 1052F (after Norris, Kroon *et al.*, 1998). See figure 1.4 for key to polarity column.

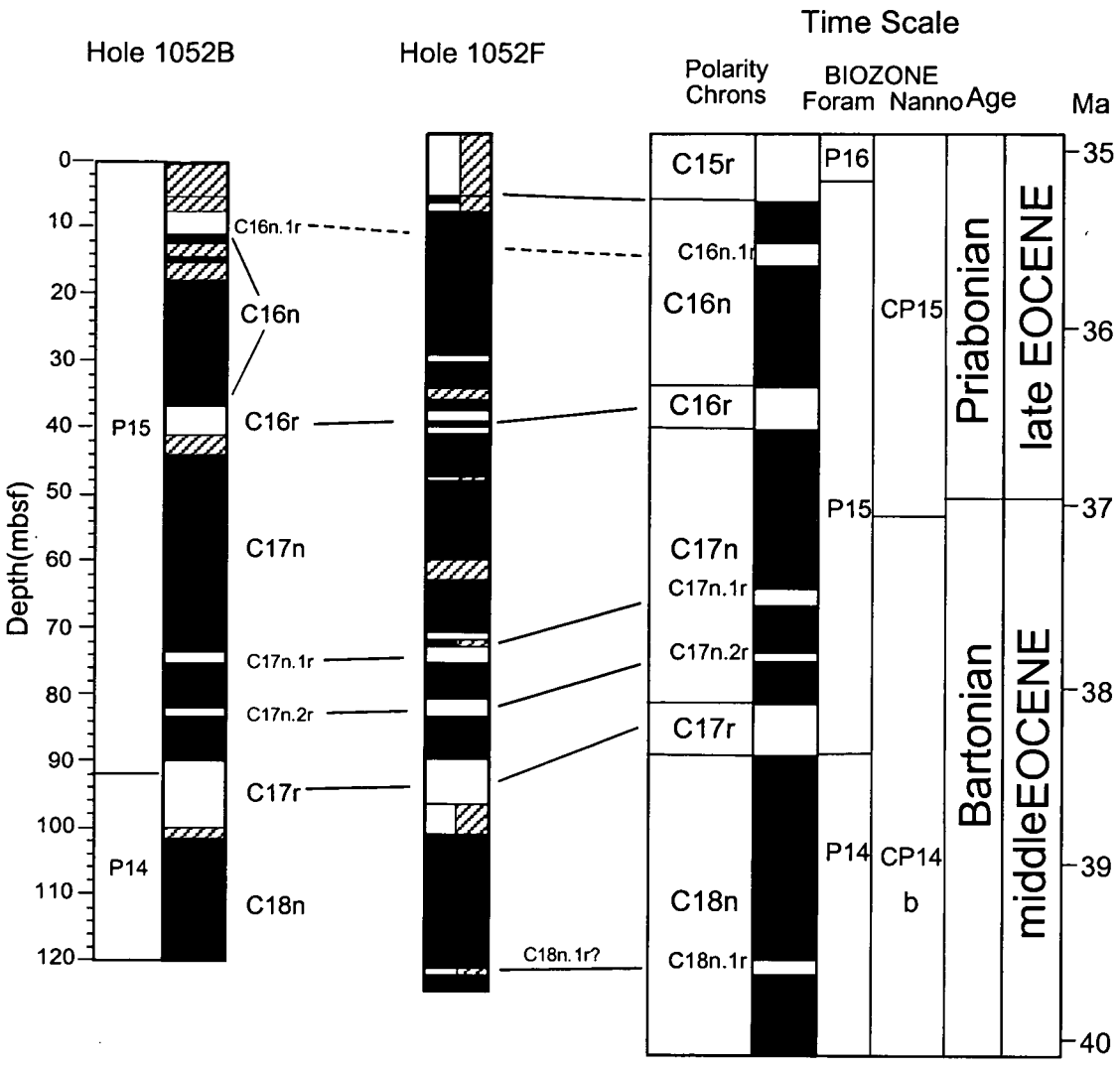

Figure 1.6. Composite magnetostratigraphy of Holes 1052B and 1052F (after Norris, Kroon *et al.*, 1998). See figure 1.4 for key to polarity column. The time-scale of Berggren *et al.* (1995) is shown on the right.

1.4 The Eocene climate

One of the most dramatic climatic changes during the history of the Earth is the transition from the hot-house world of the early Eocene to the ice-house world of the early Oligocene. Abundant palaeontological and geochemical data indicate that the Eocene climate was extremely different from the present. Early Eocene marine and terrestrial records indicate that the Earth was warmer than at any other time during the last 65 million years, representing a fundamentally different climate state than existed at any other interval in the Cenozoic. The early Eocene climate was

characterised by a reduced meridional surface temperature gradient, increased global mean temperature and the absence of large-scale continental glaciation (Rea *et al.*, 1990; Zachos *et al.*, 1994). Minor continental ice-sheets may have existed on Antarctica, although these did not reach the coastline (Mackensen and Ehrmann, 1992; Zachos *et al.*, 1993). High-latitude marine temperatures based on oxygen isotope data reveal seasonal highs of 18°C during the early Eocene (Stott *et al.*, 1990) with deep-water temperatures greater than 15°C (e.g. Shackleton and Kennett, 1975; Miller *et al.*, 1987; Zachos *et al.*, 1994).

After the warmth of the early Eocene, deep water and high-latitude temperatures began to cool. The global climatic cooling did not occur smoothly during the Cenozoic, but was marked by a number of abrupt and distinct shifts from one climatic state to another (figure 1.7). The early stages of the Cenozoic cooling trend began with a step-like climatic deterioration during the early middle Eocene (~50 to 48 Ma). The middle Eocene saw two modest increases in the $\delta^{18}O$ values of planktonic foraminifera, at the early to middle Eocene boundary and during the late middle Eocene (Shackleton and Boersma, 1981). This heralded the onset of global cooling that ultimately led to the Quaternary ice age. These increases in $\delta^{18}O$ indicate either a reduction in ocean temperature or an expansion of global ice volume. Analyses of benthic foraminifera also illustrate a cooling trend at that time, which implies a synchronous cooling in both bottom and surface ocean waters in the mid- and high-latitudes (Kennett and Shackleton, 1976). Floral and faunal records indicate a decrease in high-latitude and deep ocean temperatures (e.g., Benson, 1975; Corliss, 1979; Aubry, 1983; Keller, 1983; Boersma *et al.*, 1987). The increases in $\delta^{18}O$ have been explained as reductions in the global ocean temperature either with or without ice formation. There may have been seasonal winter ice in the Arctic region and continental ice in West Antarctica, though there is no confirmation of a major ice cap during the middle Eocene (Zachos *et al.*, 1994).

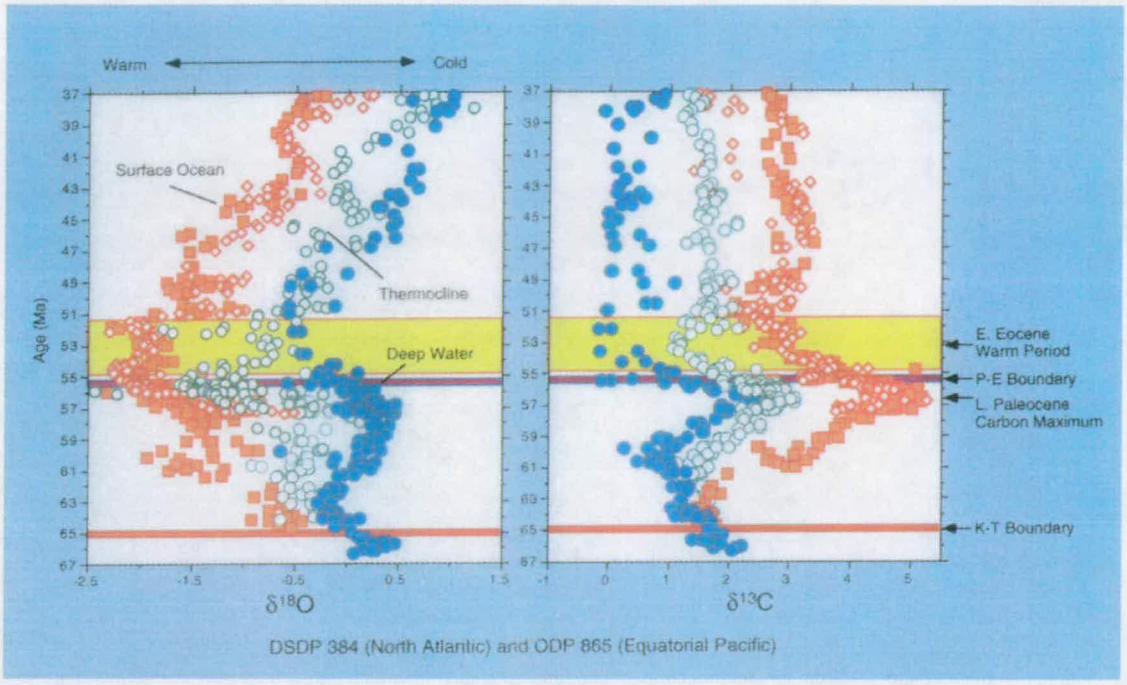

Figure 1.7. Palaeocene and Eocene global oxygen and carbon isotopic records. Palaeocene data from Deep Sea Drilling Project (DSDP) Site 384 (northwest Atlantic; Berggren and Norris, 1997), late Palaeocene and Eocene data from ODP Site 865 (north central Pacific; Bralower *et al.*, 1995). Figure courtesy of Richard Norris.

The sediments at Blake Nose provide the opportunity for investigating climate variability and sediment history during the transition from a hot-house to ice-house world. Crucial in investigating the magnitude of change in the climatic system and the succession of events are stable isotope records from planktonic foraminifers. The advantage of Leg 171B is that the middle Eocene sediments have never been deeply buried and there is a clearly defined biostratigraphy and magnetostratigraphy throughout the late middle Eocene. The record from Blake Nose therefore enables the examination of high frequency climatic variability and accurate documentation of the timing and scale of relatively short-term climatic changes in the middle Eocene Atlantic Ocean. The results from the Shipboard Scientific Party (Norris, Kroon *et al.*, 1998) indicate clear high frequency variability in the colour reflectance data (see chapter 2), which are thought to be driven by Milankovitch scale climate oscillations. The examination of planktonic foraminifera stable isotopes in association with the colour record allows climatic dynamics in the late middle Eocene to be examined

much more fully than in previous studies. This thesis explores the effect of orbital forcing (Milankovitch cycles) upon the late middle Eocene climate.

1.5 Mechanisms of Eocene climate change

The forcing factors accountable for the high-latitude climatic warmth in the early Eocene and the subsequent long-term cooling remain undetermined. Various hypotheses have been suggested that in general fall into two categories: those that call for a redistribution of energy about the Earth's surface and those that demand a change in the net amount of energy trapped by the atmosphere (Zachos *et al.*, 1994). A multiple of factors were probably responsible for the Cenozoic cooling trend.

1.5.1 Hypotheses involving the redistribution of energy

These hypotheses mostly involve changing the capability of global meridional heat transport via the atmosphere and/or ocean. This could be achieved by modifications in the position of ocean gateways and continents (e.g. Kennett and Shackleton, 1976; Kennett, 1977; Berggren and Hollister, 1977; Haq, 1981; Berggren, 1982; Horrell, 1990; Rind and Chandler, 1991). The redistribution of energy has often been cited as the principal mechanism behind high-latitude cooling in the Palaeogene (Zachos *et al.*, 1994). For example, comparatively warm global climates are associated with the existence of a circumglobal tropical ocean. Marked cooling and the development of glaciers in high-latitudes are thought to be related to the closure of low latitude oceanic seaways and the opening of high-latitude connections (Kennett, Houtz *et al.*, 1975; van Andel *et al.*, 1975; Hayes, Frakes *et al.*, 1975; Kennett, 1982). However, the exact mechanisms by which tropical oceanographic changes take place have not been identified and climatic modeling studies indicate that the high-latitude warmth and the Cenozoic cooling trend cannot be explained by changing palaeogeography and palaeoceanography alone (Barron and Washington, 1984; Barron, 1985; Sloan and Barron, 1990; Sloan *et al.*, 1992; Crowley, 1993; Fawcett and Barron, 1998; Bice *et al.*, 2000a).

Major tectonically forced events have produced significant alterations in global climate system dynamics during the Eocene (Barron and Peterson, 1991; Berner, 1994; Sloan and Rea, 1995; Mikolajewicz and Crowley, 1997). Three principal features can be distinguished in the palaeoceanographic evolution (Kennett, 1977, 1982). The first of these is the decreasing role of equatorial and low latitude oceanic circulation, as the once virtually unrestricted equatorial seaway became increasingly segmented (figure 1.8). This resulted from the closure of the Tethys seaway, the bridging of the Central American Seaway, the emergence of the south-east Asian region and the related northward migration of Australia. These palaeoceanographic changes had major consequences on the equatorial current system intensity, the associated nutrient budgets, biological productivity, upwelling and communities of fauna and flora (Kennett, 1982).

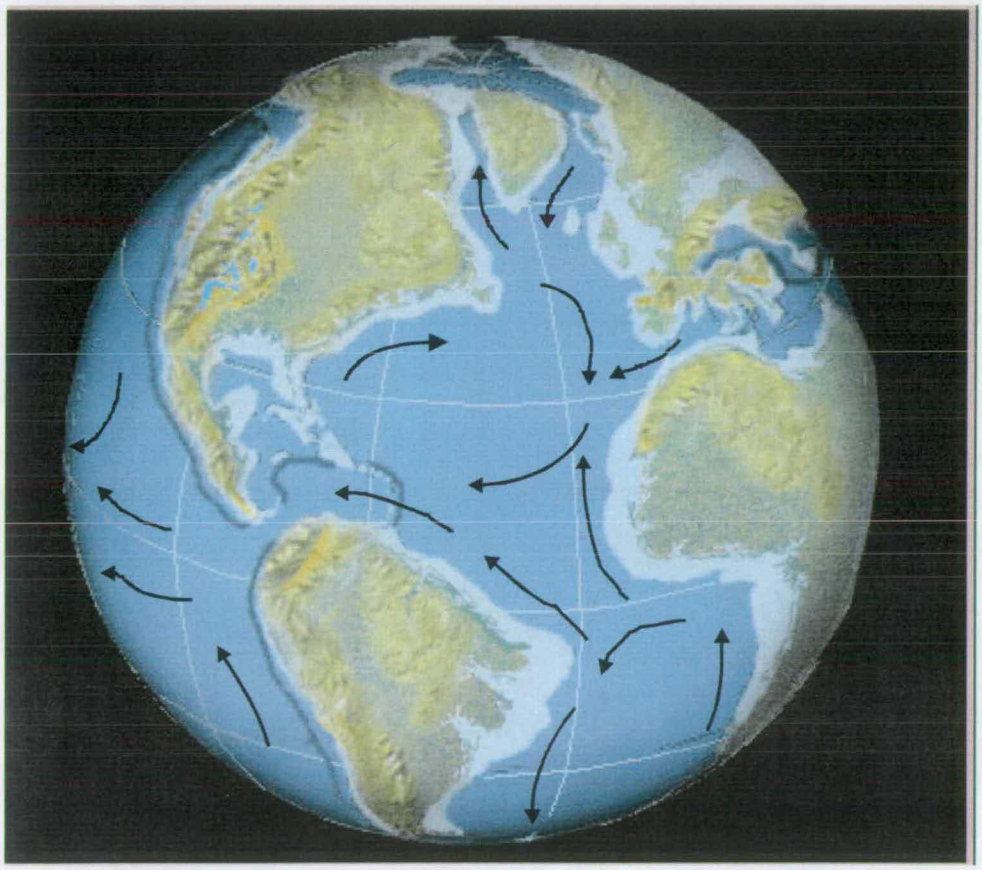

Figure 1.8. Reconstructed surface water circulation patterns in the Atlantic during the middle Eocene (after Haq, 1981).

The second major oceanographic modification was the evolution of the circum-Antarctica circulation system (Antarctic circumpolar current). This arose chiefly from the rifting of Australia and Antarctica and the opening of the Drake Passage (Lawver and Gahagan, 1998), giving rise to unrestricted flow of cold waters around Antarctica. The final element was the changing nature of the bottom-water circulation with the development of thermally driven North Atlantic Deep Water, in response to high-latitude cooling and glacial events.

1.5.2 Hypotheses involving the net amount of energy

These hypotheses tend to call for alterations in the quantity of heat trapped in the Earth's atmosphere by variations in either the Earth's albedo or the amount of greenhouse gases (e.g. Barron, 1985; Berner, 1991; Sloan *et al.*, 1992). Higher atmospheric CO_2 levels are often involved in interpretations of climate change for the Cretaceous and early Cenozoic (Crowley, 1991; Crowley and Zachos, 2000). A principal means for modifying the concentration of greenhouse gases in the Earth's atmosphere is volcanic degassing, which is governed by rates of seafloor spreading and/or subduction (Owen and Rea, 1985; Rea *et al.*, 1990; Berner, 1991).

Considerable variation has been recorded in atmospheric CO_2 during the Eocene possibly reflecting the greater instability of Earth system processes during greenhouse climates. It is indicated by Pearson and Palmer (2000) that pCO_2 decreased from 3,700 to 500 ppm between the early Eocene and Miocene. A cause and effect relationship between atmospheric CO_2 and climate change is favoured by the approximate correlation between the pCO_2 record and Palaeogene marine temperature changes in high-latitudes. However, there did not appear to be a simple correlation between CO_2, deep water temperatures and ice volume (Pearson and Palmer, 2000). Large CO_2 changes are coincident with the time period investigated here and high-resolution climate data are necessary to establish the variability of the climatic system during this transitional interval from greenhouse to ice-house states.

Another theory for Eocene climatic evolution is that these step-wise transitions characterise shifting threshold levels from water to ice in high-latitude regions. The climatic shifts were possibly the result of positive feedback upon the attainment of a specific phase of snow and ice expansion. As the ice advanced more of the incoming radiation was reflected back to space, thus changing the global albedo (Berger *et al.*, 1981). This gave rise to a feedback mechanism that helped in sustaining a new palaeoclimatic state (Kennett, 1982).

1.6 The debate over tropical sea surface temperatures (SSTs)

Tropical sea surface temperatures have been shown to be essential in verifying the character of forcing and feedback of warm climatic states (Manabe and Bryan 1985; Covey and Thompson 1989; Horrell 1990; Crowley 1991; Zachos *et al.*, 1994). However, a disparity has previously prevailed between proxy temperature interpretations derived from isotopic and other palaeontological indices for the Eocene tropics. Remarkably, stable oxygen isotopic data from planktonic foraminifera indicate that Eocene tropical SSTs were lower than present (e.g. Shackleton and Boersma, 1981; Boersma *et al.*, 1987, Zachos *et al.*, 1994; Bralower *et al.*, 1995), whilst other palaeontological proxies record SSTs equal or greater than present day temperatures (e.g. Adams *et al.*, 1990; Graham, 1994; Andreasson and Schmitz, 1998). This discrepancy in palaeoclimate proxies has significant implications for the climatic mechanisms involved in creating polar warmth. Hypotheses stating past CO_2 levels to be responsible for the Eocene warmth are not reinforced by existing calcareous $\delta^{18}O$ records which show tropical and subtropical SSTs no warmer than present (figure 1.9). If elevated high-latitude temperatures are due to increased greenhouse gases such as CO_2 and methane, then climatic models suggest that temperatures will be elevated at all latitudes (Crowley, 1991). To date, model simulations with higher atmospheric levels of CO_2 have all produced higher tropical SSTs (Manabe and Bryan, 1985; Manabe and Stouffer, 1994; Cubasch *et al.*, 1995). This disparity suggests that tropical SSTs must have been moderated by feedback processes if Eocene high-latitude warmth was greenhouse gas generated.

Difficulties exist in explaining why Eocene subtropical SSTs were cooler than today whilst high-latitude temperatures were elevated.

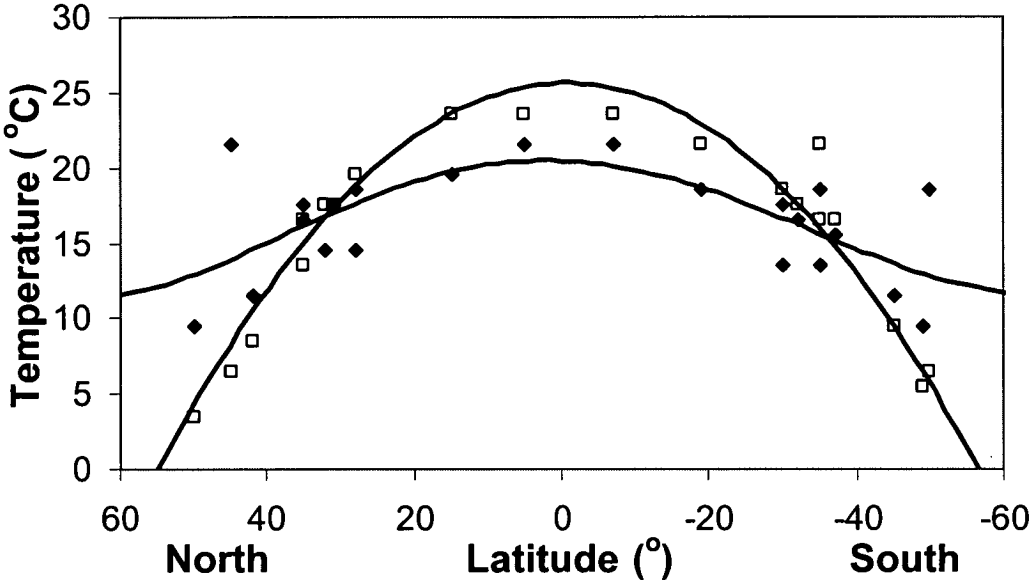

Figure 1.9. Eocene and Holocene surface water temperatures. ◆ = Eocene; □ = Holocene (after Barron, 1987).

The warm early Cenozoic polar temperatures and cool tropical surface waters are often explained by increased ocean heat transport from the low- to high-latitudes (Barron, 1987; Covey and Barron, 1988; Covey and Thompson, 1989; Horrell, 1990; Rind and Chandler, 1991; Barron *et al.*, 1993; Sloan and Rea, 1995). Climatic modeling experiments suggest that the amount of Eocene high-latitude warming and the cool tropics may be achieved by amplifying the ocean poleward heat conveyor (Barron, 1987; Rind and Chandler, 1991). This is thought to warm polar regions whilst reducing equatorial SSTs (Covey and Thompson, 1989; Horrell, 1990; Zachos *et al.*, 1994). The cooler tropical SSTs observed from calcareous oxygen isotopic evidence would suggest that amplified poleward oceanic heat transport was responsible for the high-latitude warmth. However, oceanic transport 15 to 30 per cent greater than present is reported to be necessary for such changes (Horrell, 1990; Rind and Chandler, 1991) and during intervals when meridonial and vertical thermal gradients were apparently modest compared to present day (such as the Eocene) no known physical mechanism exists to support this (Sloan *et al.*, 1995; Bice and

Marotzke, 2000). Therefore the forcing mechanism responsible continues to be problematic. Further potential feedbacks of abating tropical SSTs include amplified cloud cover which may elevate albedo and thus induce cooling (Ramanathan *et al.*, 1989; Horrell, 1990; Zachos *et al.*, 1994).

There is a possibility however, that foraminifera $\delta^{18}O$ may not always record true SST variability. Greater temperatures have been suggested by other fossil groups (e.g. Andreasson and Schmitz, 1998). The discrepancy in palaeoclimate proxies may result from the diagenetic alteration of planktonic foraminifera, foraminifer palaeoecology or errors in estimating the $\delta^{18}O$ of Eocene seawater. The conclusion needs to be examined more fully, particularly in light of feedback mechanisms and oceanic heat transport. It is clear that to test the CO_2 theory of climate change, further data are required from tropical and subtropical areas.

The results from ODP Leg 171B contribute to the debate on mechanisms of climate change by establishing subtropical SSTs from reasonably preserved material. This high-resolution study allows the middle Eocene climatic changes to be examined much more fully and leads to new insights into forcing mechanisms of the oceanic-climatic system during this period.

1.7 Milankovitch climate cycles and calibration of middle Eocene biostratigraphy to an orbital time-scale

Recent legs from the ODP provide the opportunity to study Palaeogene climate change at a high temporal resolution in the Milankovitch frequency band. The middle and upper Eocene section at Site 1052 has high sedimentation rates (~3 cm / kyr), a clearly defined magnetostratigraphy and abundant calcareous microfossils. The measurements of colour reflectance and magnetic susceptibility indicate cyclic variations in lithology. These sediments are ideal to document orbital cyclicity patterns in colour and stable isotope records to better understand Eocene climate dynamics. In this study, these data are used to tune to Milankovitch cycles to improve

the traditional middle Eocene chronology that is provided by foraminiferal and nannofossil events. The cyclostratigraphy established at Site 1052 is used to accurately reconstruct the timing of middle Eocene biostratigraphic events (chapter 2), particularly the extinction of *Morozovella spinulosa*, which is a distinct biomarker for late middle Eocene sediments. Spectral analysis is then used to identify the influence of climatic variation in response to orbital forcing (Milankovitch periodicities) on foraminiferal $\delta^{18}O$ and $\delta^{13}C$ records (chapter 4).

1.8 Objectives

By high-resolution stable isotope data from middle Eocene planktonic foraminifera, the following objectives are addressed:

1) Astronomical calibration of the colour record at Site 1052 by Pälike *et al.* (2001) is used to refine the late middle Eocene biochronology. A number of biostratigraphic datums are refined and tuned to the orbital chronology.
2) Insights are gained into the instability of transitional climate dynamics in the middle Eocene by documenting the fluctuations in surface water isotopic values and their relationship to orbital cyclicity (Milankovitch Cycles). This is accomplished by stable isotope analysis of the late middle Eocene sediments at Site 1052 from 75 – 135 metres composite depth (mcd), which represents a time span of approximately 2.3 million years. By determining orbital variability in the stable isotope records an assessment of the timing and abruptness of large climatic oscillations is made.
3) Subtropical sea surface temperatures in the middle Eocene are constrained to document if these were really cooler than modern day temperatures. This is accomplished from oxygen isotope analysis of reasonably well preserved planktonic foraminifera. The results provide information on the mechanisms that drove Eocene climatic oscillations.
4) The vertical water column temperature gradient over Blake Nose during part of the middle Eocene is reconstructed. Measurements from both planktonic and benthic foraminifera provide information on Eocene oceanic stratification, mixing / upwelling intensities and their relationship to solar insolation distributions.

5) The faunal response to climatic cooling is assessed, particularly in terms of the timing and abruptness of key extinction events.

The objectives are addressed by stable isotopic and spectral analysis of foraminifer and sedimentary cycles from ODP Leg 171B Site 1052. The long-term isotopic records of Eocene surface and deep-water are well documented (Zachos *et al.*, 1994 and references therein), however middle Eocene climate variability has not previously been examined at a high-resolution. The high-resolution study of these Eocene sediments will constrain climatic forcing mechanisms under transitional climate conditions. The stable isotope record is needed to assess the scale and timing of short-term changes in SSTs and major steps in global climatic evolution as the cryosphere develops. The results from Leg 171B will document how rapidly these changes took place and examine the stability of warm climate phases. The analysis of planktonic foraminifera permits the measurement of Eocene surface water conditions at an orbital resolution. This has never been examined at such a high-resolution in the Palaeogene and provides significant insights into climate dynamics and how these differed from those of the present day. These records hold essential information on transitional climate change and palaeoceanography that is required to interpret climate forcing and feedback mechanisms in the ocean-atmosphere system. The sediments from Site 1052 allow documentation of middle Eocene climatic variability and its relationship to biotic turnovers. The influence of Milankovitch forcing upon middle Eocene ocean dynamics is examined to understand the nature of climatic forcing mechanisms at this time.

2. ORBITAL CYCLICITY IN THE LATE MIDDLE EOCENE SEDIMENT RECORD AT BLAKE NOSE AND RECALIBRATION OF THE BIOSTRATIGRAPHY TO THE ASTRONOMICAL TIME-SCALE

2.1 Orbital forcing in Palaeogene records

It is well established that climatic variance is driven in some way by insolation changes caused by orbital forcing (Milankovitch cyclicity) (e.g. Imbrie *et al.*, 1984; Genthon *et al.*, 1987). The amount of solar radiation received and its geographical distribution are influenced by three variable elements of the Earth's orbit (figure 2.1). Periodic variations in the insolation patterns of the Earth are produced by the cycles of equinox precession (19-23 kyr), obliquity of the Earth's rotation axis (41-54 kyr), and eccentricity of the orbit around the sun (97-123 kyr for short-term and ~413 kyr for long-term components) (Milankovitch, 1941).

Over approximately a 100, 000 year cycle, the Earth's orbit changes from being circular to an elliptical shape. This eccentricity of orbit causes seasonal variations in the amount of solar insolation, by modulating the precessional cycles. Every 41, 000 years, the tilt of the Earth's axis changes between 24.5° and 22.1°, the greater the tilt the more marked the seasons, particularly at high latitudes. The time of year at which the Earth is nearest the sun (perihelion) also varies, this alternates with an average 21, 000 year cycle. This enhances the seasonal difference between the two hemispheres, with the greatest influence at low latitudes. It is these changes which appear to be responsible for remarkable variations in the complex oceanic and atmospheric systems. Changes in orbital parameters give rise to altered seasonal distributions and intensities of solar insolation that are thought to lead to changes in marine productivity, carbonate rain rates, terrestrial runoff, sediment erosion and transport among other things. How the relatively minor variations in solar insolation cause these changes is not well understood. The question addressed here is how variations

in insolation as a function of orbital cycles propagated in the climate system during the late middle Eocene.

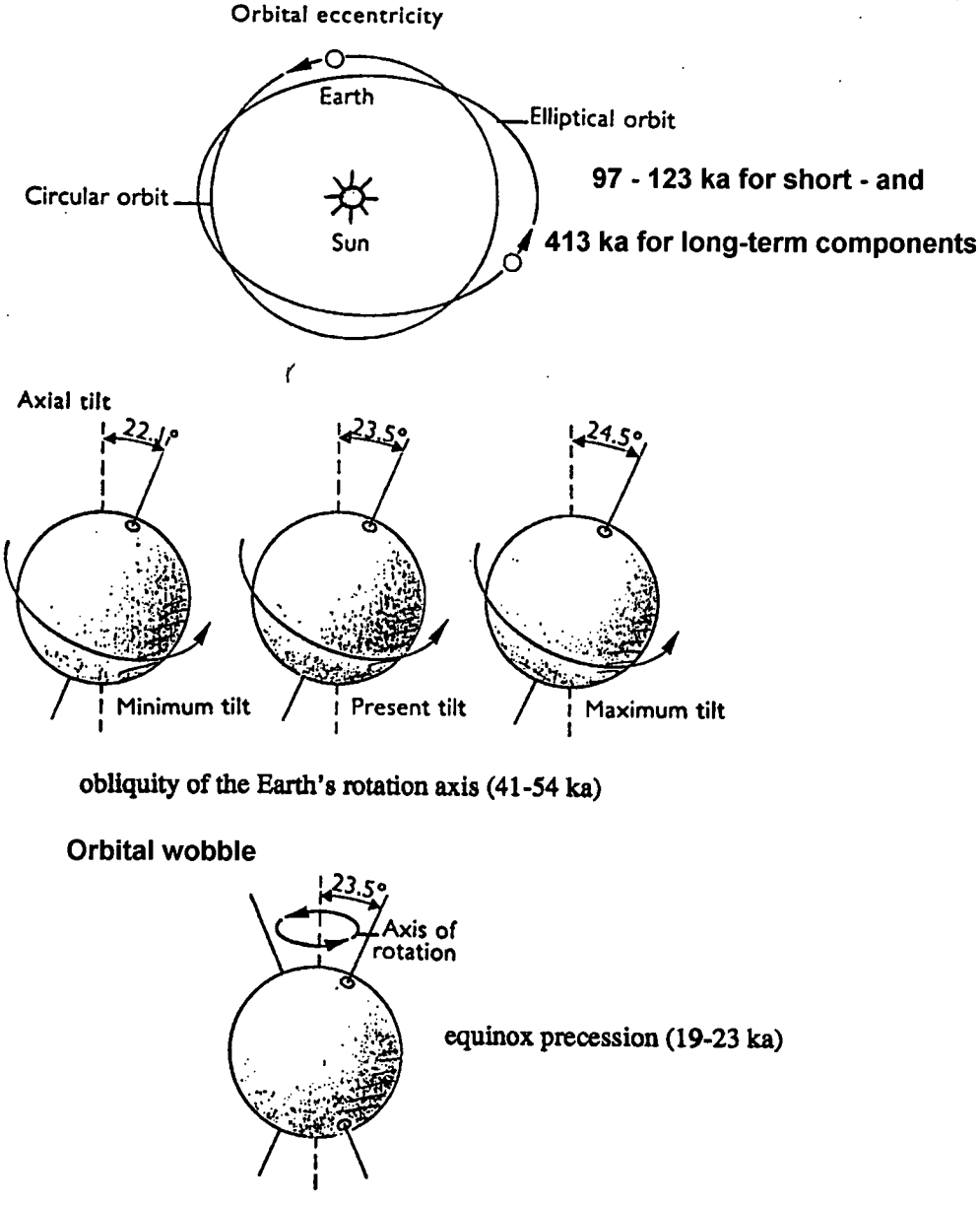

Figure 2.1. Simplified illustration of the variable elements in the Earth's orbit (after Elsom, 1992).

Evidence for orbital forcing in the Palaeogene has been provided by spectral analysis of climatic records, which has recognised orbital frequencies in foraminiferal assemblages, stable isotope data and physical property records. For example, Herbert and D'Hondt (1990) recognised precessional climate cyclicity in the South Atlantic during the Danian. Bradley (1929) and Fischer and Roberts (1991) identified oscillations with a periodicity of 19.5 and 100 kyr from the Eocene Green River Formation (Wyoming, USA). Low frequency (~ 400 kyr) oscillations in climate and carbon cycles were found by Zahn and Diester-Haass (1995) at ODP Site 689 (Weddell Sea, Antarctica) through the Eocene and Oligocene. Norris and Röhl (1999) recognised precessional frequencies in the late Palaeocene record at Site 1051 and Röhl *et al.* (2001) found both obliquity and precessional cycles in upper Danian sequences at Site 1050. Wade *et al.* (2001) documented orbital signals in colour and stable isotopic data from the middle Eocene at Site 1051.

2.2 Core to core integration

Digital reflectance data and magnetic susceptibility were measured every 5 cm at Blake Nose by the Shipboard Scientific Party (1998). These parameters indicated cyclicity that can be attributed to orbital forcing (Milankovitch cyclicity) (Norris, Kroon *et al.*, 1998). The climatically controlled lithological and colour cycles are more pronounced at Site 1052 than elsewhere on the Blake Nose due to its more proximal location and thus increased terrigenous sediment input compared with deeper water sites. The mechanisms controlling the colour signal are discussed in section 2.7. The multiple coring strategy and sediment cyclicity at Site 1052 allowed the Shipboard Scientific Party to generate a composite depth scale by splicing intervals from adjacent holes to produce a continuous sedimentary record. This prevents problems of core breaks and disturbances in the sedimentary record. The tie points used in construction of the splice were determined by the Shipboard Scientific Party (1998) and are shown in table 2.1. The metres composite depth (mcd) scale is used hereafter. This study focuses on the interval from 1052B 10H-1 83.00 cm to 1052F 14H-6 137.00 cm, equivalent to 77.26 to 131.33 mcd. Figure 2.2 illustrates the

execution of tie points from table 2.1. The composite depth scale (table 2.1) is used throughout this thesis including stable isotope examination (chapter 3).

Hole	Core, section	Interval (cm)	Depth (mbsf)	Depth (mcd)	Tied	Hole	Core, section	Interval (cm)	Depth (mbsf)	Depth (mcd)
F	8H-7	41.00	75.91	77.26	Tie to	B	10H-1	83.00	72.83	77.26
B	10H-6	119.00	80.69	85.12	Tie to	F	10H-2	84.50	83.36	85.12
F	10H-5	77.00	87.77	89.53	Tie to	B	11H-2	91.00	83.91	89.53
B	11H-5	107.00	88.57	94.19	Tie to	F	11H-1	121.00	91.71	94.19
F	11H-7	21.00	99.71	102.19	Tie to	B	12H-4	2.50	95.49	102.19
B	12H-6	11.00	98.56	105.26	Tie to	F	12H-2	85.00	102.35	105.26
F	12H-7	5.00	109.05	111.96	Tie to	B	13H-3	140.00	104.91	111.96
B	13H-4	103.00	106.03	113.08	Tie to	F	13H-1	66.00	110.17	113.08
F	13H-6	73.00	117.73	120.64	Tie to	B	14H-3	108.00	114.09	120.64
B	14H-6	115.00	118.65	125.20	Tie to	F	14H-2	123.50	121.74	125.20
F	14H-6	137.00	127.87	131.33	Tie to	A	14H-6	11.00	125.31	131.33

Table 2.1. Core to core integration at Site 1052 (Norris, Kroon *et al.*, 1998).

The spliced section allows a composite of the physical property records to be constructed. Figures 2.3 and 2.4 show the spliced Munsell hue colour record and magnetic susceptibility from Site 1052 plotted against mcd. A clear cyclicity is evident, particularly from 103 – 133 mcd with an average wavelength of ~0.7 m.

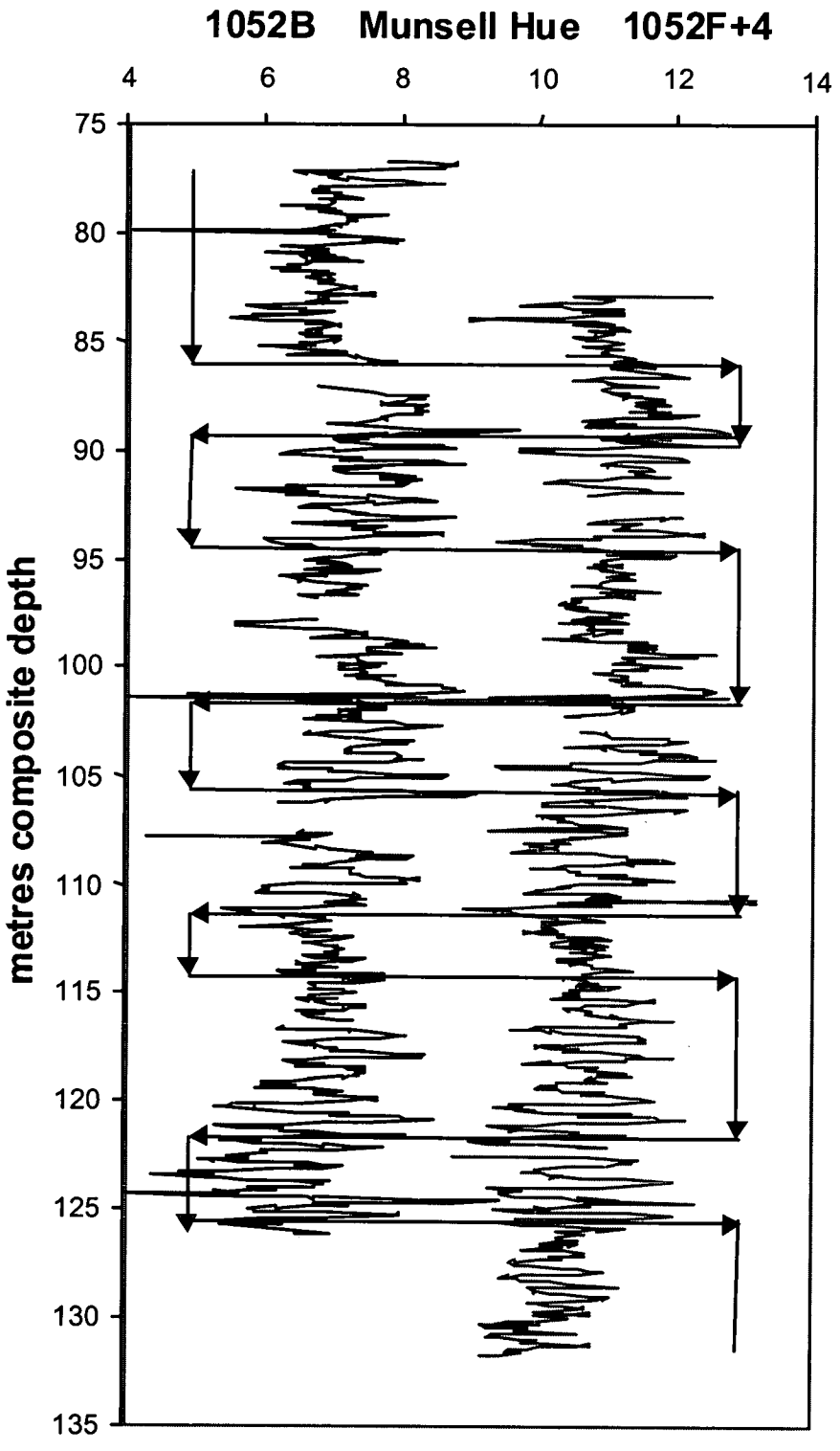

Figure 2.2. Munsell hue record from 75 – 135 mcd at Site 1052 (Holes 1052B and 1052F) after Norris, Kroon *et al.* (1998). Data from Hole 1052F has been offset by a value of +4 to distinguish data from Hole 1052B. The tie points of table 2.1 are indicated by the horizontal lines whilst the interval included in the splice is illustrated by the vertical lines.

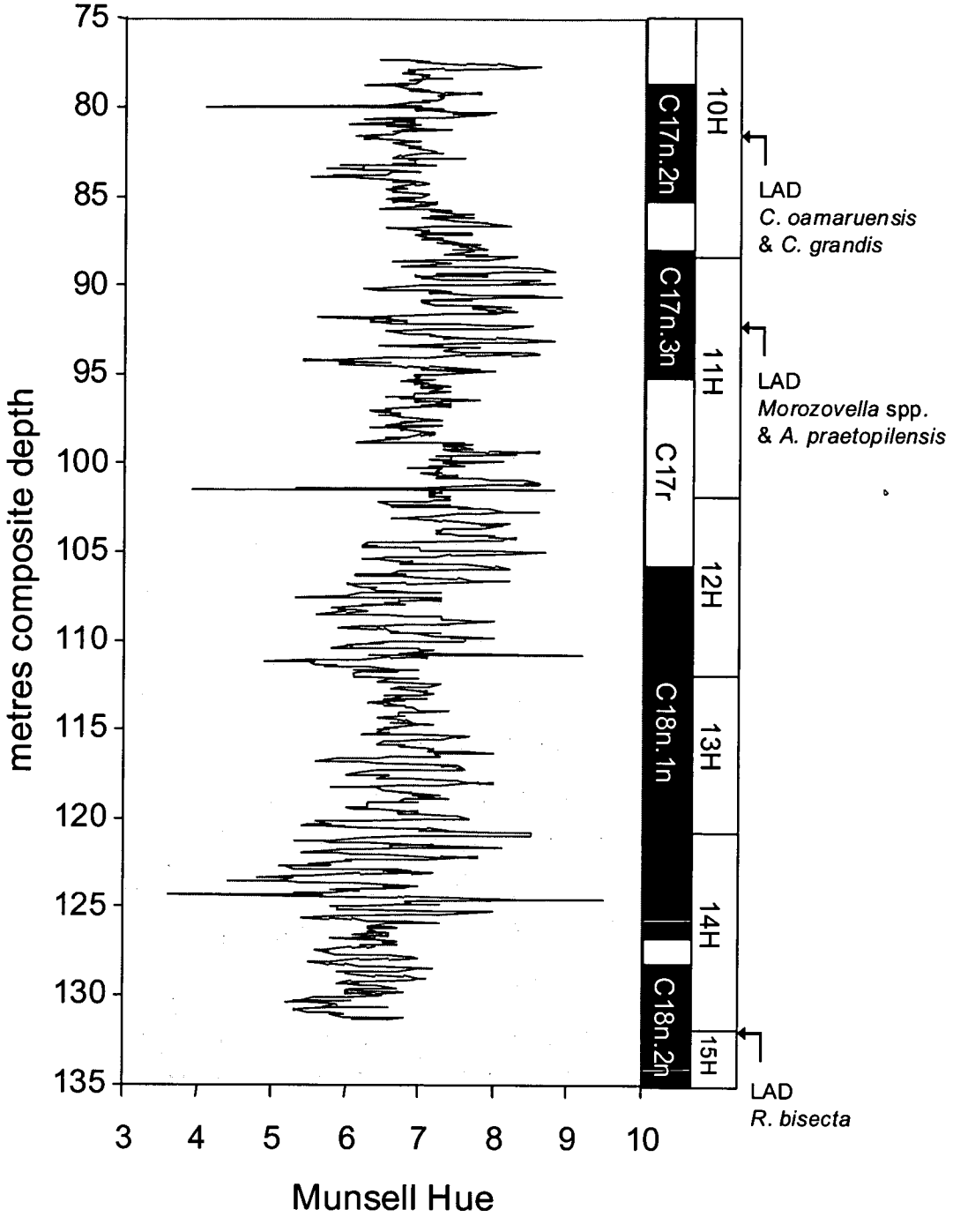

Figure 2.3. Munsell hue colour record from 75 to 135 metres composite depth at Site 1052. Magnetostratigraphy and core numbers are shown on the right. Biostratigraphic datums are also indicated (discussed in section 2.5.2). LAD = last appearance datum. *C.* = *Chiasmolithus; A.* = *Acarinina; R.* = *Reticulofenestra.* This interval corresponds to planktonic foraminifera Zones P14/P15, late middle Eocene.

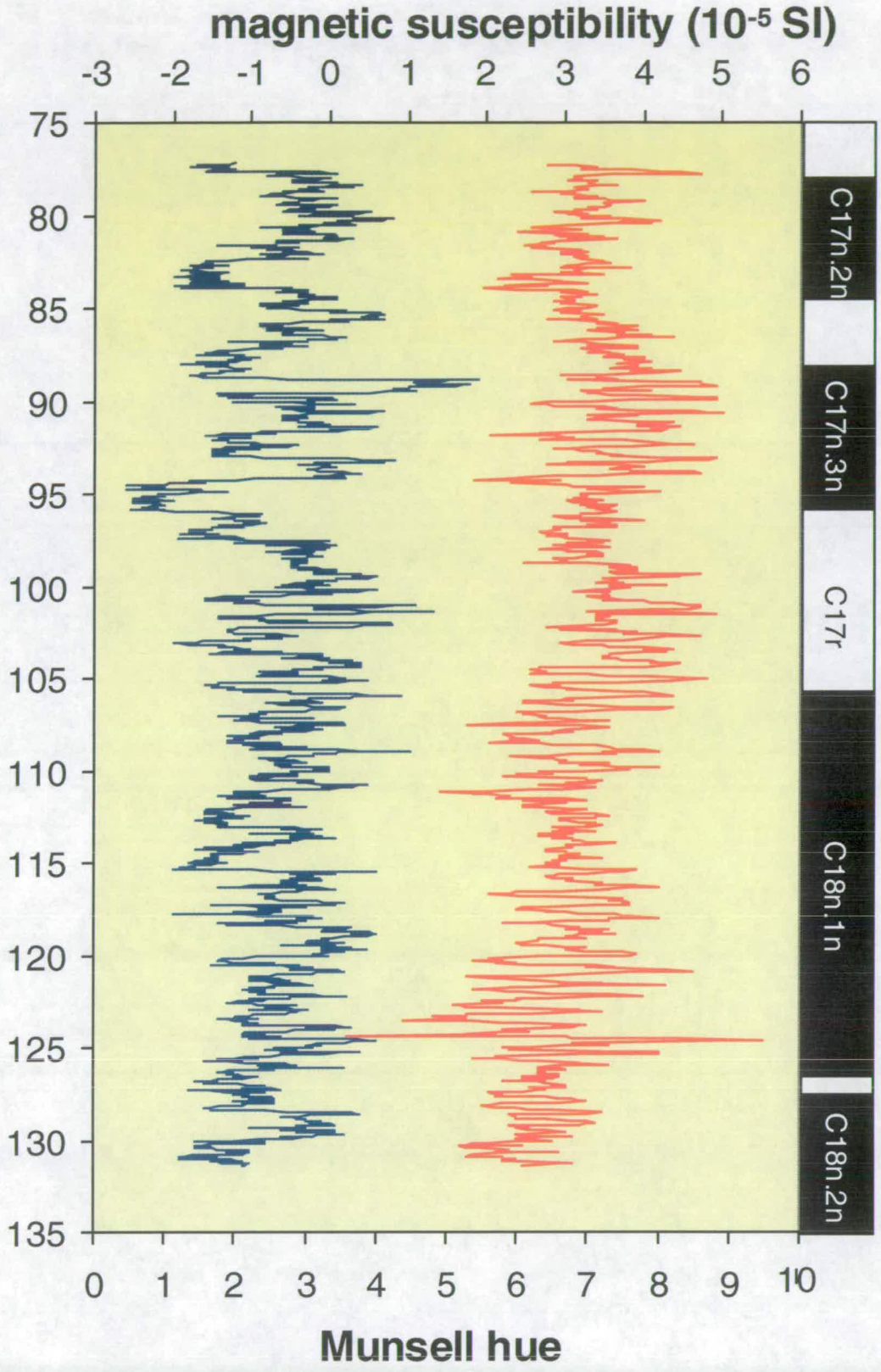

Figure 2.4. Magnetic susceptibility (left) and Munsell hue (right) record from 75 – 135 metres composite depth at Site 1052.

2.3 Age model

The combination of abundant microfossils and nannofossils, with the clear magnetostratigraphy, provided a Shipboard chronostratigraphic framework for Site 1052 that was later improved by using cyclostratigraphy. Table 2.2 lists the initial magneto- and biostratigraphic datums from Site 1052 as per the Shipboard Scientific Party (1998).

	Datum	Age (Ma)	Minimum depth (mcd)	Maximum depth (mcd)	Mean depth (mcd)
T	C17n.2n	37.604	78.46	80.00	79.23
B	C17n.2n	37.848	85.56	87.56	86.56
T	C17n.3n	37.920	88.00	89.22	88.61
B	C17n.3n	38.113	94.02	97.64	95.83
T	C18n.1n	38.426	105.26	107.80	106.53
B	C18n.1n	39.552	127.30	127.96	127.63
T	C18n.2n	39.631	128.40	129.44	128.92
B	C18n.2n	40.130	137.10	140.14	138.62
B	*C. oamaruensis*	37.000	82.19	83.59	82.89
T	*C. grandis*	37.100	82.19	83.65	82.92
B	*R. bisecta*	38.000	123.53	133.62	128.58
T	*M. spinulosa*	38.100	87.37	93.36	90.37
B	*G. semiinvoluta*	38.400	83.61	87.37	85.49
T	*O. beckmanni*	40.100	135.36	135.69	135.53
T	*C. solitus*	40.400	133.62	135.92	134.77

Table 2.2. Magnetostratigraphic and biostratigraphic age datum levels for Site 1052. B, base; T, top. All biostratigraphic datums from Hole 1052A (Norris, Kroon *et al.*, 1998) and ages from Berggren *et al.* (1995). Compare to refined magnetostratigraphic and biostratigraphic datums, tables 2.3, 2.5 and 2.6.

2.3.1 Sedimentation rates

Figure 2.5 shows the age model and sedimentation rates calibrated for Site 1052 based on the magnetostratigraphy and the age scale of Berggren *et al.* (1995) (table 2.2), assuming a constant sedimentation rate between tie points. There is considerable scatter in the biostratigraphic datums that are thought to be due to inaccuracies in the current calibration or diachronous bio-events. The age model suggests that this record is approximately 2.6 million years (myr) in duration.

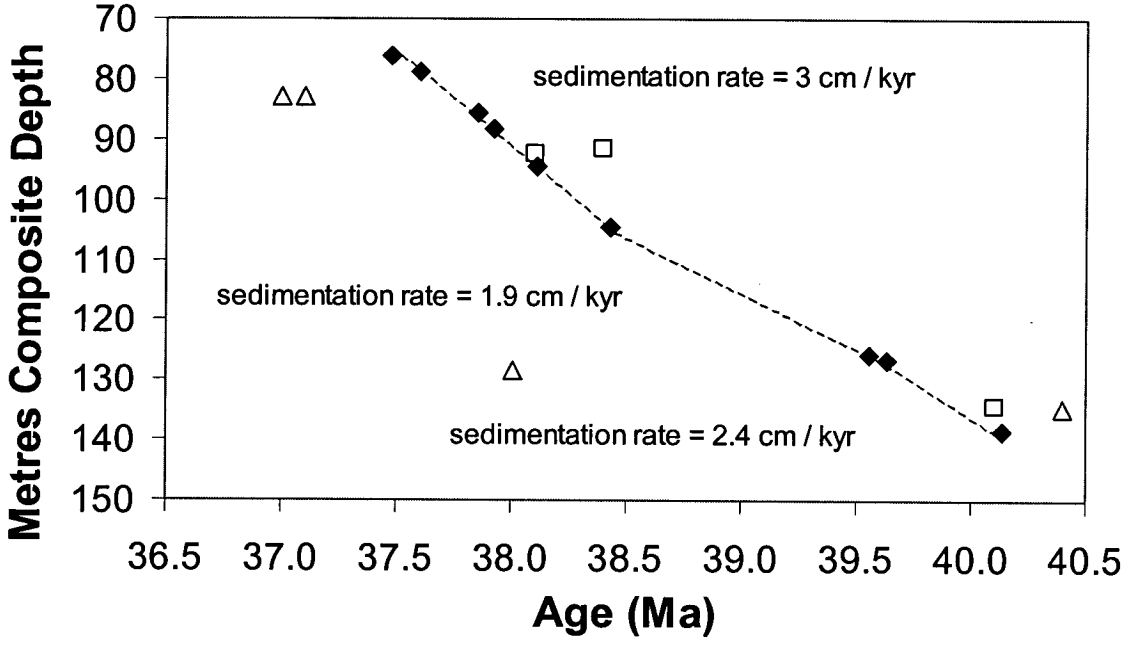

Figure 2.5. Biostratigraphic and magnetostratigraphic datums at Site 1052 plotted against the time-scale of Berggren *et al.* (1995). Age model for Site 1052 as listed in table 2.2. This is based on the bio-magnetostratigraphy from the Shipboard Scientific Party (1998), assuming a constant sedimentation rate between tie points. Points represent the mean metres composite depth (mcd) of each datum. ♦ = magnetostratigraphic datums; △ = nannofossil datums; □ = foraminifera datums.

The biostratigraphy and magnetostratigraphy allows an estimate of the sedimentation rate at Site 1052. Using the age scale of Berggren *et al.* (1995) this varied between 1.9 cm / kyr and 3 cm / kyr (figure 2.5). The magnetochronology implies a significant decrease in the sediment accumulation rate during chron C18n.1n (106.53 – 127.63 mcd). Alternatively, this magnetochron could be truncated by one or more unconformities (evidence for which is discussed in section 2.5.1).

2.4 Spectral analysis of the sedimentary record

Spectral analysis was conducted on the digitised sediment colour records from Site 1052 using the Blackman-Tukey method in the *Analyseries* software package (Paillard *et al.*, 1996). The Munsell hue record was detrended with a 21-point moving average. To document the frequency of significant cycles in the Munsell hue record, spectral analysis was performed on a series of overlapping 10 m sliding windows (figure 2.6). Performing spectral analysis in this way allows the change in short-term (precessional) cycle frequencies over time to be isolated and identified. The overlapping windows document variations in sediment accumulation rate and constancy of the spectral peaks. As the data has been detrended to remove the long-term periods other Milankovitch frequencies such as the eccentricity cycle (~400 and 100 kyr) are not seen.

The Munsell hue colour record from 75 to 135 mcd shows pronounced cyclicity at a wavelength of 1.4 ± 0.2 cycles / metre (figure 2.6) throughout the record, suggesting a recurrent variation in the depositional environment. This is visually apparent in both the evolving spectral analysis (figure 2.6) and within the raw data (figures 2.2, 2.3 and 2.4). The sediment accumulation rates obtained by the bio and magnetostratigraphic age model (figure 2.5) provide an estimate of the periodicity in the Munsell hue record. The sedimentation rate averages ~3 cm / kyr during Chron C17n.2n and C17n.3n (75 – 105 mcd) suggesting that the ~0.7 metre oscillations are attributed to the 21 kyr precessional periodicity. There are a number of magnetostratigraphic and biostratigraphic datums for this interval and therefore the sedimentation rate for this section is better constrained than further downhole. The estimated sediment accumulation rate of magnetochrons C17n.2n, C17n.3n and C17r are consistent with the ~0.7 metre cycles assigned to the precessional period.

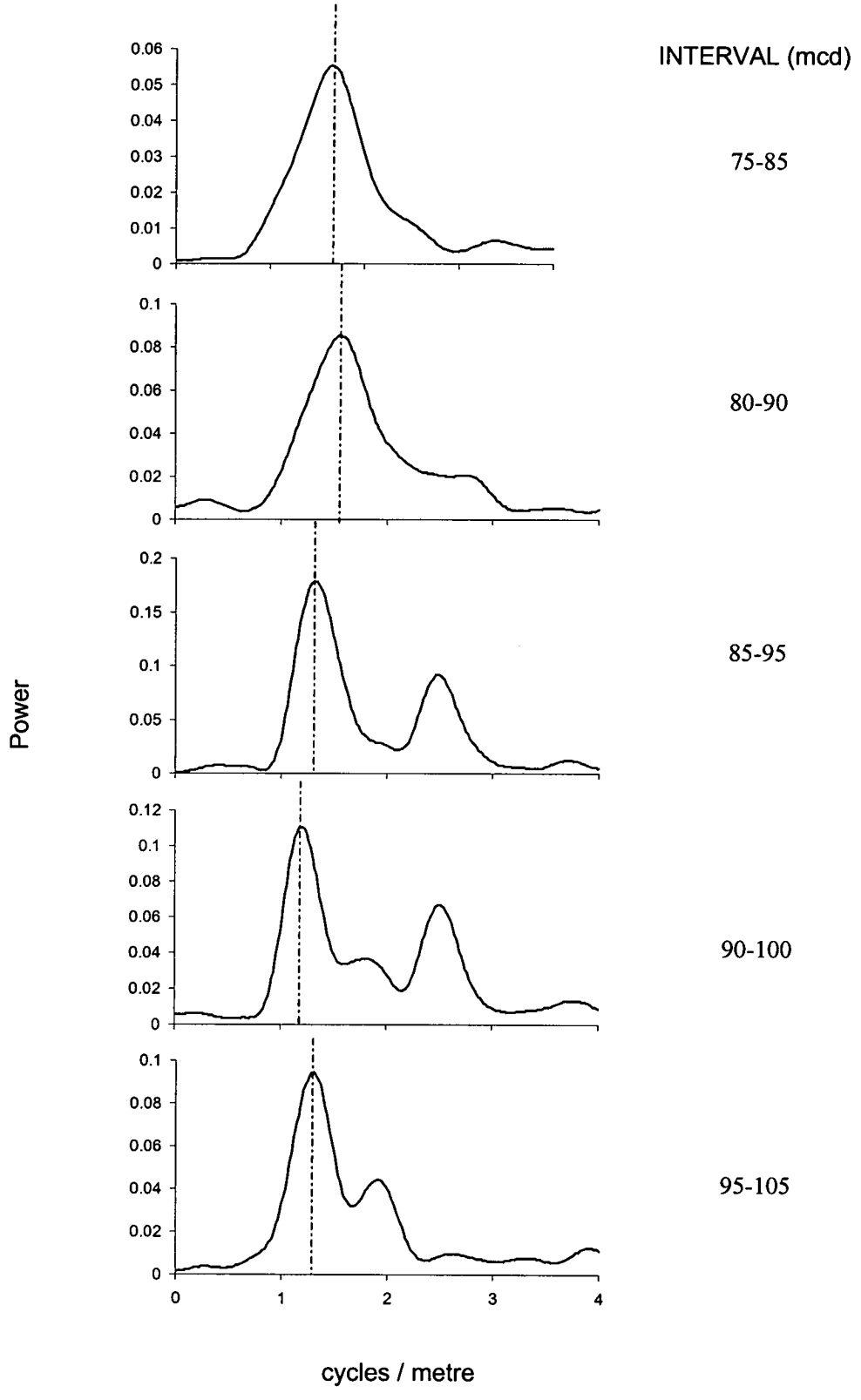

Figure 2.6a. Power spectra of 10 m intervals of the Munsell hue record at Site 1052. Note changes in scale on the y-axis. The dotted line indicates the main cycle frequency corresponding to precession (~21 kyr).

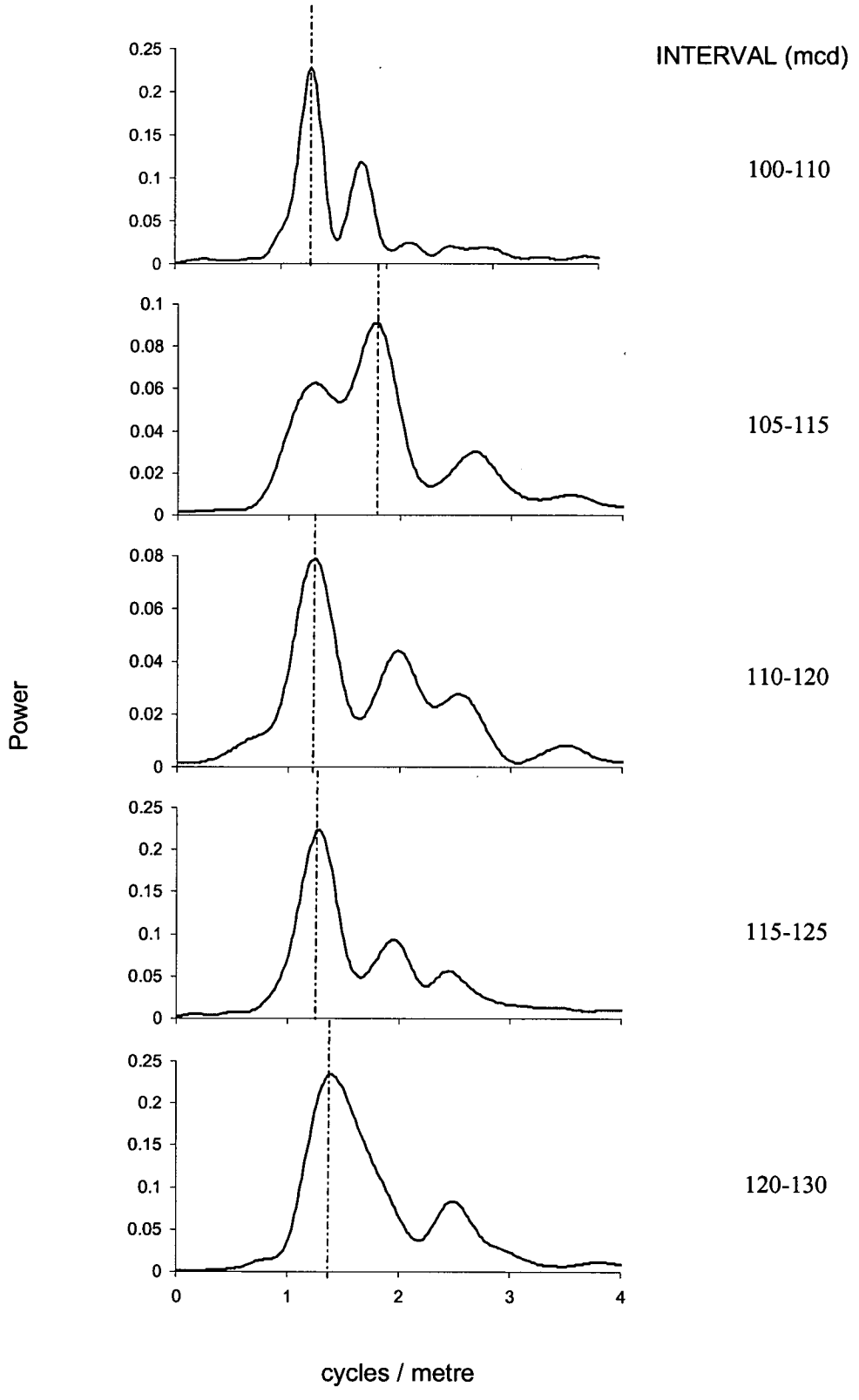

Figure 2.6b. Power spectra of 10 m intervals of the Munsell hue record at Site 1052. Note changes in scale on the y-axis. The dotted line indicates the main cycle frequency corresponding to precession (~21 kyr).

There is a shift in the dominant cycle from 1.2 to 1.8 cycles / metre at 105 – 115 mcd. This reflects a change in mean sedimentation rate from 3.8 cm / kyr to 3.0 cm / kyr over this interval. There is also a secondary frequency at 2.3 ± 0.38 cycles / metre. This may relate to smaller maxima of precession and has been recorded in previous studies (e.g. Herbert and D'Hondt, 1990; Crowley *et al.*, 1992; Hagelberg *et al.*, 1994; Olago *et al.*, 2000; Wade *et al.*, 2001). Alternatively, the subsidiary cycles may relate to secondary harmonics, which are frequent in time series against depth (Weedon, 1989; Weedon *et al.*, 1997). Small fluctuations in sedimentation rate account for the variations in the orbital peaks with depth.

2.5 Astronomical calibration of the middle Eocene time-scale

As demonstrated for Pleistocene palaeoclimatology, orbital cyclicity provides an effective means to gauge time. It therefore has the capacity to significantly improve the temporal resolution of geomagnetic polarity time-scales (e.g. Cande and Kent, 1992, 1995; Berggren *et al.*, 1995). The recognition of Milankovitch cyclicities in stable isotope, colour, magnetic susceptibility and other geochemical data has allowed astronomical calibration of parts of the Palaeogene time-scale (Herbert and D'Hondt, 1990; Norris and Röhl, 1999; Shackleton *et al.*, 1999, 2000; Pälike *et al.*, 2001).

The expanded sediments from the Eocene at Site 1052 contain abundant calcareous and siliceous microfossils and a good magnetostratigraphic record that reveal pronounced Milankovitch-related cyclicity in the colour and magnetic susceptibility data (section 2.4; figures 2.3, 2.4 and 2.6). Elemental concentrations from Site 1052 sediment cores were obtained by Pälike *et al.* (2001) through X-ray fluorescence (XRF) scanning. Pälike *et al.* (2001) have calibrated the cyclic record in calcium – iron ratios (Ca/Fe) and colour data at Site 1052 to astronomical frequencies in order to retune the time-scale of the middle and late Eocene and thus refine the late and middle Eocene magnetochronology.

The true character of precessional and obliquity cycles are only reliably calculated for the last 10 - 20 Ma (Laskar *et al.*, 1993). Therefore for astronomical tuning of sediments older than 20 Ma a different method needs to be employed. As Eocene astronomical calculations cannot be determined, present day values for dynamical ellipticity and tidal dissipation from Laskar *et al.* (1993) were used by Pälike *et al.* (2001) to fine-tune the lithological record. The tuning methodology was similar to that described in Shackleton *et al.* (1999) and Lourens *et al.* (2001). Precession, obliquity and eccentricity values were normalised and used to create an artificial curve. The precessional signal was reversed to account for Northern Hemisphere insolation. These values are then added together to construct an "eccentricity-tilt-precession" curve (ETP). The most constant feature of orbital climatic cycles is that of the ~400 kyr cycle modulation (Laskar, 1990; Berger *et al.*, 1992; Laskar, 1999). Pälike *et al.* (2001) used the amplitude modulation of the precessional signal by the long-period eccentricity cycle (400 kyr) in these sediments as the primary tuning target.

Pälike *et al.* (2001) concluded that the dominant lithological cycle during the middle Eocene was precession. This was determined by studying the amplitude of modulation over longer time series and comparisons to the present-day astronomical calculations of Laskar *et al.* (1993) (figure 2.7). The results are consistent with those from Site 1051 where a dominant orbital cyclicity of precession (1.0 to 1.4 cycles / metre) is seen in the colour records (Wade *et al.*, 2001). Pälike *et al.* (2001) further verified their time-scale by time-series analysis and studying the modulation pattern in the data. This is discussed further in section 2.6.

Whilst the long-period eccentricity signal may be stable over time, an absolute age datum is required to tie the record to. The presence of an ash layer at 101.39 – 101.47 mcd provides an Ar/Ar age of 37.81 ± 0.91 Ma (Smit, pers. comm.). It was therefore possible for Pälike *et al.* (2001) to correlate the maximum eccentricity of Laskar *et al.* (1993) to amplitude maxima in the lithological records.

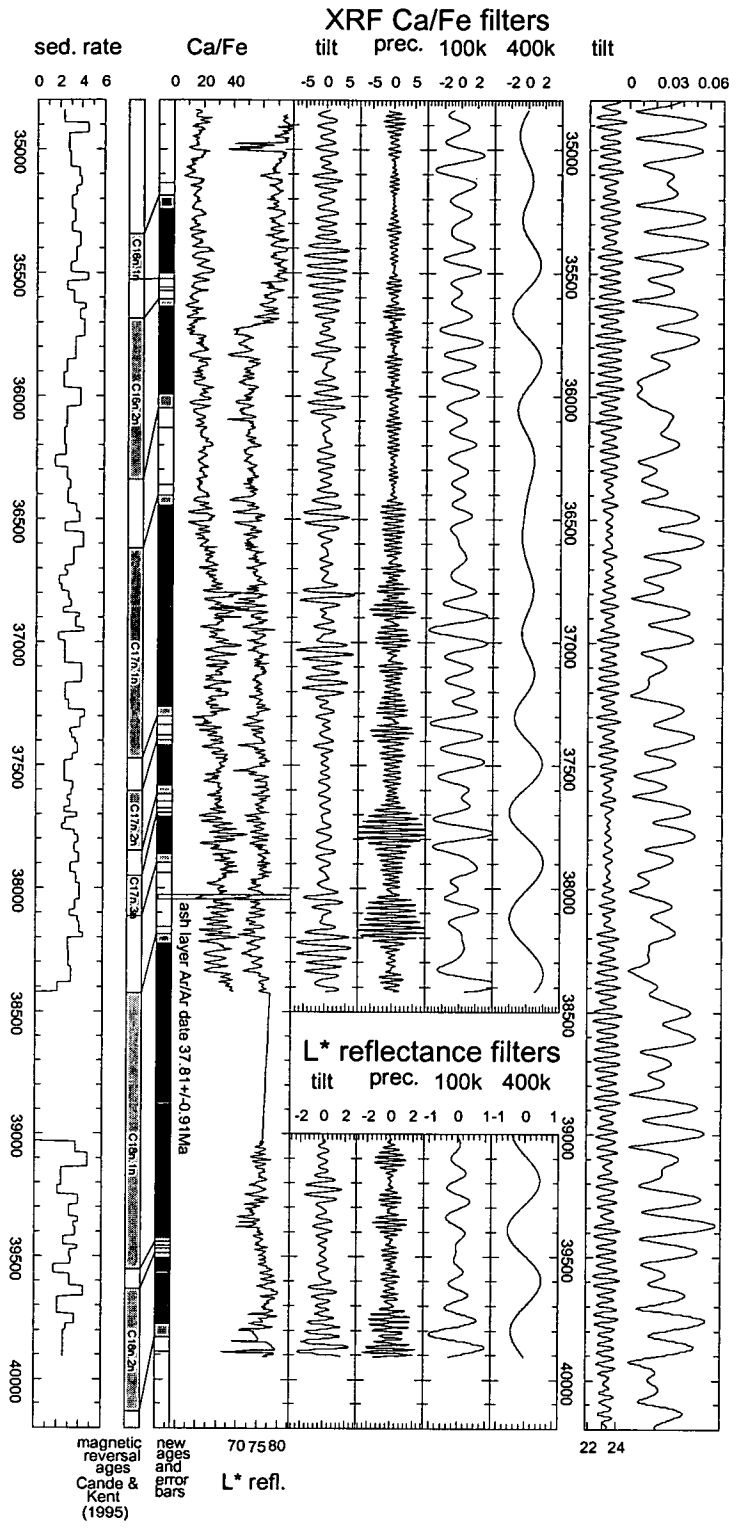

Figure 2.7. Spliced lithological data and astronomical time-scale at Site 1052 from Pälike *et al.* (2001). The revised sedimentation rate in cm / kyr is shown on the left with the magnetochronology (Cande and Kent, 1995) and revised magnetochronology. Bandpass filters are displayed for the main orbital frequencies within the XRF and colour data. The orbital target curve is shown on the right.

The time-scale generated by Pälike *et al.* (2001) is used here to refine the middle late Eocene biostratigraphy and establish the precise timing of rapid fluctuations in planktonic foraminiferal stable isotope records (chapter 4). Tables 2.3 and 2.4 indicate the revised ages and durations of the middle Eocene magnetochronology as per Pälike *et al.* (2001). The duration of polarity chrons do not significantly deviate from those of Berggren *et al.* (1995), suggesting that the tuned time-scale of Pälike *et al.* (2001) is largely correct. The biostratigraphic implications for the revised time-scale are discussed in section 2.5.2.

	Datum	mcd	Age (Ma)*	Revised Age (Ma)$^{\$}$
T	C17n.2n	79.23	37.604	37.399
B	C17n.2n	86.56	37.848	37.618
T	C17n.3n	88.61	37.920	37.692
B	C17n.3n	95.83	38.113	37.897
T	C18n.1n	106.53	38.426	38.186
B	C18n.1n	127.63	39.552	39.441
T	C18n.2n	128.92	39.631	39.486
B	C18n.2n	138.62	40.130	39.828

Table 2.3. Revised late middle Eocene magnetochronology. * = time-scale of Berggren *et al.* (1995); $^{\$}$ = Pälike *et al.* (2001). B = base; T = top; mcd = metres composite depth.

Chron	Duration (kyr)*	Revised duration (kyr)$^{\$}$	Difference (kyr)
C17n.2n	244	219	-25
C17n.3n	193	205	+12
C17r	313	289	-24
C18n.1n	1126	1255	+129
C18n.2n	499	342	-157

Table 2.4. Revision of chron duration. * = time-scale of Berggren *et al.* (1995); $^{\$}$ = Pälike *et al.* (2001).

2.5.1 Revised sedimentation rates

Sedimentation rates generally range between 2 – 5 cm / kyr (figure 2.7) with a mean of 3 cm / kyr. There is a hiatus of 613 kyr duration within chron C18n.1n. Pälike *et al.* (2001) have implicated a hiatus at 113 mcd based on cycle duration and loss in magnetic susceptibility, XRF signal and reflectance (figure 2.8). This is confirmed by the oxygen isotope record (chapter 3) which shows an abrupt short-term shift to negative values at 113 mcd. Detailed XRF analysis and studies of the colour record exclude errors in the composite depth scale.

Cycle counts reveal approximately 24 cycles within C18n.1n (figure 2.8). Based on a precessional period this accounts for a duration of 504 kyr. This would suggest that approximately 30 precessional cycles are missing (630 kyr). An alternative explanation is that there is not a hiatus and that these cycles reflect the obliquity period. However, this explanation would require a shift in the dominant orbital periodicity and is not supported by the consistency of the Munsell hue power spectra (figure 2.6).

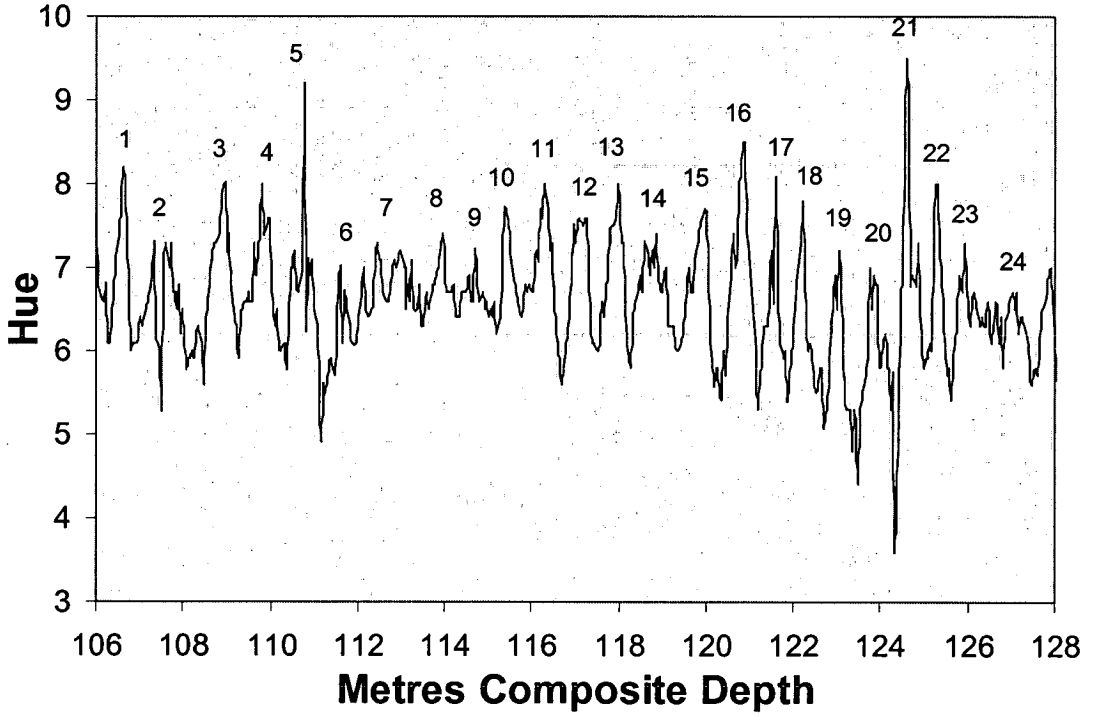

Figure 2.8. Cycle count of the Munsell hue record for chron C18n.1n. There is a loss in the cyclic signal at ~113 mcd probably due to a hiatus (discussed in text).

The presence and length of the hiatus is also constrained by the amplitude modulation of the precessional cycles within the colour record. The absence of a hiatus within C18n.1n would suggest large variations in the total duration of C18n.1n and thus significant fluctuations in sea-floor spreading rate. The hiatus is consistent with assignment of 0.7 metre cycles to the precessional period and that little change in sediment accumulation rate occurred pre or post hiatus (figure 2.9). The revised sediment accumulation rates with the bio- and magnetostratigraphic datums are shown in figure 2.9.

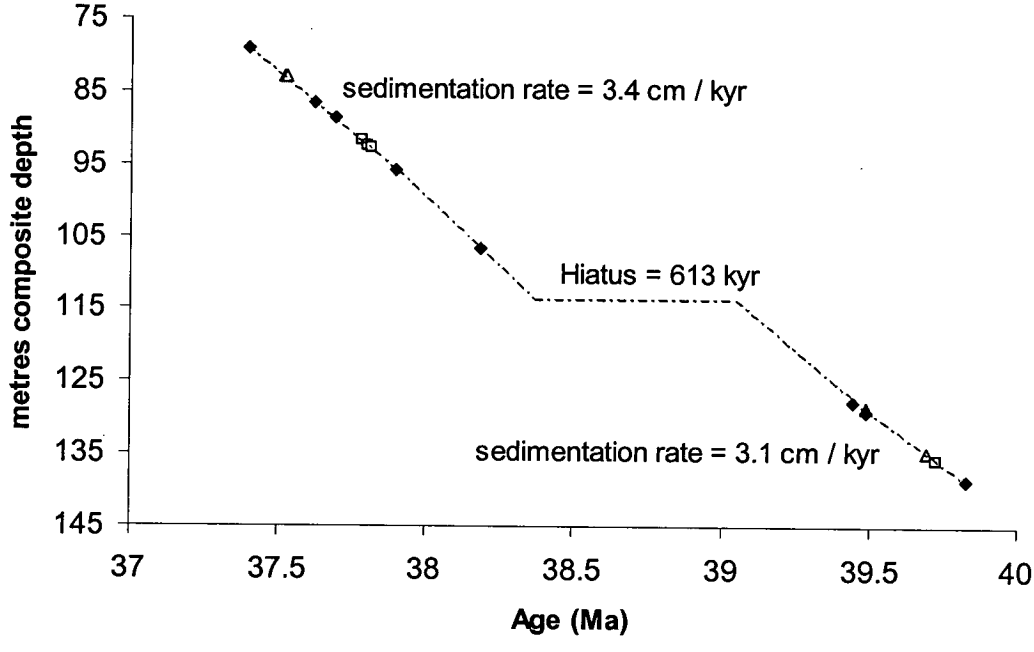

Figure 2.9. Recalibrated biostratigraphic and magnetostratigraphic datums at Site 1052 as listed in tables 2.3; 2.5 and 2.6. Points represent the mean metres composite depth (mcd) of each datum. ♦ = magnetostratigraphic datums; △ = nannofossil datums; □ = foraminifera datums. Small changes in sedimentation rate occur through this interval.

2.5.2 *New and revised biostratigraphic events and calibration to the orbital time-scale*

The astronomical time-scale and the high-resolution analysis applied here has allowed a number of new and existing biostratigraphic datums to be revised to the orbital chronology (tables 2.5 and 2.6). Samples were analysed for planktonic

foraminifera biostratigraphic purposes every 10 cm, permitting datums to be constrained to within 3 kyr (based on average sedimentation rates). Planktonic foraminifera species of biostratigraphic significance are shown in Plate 1. The preservation of foraminifera is discussed in chapter 3.

	Datum	Hole	Interval (cms)	Depth (mbsf)	Depth (mcd)	Age (Ma)*	Revised age (Ma) †
T	*S. linaperta*	10H-1	73-76	72.75	77.18	37.7	<37.341
T	*M. spinulosa*	11H-4	93-96	86.95	92.57	38.1	37.802
T	*M. crassata*	11H-4	93-96	86.95	92.57	-	37.802
T	*A. praetopilensis*	11H-4	133-136	87.25	92.87	-	37.810
B	*G. semiinvoluta*	11H-4	3-6	86.05	91.67	38.4	37.778
T	*Planorotalites* spp.	10H-1	73-76	72.75	77.18	38.5§	<37.341
T	*O. beckmanni*	15H-CC	14-16	129.67	135.69	40.1	39.723

Table 2.5. New and revised planktonic foraminifera datums. * = time-scale of Berggren *et al.* (1995); † = this study; § = Nocchi *et al.* (1986); - = no previous age assignment; < = younger than; T = top; B = base. All biostratigraphic datums from Hole 1052B except top *O. beckmanni* from Hole 1052A (Norris, Kroon *et al.*, 1998).

The first occurrence (FO) of *Globigerinatheka semiinvoluta* was determined at 91.67 mcd within chron C17n.3n. This is younger than that of Berggren *et al.* (1995), where the FO of *G. semiinvoluta* is close to the base of C17r and is older than the last occurrence (LO) of *Morozovella spinulosa*. This discrepancy was also found by several other workers (e.g. Benjamini, 1980; Nocchi *et al.*, 1986; Pearson and Chiasson, 1997; Norris, Kroon *et al.*, 1998) suggesting that the diachronism of the FO of *G. semiinvoluta* should be investigated further. Specimens here intergraded from *Globigerinatheka* spp. making the actual FO difficult to determine. *G. semiinvoluta* is usually very rare at its FO (Pearson pers. comm.) and this discrepancy stresses the importance of examining all size fractions at a high-resolution. The extinction of *Morozovella* spp. and *Acarinina praetopilensis* are discussed in detail in chapter 6.

Plate 1. Late middle Eocene planktonic foraminifera of biostratigraphic significance. Scale bars represent 50μm in (a) – (c) where specimens from the 63 to 125 μm size fraction. Scale bars represent 100 μm in (d) – (h) where specimens are from the 250 to 355 μm size fraction. Specimens (a) to (c) from sample 171B, 1052F, 10H-4, 73 – 76 cm (88.01 mcd). Specimens (e) – (h) from sample 171B, 1052B, 11H 4, 143 – 146 cm (93.07 mcd).

(a) *Planorotalites pseudoscitula* umbilical view;
(b) *Planorotalites pseudoscitula* spiral view;
(c) *Planorotalites pseudoscitula* side view;
(d) *Subbotina linaperta* side view, from sample 171B 1052B, 10H-1, 83-86 cm (77.28 mcd);
(e) and **(f)** *Morozovella spinulosa* umbilical view;
(g) *Morozovella crassata* umbilical view;
(h) *Globigerinatheka semiinvoluta* ?. Specimen does not show strong thickening around the apertures.

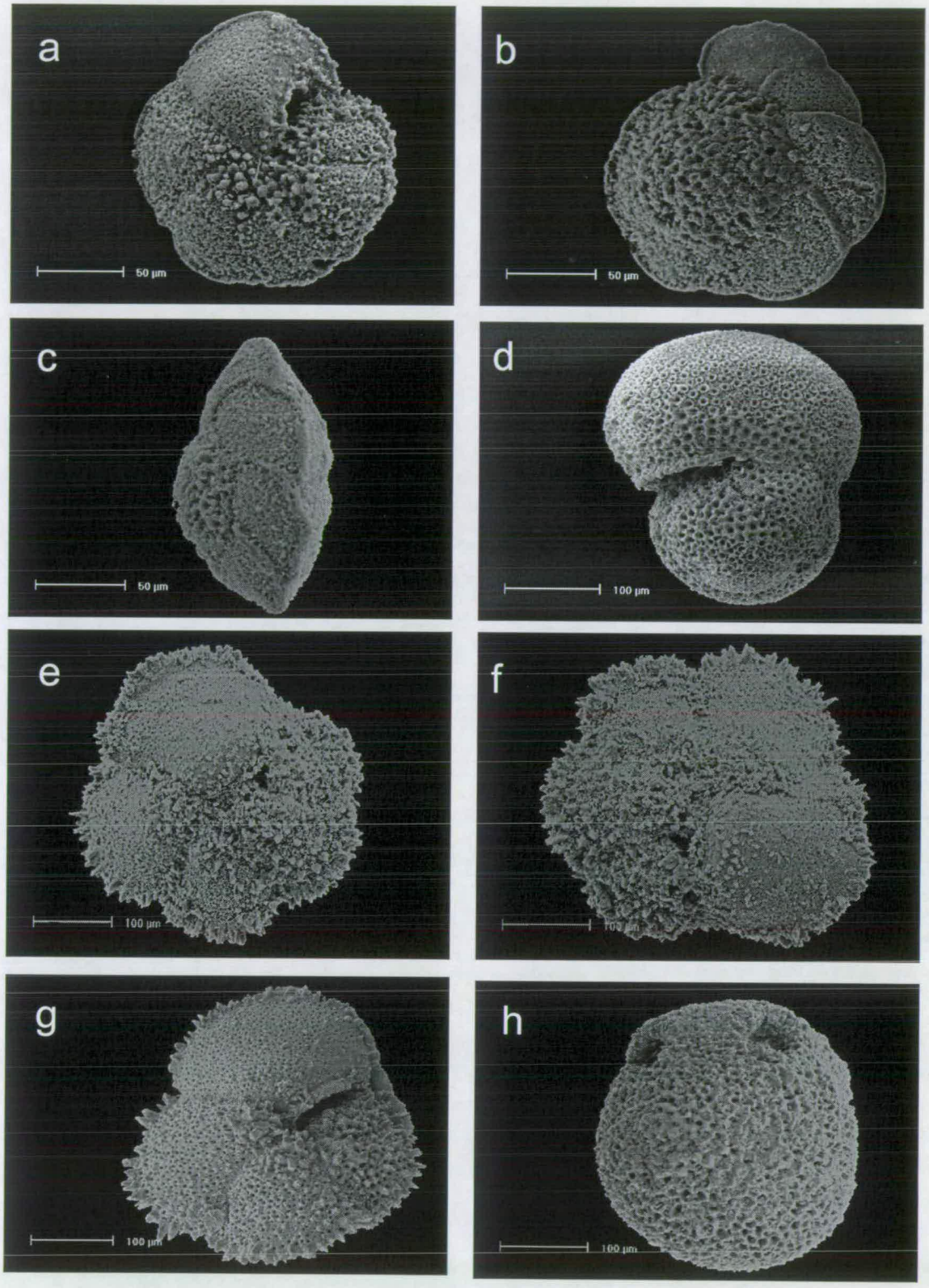
a
50 µm
b
50 µm
c
50 µm
d
100 µm
e
100 µm
f
g
100 µm
h
100 µm

The LO of *Subbotina linaperta* was reported by Berggren *et al.* (1995) to be within C17n.2n (37.7 Ma), based on the calibration of datums from Maud Rise (Weddell Sea, Antarctica). Here the LO of *S. linaperta* was found at Site 1052 to be younger than 37.341 Ma. This species was present at the top of the studied section (77.18 mcd) and therefore its LO is younger than identified here. Jenkins (1971) and Blow (1979) reported that *S. linaperta* persisted into the late Eocene Zone P16. Although this study does not continue into P16, the duration of *S. linaperta* does extend beyond that of Berggren *et al.* (1995). *Planorotalities* spp. are also present to the top of the section studied. This disagrees with previous work that has suggested an extinction of *Planorotalities* spp. within P14 (Schmidt and Raju, 1973; Toumarkine and Luterbacher, 1985; Nocchi *et al.*, 1986).

Several foraminiferal datums published in previous chronologies such as Berggren *et al.* (1995) have not been revised. These are the last occurrences of *Acarinina collactea, A. primitiva and Subbotina frontosa.* This was because *A. collactea* and *A. primitiva* were rare within the samples studied, whilst *S. frontosa* graduated to *Turborotalia* spp. which prevented the last occurrence being defined.

A number of calcareous nannofossil datums can also be revised to the astronomical time-scale (table 2.6). There is a major revision in the base of *Reticulofenestra bisecta* from 38.0 Ma to 39.330 – 39.650 Ma. However, the event horizons of calcareous nannofossil datums are relatively less well constrained compared to the planktonic foraminifera datums (10 cms) in this study due to the lower resolution employed by the Shipboard Scientific Party (1998) (1.5 metres). These dates are likely to be revised by more detailed biostratigraphic work in the future.

	Datum	Hole	Min. depth	Max. depth	Age (Ma)*	Min. age (Ma)$	Max. age (Ma)$
B	*C. oamaruensis*	A	82.19	83.59	37.0	37.474	37.568
T	*C. grandis*	A	82.19	83.65	37.1	37.474	37.570
B	*R. bisecta*	A	123.53	133.62	38.0	39.330	39.650
T	*C. solitus*	A	133.62	135.92	40.4	39.650	39.731

Table 2.6. Revised calcareous nannofossil datums. * = time-scale of Berggren *et al.* (1995); $ = datums provided by the Shipboard Scientific Party (1998) and tuned to the time-scale of Pälike *et al.* (2001).

2.6 Orbital variations in the lithological record

The astronomical time-scale of Pälike *et al.* (2001) has been used to investigate the downcore physical properties of Site 1052 (figure 2.10). Spectral analysis of the Munsell hue versus the astronomical time-scale reveals strong spectral power at 0.0023, 0.0430 and 0.0458 cycles / kyr (figure 2.11) These represent the single peak of the long-term eccentricity cycle (427.5 kyr) and the characteristic double precessional peaks (23.2 and 21.8 kyr) respectively. The double precessional peak was also seen in the colour record at Site 1051 (Wade *et al.*, 2001). Pälike *et al.* (2001) found significant power at the additional orbital frequencies of short-term eccentricity (126 and 98 kyr), obliquity (54 and 41 kyr) and short-term precession (19 kyr) within the Ca/Fe data from the late and middle Eocene at Site 1052.

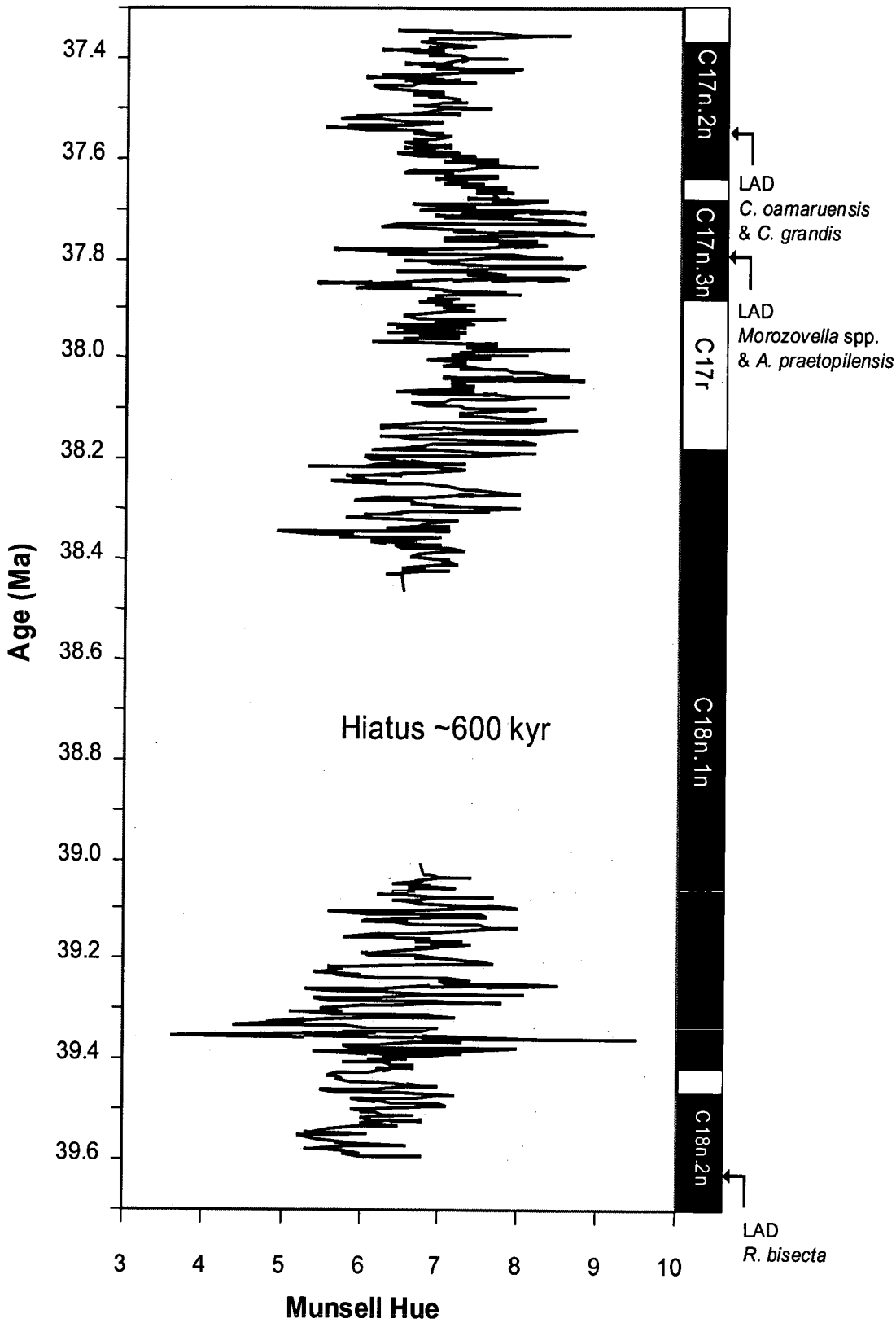

Figure 2.10. Munsell hue record at Site 1052 against the astronomical chronology of Pälike *et al.* (2001). Revised biostratigraphic datums and magnetochronology are shown on the right.

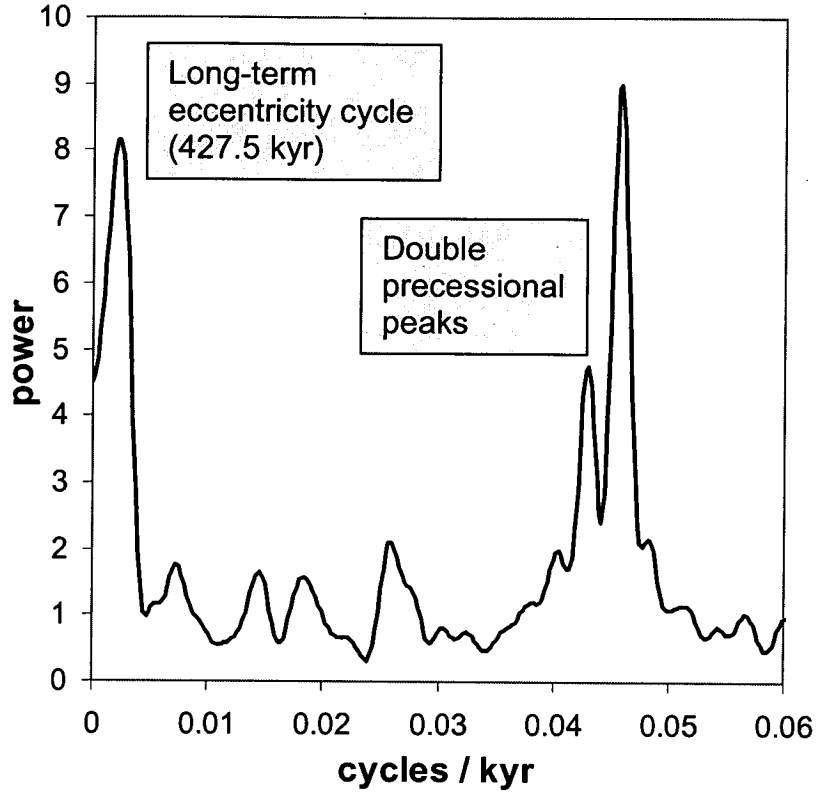

Figure 2.11. Power spectra of the Munsell hue colour record at Site 1052.

The long-term eccentricity cycle within the raw data is indicated in figure 2.12. The ~400 kyr cycle results from the modulation by Venus and Jupiter of the Earth's precession and is the most invariable orbital period over geological time (Laskar, 1990; Berger *et al.*, 1992; Laskar, 1999). Precessional variations modify the amount of seasonal and annual insolation received at the Earth's surface. The effects are particularly strong in tropical and subtropical regions (Ruddiman *et al.*, 1989; Imbrie *et al.*, 1992). The strong power at the precessional period indicates that the colour record is primarily controlled by low-latitude changes in solar insolation. The variations in the colour record most probably represent fluctuations in the relative proportions of biogenic and lithic sediment components. These could derive from modifications in factors such as biogenic productivity, wind strength, weathering rates and runoff (see section 2.7). The strong precession period in the Munsell hue data suggests that the record here is primarily influenced by low and mid latitude variations in solar insolation.

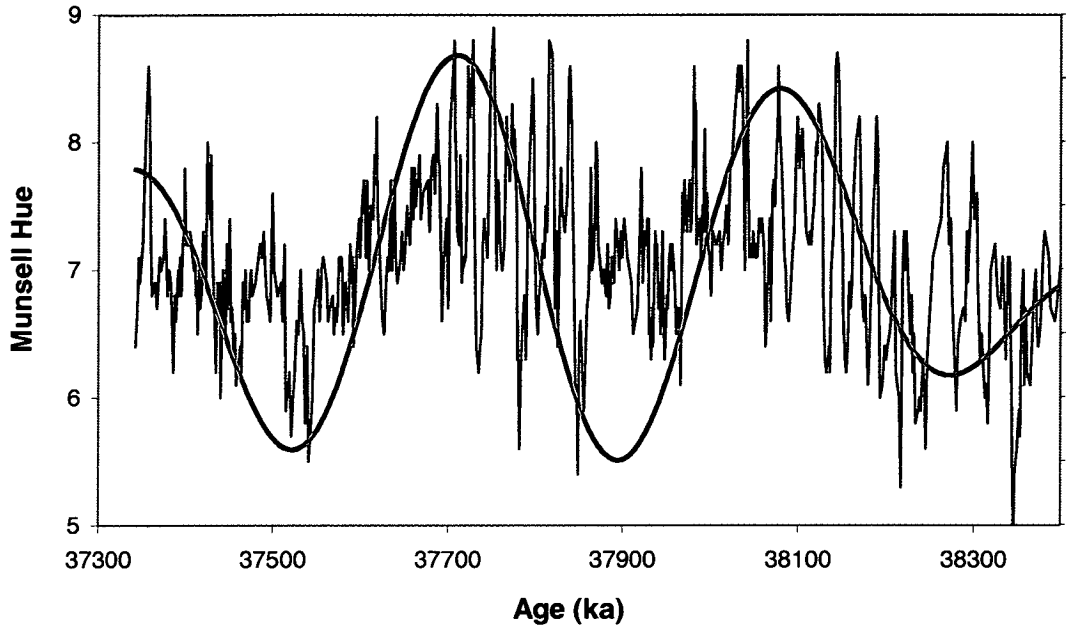

Figure 2.12. Munsell hue colour record at Site 1052 (raw data = blue line). Data has been filtered to indicate the long period eccentricity cycle (red line). Visually apparent in the colour record are precessional cycles and their amplitude modulation by the long-term eccentricity signal (~400 kyr).

To isolate the precessional period, a band-pass gaussian filter was applied to the Munsell hue colour record with a filter central frequency and bandwidth of 0.05 ± 0.02 respectively. Figure 2.13 shows the filtered Munsell hue record against the calculated precessional frequency of Berger (1978). Both the calculated precession and the filtered Munsell hue colour record clearly show the modulation of the precessional period by the long-term eccentricity cycle. The relationship between the calculated precession and the filtered Munsell hue record confirms that the time-scale of Pälike *et al.* (2001) is consistent with calculated orbital variations.

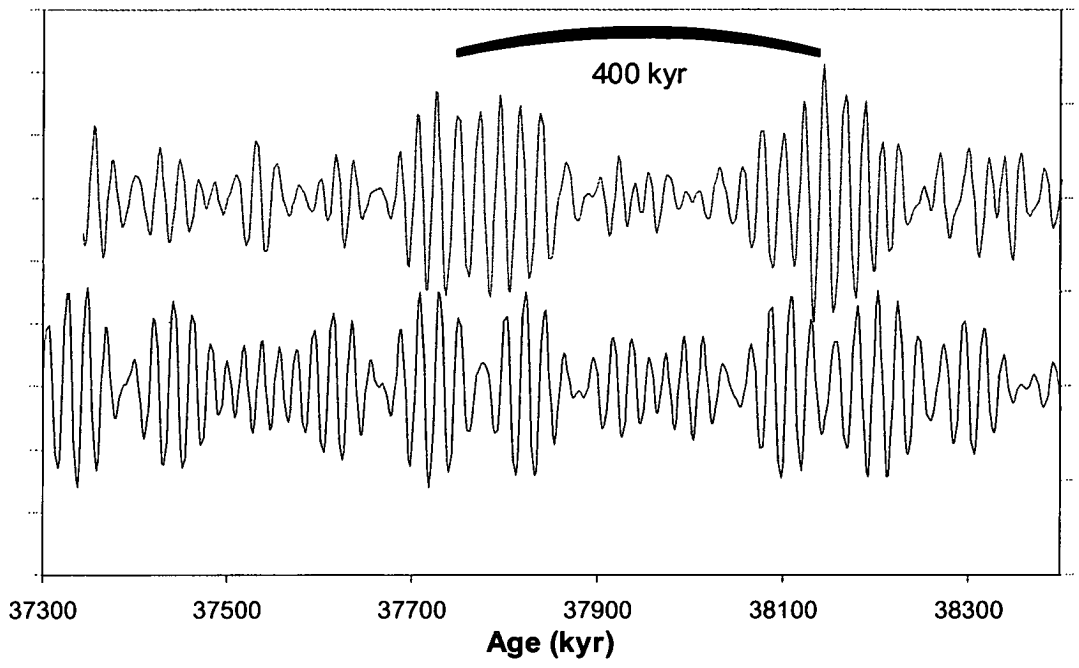

Figure 2.13. Filtered Munsell hue colour record (upper blue line) from Site 1052 and the calculated precessional frequency (lower red line) of Berger (1978).

2.7 Origin of the Munsell hue signal

The sediment properties at Site 1052 are clearly influenced by orbital frequencies. The relationship between the magnetic susceptibility and the Munsell hue record is demonstrated in figure 2.14, where positive magnetic susceptibility values are associated with increased Munsell hue (darker sediments). Magnetic susceptibility and sediment colour can be used as an indirect proxy for climatic – palaeoceanographic changes in terrigenous input and relative carbonate abundance. The increases in magnetic susceptibility are generally associated with darker coloration and increased Fe values, which can be inferred to reflect additional terrigenous input relative to carbonate content. Increases in the relative carbonate abundance is indicated by lower magnetic susceptibility, lighter sediments and decreased Fe. This is confirmed by Ca/Fe data from Pälike *et al.* (2001) over part of this interval.

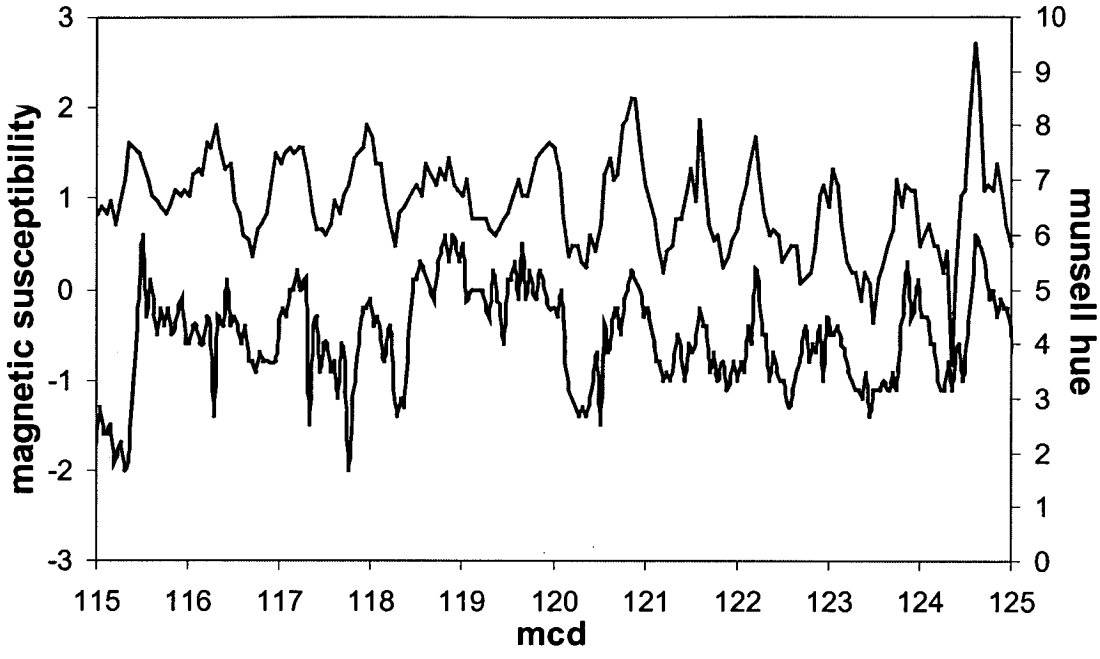

Figure 2.14. Magnetic susceptibility (10^{-5} SI) (lower line) and Munsell hue record (upper line) from 115 – 125 mcd at Site 1052. Strong cyclic oscillations at an interval of ~0.7 metres are present in both the Munsell hue colour record and the downhole log of magnetic susceptibility, reflecting precessional cycles.

The sediment cyclicity can be attributed to variations in terrestrial input and/or surface water productivity. There is also the possibility that cyclic dissolution by deep water caused periodic decreases in carbonate content. However, at a depth of only 1200 mbsl (Shipboard Scientific Party, 1998) dissolution cycles are less likely and the cyclicity is more developed in the shallower rather than deeper sites. The variability in the colour and magnetic susceptibility records are therefore consistent with alterations between terrigenous and carbonate rich horizons. These variations are ascribed to periodic alterations in the amount of terrigenous material supplied by atmospheric transport and/or runoff from the North American continent versus local carbonate productivity. The influence of precessional forcing was therefore clearly significant in controlling the relative fluxes of carbonate and clay at Blake Nose.

The results of all spectral analysis show that orbital forcing clearly propagates through the climatic system and that orbital forcing was an important short-term and long-term component of late middle Eocene climate change at Blake Nose.

Developing a tuned time-scale is critical for examining the timing and abruptness of palaeoceanographic and biological events and this can only be assessed by utilising a high-resolution record, such as that from ODP Leg 171B. Astronomical calibration of the time-scale is used to establish the timing of abrupt shifts in palaeoceanographic events in the Atlantic Ocean (chapter 4).

2.8 Summary

1) High-resolution physical property data from Site 1052 illustrate regular oscillations in Munsell hue and magnetic susceptibility.
2) Lithological oscillations have a precessional cyclicity, which is modulated by the long-term eccentricity cycle (~400 kyr).
3) Cyclicity in the colour and magnetic susceptibility records can be attributed to precessionally forced variations in wind blown terrigenous input or runoff from the North American continent versus surface water productivity.
4) Selected planktonic foraminiferal biostratigraphic events have been examined with a sampling resolution of 10 cm from Site 1052. The new and revised biostratigraphic datums of the middle Eocene have been orbitally calibrated to the astronomical time-scale of Pälike *et al.* (2001).

3. HIGH-RESOLUTION STABLE ISOTOPE VARIATIONS AT SITE 1052

3.1. Introduction

Whilst recent research has concentrated on understanding past greenhouse worlds, little is known about transitional climate dynamics and their stability. This thesis presents the first high-resolution planktonic foraminiferal stable isotope record in the late middle Eocene and provides a unique analysis of the palaeoceanographic changes and their possible origins. The ability to understand Eocene climate change has been previously hindered by sampling resolutions. The high-resolution record from Site 1052 enables the examination of high frequency climatic variability and accurate documentation of the timing and scale of relatively short-term climatic changes.

Site 1052 (29°57'N, 76°37'W) is the shallowest site of the depth transect and is located at a water depth of ~1345 m. This site comprises an expanded Eocene section consisting predominantly of a siliceous nannofossil ooze (Norris, Kroon *et al.*, 1998). High-resolution stable isotopic investigations ($\delta^{18}O$, $\delta^{13}C$) were conducted on late middle Eocene foraminifera from 75 to 135 mcd from a composite of Holes 1052B and 1052F. Samples have been analysed every 10 cm with an average sampling resolution of approximately 3,000 years. High frequency variability is seen in the colour reflectance data and magnetic susceptibility data (chapter 2), which are thought to be driven by Milankovitch scale climate oscillations. The aim of this work was to examine the stability of subtropical surface water conditions at a high temporal resolution in the Milankovitch frequency band. The effect of orbital forcing upon the late middle Eocene climate is explored in chapter 4. The results reveal large and abrupt shifts in $\delta^{18}O$ that are greater than those seen during the Pleistocene.

3.2. Methods and procedures

3.2.1. Sample preparation

For isotopic analyses, 20cc samples from a composite of Holes 1052B and 1052F were examined at 10 cm intervals. All samples were dried and wet sieved on a 63 μm mesh. For planktonic foraminiferal analyses the >63 μm fraction was dry sieved into three different size fractions: >355 μm, 250 - 355 μm and <250 μm. Isotopic measurements were conducted on planktonic foraminifera from the 250 - 355 μm size fraction. A narrow size fraction was selected to constrain vital and ontogenetic effects on stable isotopic interpretation (Shackleton *et al.*, 1985; Corfield and Cartlidge, 1991; Pearson *et al.*, 1993; Norris, 1998).

3.2.2. Isotopic examination

The applications and restrictions of stable isotopic analyses have been introduced in chapter 1. To generate a $\delta^{18}O$ record multiple species of mixed layer planktonic foraminifera are required. In this study stable isotopic measurements from the species *Morozovella crassata, M. spinulosa, Acarinina praetopilensis* and *Globigerinatheka mexicana* have been used. In addition to these species, measurements have been made from *Turborotalia cocoaensis*, *Subbotina utilisindex*, *Hantkenina alabamensis*, *Chiloguembelina cubensis*, bulk carbonate and the benthic foraminifer *Nuttalides truempyi* in selected intervals. A selection of species used in stable isotopic examination is shown in Plate 2.

Plate 2. Middle Eocene planktonic foraminifera used in isotopic investigation. All specimens are from the 250 – 355 μm size fraction. Scale bar represents 100 μm.

(a) *Morozovella crassata* umbilical view, from sample 171B, 1052B, 14H-4, 23 – 26 cm (121.30 mcd).

(b) *Morozovella crassata* spiral view, from sample 171B, 1052F, 11H-5, 33 – 36 cm (99.33 mcd).

(c) *Morozovella crassata* side view, from sample 171B, 1052B, 14H-4, 23 – 26 cm (121.30 mcd).

(d) *Morozovella spinulosa* umbilical view, from sample 171B, 1052F, 11H-5, 33 – 36 cm (99.33 mcd).

(e) and **(f)** *Globigerinatheka mexicana*, from sample 171B, 1052B, 10H-1, 83 – 86 cm (77.28 mcd).

(g) *Subbotina utilisindex* umbilical view, from sample 171B, 1052B, 11H-4, 103 – 106 cm (92.67 mcd).

(h) *Subbotina utilisindex* spiral view, from sample 171B, 1052B, 11H-4, 103 – 106 cm (92.67 mcd).

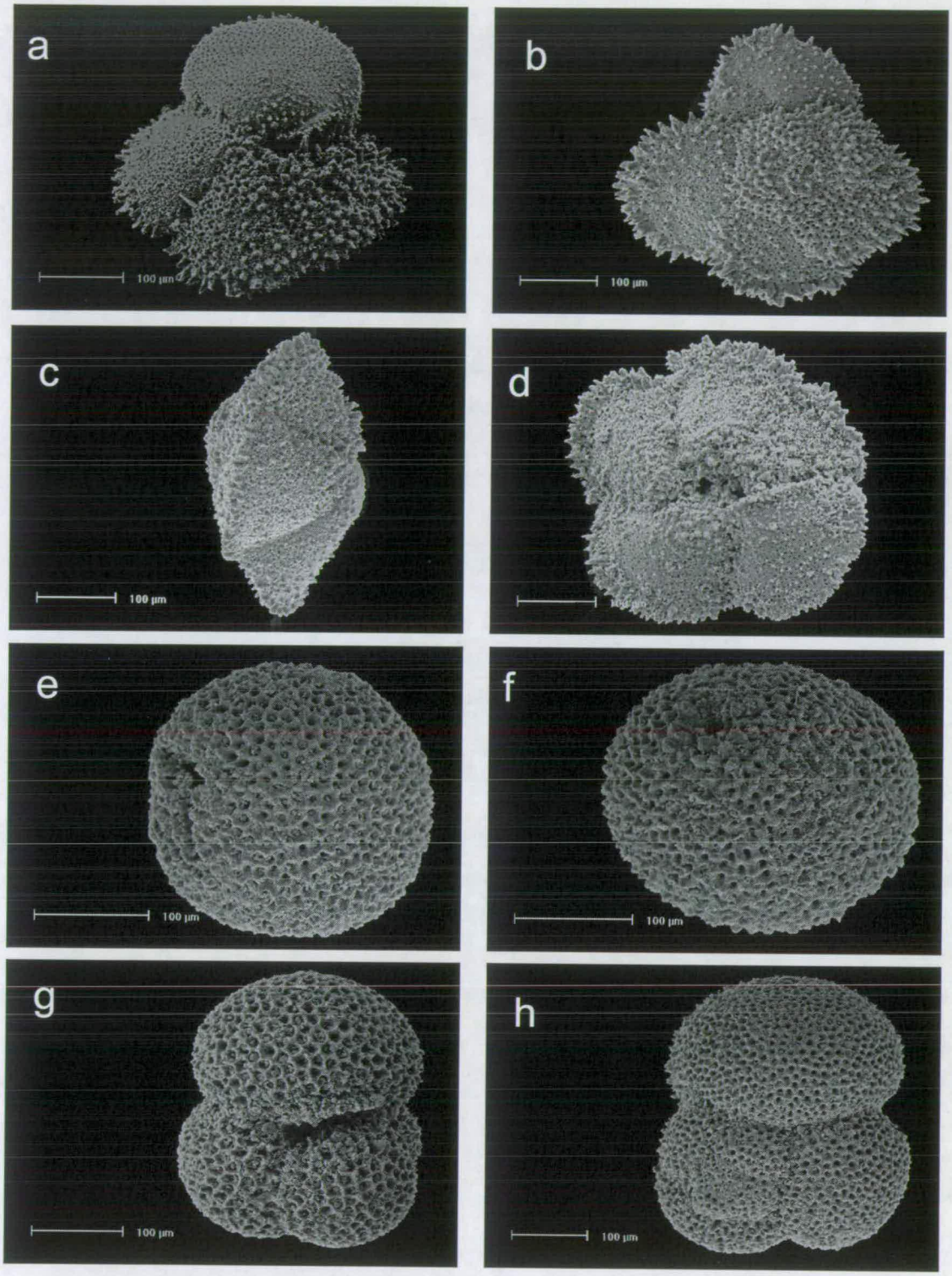
a
100 µm
b
100 µm
c
100 µm
d
e
100 µm
f
100 µm
g
100 µm
h
100 µm

For isotopic investigation between 2 and 23 monospecific tests of mixed layer planktonic foraminifera were picked for each sample studied. The analysis of multiple specimens provides results that are nearer to the species mean stable isotopic value than analyses conducted on singular specimens, however, using this method, data on intraspecific deviation is lost (Pearson and Shackleton, 1995). The species *M. crassata* was preferentially selected for analysis due to its surface dwelling habitat, ease of identification and abundance within the samples, although this species was not present in all samples. When *M. crassata* was unavailable, *M. spinulosa, A. praetopilensis* or *G. mexicana* were selected as alternatives due to their mixed layer habitat (Pearson *et al.*, 1993; Norris, 1998).

Sample weights were typically 0.17 ± 0.03 mg. Prior to analysis, specimens were sonicated in methanol to dislodge attached fine calcite particles. Ultrasonic cleaning was repeated when visual examination proved this to be required. All planktonic foraminiferal samples were analysed isotopically using a VG Isogas Prism III mass spectrometer at the University of Edinburgh, Scotland. Normal corrections were employed and results of stable isotope measurements are expressed in ‰ relative to the Pee Dee Belemnite (PDB) standard reference carbonate of zero (Craig, 1957). Silver Mine (SM) calcite powdered standard was measured concurrently (mean = 0.20 mg) to record analytical precision and instrument calibration. Replicate analyses of standards yields standard deviations of 0.09‰ for $\delta^{18}O$ and 0.05‰ for $\delta^{13}C$. In total 772 measurements were taken from Holes 1052B and 1052F (cores 10H-14H). All isotopic data are listed in Appendix 1. Low sample weights (<0.06 mg) commonly resulted in anomalous values for $\delta^{18}O$. These results were rejected from the data set. The criteria for data rejection are discussed in the Appendices.

3.2.3. Age model and sedimentation rates

The record at Site 1052 is the highest resolution record currently available for the late middle Eocene, with clearly defined cyclostratigraphic and magnetostratigraphic control. This study focuses on approximately 2.3 million years in the late middle Eocene, equivalent to planktonic foraminiferal biozones P14 and P15 and

magnetochrons C17n.2n to C18n. 2n. During this interval the sediment accumulation rate averages 34 m / m.y. This is moderately high for an open-ocean pelagic environment and is due to the high siliceous and calcareous plankton productivity. Sampling was at 10 cm intervals and therefore the time span between each sample is approximately 3, 000 years. Bioturbation will undoubtedly have smoothed the results to some extent. Each sample covers over 2 cms of core and therefore represents a period of approximately 600 years. However, the large cyclic fluctuations in the colour (chapter 2) and isotopic records (section 3.5) suggest that the smoothing effect of bioturbation is minimal. Mixed layer dwellers are identified to yield surface water temperatures at this subtropical site. Spectral analysis was conducted on the $\delta^{18}O$ and $\delta^{13}C$ records to obtain information on orbital cyclicity in the middle Eocene (chapter 4).

3.2.4. Planktonic foraminiferal assemblages

All of the samples analysed contained abundant planktonic foraminifera. The fauna present at Blake Nose, Site 1052 is distinctive of subtropical environments of the middle Eocene. The samples are typically characterised by *Morozovella spinulosa, M. crassata, Acarinina praetopilensis, Subbotina utilisindex, Globigerinatheka mexicana, Turborotalia cerroazulenis* and *Catapsydrax unicavus*, indicating planktonic foraminiferal Zones P14 and P15 (upper middle Eocene). A late middle Eocene age is also indicated by radiolarian assemblages characteristic of the *Podocyrtis geotheana* Zone (Zone R11) (Norris, Kroon *et al.*, 1998).

3.3. Foraminifera preservation

Foraminifer preservation is generally moderate to good under visual examination. Despite the shallow burial of middle Eocene sediments at Blake Nose, the preservation of planktonic foraminifera cannot be described as excellent. All specimens showed evidence of recrystallisation (e.g. Plate 3). Carbonate infilling was evident in some specimens, this usually consisted of amorphous calcite. Minor amounts of fine carbonate debris, mainly coccoliths, are seen attached to the test surfaces, however ultrasonic cleaning removed a large majority of this material.

Specimens have been examined under the scanning electron microscope (SEM) from intervals where both light (-1.9‰) and heavy (-0.5‰) results were recorded. These showed no obvious preservational differences (Plate 3). As diagenetic overprint may have affected some intervals, the recorded stable isotopic values (particularly those of oxygen) should not be considered as absolute. The effects of recrystallisation upon the stable isotopic results and reconstructed sea surface temperatures are discussed in chapter 5.

3.3.1. Size variations in the tests of Globigerinatheka mexicana.

For isotopic investigation between 77.18 and 91.97 mcd, 15 specimens of *G. mexicana* were picked and weighed per sample from the 250 – 355 μm size fraction. Large variations in the size and weight of *G. mexicana* occurred over time, with mean values ranging from 0.008 to 0.028 mg for individual specimens (figure 3.1). However, when test weight is compared with oxygen and carbon isotopic data (figure 3.2), these factors do not appear to be related. Test weight is therefore not obviously controlled by factors that influence $\delta^{18}O$ or $\delta^{13}C$ such as temperature, salinity, ice volume and productivity. Calcite infilling, recrystallisation or dissolution may also influence test weight. However, the variations in weight recorded here are thought to be a primary signal as visual examination suggested a direct correlation between test size and test weight. Even if this is a diagenetic signal, the absence of a relationship between test weight and isotopic variation (figure 3.2) indicates that the stable isotope results are robust, although the actual values should not be considered unequivocal.

Plate 3. Preservation of middle Eocene planktonic foraminifera at Blake Nose. Note changes in scale bar. Specimens on the left are all from samples where heavy oxygen isotope values were recorded (-0.5‰). Specimens on the right are all from intervals where light oxygen isotope values were recorded (around -1.9‰). Preservation of foraminifera is variable however, no obvious differences were identified between light and heavy $\delta^{18}O$ intervals.

(a) *Morozovella crassata* from sample 171B, 1052F, 12H-5, 53 – 56 cm (109.46 mcd). A large amount of calcite debris and coccoliths are seen attached to the test surface.

(b) Test surface of *M. crassata* from sample 171B, 1052B, 14H-4, 23 – 26 cm (121.30 mcd).

(c) Test surface of *M. spinulosa* from sample 171B, 1052F, 13H-2, 123 – 126 cm (115.16 mcd).

(d) Test surface of *M. spinulosa* from sample 171B, 1052B, 14H-4, 23 – 26 cm (121.30 mcd).

(e) Test surface of *M. crassata* from sample 171B, 1052F, 13H-2, 123 – 126 cm (115.60 mcd).

(f) Test surface of *M. crassata* from sample 171B, 1052B, 13H-4, 103 – 106 cm (113.10 mcd).

(g) *Acarinina praetopilensis* from sample 171B, 1052F, 12H-5, 53 – 56 cm (109.46 mcd).

(h) *Globigerinatheka semiinvoluta* from sample 171B, 1052B, 10H-5, 3 – 6 cm (82.48 mcd).

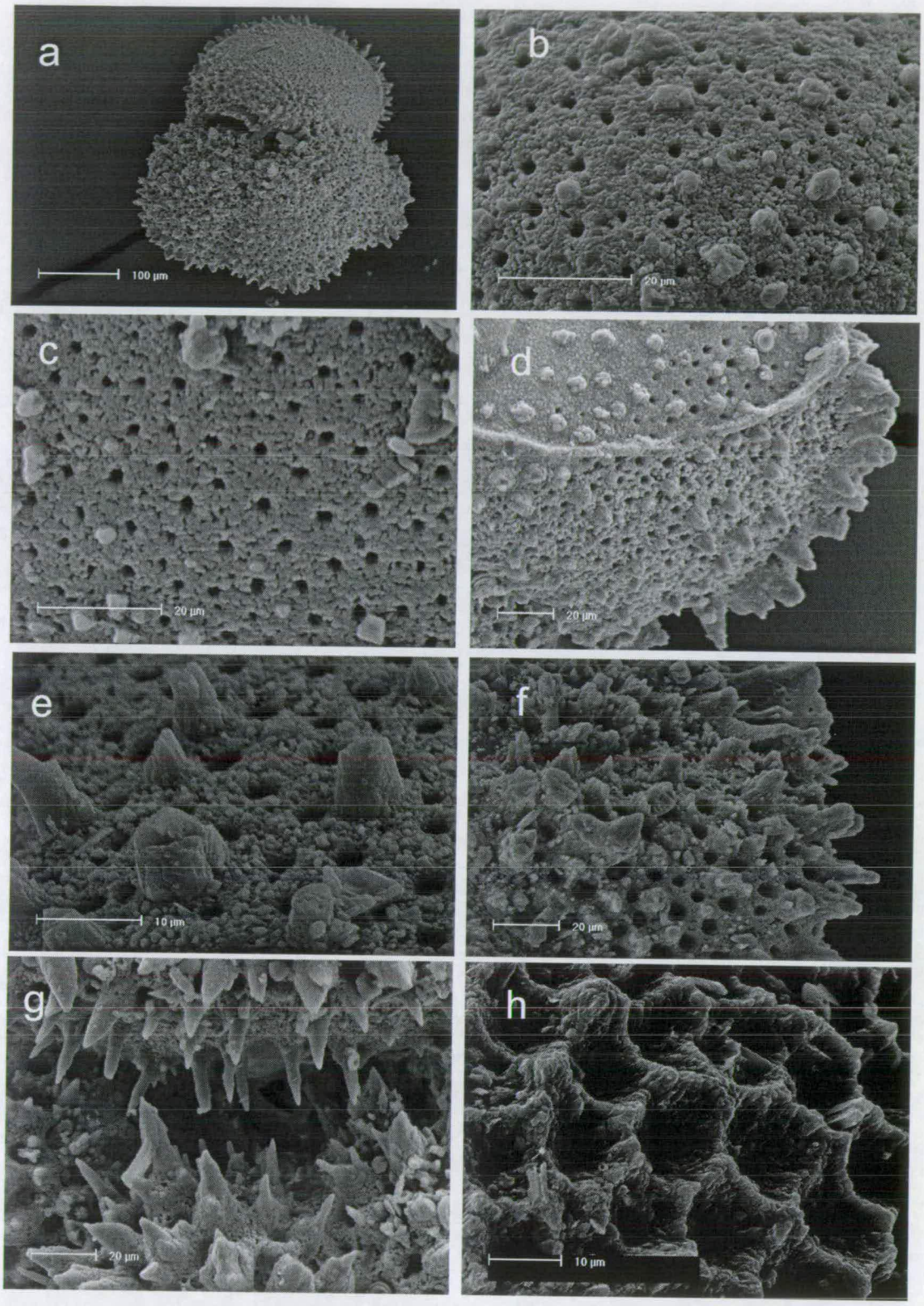
a
100 µm
b
20 µm
c
20 µm
d
20 µm
e
10 µm
f
20 µm
g
20 µm
h
10 µm

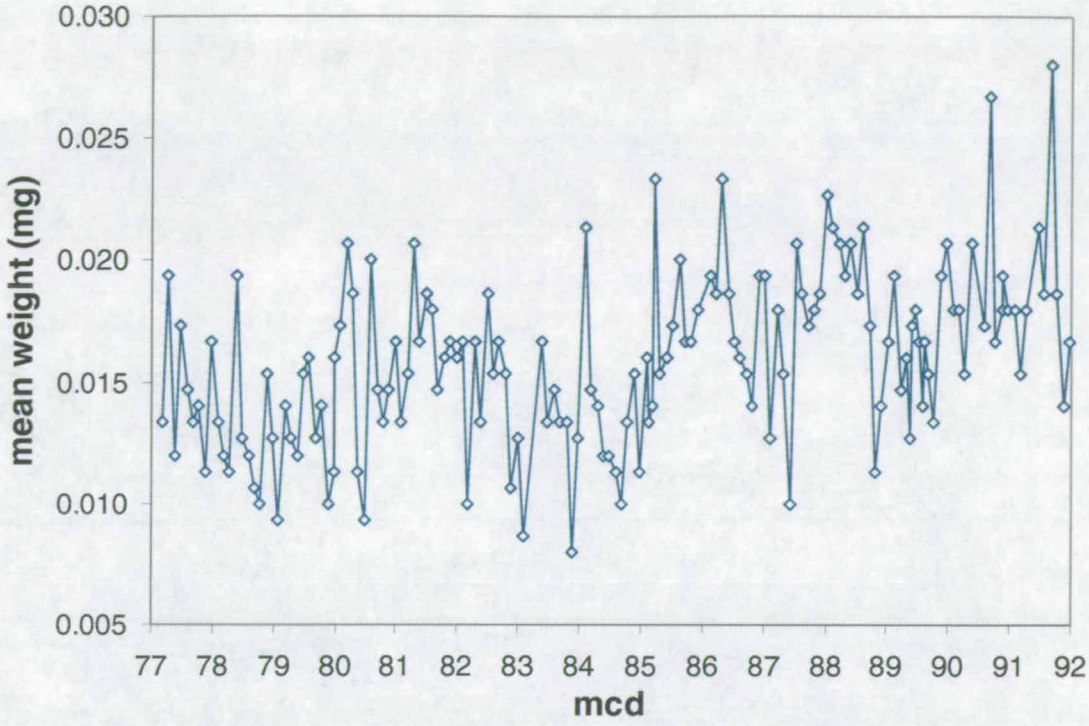

Figure 3.1. Weight variations in the tests of *Globigerinatheka mexicana*.

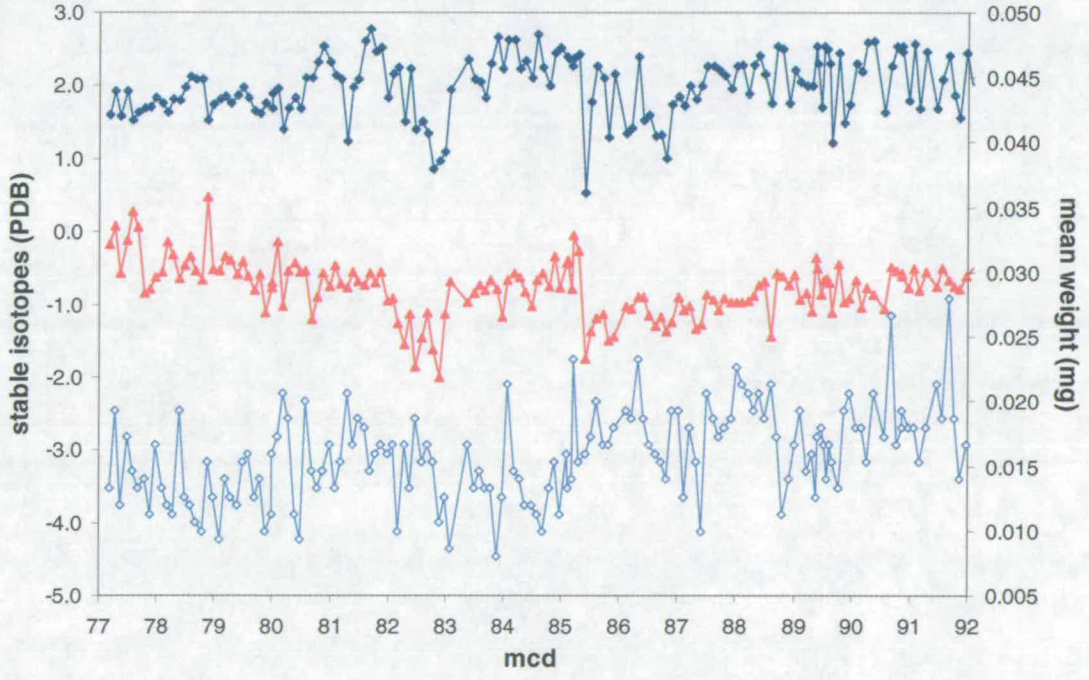

Figure 3.2. Stable isotope and weight variations of *G. mexicana*. ◇ = mean weight of 15 tests of *G. mexicana*; ♦ = carbon isotopes; ▲ = oxygen isotopes. The isotopic results are discussed in section 3.5.

3.4. Stable isotope results

All oxygen and carbon isotope results using various species from Site 1052 are shown against depth in figures 3.3 and 3.4 respectively. Offsets in $\delta^{18}O$ and $\delta^{13}C$ can be seen between species. These are attributed to interspecific variation such as depth habitat or season of reproduction. The implications of these offsets are explored here, prior to the reconstruction of a continuous time-series for both $\delta^{18}O$ and $\delta^{13}C$. The isotopic results are described in section 3.5.

3.4.1. Depth stratification of planktonic foraminifera

The depth of calcification is reflected in both the oxygen and carbon isotopic ratios of foraminiferal tests and is a well-established method in determining foraminiferal palaeoecology and depth habitat (e.g. Boersma and Premoli Silva, 1986; Pearson *et al.*, 1993; Pearson, 1998; Spero, 1998; Coxall *et al.*, 2000). Planktonic foraminifera inhabiting the uppermost mixed layer (surface dwellers) will have the most depleted $\delta^{18}O$ values as they encounter the warmest water temperatures (Emiliani, 1954). However, notable variations in modern surface water temperatures occur on an annual cycle, which result in seasonal variation in the oxygen isotope record of planktonic foraminifera (Erez and Honjo, 1981; Williams *et al.*, 1981). This is seen in the Sargasso Sea, where seasonal temperature variations result in $\delta^{18}O$ changes of approximately 1‰ in surface water foraminiferal calcite (Deuser *et al.*, 1981; Deuser, 1987; Deuser and Ross, 1989).

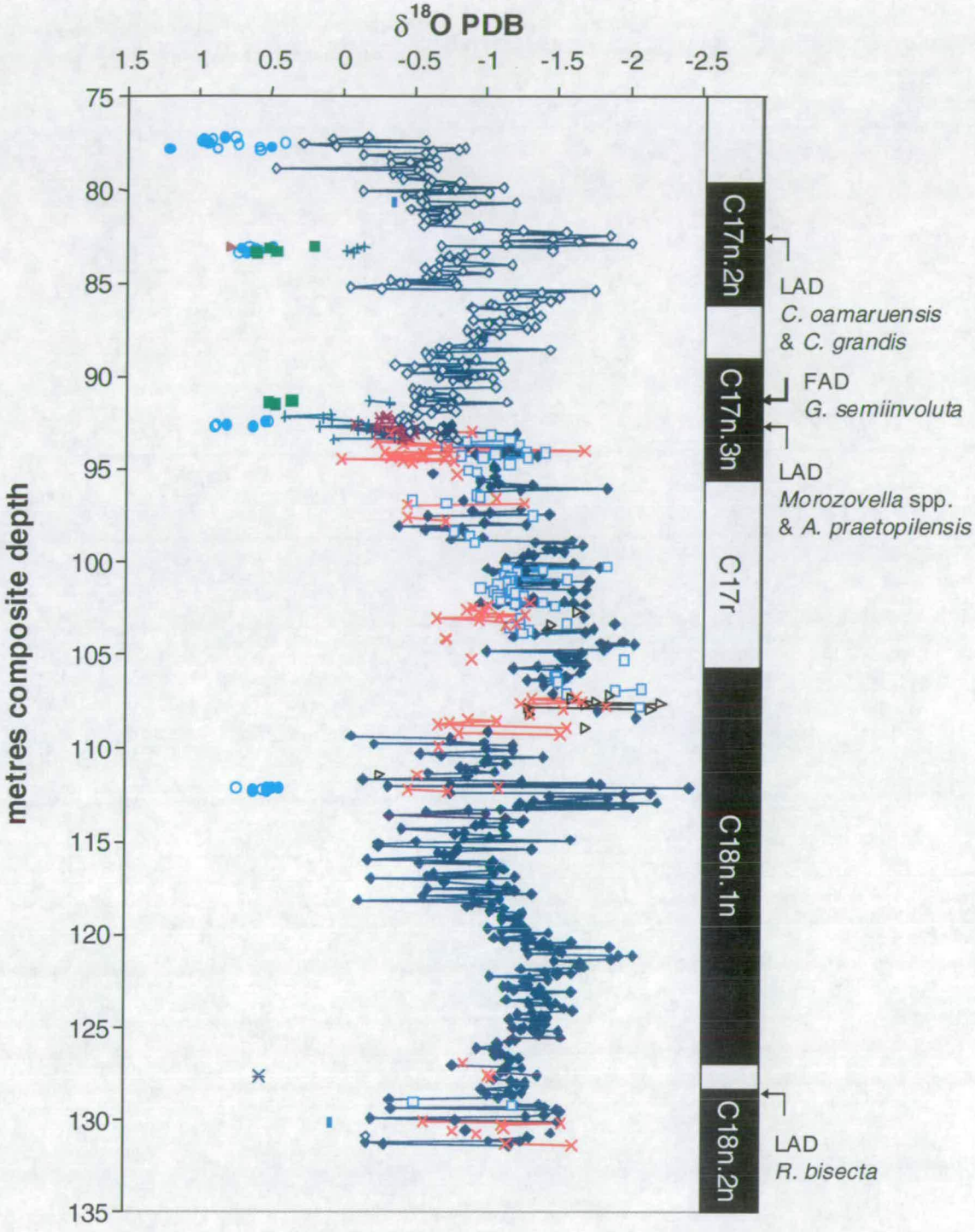

Figure 3.3. All oxygen isotope data from Site 1052. ♦ = *Morozovella crassata*; □ = *Morozovella spinulosa*; ▷ = *Morozovella* spp.; × = *Acarinina praetopilensis*; ✳ = *Turborotalia cocoaensis*; ◇ = *Globigerinatheka mexicana*; + = *Subbotina utilisindex*; ▬ = *Hantkenina alabamensis*; ○ and ● = Bulk carbonate; ✳ = *Chiloguembelina cubensis*; ■ = *Nuttalides truempyi*; ▶ = mixed benthic species.

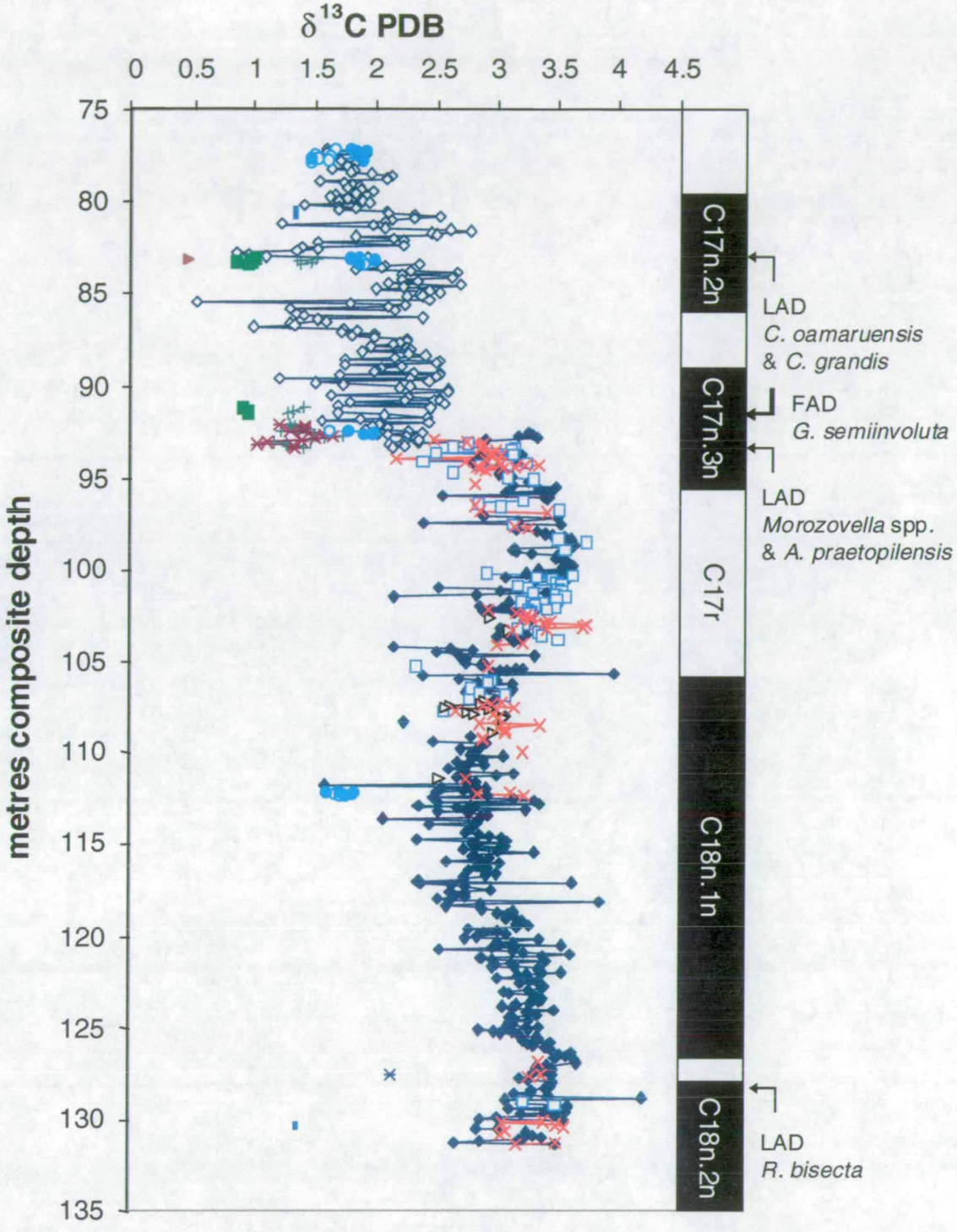

Figure 3.4. All carbon isotope data from Site 1052. ♦ = *Morozovella crassata*; □ = *Morozovella spinulosa*; ▷ = *Morozovella* spp.; × = *Acarinina praetopilensis*; ✳ = *Turborotalia cocoaensis*; ◇ = *Globigerinatheka mexicana*; + = *Subbotina utilisindex*; ▬ = *Hantkenina alabamensis*; ○ and ● = Bulk carbonate; ✳ = *Chiloguembelina cubensis*; ■ = *Nuttalides truempyi*; ▶ = mixed benthic species.

Independent evidence for planktonic foraminiferal palaeodepth habitat relative to other planktonic species can be derived from their characteristic carbon isotope value. Surface waters are enriched in $\delta^{13}C$ by the preferential extraction of ^{12}C by algal productivity. The sinking of isotopically depleted organic carbon through the water column from the ocean surface to depth causes sea surface bicarbonate to be enriched in ^{13}C relative to ^{12}C. This declines quickly with depth and hence a gradient in $\delta^{13}C$ from surface to deep waters is established (Kroopnick, 1974, 1985). Carbon isotopic values of near-surface dwelling planktonic foraminifera should consequently be more enriched than those living in deeper depths. Therefore the heaviest $\delta^{13}C$ and lightest $\delta^{18}O$ values should be recorded by foraminifera living in the uppermost mixed layer. Other factors can also affect surface water oxygen and carbon isotopic values, including primary productivity, strength and depth of the thermocline, freshwater input and light penetration (Pearson *et al.*, 1993).

3.4.2. Intertaxa variation

Oxygen and carbon isotopic results are plotted for all species analysed in figure 3.5. This shows results similar to those of previous studies of these genera (e.g. Boersma and Premoli Silva, 1986; Boersma *et al.*, 1987; Pearson *et al.*, 1993). Photosymbionts preferentially uptake ^{12}C and therefore photosymbiotic species theoretically have a more positive $\delta^{13}C$ signal than asymbiotic taxa (Spero *et al.*, 1991). Lighter $\delta^{18}O$ and heavier $\delta^{13}C$ are displayed by the taxa *Morozovella* and *Acarinina* in comparison with other species, supporting their mixed layer symbiotic habitat.

A greater degree of variability is seen in the mixed layer group than the thermocline group (figure 3.5). Seasonal variations in SST or habitat depth are probably responsible for small differences in oxygen isotope values between co-existing taxa. This is comparable with previous work (e.g. Pearson *et al.*, 1993) and is probably due to seasonal temperature variations that affect the surface, but not the deep waters. There are also a greater amount of analyses in the mixed layer dwellers compared to thermocline dwellers, allowing a greater range of values to be recorded.

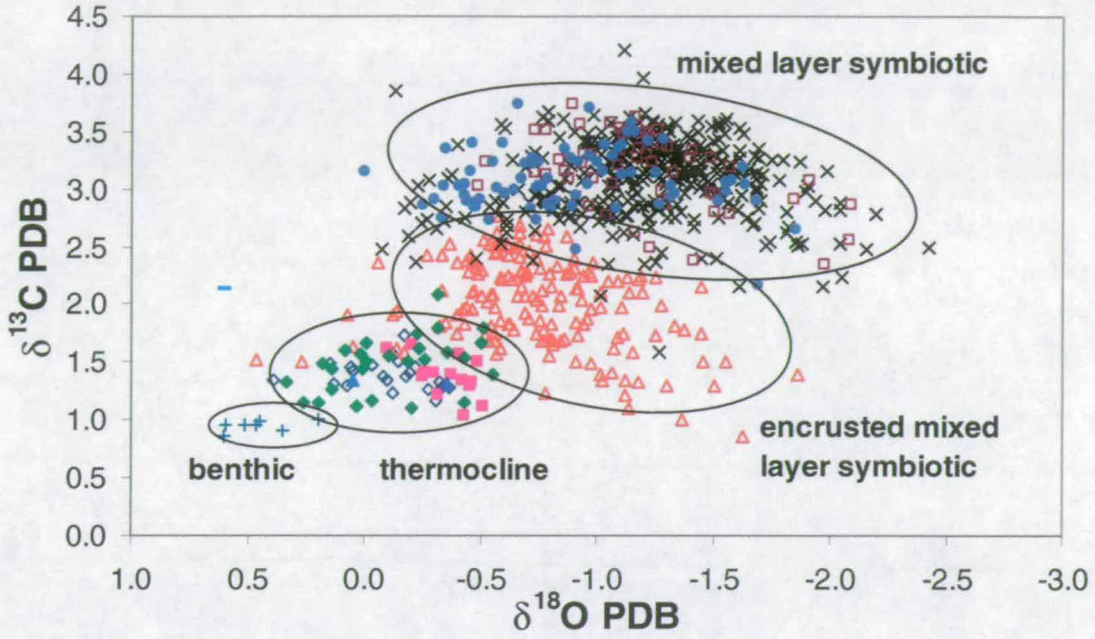

Figure 3.5. Oxygen vs. carbon isotopic results for all data at Site 1052. × = *Morozovella crassata*; □ = *Morozovella spinulosa*; ● = *Acarinina praetopilensis*; △= *Globigerinatheka mexicana*; ◇ = *Subbotina utilisindex*; ♦ = *Catapsydrax unicavus*; ■ = *Turborotalia cocoaensis*; ▲= *Hantkenina alabamensis*; + = *Nuttalides truempyi*; − = *Chiloguembelina cubensis*. All isotopic data from Site 1052 except *Catapsydrax unicavus* data from Site 1051 hole A.

3.5. The construction of a continuous time series of $\delta^{18}O$ and $\delta^{13}C$

To reconstruct sea surface temperatures and examine periodicities within the isotopic data, a composite time series of planktonic foraminifera oxygen and carbon isotope values is required. This calls for the oxygen and carbon isotopic results to be corrected to uniform mixed layer values. The isotopic values of *G. mexicana* and *A. praetopilensis* are offset from those of *Morozovella* species due to habitat preferences and/or vital effects (figures 3.3, 3.4 and 3.5). These results are similar to previous works (e.g. Boersma *et al.*, 1987; Pearson *et al.*, 1993), where acarininids record $\delta^{18}O$ values heavier than those of *Morozovella*. The isotopic values were therefore corrected for these species to provide a continuous mixed layer planktonic

foraminifera record for palaeo SSTs to be reconstructed. Correction values were calculated from the mean isotopic difference between species within the same samples. Correction factors of -0.28‰ and -0.50‰ were applied to oxygen isotope values of *G. mexicana* and *A. praetopilensis* respectively based on deviations from the mean values of *Morozovella* spp. For carbon isotopic values a correction factor of +0.77‰ was applied to *G. mexicana*. No correction factor was applied to the carbon isotopic values of *A. praetopilensis,* as these did not significantly deviate from *Morozovella* spp.

This method for reconstructing surface water conditions is the most appropriate in this case. Ideally, the same planktonic foraminiferal species would be analysed throughout, although this is rarely possible due to changes in species abundance and evolution. The correction factors applied here are first order approximations, as the offsets probably deviate both spatially and temporally. However, the correction factors are unlikely to change the conclusions drawn from the data. Figures 3.6 and 3.7 show the composite planktonic foraminifera $\delta^{18}O$ and $\delta^{13}C$ record for Site 1052. Both the oxygen and carbon isotopic results are shown in figure 3.8. The continuous and corrected stable isotopic data are tabulated in Appendix 2.

3.5.1. The composite oxygen isotope record

Large and rapid shifts are recorded in the surface dwelling planktonic foraminifera oxygen isotope record (figure 3.6). Between 129 and 132 mcd $\delta^{18}O$ values fluctuate between -1.65‰ and -0.20‰. Similar values are recorded between 113 and 118 mcd and between 109 and 112 mcd. In the interval between 118 and 129 mcd, oxygen isotope values vary between -0.79‰ and -1.94‰. Although this is a 1.15‰ variance, the $\delta^{18}O$ values are commonly less variable than those seen in other parts of the record. There is a steady decrease in values from 128 to 121 mcd, followed by a rise between 120 and 118 mcd. For a short interval, between 113 and 112 mcd $\delta^{18}O$ values decrease rapidly from -0.60‰ to -2.42‰. This shift of almost 2‰ occurs in a stepwise fashion, before crashing to values of -0.17‰ at 111.7 mcd. From 108 to 92 mcd $\delta^{18}O$ values increase from -2.23‰ to -0.43‰. From 92 to 85 mcd $\delta^{18}O$ values

decline from -0.71 to -2.03‰. There is then a sharp increase at 85 mcd from -2.03‰ to –0.33‰. Above 85 mcd oxygen isotope values become lighter to a maximum of -2.28‰ at 83 mcd. Oxygen isotope values then become heavier at the top of the measured interval with maximum values of 0.18‰ at 79 mcd.

3.5.2. The composite carbon isotope record

Like the oxygen isotope record, the $\delta^{13}C$ record at Site 1052 reveals pronounced variation between 1.3‰ and 4.0‰ (figure 3.7). There is a general decrease in $\delta^{13}C$ from 3.5‰ at the base of the analysed section at 130 mcd, to 2.8‰ at 113.5 mcd. Carbon isotope values then increase to 3.7‰ at 98.5 mcd. After 98.5 mcd, $\delta^{13}C$ values fall once more to approximately 2.8‰ at 92 mcd. From 92 to 77 mcd $\delta^{13}C$ values fluctuate between 3.55‰ and 1.3‰. The carbon isotope record appears to have a long-term cycle, where values go from highs at 128 mcd and 98 mcd with a low at 112 mcd.

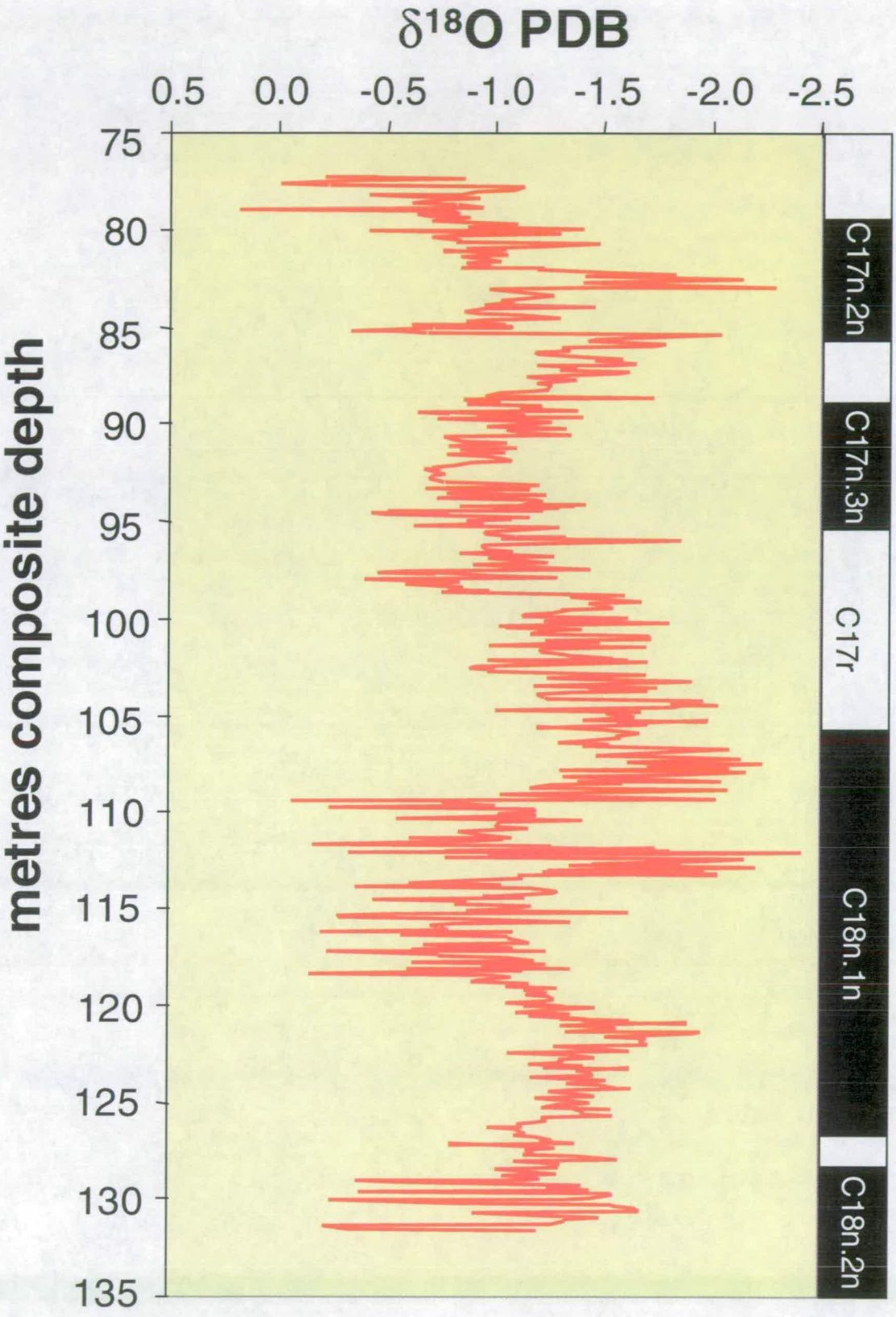

Figure 3.6. Composite oxygen isotope record at Site 1052

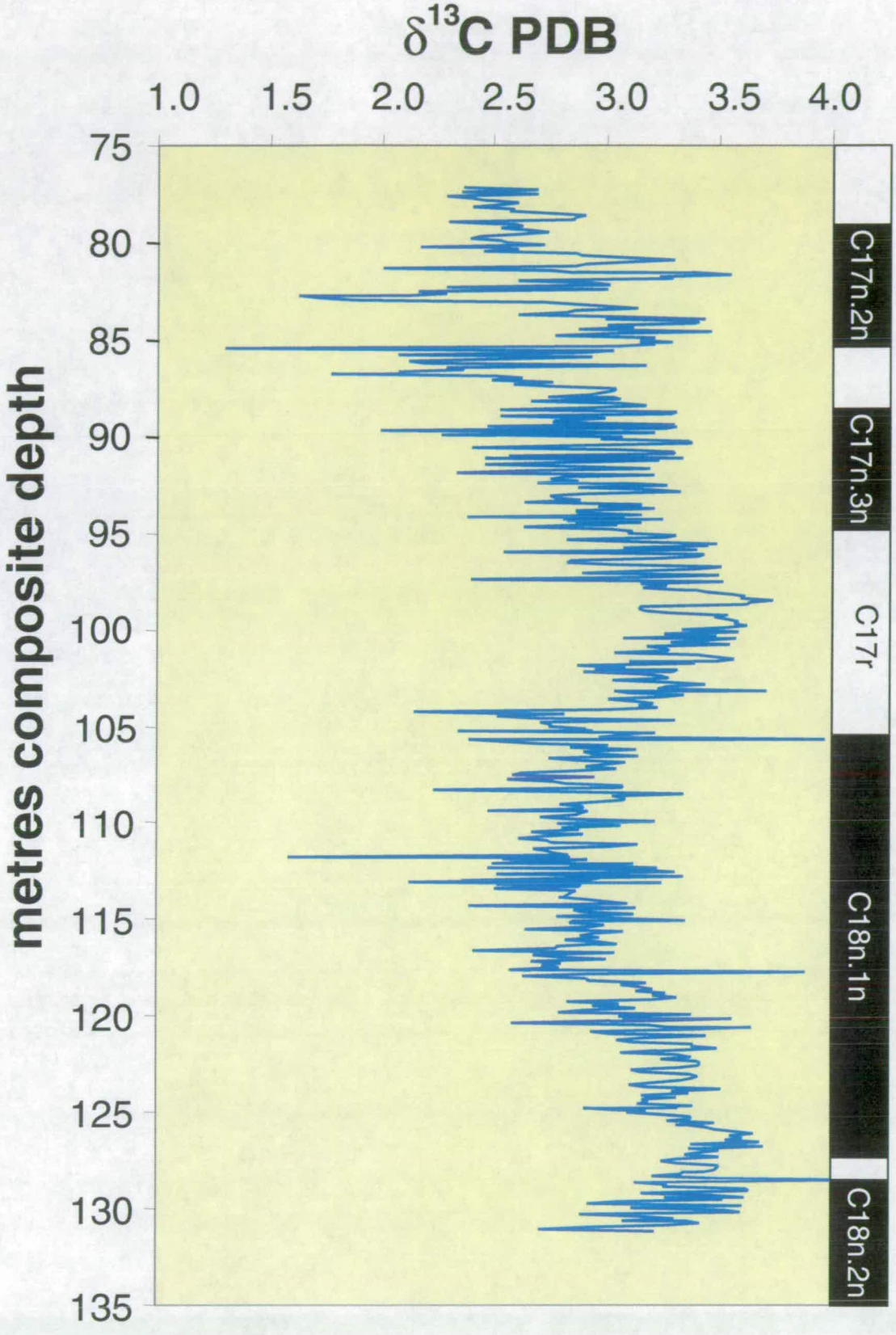

Figure 3.7. Composite carbon isotope record from Site 1052

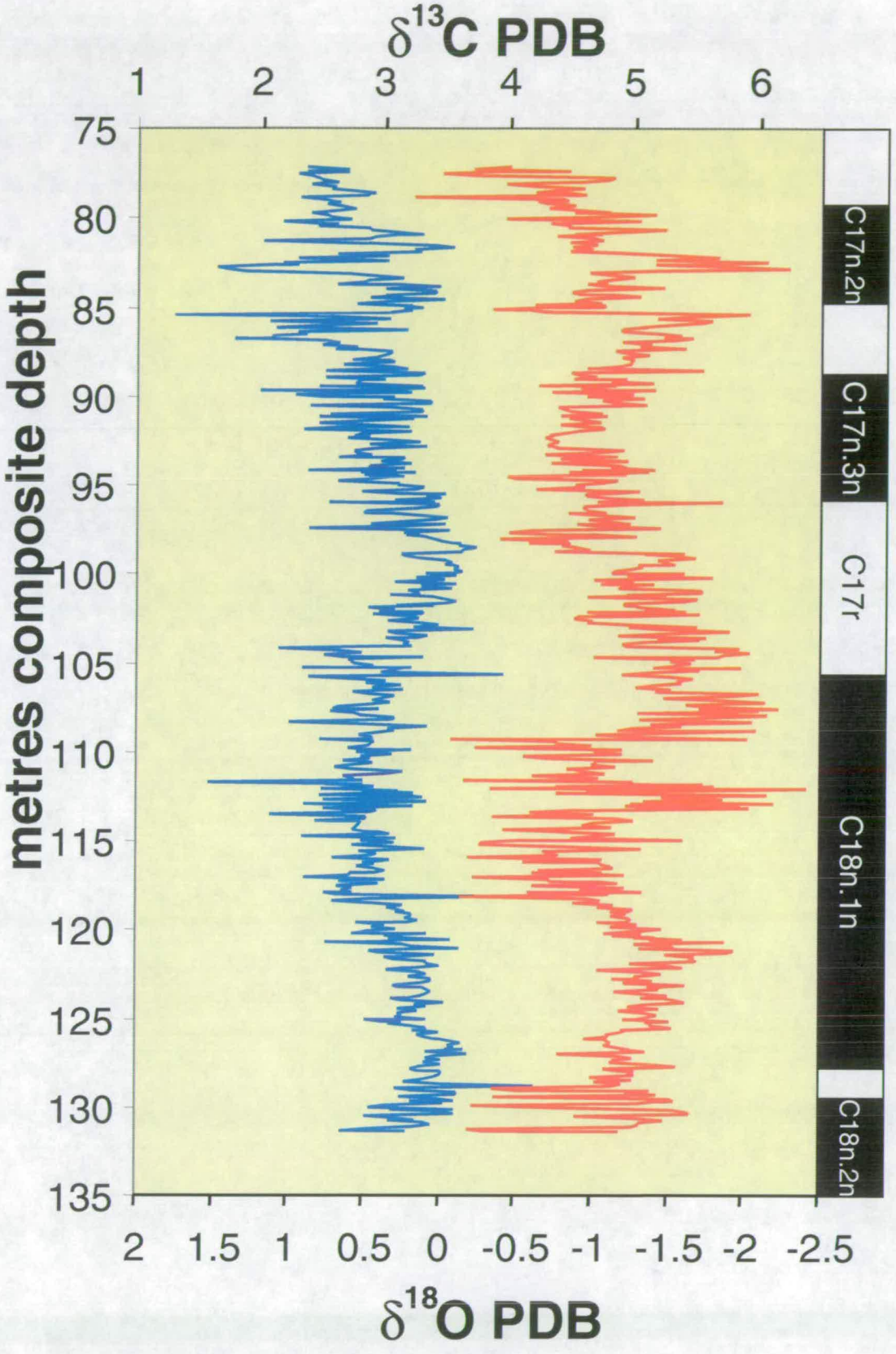

Figure 3.8. Oxygen and carbon isotopic results at Site 1052 against metres composite depth

3.6. High amplitude and abrupt isotopic shifts

The planktonic foraminiferal isotope record at Site 1052 represents the highest resolution study of the middle Eocene and therefore provides a new understanding of climate dynamics during this transitional climate interval. The record shows outstanding and rapid oscillations in mixed layer planktonic foraminifera $\delta^{18}O$ and $\delta^{13}C$ between +0.2 and –2.4‰ and 4.0 and 1.3‰ respectively (figure 3.8), at a time interval when climate was previously accepted to be relatively stable. The isotopic results from Blake Nose reveal substantial shifts in planktonic foraminifera $\delta^{18}O$, which are commonly greater than 1‰ PDB (figure 3.6). This is particularly evident at 85 and 112 mcd when $\delta^{18}O$ values shift from less than -1.5‰ to 0.0‰. This magnitude of variation is greater than shifts during the glacial / interglacial events of the Pleistocene (e.g. Berger and Gardner, 1975; Chapell and Shackleton, 1986; Fairbanks, 1989). Large and abrupt variations are also seen in the $\delta^{13}C$ record from Blake Nose (figure 3.7). These fluctuations are particularly apparent in the record from 80 to 90 mcd when shifts of >1‰ are recorded. The large and abrupt stable isotope variations suggest that unstable climatic conditions prevailed in the western North Atlantic during the middle Eocene.

3.7. Long-term trends in the isotope records

Long-term trends are also evident in the isotopic records with periodically heavy $\delta^{18}O$ values recorded at 130, 116, 109, 93 and 77 mcd. Cyclic variation is also seen in the carbon isotope record with heavy $\delta^{13}C$ values recorded at 130 mcd and again at 100 mcd (figure 3.7). These trends may reflect orbital variability. Whilst both the $\delta^{18}O$ and $\delta^{13}C$ indicate high amplitude variability, the long-term trends in the isotopic data do not closely covary (figure 3.8). The periodicity of the cycle length appears to be longer in the $\delta^{13}C$ record. The relationship and periodicity of this apparent cyclicity is discussed in chapter 4.

3.8. Comparison with other records

The main focus for this study was to reconstruct surface water conditions by utilising moderately well preserved calcareous microfossils at ODP Site 1052. Despite observing only ~2 million years of sediment history during the late middle Eocene, the high-resolution study of Site 1052 reveals many significant attributes which were not determined in low-resolution studies and presents a significant new understanding of subtropical palaeoceanography in the western North Atlantic.

The short-term, high amplitude (~1‰) variability in planktonic foraminifera $\delta^{18}O$ and $\delta^{13}C$ values at Blake Nose (figure 3.8) are remarkable and have not been seen elsewhere. Several reasons may account for this; the record here is at a much higher resolution than in many other Eocene studies, with approximately 2, 000 to 4, 000 years between data points, allowing the high amplitude oscillations at this site to be documented. There may also be large changes in the oceanography at Blake Nose such as upwelling, productivity or salinity changes which may also account for the greater $\delta^{18}O$ and $\delta^{13}C$ variability at this locality compared to previous studies.

Whilst the large amplitude fluctuations have not previously been recorded, the mean carbon isotopic values recorded are typical of planktonic foraminifera bearing algal symbionts and inhabiting surface waters. These values compare well with previous studies of the Eocene (e.g. Keigwin and Corliss, 1986; Boersma *et al.*, 1987; Pearson *et al.*, 1993; Bralower *et al.*, 1995). The oxygen isotope results recorded here are periodically far lighter than those recorded in earlier investigations. Typical $\delta^{18}O$ values from the middle Eocene are -0.5‰ PDB (e.g. Keigwin and Corliss, 1986; Boersma *et al.*, 1987; Zachos *et al.*, 1994; Bralower *et al.*, 1995; Coxall *et al.*, 2000). Oxygen isotopic results less than –1.5‰ are lighter than those recorded in the early Eocene tropics (Bralower *et al.*, 1995). The mean oxygen isotope values recorded here are thus 0.6‰ to 1.4‰ lighter than other studies. There are several possible reasons why these values are not recorded in other studies of the late middle Eocene. A first explanation is that previous low-resolution investigations missed the negative

$\delta^{18}O$ shifts recorded in this study. By virtue of sampling the record at a resolution of less than 4, 000 years between data points, I have identified short-term events in the isotopic record. Previous studies (e.g. Keigwin and Corliss, 1986; Bralower *et al.*, 1995) may have been aliased with average sampling spacing of approximately 175, 000 years or greater, sufficient to document the long-term trends but not the short-term fluctuations. A second explanation is that recrystallisation or dissolution caused a more serious preservational effect in previous studies. This could potentially bias planktonic $\delta^{18}O$ estimates towards heavier oxygen isotope values (Paull *et al.*, 1988; Wu *et al.*, 1990). A third explanation is that the palaeoceanography of Blake Nose is in some way unique and perhaps the results here do not reflect temperature effects, but instead decreases in surface water salinity that gave rise to isotopically light $\delta^{18}O$ values.

3.9. Summary

The examination of planktonic foraminifer stable isotopes at an orbital scale (~3 kyr) sampling resolution allows climatic dynamics in the late middle Eocene to be examined in much greater detail than in previous studies. Milankovitch cyclicity within the planktonic foraminifera isotopic records is discussed in chapter 4. Reconstructed sea surface temperatures and the implications of these large isotopic variations are presented in chapter 5 and 7 respectively.

1) High-resolution stable isotopic investigations ($\delta^{18}O$, $\delta^{13}C$) were conducted on late middle Eocene foraminifera to examine the stability of subtropical surface waters at a high temporal resolution.
2) Isotopic results record variations of –2.4 to +0.2‰ in $\delta^{18}O$ and 1.3 to 4.0‰ in $\delta^{13}C$. These shifts in $\delta^{18}O$ are abrupt and are greater than those seen during the Pleistocene.
3) The $\delta^{18}O$ results are periodically lighter than those recorded in previous studies of the middle Eocene.
4) Long-term trends can be identified in both the oxygen and carbon isotope records that may reflect orbital cycles.

4. ORBITALLY FORCED MIDDLE EOCENE CLIMATE OSCILLATIONS

Previous work and the application of astronomical time-series have been discussed in chapter 2. The tuned chronology and the high-resolution (~3 kyr) stable isotopic records at Blake Nose provide the opportunity to identify the full suite of orbital climate signatures and allow the influence of Milankovitch cyclicity on surface water characteristics to be identified. The composite planktonic foraminifera stable isotope data set (chapter 3) is here plotted versus the tuned chronology of Pälike *et al.* (2001), discussed in chapter 2 (figures 4.1 and 4.2). This enables the pace and timing of the $\delta^{18}O$ and $\delta^{13}C$ events to be determined and high temporal climate fluctuations within the Milankovitch frequency band to be investigated. Here the effects of orbital forcing upon Eocene climate are examined with the aim of understanding the character of transitional Eocene palaeoceanography. The composite isotopic data is tabulated against time in Appendix 2.

4.1. Spectral analysis on middle Eocene stable isotopic time-series

The visually apparent cycles (see section 3.7) suggest that orbital periodicities are recorded in the stable isotopic time series. Spectral analyses were conducted on the composite planktonic foraminifera stable isotopic record from Site 1052 using the Blackman-Tukey method (*Analyseries* software) to determine the frequency of both the short- and long-term oscillations. To enhance the visual cyclicity, frequencies at 21, 41, 100 and 400 kyr were isolated in the composite isotopic records by applying band-pass gaussian filters. Filter central frequencies and bandwidths were 0.05 ± 0.02, 0.0244 ± 0.01, 0.01 ± 0.004, and 0.0025 ± 0.001 respectively.

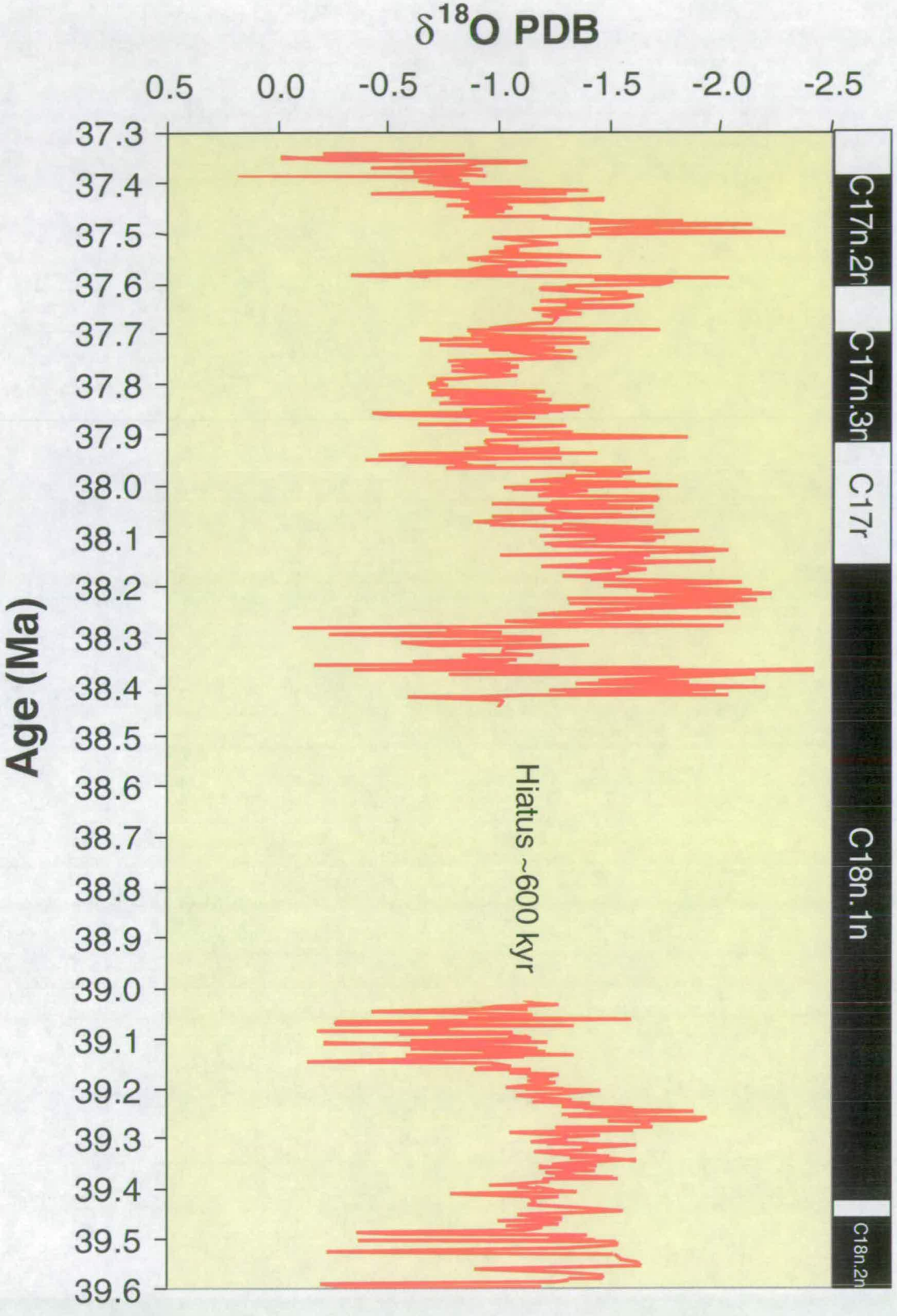

Figure 4.1. Composite oxygen isotope record at Site 1052 plotted against the astronomical time-scale.

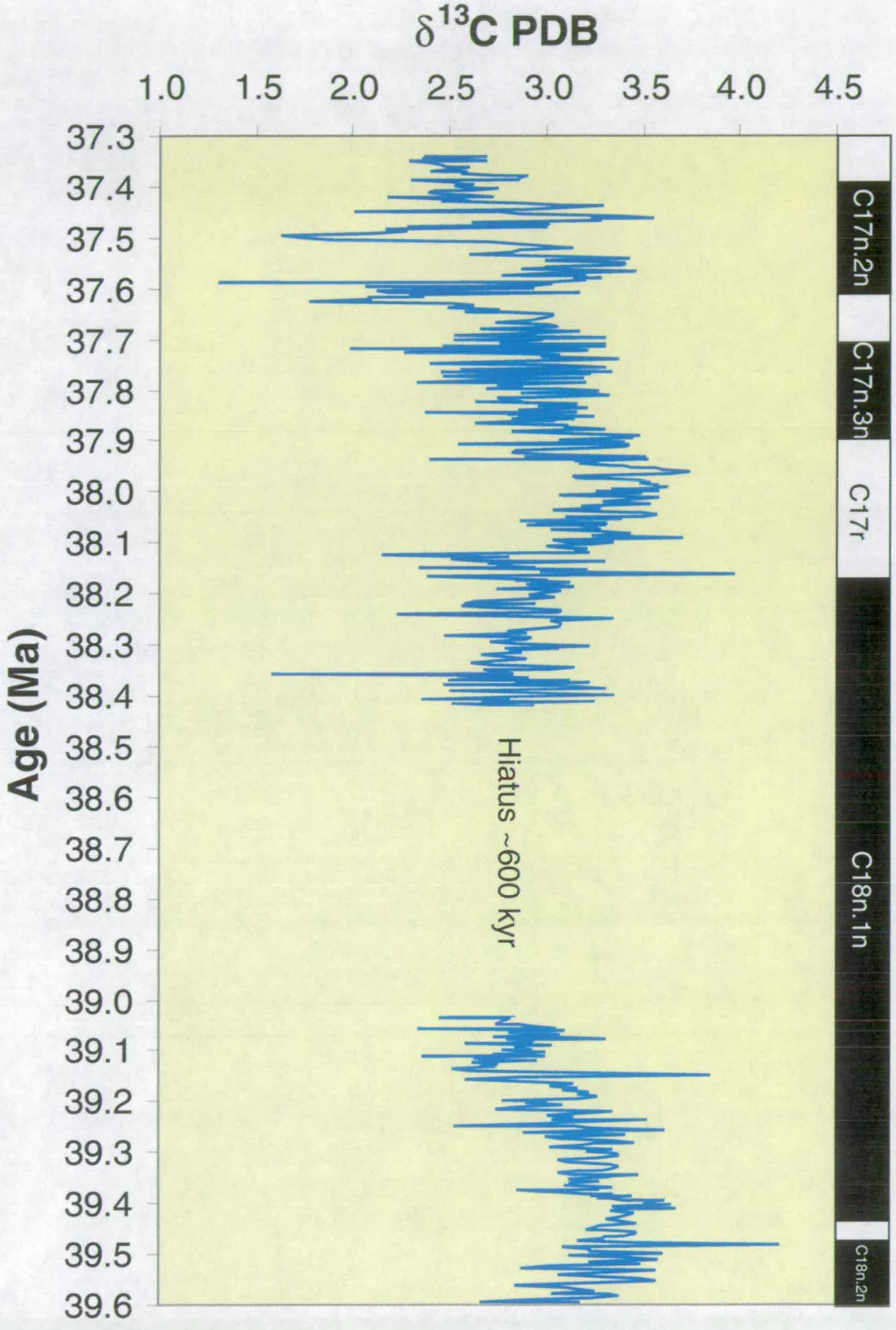

Figure 4.2. Composite carbon isotope record at Site 1052 plotted against the astronomical time-scale.

4.2. Modulation of surface waters by the eccentricity cycle (400 and 100 kyr)

4.2.1. Eccentricity forced variations in $\delta^{18}O$

The oxygen isotope record displays long-term trends and high-frequency variability that are thought to be influenced by orbital forcing. When examining the oxygen isotope record (figure 4.1) it can be seen that heavy $\delta^{18}O$ values are periodically recorded at 39.5, 39.1, 38.3, 37.8 and 37.4 Ma. All these intervals are ~400 kyr apart (accounting for the hiatus) suggesting that the long-term trends in the oxygen isotope record have a strong long-term eccentricity influence. This is shown in figure 4.3, where the data was filtered to reveal the 400 kyr eccentricity cycle.

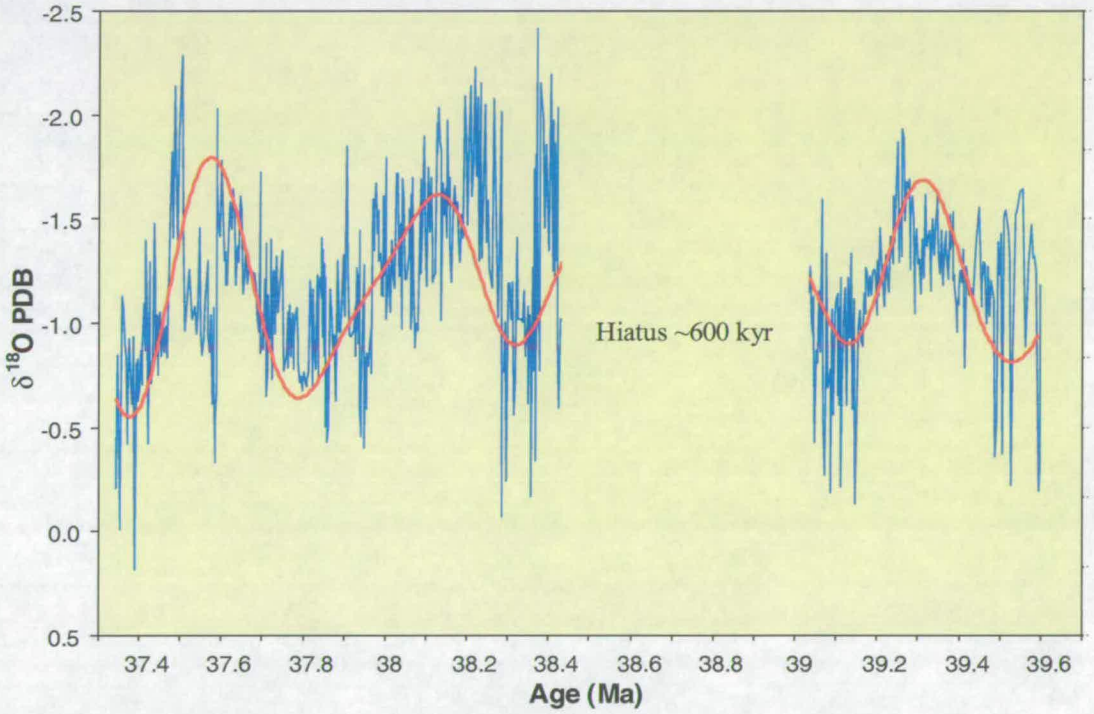

Figure 4.3. Oxygen isotope record at Site 1052 (blue line) against the astronomical time-scale. Data has been filtered to reveal the long-term eccentricity cycle (400 kyr) (red line).

Spectral analysis of the middle Eocene $\delta^{18}O$ record (figure 4.4) confirms the presence of a notable ~400 kyr periodicity and reveals strong power at 0.00235 cycles per kyr, corresponding to a cycle frequency of 425 kyr. There are also low power spectral peaks at 0.0127, 0.0282 and 0.0513 cycles per kyr. These concur to cycle frequencies of 82, 37 and 19.5 kyr and may represent the short-term

eccentricity component, obliquity and the precessional peaks respectively. However power at these periods is not strong and it is difficult to recognise these frequencies in the entire data set.

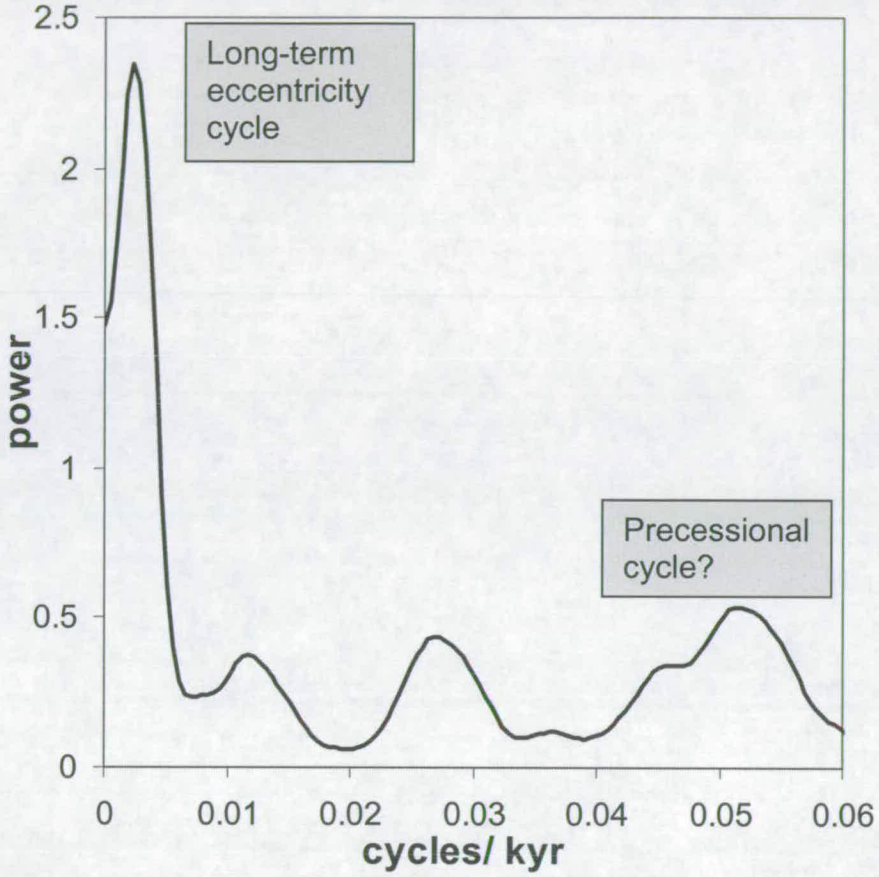

Figure 4.4. Power spectra of the oxygen isotope record determined using the Blackman-Tukey method.

Whilst there is a prominent 400 kyr cycle from 37.6 to 39.6 Ma, the long-term eccentricity signal is less apparent in the record from 37.3 to 37.6 Ma (figure 4.3). Filtering the data indicates that the short-period eccentricity signal is more prominent here (figure 4.5). The shift in the dominant frequency from long- to short-term eccentricity in the oxygen isotope record at ~37.6 Ma could be a bias caused by the termination of the record at 37.3 Ma. Alternatively this could reflect a real change in climate modulation in response to surface water cooling and the expansion of the cryosphere. Only the analysis of longer time-series data or high-resolution coeval sections will be able to address this.

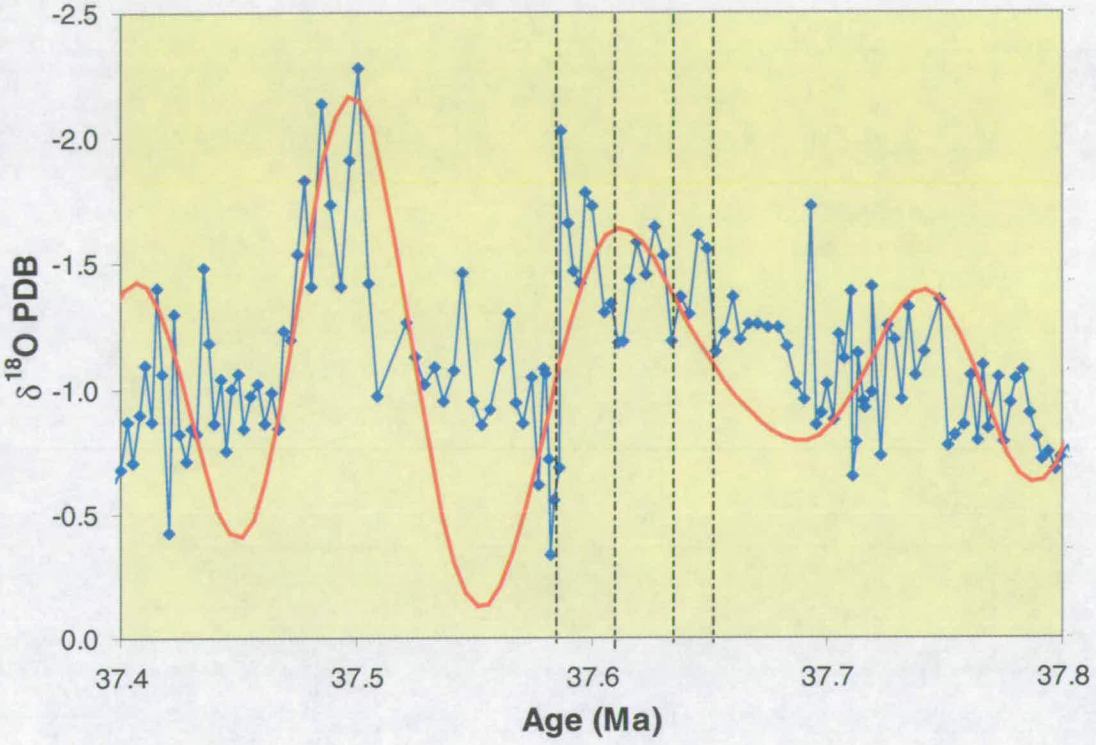

Figure 4.5. Oxygen isotope record at Site 1052 (blue line) against the astronomical time-scale. Data has been filtered to reveal the short-term eccentricity cycle (100 kyr) (red line). The vertical lines indicate regular cycles that may correspond to precession.

4.2.2. Eccentricity forced variations in $\delta^{13}C$

Power spectra of the carbon isotopic record suggests the presence of a dominant frequency at 0.0084 cycles / kyr (figure 4.6). This corresponds to a cycle period of 120 kyr and is thought to represent the short-term eccentricity cycle. Spectral analysis also indicates a cycle of 19 kyr wavelength (0.0516 cycles / kyr) that may be the precessional signal.

Unlike the oxygen isotope record, the $\delta^{13}C$ record does not show a prominent 400 kyr signal. This is indicated in figure 4.7, where the $\delta^{13}C$ record has been filtered to a 400 kyr period. What appears to be more influential in the $\delta^{13}C$ signal is the short-term eccentricity period (100 kyr) which is particularly strong in the upper 15 metres of the record (figure 4.8).

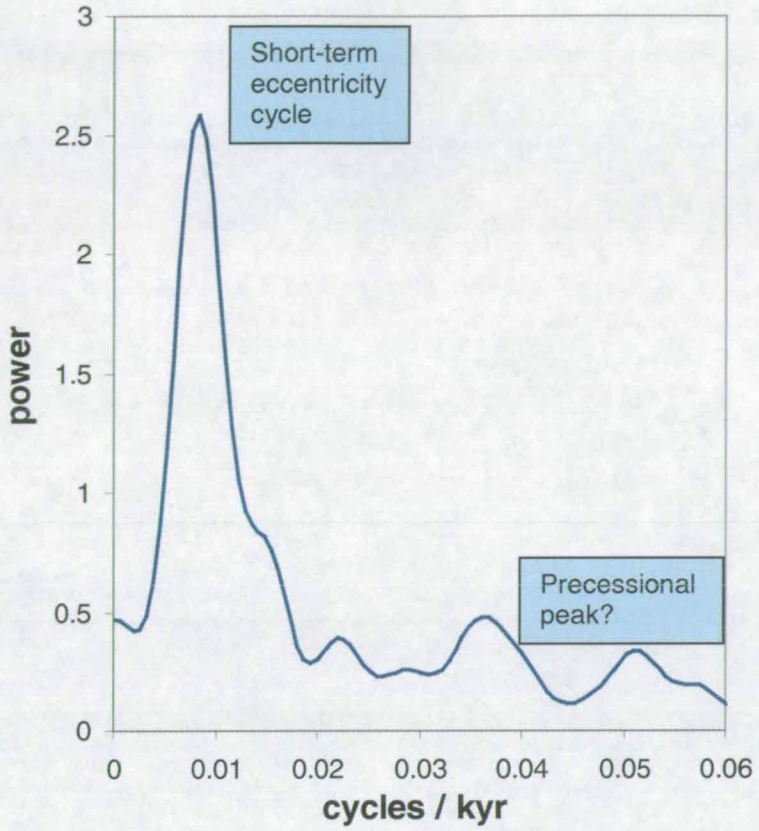

Figure 4.6. Power spectra of the carbon isotope record at Site 1052 determined using the Blackman-Tukey method.

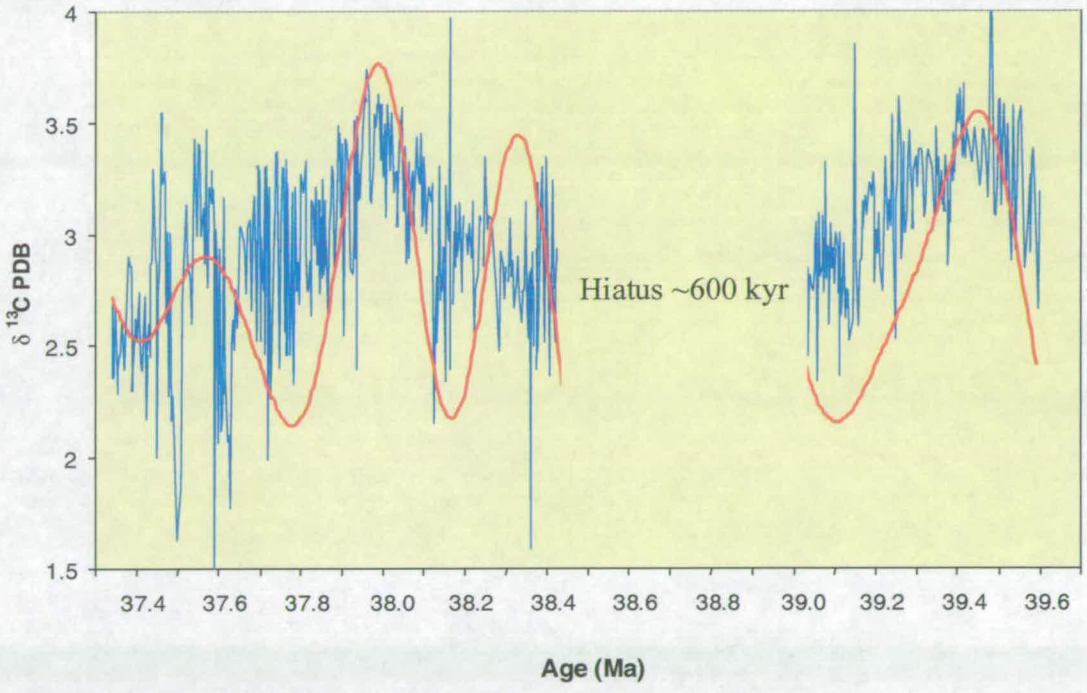

Figure 4.7. Carbon isotope record at Site 1052 (blue line), plotted against the astronomical time-scale. Data has been filtered to a 400 kyr period (red line).

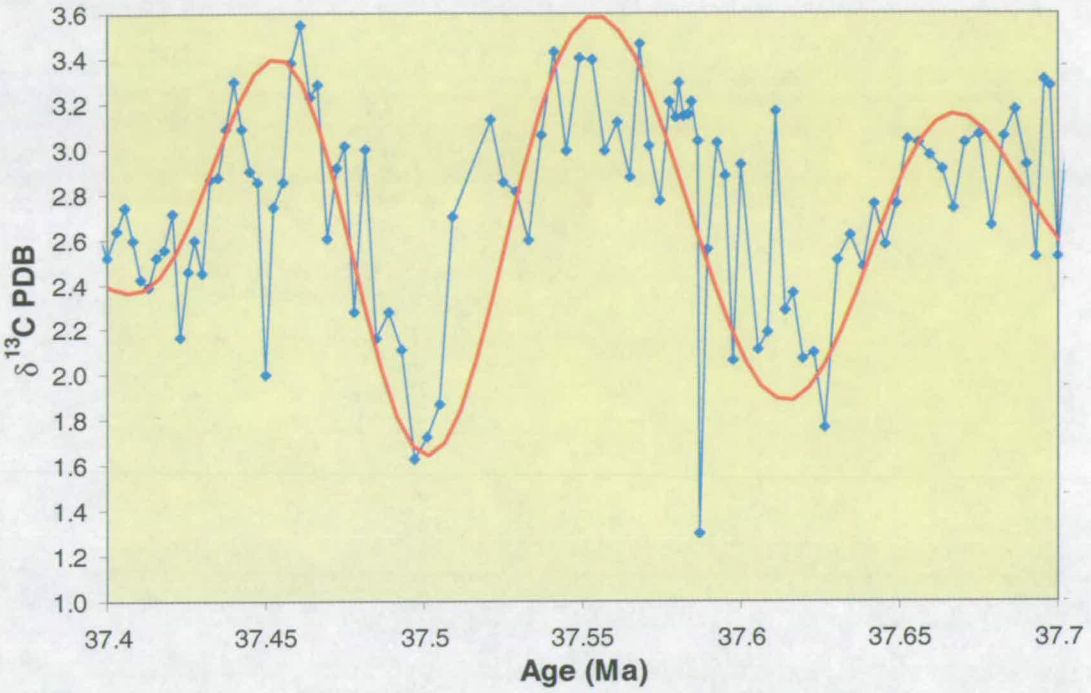

Figure 4.8. Carbon isotope record at Site 1052 (blue line), plotted against the astronomical time-scale. Data has been filtered to reveal the short-term eccentricity cycle (~100 kyr) (red line).

4.3. Isotopic variations at the obliquity period

The obliquity period causes changes in the latitude of the polar circle, which influences the meridonial distribution of solar energy. This has a large climatic influence in the high latitude regions due to variations in seasonality (Imbrie *et al.*, 1992, 1993), although this may also effect the balance of evaporation and precipitation in the tropics and subtropics (Park and Oglesby, 1990). Whilst there is a pronounced eccentricity signal in the stable isotopic records at Site 1052 there is little indication of the influence of the obliquity period (41 kyr). This is in accordance with local forcing of subtropical climate. Figures 4.9 and 4.10 indicate the possible influence of the obliquity period on the oxygen and carbon isotope records, though this is not as clear as the eccentricity cycles and the signal is weak.

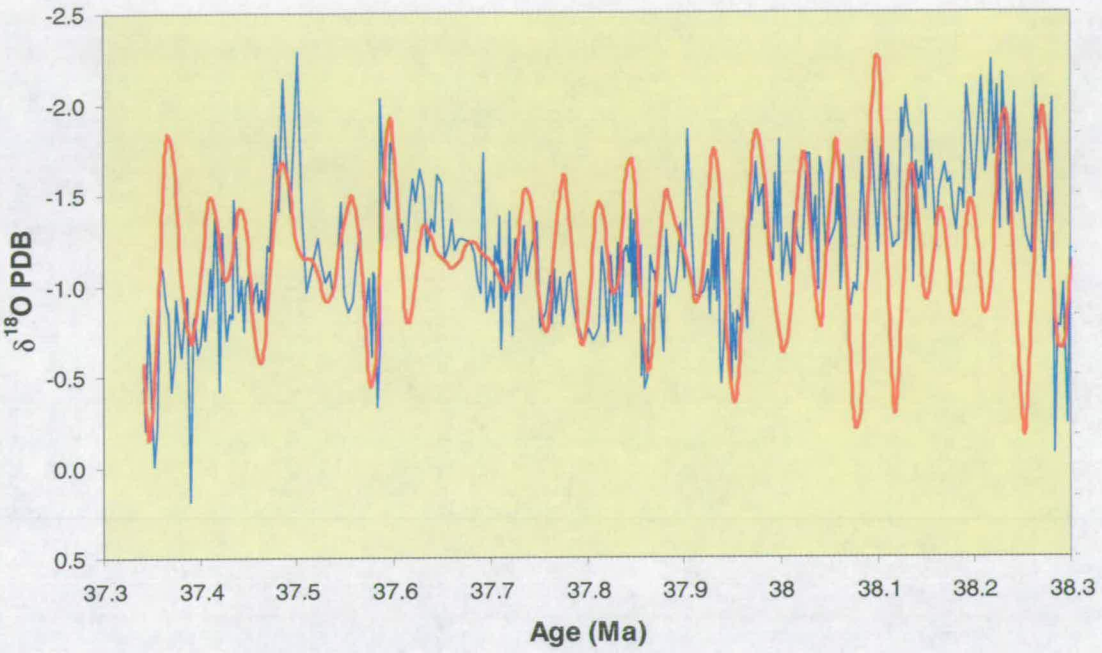

Figure 4.9. Oxygen isotope record at Site 1052 (blue line) against the astronomical time-scale. Data has been filtered to reveal possible obliquity cycles (red line).

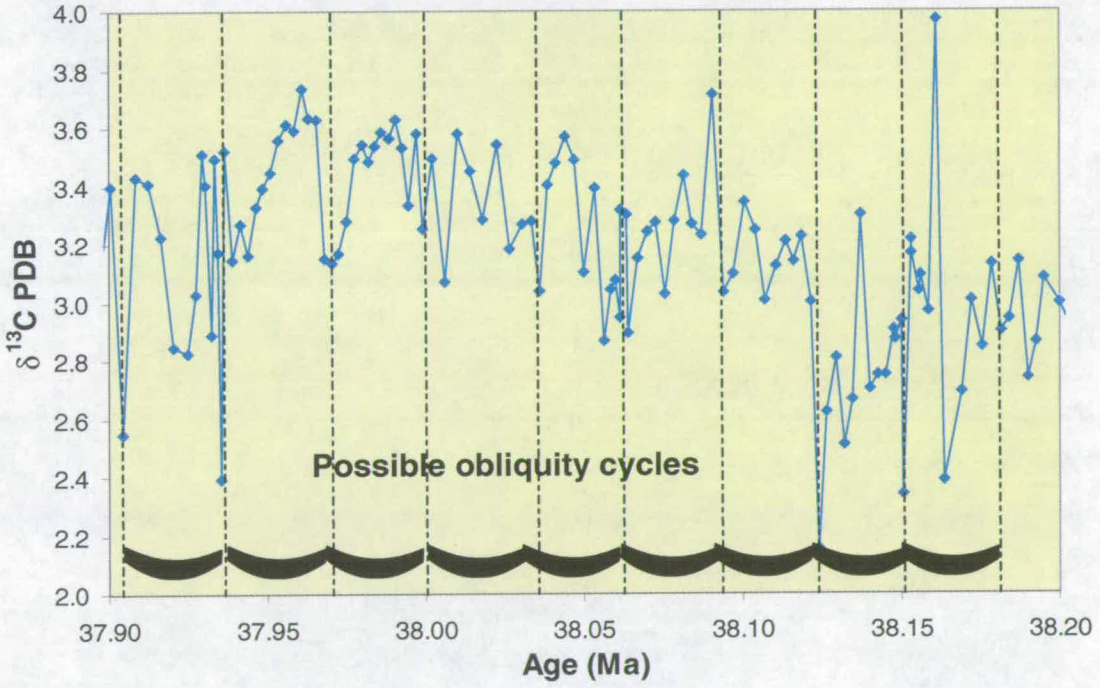

Figure 4.10. Carbon isotope record at Site 1052 (blue line) against the astronomical time-scale. Vertical hashed lines indicate the possible obliquity cycles.

The obliquity period is not a strong influence on the record, suggesting that high latitude water masses did not significantly affect the Blake Nose area. This confirms dinoflagellate faunal results (e.g. van Mourik *et al.*, 2001) that do not record high latitude fauna in the samples from Blake Nose. The lack of obliquity signal in the middle Eocene $\delta^{18}O$ record also confirms the absence of large scale ice-sheets on Antarctica at this time.

4.4. Isotopic variations at the precessional period

4.4.1. Evidence of the precessional period in the stable isotopic record

There are several lines of evidence that point to the presence of a precessional periodicity in the stable isotopic records. The power spectrum indicates weak power at 0.0513 and 0.0516 cycles per kyr in the oxygen and carbon isotopic records respectively. These correspond to cycle frequencies of 19 kyr that may represent the short-term component of precession. The 19 kyr frequency does not match the power spectra of the Munsell hue record (figure 2.11) which indicated power at 23 and 21 kyr. However, cross-spectral analysis by Pälike *et al.* (2001) showed coherency at all the precessional frequencies (23, 21 and 19 kyr) in the Ca / Fe record at Site 1052. There is also a visual co-variation between the precessional forced Munsell hue record and the $\delta^{13}C$ record (figure 4.13).

The eccentricity component of orbital frequencies is due to the amplitude modulation of the precessional period. The presence of a significant 400 kyr signal in the $\delta^{18}O$ record (figure 4.4) and the clear precessional frequencies in the lithological record (figure 2.6) suggest that the precessional period was an important component of subtropical Eocene climate.

The precessional period is not easily recognised within the stable isotopic data. This is probably due to unknown offsets in the data. The exact season of reproduction and position of *Morozovella crassata* and *Globigerinatheka mexicana* within the middle Eocene water column in unknown. Temporal shifts in depth habitat may obscure the precessional periodicities within the data set. It is also more difficult to recognise

these short period orbital frequencies as the data points involved in a full cycle are much fewer than longer orbital periods (e.g. precession = 7 data points, long-term eccentricity = 140 data points, based on mean sedimentation rates). Further statistical analyses or higher sampling frequencies are probably necessary to significantly show the precessional period within Palaeogene planktonic foraminifera data.

4.4.2. Precessionally forced climate variability

The amount of seasonal and annual insolation at a given latitude is modified by precessional variations, particularly in the tropics and subtropics (Ruddiman *et al.*, 1989; Imbrie *et al.*, 1992). Positive feedback increases the effects of these small variations in solar insolation through non-linear response (Herbert, 1997). The precessional frequencies in the Munsell hue record indicate a strong influence of low latitude insolation on the subtropical climate. The primary feature of eccentricity is to regulate the magnitude of the precessional influence. The modulation of the precessional signal by the 400 kyr cycle is apparent in the $\delta^{18}O$ record (figure 4.11). It can be seen that mixed layer planktonic foraminifera $\delta^{18}O$ fluctuations are greater from 39.49 to 39.60 Ma and again 400 kyr later at 39.04 to 39.15 Ma. The precessional period may be responsible for the low amplitude oscillations in the planktonic foraminifera stable isotopic record. This probably reflects temperature and productivity changes associated with changes in subtropical insolation.

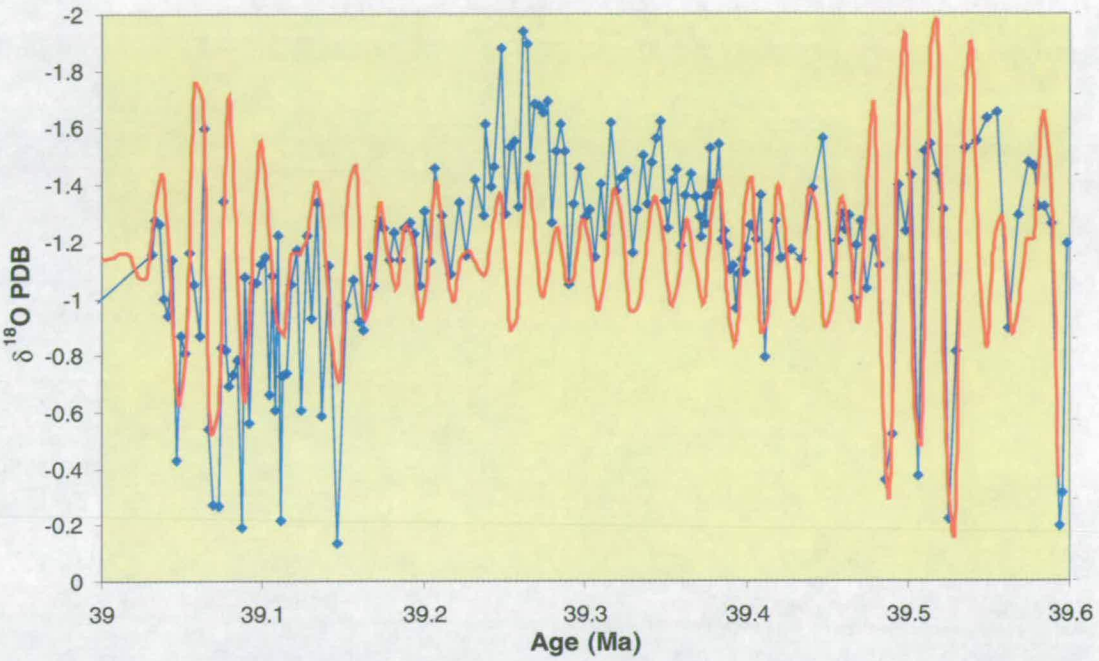

Figure 4.11. Oxygen isotope record at Site 1052 (blue line) plotted against the astronomical time-scale. Data has been filtered to reveal the possible precessional signal (red line).

4.4.3. Precessionally forced variations in productivity

As with the $\delta^{18}O$ record, short-term frequencies in the $\delta^{13}C$ record are probably influenced by precession (figure 4.12). Factors that may have enhanced the effects of precessional insolation changes include modifications in heat transport, pCO_2, carbon cycling and precipitation (Ruddiman and McIntyre, 1981; Pisias *et al.*, 1990; Crowley *et al.*, 1992; Herbert, 1997). However, the modulation of precession by the 400 kyr cycle within the $\delta^{13}C$ is less obvious. Flower *et al.* (1997) attributed the 400 kyr cycle in Oligocene - Miocene isotopic records from Ceara Rise to variations in the East Antarctic ice sheet and rates of burial / oxidation of organic matter. The lack of a prominent 400 kyr cyclicity in the $\delta^{13}C$ record here suggest that the systems controlling $\delta^{13}C$ and $\delta^{18}O$ on long time-scales were not coupled during the middle Eocene. The uncoupled climate and carbon systems are discussed further in chapter 7.

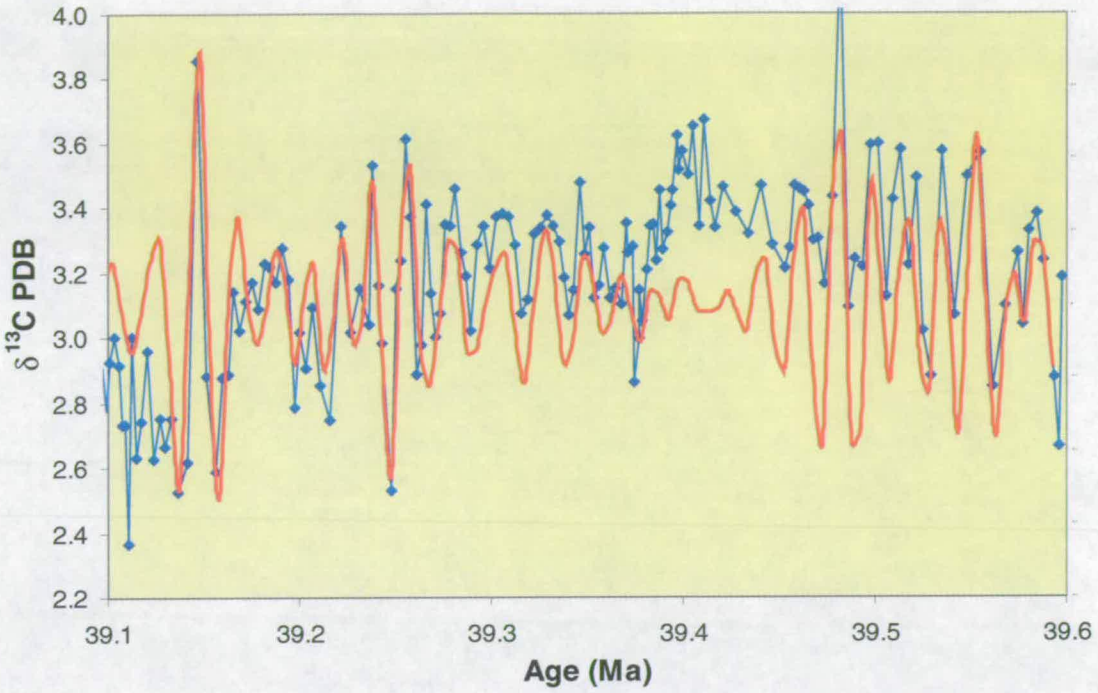

Figure 4.12. Carbon isotope record at Site 1052 (blue line) plotted against the astronomical time-scale. Data has been filtered to reveal the possible precessional period (red line).

4.5. Non-Milankovitch climate variability

Whilst eccentricity frequencies are clearly represented in the stable isotopic records at Blake Nose, some variability cannot be explained by this means. There are intervals when isotopic variability is irregular. This could be attributed to planktonic foraminiferal vital effects, non-Milankovitch variability, or alternatively that the orbital signals of precession, sub-precession and obliquity are superimposed, thus making cycles difficult to determine.

4.6. Comparison of the cyclicity in the lithological and stable isotopic records

It has already been established in chapter 2 that the middle Eocene lithological sequence at Site 1052 has a strong precessional period. In figures 4.13 and 4.14 the isotopic results of carbon and oxygen respectively are plotted with the Munsell hue record against time. Both records indicate a precessional cyclicity, although this is

visually more perceptible in the Munsell hue record, because the colour record was sampled at a higher resolution (5 cm). Heavy $\delta^{13}C$ results are associated with lighter sediment colour (increased carbonate), suggesting that this could be in response to wind blown terrestrial input which provides nutrients to the surface water and therefore increases carbonate productivity.

Whilst the precessionally forced cycles are very prominent within the colour record, it is harder to identify individual cycles within the planktonic foraminifera $\delta^{18}O$ record. Pearson *et al.* (1997) also noted a lack of association between the stable isotopic and colour cycles in sediments from the Ceara Rise. This is probably due in part to species vital effects, but also local and global influences. The colour cycles are a local signal probably controlled by wind driven terrigenous input (see section 2.7). The isotopic records are however also influenced by wider scale and global changes in the evaporation / precipitation balance, ice volume and global carbon flux. These factors will cause changes in the stable isotopic records that may not be recorded in the lithological physical properties data. High frequency variability, differences in sampling resolution and possible phase leads and lags may also distort the visible relationship between lithological and isotopic data.

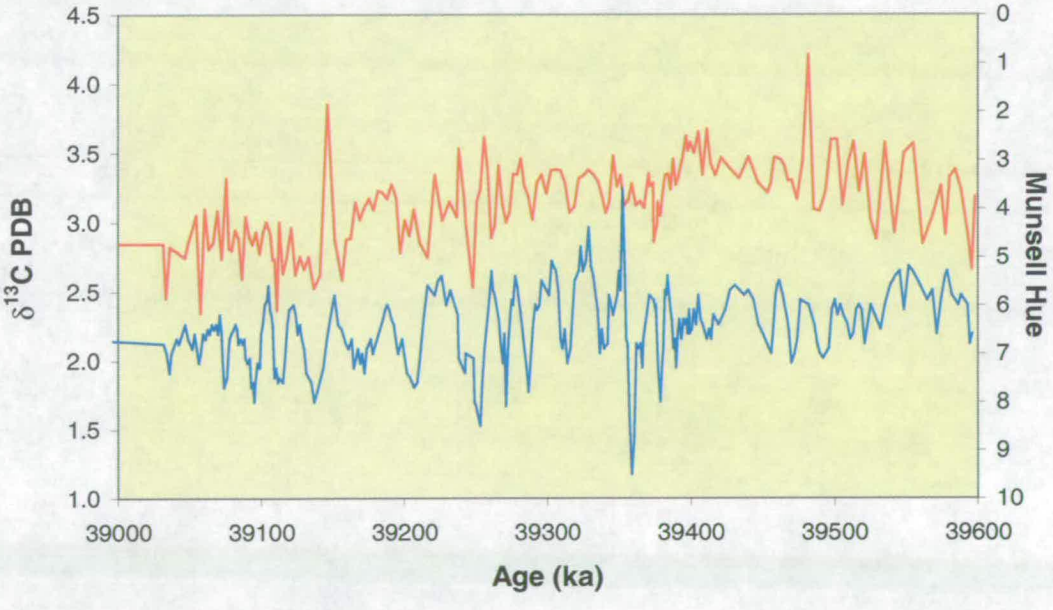

Figure 4.13. The carbon isotope record (red line) and Munsell hue record (blue line) from 39.0 to 39.6 Ma at Site 1052.

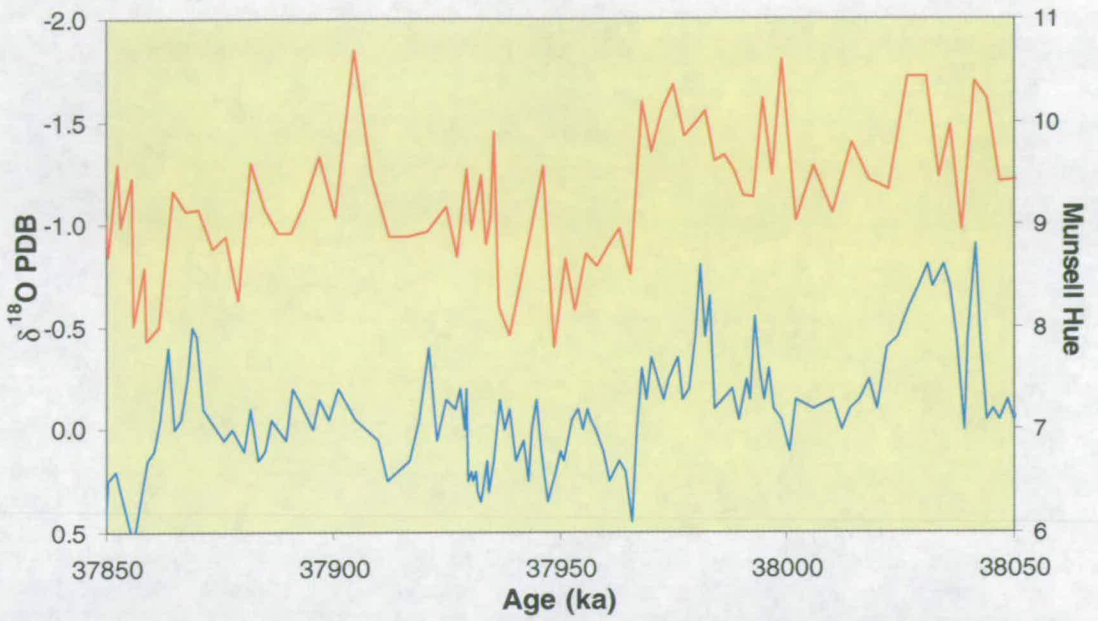

Figure 4.14. The oxygen isotope record (red line) and Munsell hue record (blue line) from 37.85 to 38.05 Ma at Site 1052.

4.7. Implications of orbital control on the Eocene climate

Fourier analysis shows the predominance of certain Milankovitch frequencies in the isotopic records. The spectral power is particularly significant in the oxygen isotope record at the long-term eccentricity period (~400 kyr), whilst the short-term eccentricity period (100 kyr) dominates the $\delta^{13}C$ record. The respective significance of the short-term and long-term eccentricity components within the oxygen isotope record varies through the analysed interval. The long-term eccentricity signal is dominant in the interval from 37.6 to 39.6 Ma. The short-term eccentricity becomes a significant component in the upper interval from 37.3 to 37.6 Ma.

Precessional variations in solar insolation are most probably acting on Eocene subtropical surface waters, although the precessional period within the $\delta^{18}O$ and $\delta^{13}C$ records is not clear throughout the analysed interval. Long-term orbital effects, perhaps due to shifts in wind systems, then modulate this precessional forcing to give rise to a strong 400 kyr signal where periodically heavy $\delta^{18}O$ are recorded. Eccentricity forcing indicates that the subtropical climate is responding to the modulation of regional variations in solar insolation.

It has been indicated that certain climatic factors are sensitive to orbital forcing. The weak precessional variations in the $\delta^{18}O$ and $\delta^{13}C$ record could reflect Ekman driven upwelling, changes in the strength of the thermocline or variations in continental runoff or evaporation / precipitation which are sensitive to precessional forcing. Climatic modeling studies of the Eocene have forecast sensitivity to precessional forcing in the western North Atlantic that gave rise to Ekman driven upwelling and changes in wind systems (e.g. Bice *et al.*, 2000b; Sloan and Huber, 2001a, 2001b). This is discussed further in chapter 7.

Long-period eccentricity variation has been recognised in Palaeogene sediments from both high and low latitudes (e.g. Zahn and Diester-Haass, 1995; Zachos *et al.*, 1996; Zachos *et al.*, 1997; Zachos *et al.*, 2001b). However, sampling resolutions and sediment accumulation rates have been insufficient to significantly resolve the full spectra of orbital frequencies in Palaeogene studies. The persistence of the eccentricity period within climatic records signifies a firm association between climatic variance and insolation forcing (Zachos *et al.*, 2001b). Herbert (1997) showed that the 400 kyr eccentricity period was a particularly important component of climate change prior to extensive glaciation on Antarctica. The strong 400 and 100 kyr cycles in the isotopic records provide further confirmation of the importance of the eccentricity frequencies within past climatic regimes.

The carbon isotopic record indicates power in the short-term eccentricity band. However, the long-term trends in oxygen and carbon isotope are not the same (figure 3.8). There is a longer-term periodicity in the $\delta^{13}C$ record with heavy carbon isotope values recorded at 38.0 and 39.4 Ma. The carbon record does not exhibit the 400 kyr eccentricity cycle and the precessional $\delta^{13}C$ variations are not clearly modulated in this way. Zachos *et al.* (2001b) suggest that the strong long-term eccentricity cycle in sediments of Miocene age and older is related to atmospheric pCO_2 and the global carbon cycle. However, if this theory is correct, why does the carbon isotopic record of Blake Nose not show a strong 400 kyr modulation? The long-term amplitude modulation within the $\delta^{13}C$ is probably controlled by non-orbital variations in the

carbon cycle flux such as changes in the carbon reservoir, geochemical cycling of carbon or pCO_2 with a periodicity greater than 400 kyr.

It is unknown how the relative changes in the Earth's solar insolation give rise to the significant climate variability recorded in the lithological and stable isotope cycles. The eccentricity signal cannot be caused directly by variations in solar insolation, as the eccentricity influence on insolation is small. The strong eccentricity periodicities suggest both short- and long-term feedbacks that amplify the modulation of precession. The mechanisms responsible for the sensitivity and increase in the 400 kyr forcing are not known, but shifts in wind fields and atmospheric circulation patterns are suspected (discussed in chapter 7). Changes in SST, surface water chemistry and thermal gradient are probably involved, either directly or indirectly via feedback mechanisms.

The evidence of orbitally induced climate change in the middle Eocene adds support to the fact that Milankovitch variations were important during all modes of past climate. These results provide further evidence for the sensitivity of climate to orbital variations in pre-Pleistocene times. Orbitally induced variations in solar insolation have a direct correspondence with variations in surface water properties, although it is not yet fully understood exactly how. Orbital periodicities in the stable oxygen isotope record indicate an oceanic - climatic system that is extremely dynamic. Both short- and long-term variations resulted within the Eocene climatic system, induced either directly or indirectly by external variations in solar insolation.

4.8. Summary

1) Stable isotopic results have been plotted against the astronomical chronology established in chapter 2.
2) Power spectra of the late middle Eocene planktonic foraminifera stable isotopic time series indicates periodicities that may reflect obliquity, precession and eccentricity cycles.

3) The oxygen isotope record indicates that the long-term eccentricity cycle periodically gave rise to heavy $\delta^{18}O$ values.
4) The 100 kyr eccentricity cycle is more prominent in the $\delta^{18}O$ record from 37.6 to 37.3 Ma.
5) The carbon isotopic record does not indicate the long-period eccentricity cycle (400 kyr), and the short-period eccentricity cycle (100 kyr) dominates this isotopic record.
6) The positive relationship between increased carbonate and increased $\delta^{13}C$ suggests precessional forced variations in productivity attributed to wind blown terrigenous material from the North American continent.
7) The results confirm the importance of orbitally induced climate change within pre-Pleistocene sediments and indicate a highly dynamic climate system in the middle Eocene.

5. LATE MIDDLE EOCENE SEA SURFACE TEMPERATURES AND MECHANISMS CONTROLLING THE LARGE AND RAPID OXYGEN ISOTOPE SHIFTS

High-resolution stable isotope investigations allow the variability of the climate system during the late middle Eocene to be quantified. During 2.3 million years in the late middle Eocene the planktonic $\delta^{18}O$ record at Blake Nose ranges from +0.2 to –2.4‰, with values generally between 0.0 and –2.0‰. If the isotopic shifts in $\delta^{18}O$ are wholly attributed to temperature, then SSTs fluctuated more than 10°C (~0.25‰/1°C, Epstein *et al.*, 1953). These temperature shifts are massive and exceed the magnitude recorded in the tropical Pacific Ocean during El Niño events (e.g. Elliott *et al.*, 2001). It is difficult to account for such large temperature shifts in the subtropics. To understand what caused the rapid and high amplitude oxygen isotopic shifts it is important to quantify the effects of ice volume, temperature, atmospheric vapour transport and oceanic circulation on the $\delta^{18}O$ signal.

5.1. Ice volume effect

The early Eocene was a greenhouse world in comparison to the modern, with elevated CO_2 levels (Pearson and Palmer, 2000), increased temperatures at high latitudes and insignificant global ice volume compared to today (Zachos *et al.*, 1994 and references therein). The earliest accepted evidence of ice on the Antarctic continent is the early middle Eocene (Hambrey *et al.*, 1991; Wise *et al.*, 1991; Browning *et al.*, 1996; Abreu and Anderson, 1998). Glacio-marine deposits are found in Prydz Bay from ~43 Ma, however, little is known quantitatively about early ice-sheet development on Antarctica and ice may have existed on high regions of East Antarctica millions of years before advancing to the coastline. Large scale continental glaciation did not occur until the earliest Oligocene (Miller *et al.*, 1987, 1991; Zachos *et al.*, 1992, 1993, 1999; Lear *et al.*, 2000).

Whilst ice volume can be quantified to some extent, it is unclear what the isotopic composition of early Antarctic ice was. The Antarctic ice sheet is formed from high-latitude precipitation. The isotopic formation of precipitation is related to the mean surface air temperature, water saturation vapour pressure and airmass transport distance (Robin, 1988). It is likely that during intervals of high-latitude warmth there would have been less fractionation of oxygen and therefore less depleted $\delta^{18}O$ in precipitation. However, this has not yet been quantified.

Lear *et al.* (2000) estimated the ice volume effect in the late middle Eocene $\delta^{18}O$ to be –0.5‰ Standard Mean Ocean Water (SMOW). Results of Lear *et al.* (2000) are comparable with benthic foraminifer stable isotope data from Blake Nose. Benthic foraminifer oxygen isotope values fluctuate by 0.7‰ in the middle Eocene at Site 1051 (Wade *et al.*, 2001) and are consistent with variations recorded at Site 1052 (Appendix 1 and Pälike, pers. comm.). The low amplitude oscillations (~0.7‰ PDB) in deep sea $\delta^{18}O$ reflect small changes in Antarctic ice volume, deep sea temperature or both. It cannot be assumed that all ice will be advancing and retreating and therefore a maximum ice volume effect on middle Eocene $\delta^{18}O$ was probably ~0.5‰ PDB or less. This is a minor fraction of the isotopic shifts seen recorded in planktonic foraminifera $\delta^{18}O$ at Site 1052 and ice volume cannot account for the high-amplitude shifts of >1‰ PDB. Further mechanisms must therefore be sought to explain the planktonic foraminifera $\delta^{18}O$ shifts of 1 to 2‰ PDB.

5.2. Atmospheric vapour transport, freshwater and seawater $\delta^{18}O$

A strong relationship exists between surface ocean salinity and the local oxygen isotope composition of seawater ($\delta^{18}O_{sw}$), as they are both controlled by the same processes (figure 5.1). A number of factors may influence $\delta^{18}O_{sw}$ including atmospheric vapour transport, ocean circulation, runoff and the magnitude and location of precipitation and evaporation.

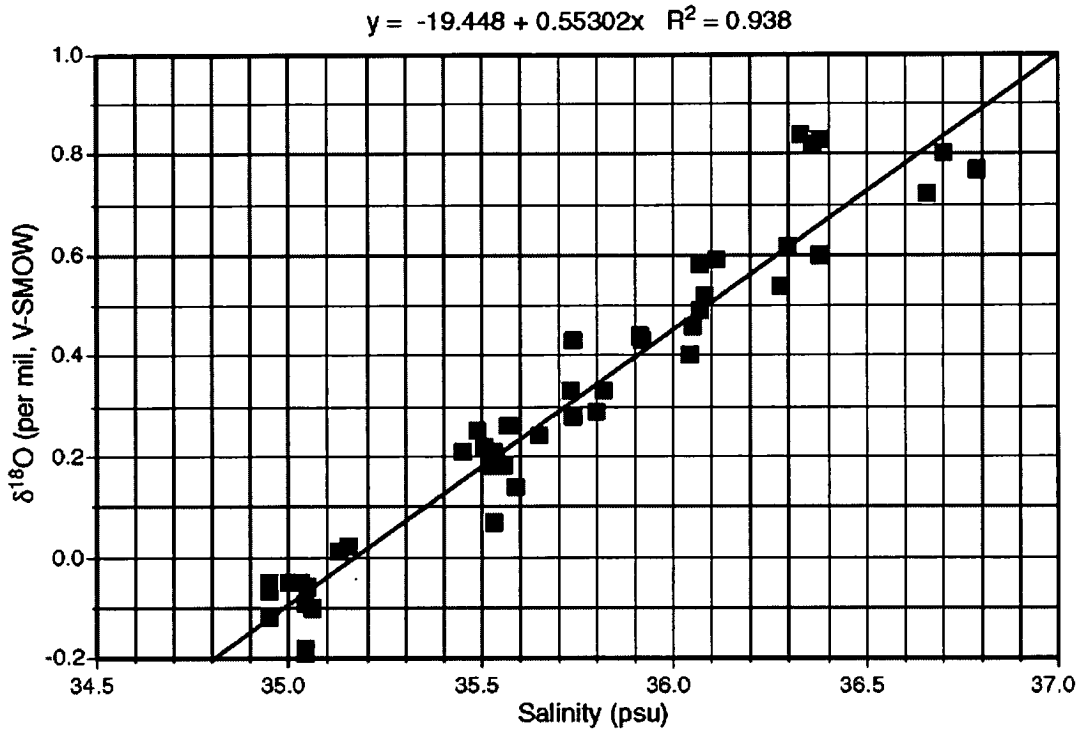

Figure 5.1. The relationship between surface water salinity and $\delta^{18}O$ in the modern Atlantic Ocean (Ganssen and Kroon, 2000).

A possible explanation is that the oxygen isotope signal of planktonic foraminifera reflects decreases in surface water salinity that caused isotopic depletion of the mixed layer and gave rise to isotopically light $\delta^{18}O$ values. It may be that the amount of freshwater required is not substantial especially if this water is very isotopically light. Perhaps at periodic intervals large amounts of water enriched in ^{16}O (warm, low salinity water), possibly from the ancestral Mississippi outflow entrained in the proto Gulf Stream, were transported from the Gulf of Mexico, north over Blake Nose. Seismic evidence suggests that the position of the Gulf Stream periodically shifted across the Blake Plateau during the Cenozoic (Pinet and Popenoe, 1985). The temporal, climatically forced variations in the strength and location of the Gulf Stream, associated with freshwater input could result in the fluctuations in planktonic foraminiferal $\delta^{18}O$ observed at Blake Nose. This would also explain the shifts in $\delta^{13}C$, as $\sum CO_2$ in freshwater tends to be depleted in ^{13}C relative to marine water, although interpretation of the carbon isotope record is complicated by vital effects. However, significant changes in local $\delta^{18}O_{sw}$ are required for the isotopic fluctuations

recorded at Blake Nose. If a constant temperature is invoked, the $\delta^{18}O_{sw}$ must have changed by 1 – 2‰, equivalent to a 4‰ shift in salinity (see figure 5.1 and also Broecker, 1989).

Modern flooding of the Mississippi Valley has given rise to a decrease in salinity of up to 4‰ in the Florida Current, Florida Straits and Gulf of Mexico by providing massive inputs of freshwater (Gilbert *et al.*, 1996). If recent flooding of the Mississippi valley is comparable to dramatic climatic changes in the middle Eocene that featured regular and intense precipitation events then this is a potential way to lower $\delta^{18}O_{sw}$ by 2‰. However, annual variations in salinity at Blake Nose are currently small (0.27‰) (Levitus *et al.*, 1994) and planktonic foraminifera are normally not tolerant of low salinity environments. This change is considered too large to be consistent with the open ocean setting for Site 1052.

Neither ice volume nor salinity alone can account for the high amplitude planktonic foraminifera $\delta^{18}O$ shifts and temperature must play a significant role. It is unlikely that temperature shifts occurred without variations in salinity due to evaporation and precipitation. Therefore the shifts in $\delta^{18}O$ probably occur as a result of a combination of temperature, ice volume and salinity changes.

5.3. Temperature

Even after ice volume effects have been taken into account (0.5‰ SMOW, Lear *et al.*, 2000), there still remains isotopic shifts of 1.5‰ to be accounted for and the amplitude of the temperature shifts are still a minimum of 6°C.

Glacial – interglacial shifts of 2.8‰ were recorded in the tropical western Atlantic at Site 1006 on the Great Bahama Bank (24°N) by Kroon *et al.* (2000) (figure 5.2). Such a magnitude of variation is slightly easier to explain during the Pleistocene as ice volume / sea-level effects can account for 1.2‰ of the signal (Berger and Gardner, 1975; Chapell and Shackleton, 1986; Fairbanks, 1989). During glacial-

interglacial intervals tropical SSTs can change by 4 to 5°C (Guilderson *et al.*, 1994, 2001; Cortijo *et al.*, 1999; Keigwin and Boyle, 1999; Pelejero *et al.*, 1999), thus accounting for a further 0.9 to 1.1‰ PDB of the isotopic variation. The remaining 0.5‰ can be attributed to local variation in surface water $\delta^{18}O$, such as upwelling, runoff or atmospheric moisture transport. However, during the middle Eocene the magnitude of the ice volume effect was smaller. This means that the temperature or $\delta^{18}O_{sw}$ fluctuations needed to account for the oxygen isotope shifts are significantly greater than those during the glacial / interglacial shifts of the Pleistocene.

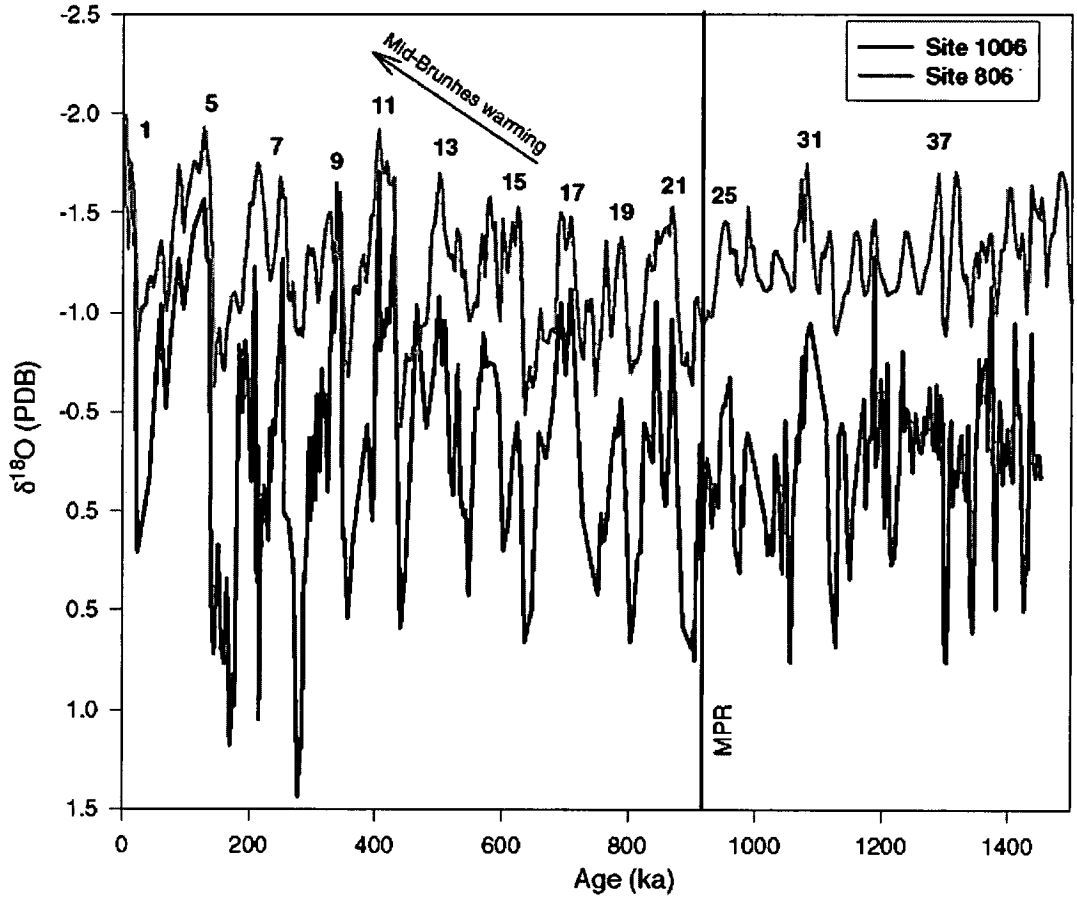

Figure 5.2. Oxygen isotope records from Site 1006 (tropical western Atlantic) and Site 806 (western Pacific), from Kroon *et al.* (2000). MPR = Mid-Pleistocene Revolution.

The high amplitude (2‰) negative oxygen isotope shifts recorded at Blake Nose cannot be explained by a single forcing mechanism. They are probably caused by a combination of ice volume decrease, subtropical warming, freshwater input and ocean circulation. The possible magnitude of the ice volume, salinity and temperature effects is illustrated in figure 5.3. A dramatic fall in $\delta^{18}O$ of almost 2‰ PDB is evident at 85.2 mcd (figure 5.3). This cannot represent ice volume alone, as this is nearly two times greater than the glacial-interglacial differences of the Pleistocene. If this shift reflects temperature, then this is a 7°C crash in surface water temperatures over approximately 2,000 years (~0.25‰/1°C, Epstein *et al.*, 1953). For this to be due to changes in salinity it would require a salinity shift of 4‰ (Broecker, 1989) to 10‰ (Fairbanks *et al.*, 1992). This is considered too large for an open ocean environment. It is likely that the $\delta^{18}O$ shifts reflect a mixture of temperature, salinity and ice volume fluctuations but without an independent temperature proxy these effects cannot be separated. It is thought to primarily reflect temperature, although ice volume and salinity will also have an influence.

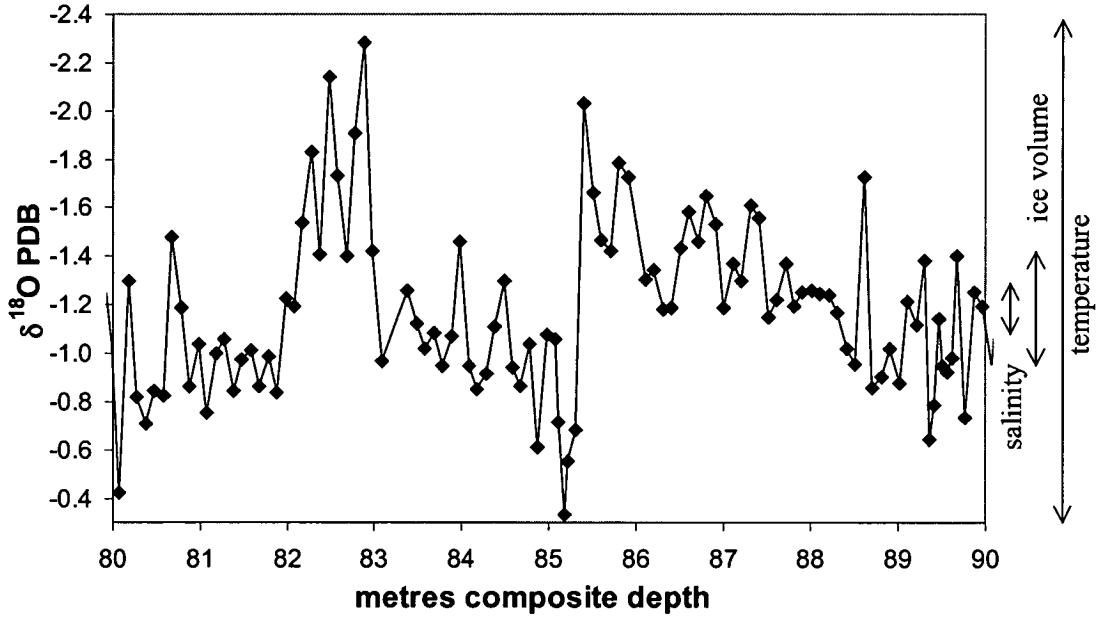

Figure 5.3. Planktonic foraminifer oxygen isotope record from Site 1052 from 80 to 90 mcd. Arrows indicate the maximum amount of $\delta^{18}O$ variation that can be attributed to salinity, ice volume and temperature. Salinity variation is kept at modern day values (0.27‰).

5.4. Middle Eocene subtropical sea surface temperatures

5.4.1. Palaeotemperature reconstruction

In order to determine the forcing mechanisms that produced past climatic states it is critical to ascertain marine palaeotemperatures. Sea surface temperatures (SSTs) were calculated using the calcite-water $\delta^{18}O$ temperature equation of Erez and Luz (1983):

$$T°C = 16.998 - 4.52\,(\delta^{18}O_{cc} - \delta^{18}O_{sw}) + 0.028\,(\delta^{18}O_{cc} - \delta^{18}O_{sw})^2 \qquad (1)$$

where $\delta^{18}O_{cc}$ is the oxygen isotope composition of the sample calcite relative to PDB, and $\delta^{18}O_{sw}$ is the oxygen isotope composition of the ambient seawater relative to SMOW.

5.4.2. Atmospheric vapour transport, $\delta^{18}O_{sw}$ and salinity

It is imperative that the mean oxygen isotope composition of the seawater in which the calcite was precipitated ($\delta^{18}O_{sw}$) is constrained in the calculation of palaeotemperatures from equation 1. This is influenced by ice volume, runoff, precipitation and fractionation by freezing and evaporation. During the Eocene, in the absence of significant continental ice, the estimated mean composition of seawater is -0.5‰ SMOW (Lear *et al.*, 2000), based on magnesium / calcium data from benthic foraminifera. Instead of applying a mean $\delta^{18}O$ value for the entire ocean when calculating SSTs from planktonic foraminifera, it is desirable to account for local variations in sea surface $\delta^{18}O$ as a function of latitude. This value is dependent on evaporation, precipitation and atmospheric vapour transport in the open ocean. There is presently no direct measure of palaeoseawater $\delta^{18}O$.

Zachos *et al.* (1994) introduced an equation to calculate the influence of atmospheric moisture transport and evaporation on regional $\delta^{18}O$:

$$y = 0.576 + 0.041\,x - 0.0017\,x^2 + 1.35*10^{-5}\,x^3 \qquad (2)$$

where y is the oxygen isotopic composition of the seawater ($\delta^{18}O$, SMOW) and x is the absolute latitude in the range of 0° to 70°. This equation is applied to decrease the effect of the surface water $\delta^{18}O_{sw}$ gradient on palaeotemperature reconstruction. The equation infers that the zonally averaged meridional surface water $\delta^{18}O$ gradient was similar to that of the present day. Although it is conceivable that the latitudinal $\delta^{18}O$ gradient was different in the middle Eocene, there is no indication that the amplitude or direction of this gradient was significantly dissimilar to the present (Crowley and Zachos, 2000). Eocene model simulations (e.g. Manabe and Bryan, 1985; Rind, 1986; Sloan and Rea, 1995) indicate that the balance of precipitation / evaporation which establish the salinity patterns of the ocean are comparable in the Eocene to today (Crowley and Zachos, 2000).

Errors in estimating surface ocean salinity may cause serious biases in calculations of past SSTs. As the actual isotopic composition of the middle Eocene seawater cannot be determined, two constant values of $\delta^{18}O_{sw}$ were considered in the calculation of sea surface temperatures. These were: i) -0.5‰ (SMOW) where the net evaporation effect on $\delta^{18}O_{sw}$ is not considered and ii) +0.14‰ (SMOW) where the palaeolatitudinal dependant effect on $\delta^{18}O_{sw}$ was determined from equation 2 (Zachos *et al.*, 1994) and the resulting value reduced by –0.5‰ to account for global conditions (Lear *et al.*, 2000). The palaeolatitude of Site 1052 is comparable to today ~29°N (Ogg and Bardot, 2001). The $\delta^{18}O_{sw}$ value of +0.14‰ translates to a palaeosalinity of 35.5‰ (using the equation of Broecker, 1989).

Palaeotemperatures were reconstructed using the assumption that local salinity did not severely fluctuate and thus temperature was the primary influence on the stable oxygen isotope record. Variations in ice volume and $\delta^{18}O_{sw}$ will have also influenced $\delta^{18}O$ to some extent. Future work on these specimens will involve the quantification of the $\delta^{18}O_{sw}$ influence that accompanied changes in foraminiferal $\delta^{18}O$ (see section 7.5.1). It is possible that the assumption of constant salinity is incorrect but there is no direct means of quantifying the salinity effect on surface water $\delta^{18}O$ at this stage.

5.5. Sea surface temperatures at Site 1052

Modern species of planktonic foraminifera vary their depth habitat and season of reproduction. It is not known in which season *Morozovella* lived but it is likely that they were similar to the modern species *Globigerinoides ruber* and lived year-round. The SSTs calculated here are therefore considered to be mean annual temperatures. It should be noted that isotopic palaeotemperatures have a ±2 °C degree of uncertainty (see Crowley and Zachos, 2000 for discussion). All following palaeotemperatures should thus be considered as minimal values and not absolute.

The calculated sea surface temperatures at Site 1052 are shown in figure 5.4. When applying a $\delta^{18}O_{sw}$ value of -0.5‰ (SMOW), temperatures range between 13.9°C and 25.8°C. These values are increased by 3°C when the equation of Zachos *et al.* (1994) (equation 2) is employed to estimate palaeotemperatures between 16.8°C and 28.8°C. Previously, the general consensus of palaeoceanographers seems to have been that the middle Eocene was a time of stable, equable climate. However, results indicate large fluctuations in surface water temperatures with shifts as great as 12°C, assuming no change in ice volume and $\delta^{18}O_{sw}$. This suggests a very unstable climatic / oceanographic system that experienced abrupt changes in temperature.

The vertical line of figure 5.4 indicates modern mean temperatures at Blake Nose (from Bottomley *et al.*, 1990). Maximum recorded SSTs of 29°C are comparable to today's summer maxima. It is evident that if indeed the SSTs reconstructed for the Eocene reflect annual temperatures then there are intervals (yellow shaded areas) when annual temperatures were up to 5°C warmer than modern mean annual temperatures, using the equation of Zachos *et al.* (1994). These may reflect periods of abrupt warming when the greenhouse conditions that are characteristic of the early Eocene were restored. There are also intervals when SSTs were 7°C cooler than modern mean temperatures (blue shaded areas). The forcing factors accountable for these heavy $\delta^{18}O$ intervals are discussed in sections 5.8 and 5.9.

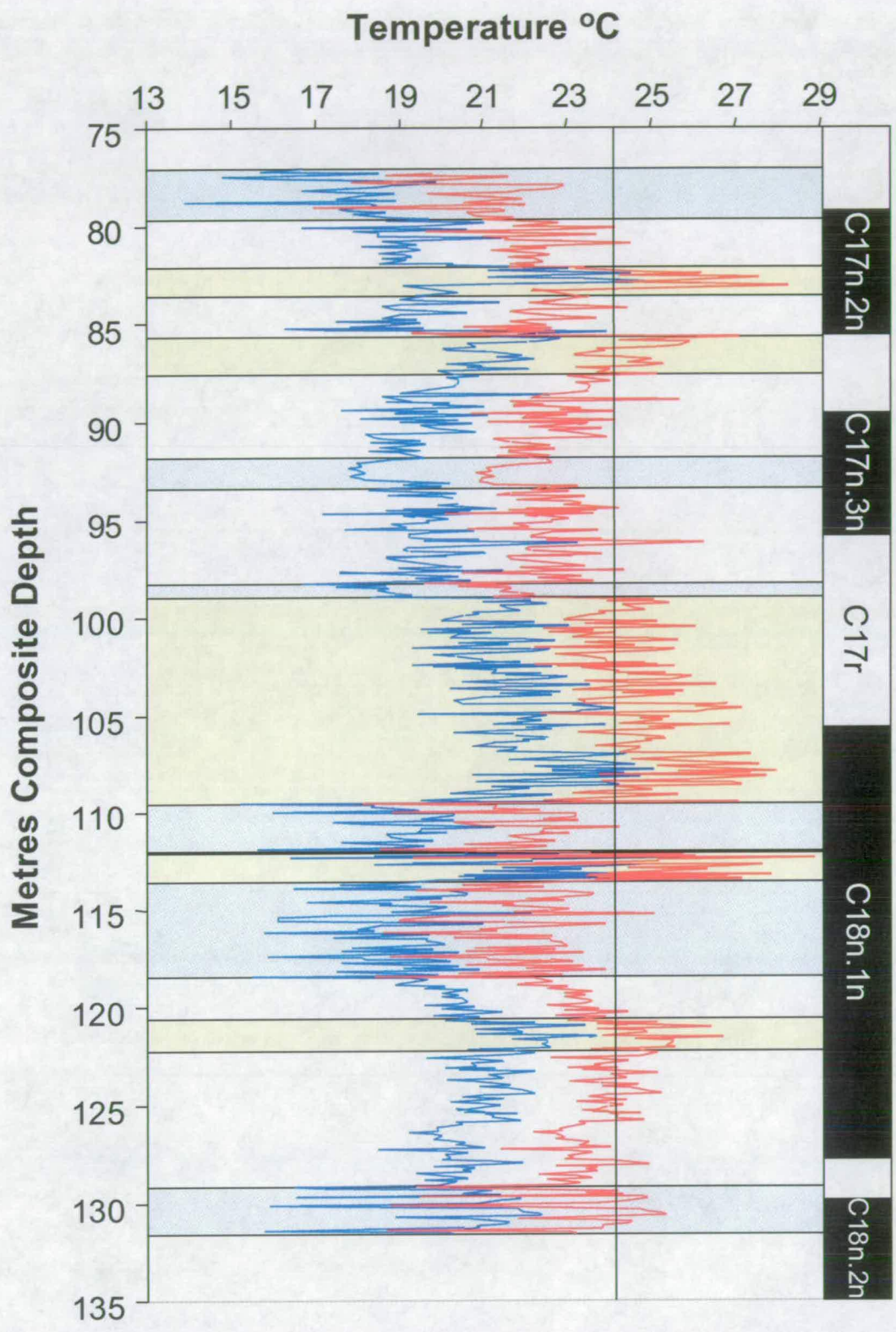

Figure 5.4. Surface water palaeotemperatures at Site 1052 using $\delta^{18}O_{sw}$ values of –0.5‰ (SMOW) (blue line) and +0.14‰ (SMOW) (red line). Vertical line indicates the modern mean annual temperature. Blue shaded areas are intervals where surface waters record heavy $\delta^{18}O$ and yellow shaded areas are intervals where surface waters record light $\delta^{18}O$.

Figure 5.4 indicates how sensitive the palaeotemperature calculations are to changes in seawater $\delta^{18}O$. Temperatures can be shifted by 3°C simply by changing the local $\delta^{18}O_{sw}$. The relationship between seawater $\delta^{18}O$ and temperature for varying isotopic values are shown in figure 5.5. At 29°N, Blake Nose is situated in a zone of net evaporation, leading to high $\delta^{18}O_{sw}$ and salinity. The modern $\delta^{18}O_{sw}$ at Blake Nose is high compared to the open ocean, 1.2‰ SMOW (Fairbanks *et al.*, 1992), with a salinity of 36.5‰ (Levitus *et al.*, 1994). If these modern values are applied to the palaeotemperature equation then sea surface temperatures are increased further and vary between 19 and 31°C (figure 5.5).

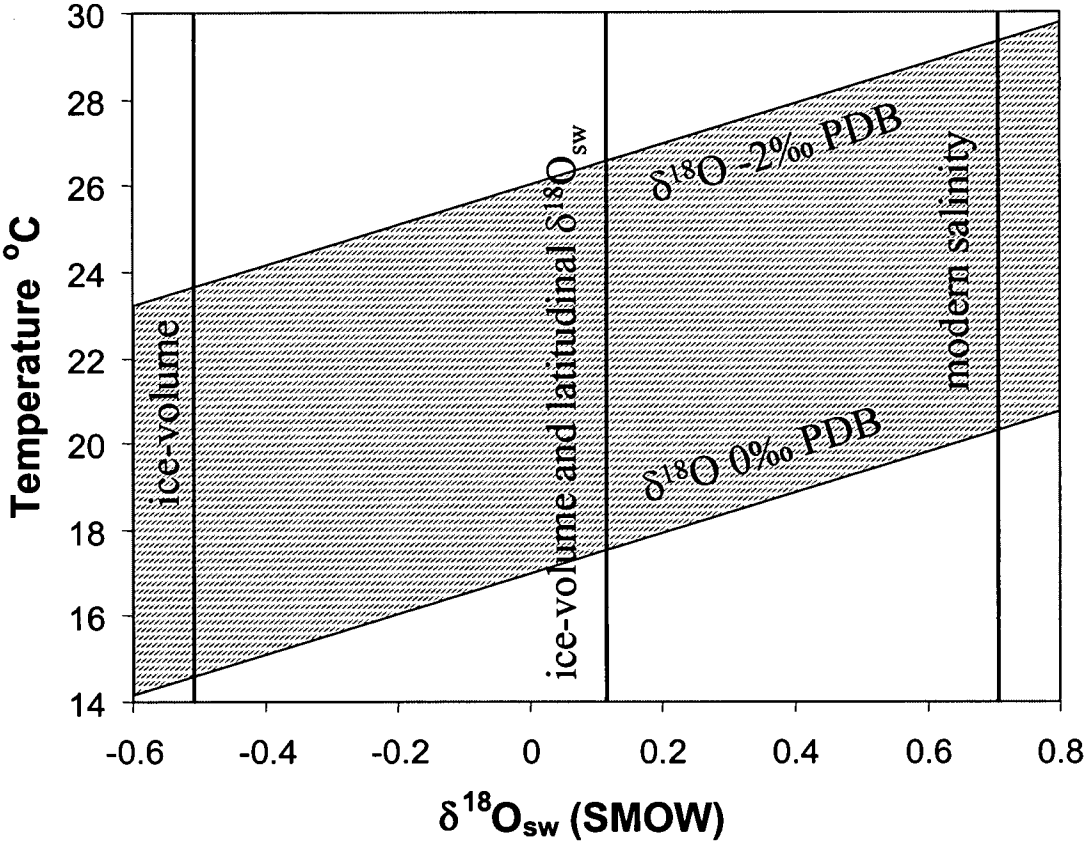

Figure 5.5. The relationship between temperature and differing $\delta^{18}O_{sw}$. The lower line and upper line represent $\delta^{18}O$ values of 0 and -2‰ PDB respectively. Shaded area represents the common range of sea surface temperatures. Vertical lines indicate the varying $\delta^{18}O_{sw}$ values applied in the palaeotemperature calculations.

It is probable that the palaeotemperatures deduced using the latitudinal adjustment of Zachos *et al.* (1994) are the most reliable. During the middle Eocene, with limited ice volume in comparison to modern, the surface water salinity was probably slightly less than today. Oceanic circulation will also influence the $\delta^{18}O_{sw}$ at Blake Nose. During the Eocene the central American seaway was open, which probably resulted in more uniform $\delta^{18}O_{sw}$ values between the Atlantic and Pacific Oceans.

5.5.1. Recrystallisation

There is the possibility that the reconstructed SSTs at Blake Nose are considerably lower than actual temperatures. Recrystallisation of foraminifer calcite at low temperatures is likely to have produced heavier $\delta^{18}O$ values (Killingley, 1983; Schrag *et al.*, 1995) and thus could potentially reduce estimates of SSTs at low latitudes by several degrees. Pristine foraminifera from Tanzanian clays record middle Eocene $\delta^{18}O$ values 2‰ lighter than those from marine oozes and chalks (Pearson, 2001). If indeed the Blake Nose samples have been affected by a 2‰ recrystallisation effect, this would give rise to $\delta^{18}O$ values of –1.8 to –4.4‰ PDB corresponding to SSTs of 26 to 38°C (assuming the degree of recrystallisation is constant). These SSTs are greater than those recorded in the mid Cretaceous by Norris and Wilson (1998). Surface water temperatures between 10 and 14°C greater than today have not been documented in any part of the geological record. The recrystallisation effect is therefore probably <2‰ PDB. It is also possible that differing degrees of diagenesis have also affected the record. However, the SEM images appear consistently recrystallised between intervals of both light and heavy $\delta^{18}O$ and there is no means for documenting the affects of diagenesis on the isotopic record for each sample. Despite not being able to quantify the effects of recrystallisation, the $\delta^{18}O$ shifts and thus comparable shifts in temperatures are believed to be a true record of Eocene climate variability.

5.6. Comparison with modern conditions at Blake Nose

Present day temperatures at Blake Nose range between 20°C and 28.5°C, with a mean value of 24°C (Bottomley *et al.*, 1990). Existing palaeotemperature equations reveal late middle Eocene SSTs to range between 16.8 and 28.8°C, with mean SSTs of 23°C (figure 5.4) when palaeolatitudinal dependent effects on $\delta^{18}O_{sw}$ are considered and ice volume taken into account. The temperatures reconstructed at Blake Nose are therefore, in parts of the record comparable to, or slightly cooler than present, by no more than 1 to 4°C depending on the $\delta^{18}O_{sw}$ value used.

Other palaeontological data support that SSTs at Blake Nose were comparable to today. Dinocyst assemblages from Site 1053 (van Mourik *et al.*, 2001) reveal middle Eocene conditions typical of warm to temperate surface waters. Cold-water species were absent suggesting that subtropical conditions continued in the middle Eocene and that northern water masses did not influence Blake Nose. Middle and late Eocene palynofloras from the Caribbean basin also indicate palaeotemperatures within the range of modern values (Graham, 2000). These temperatures are also comparable to the results of Tripati and Zachos (2000) and Andreasson and Schmitz (1996, 2000), who recorded middle Eocene SSTs between 14 and 28°C from tropical and temperate molluscan stable isotope profiles.

Whilst the SSTs reconstructed for the late middle Eocene at Blake Nose are comparable to modern day values at this site, SSTs are periodically significantly higher and substantially more variable than those recorded in previous planktonic foraminiferal studies from the middle Eocene (e.g. Keigwin and Corliss, 1986; Boersma *et al.*, 1987; Zachos *et al.*, 1994; Bralower *et al.*, 1995). Minimal planktonic foraminifera $\delta^{18}O$ values are regularly less than -1‰ PDB. These values are more typical in the early Eocene (e.g. Barrera and Huber, 1991; Zachos *et al.*, 1994; Bralower *et al.*, 1995), a period of pronounced warming. Blake Nose planktonic foraminiferal oxygen isotopic values lighter than -1‰ PDB suggest that there may have been several warming intervals during the middle Eocene.

5.7. Bottom water temperatures

The isotopic measurement of benthic foraminifera to reconstruct the surface to benthos isotopic gradient at Site 1052 is beyond the scope of this study. However, measurements of the benthic foraminifera *Nuttalides truempyi* were made from 77.48 to 89.57 mcd by Pälike *et al.* (unpublished data), which help to constrain the surface to benthos thermal gradient.

In modern benthic foraminifera it has been demonstrated that in certain species the stable isotopic composition is not in equilibrium with the surrounding seawater (Duplessy *et al.*, 1970; Shackleton, 1974; Woodruff *et al.*, 1980; Belanger *et al.*, 1981; Graham *et al.*, 1981; Shackleton *et al.*, 1984; Keigwin and Corliss, 1986; Zachos *et al.*, 1992). The recorded stable isotopic values of oxygen are reduced compared to the forecast equilibrium values (Boersma *et al.*, 1979). In many studies the measured oxygen isotope values are adjusted to account for this disparity. The proposed "correction factors" range from +0.35‰ to +0.6‰ (Shackleton *et al.*, 1984; Keigwin and Corliss, 1986; Kennett and Stott, 1990; Barrera and Huber, 1991; Zachos *et al.*, 1992, 1994). I have applied an adjustment of +0.4‰ (Shackleton *et al.*, 1984) to the measured $\delta^{18}O$ values of *Nuttalides* to account for the suspected species-specific non-equilibrium fractionation, and allow comparison with previous work. The corrected benthic foraminifera values are used in figure 5.6.

The results of Pälike *et al.* (unpublished data) are comparable to those at Site 1051 (Wade *et al.*, 2001) and fluctuate between 0.98 and 1.70‰, corresponding to palaeotemperatures of 7 to 11°C. These deep intermediate water temperatures are significantly higher than modern temperatures and are similar to intermediate and bottom water temperatures recorded in previous Palaeogene and Late Cretaceous studies (e.g. Boersma *et al.*, 1987; Barrera and Huber, 1991; Corfield and Norris 1996, 1998 and references therein; Lear *et al.*, 2000; Zachos *et al.*, 2001a).

5.8. Surface to benthos $\delta^{18}O$ and thermal gradient

The low amplitude oscillation in benthic foraminiferal $\delta^{18}O$ at sites 1051 and 1052 suggest that the large variations in surface water $\delta^{18}O$ are purely a surface water phenomenon and did not affect deep waters. Limited measurements of the thermocline dwelling *S. utilisindex* have been made (Appendix 1) and indicate that oxygen isotope results vary between –0.37 and +0.39‰ (figure 3.3). If the limited benthic and thermocline foraminifer isotope values are applied to the whole data set, this implies massive fluctuations in the $\delta^{18}O$ gradient. This is indicated in figure 5.6, which shows the composite oxygen isotope record against the astronomical time-scale. The mean thermocline values are shown as a dotted line, whilst benthic values are indicated by the blue shaded area.

The isotopic gradient between surface and deep-water periodically shifts from a minimum of 1.2‰ to a maximum of ~4.0‰, equal to thermal gradients of 4.8 to 16°C. There are periods when very light isotopic values are recorded and SSTs are up to 5°C warmer than today at 37.5, 37.65, 38.2, 38.4 and 39.3 Ma (figure 5.6). Here the $\delta^{18}O$ gradient is expanded (3‰), stratification is strong and thermal gradients are equivalent to 12°C. However, the vertical gradient is dramatically reduced to only 6°C (1.5‰) at 39.5, 39.1, 38.3 and 37.75 Ma. The periodic breakdown of the isotopic gradient from surface to deep waters is in response to variations in vertical stratification, reducing SSTs to 17°C.

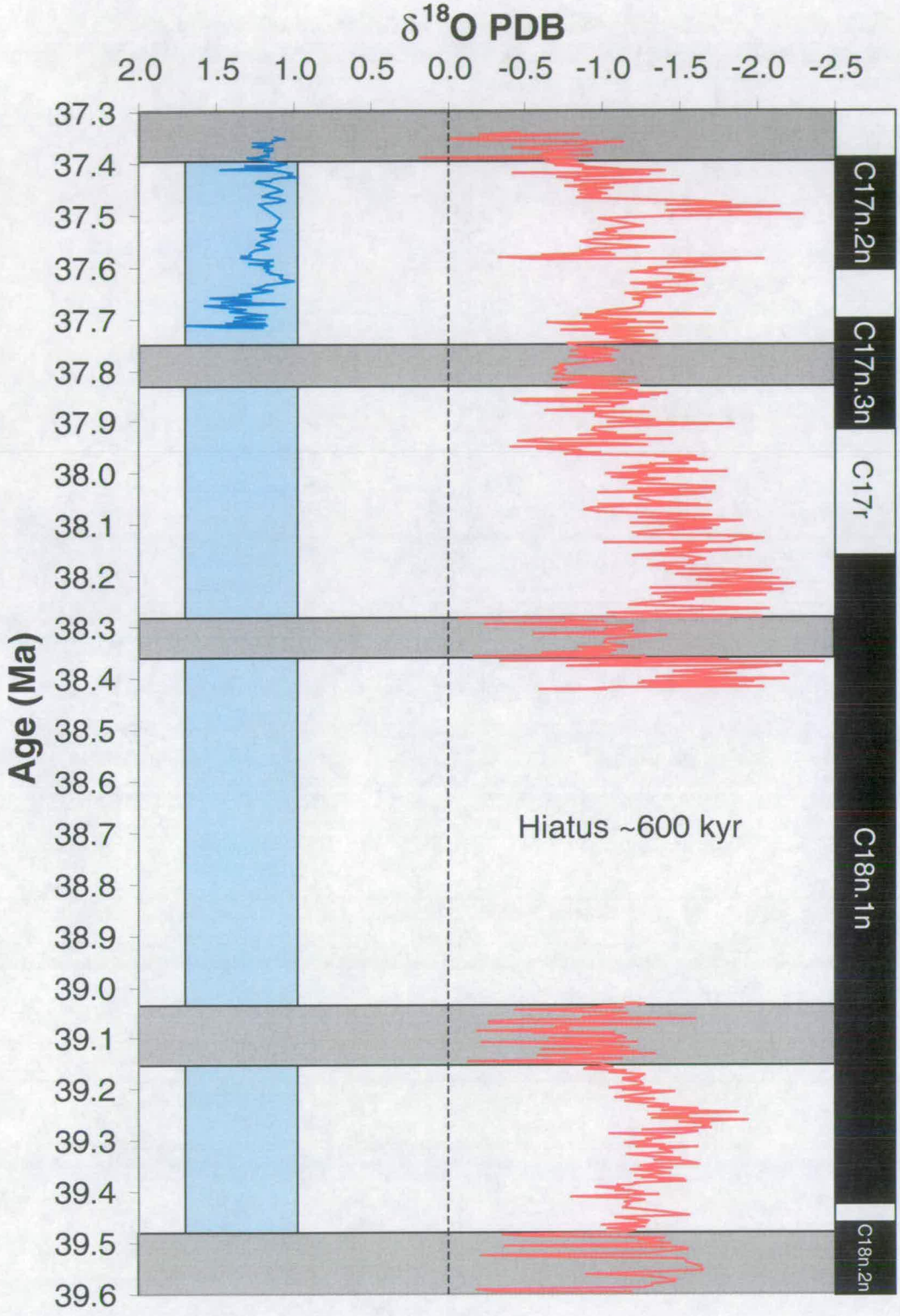

Figure 5.6. Middle Eocene oxygen isotope variability at Site 1052. Blue shaded area indicates the range of benthic foraminifer values. Hashed line = thermocline depth. Horizontal shaded areas indicate periods of intense upwelling where the vertical $\delta^{18}O$ gradient is reduced to 1.5 – 2.5‰ PDB. These events periodically occur every 400 kyr and last ~100 kyr.

5.9. Orbital cyclicity in thermal stratification

Fluctuation in sea surface $\delta^{18}O$ and the periods of weak thermal gradient, where mean SSTs were much cooler than today recurred with a 400 kyr cyclicity, (indicated by the shaded areas in figure 5.6) attributed to the long-term eccentricity cycle. During these intervals sea surface temperatures were periodically reduced by 2 to 6°C and the vertical temperature gradient over Blake Nose almost collapsed. The periods of inferred upwelling when heavy $\delta^{18}O$ are recorded are all 109 ± 8 kyr in duration. This ~100 kyr period of cold SSTs suggest that the modulation of precessional insolation by the short-term eccentricity cycle is also important. This regularity suggests that there is a periodic shift in the dominant climate signal, probably related to the modulation of solar insolation by the short-term eccentricity cycle.

5.9.1. Causes of thermal stratification breakdown

Water column stratification fluctuates every 400 kyr indicating that western North Atlantic oceanography was forced by the long-term eccentricity cycle. A possible explanation is that these abrupt shifts in surface water $\delta^{18}O$ and the collapse of the $\delta^{18}O$ gradient may represent an unstable water column, in response to orbitally forced intense upwelling that drives cold deep water to the ocean surface. Changes in temperature gradient or enhanced North American zonal wind stress forced by orbital variations in insolation may have given rise to periodic intense upwelling events and ~400 kyr cyclic collapse of water column stratification. The generally reduced surface to benthos temperature gradient in the Eocene compared to the present day may have facilitated the upwelling of deep water to the surface ocean. The upwelling hypothesis is favoured as it can account for the large variations in $\delta^{18}O$, the reduction of the thermal gradient and the high abundance of siliceous microfossils in the samples. By investigating longer time-series it may be possible to ascertain whether this 400 kyr variability was continuous or if this feature effectively was turned on and off. This will lead to significant further understanding of the climate system during warm climatic phases.

There is a disparity in the relationship between oxygen and carbon isotopic values within the planktonic foraminifer record. Whilst the fluctuations in the oxygen isotope record are consistent with an upwelling system, this contradicts the isotopic shifts seen in the carbon data. If the variations in surface water $\delta^{18}O$ reflected variations in upwelling, then one would expect to see positive shifts in $\delta^{18}O$ to be associated with negative shifts in $\delta^{13}C$, as deep water was upwelled to the surface. However, in this record the long-term trends in $\delta^{18}O$ and $\delta^{13}C$ are not controlled in the same way (chapter 4). This would suggest that upwelling is not the obvious cause of the $\delta^{18}O$ fluctuations and that some other factor could be held responsible. Variations in SST may also be caused by shifts in the subtropical gyre or inter-tropical convergence zone. These are discussed further in chapter 7.

One way to test the upwelling hypothesis is to use a secondary temperature proxy to document the magnitude of temperature change. Samples from Site 1052 12H have been analysed for alkenones by Tim Herbert (Brown University). Unfortunately no alkenones were found in the samples. Future work could involve the use of other geochemical proxies such as biogenic silica, where, in theory the biosiliceous content of the samples should increase during periods of enhanced upwelling as nutrient rich waters are brought to the surface ocean.

5.10. Summary

It is clear that the climate system in the late middle Eocene was highly fluctuating and dynamic, where modulation of solar insolation patterns by the long period eccentricity cycle can induce massive changes in vertical stratification and SSTs. The variations in insolation alone are too small to induce these large oceanographic shifts and feedback effects to climatic modulation must have been an important forcing factor.

1) The possible causes of the large oxygen isotope shifts are discussed. The required changes in ice volume or surface water $\delta^{18}O$ are considered too large to cause the recorded shifts in planktonic foraminifer $\delta^{18}O$.

2) It is concluded that temperature has the dominant role here and the dataset represents unstable SSTs during the middle Eocene.
3) SSTs have been reconstructed at Blake Nose using two different $\delta^{18}O_{sw}$ values.
4) SSTs range between 17 and 29°C when latitudinal changes in $\delta^{18}O_{sw}$ are considered.
5) Rapid and abrupt fluctuations in SSTs are evident of up to 12°C.
6) There are periodic intervals when SSTs were up to 5°C greater than modern suggesting greenhouse conditions returned to the subtropics.
7) Heavy $\delta^{18}O$ values periodically occurred with a 400 kyr cyclicity. These intervals are all ~100 kyr in duration and caused SSTs to cool by 2 – 6°C.
8) The collapse of the vertical temperature gradient is attributed to periodically intense upwelling events.

6. THE EXTINCTION OF MURICATE PLANKTONIC FORAMINIFERA AND CAUSES OF THE LATE MIDDLE EOCENE BIOTIC TURNOVER

6.1. Introduction and previous work

The muricate† genera *Morozovella* and *Acarinina* are abundant and diverse within Palaeocene and Eocene sediments. The diversity of the muricate group decreased throughout the middle Eocene and all muricate forms were extinct by the Eocene / Oligocene boundary. A major faunal turnover in planktonic foraminifera occurred during the late middle Eocene (magnetochron C17n.3n) which saw the extinction of the *Morozovella* lineage and a major decline in the *Acarinina* lineage. The final extant members of the *Morozovella* genus were *M. spinulosa* and *M. crassata*. Other marine and terrestrial faunal and floral groups also indicate a biotic turnover around this time (Prothero, 1994). Extinctions at the Bartonian / Priabonian boundary have been found in land mammals, terrestrial pollen and whales. The majority of species becoming extinct around this time were highly diversified tropical species (Berggren and Prothero, 1992), suggesting a causal link between climatic deterioration and biotic turnover.

Whilst research has established that the muricate forms were the dominant surface dwelling group during the middle Eocene with probable algal symbionts (Pearson *et al.*, 1993; D'Hondt *et al.*, 1994; Norris, 1998), the reason for the extinction of the muricate planktonic foraminifera genus *Morozovella* has not previously been studied at a high-resolution. Previous workers (e.g. Toumarkine and Luterbacher, 1985) have noted that the extinction was abrupt though the exact timing of events was not known. The excellent recovery and chronostratigraphic framework for Site 1052 present the opportunity to investigate whether the extinction of the *Morozovella* genus was in response to Eocene climatic deterioration and allows the rate and

† Type of planktonic foraminifera wall structure, consisting of short multiple projections from the test surface (Blow, 1979).

timing of planktonic foraminifera extinction to be documented. The stable isotopic analysis of several species of planktonic foraminifera permits the structure of the Eocene ocean to be determined. This work details the middle Eocene extinction of morozovellids at a high temporal resolution (3 kyr sampling) and thus enables the rate and timing of biotic turnover to be defined and an understanding of climatic / oceanographic change at this time.

6.2. Methods and procedures

Stable isotope analyses have been conducted on six species of planktonic foraminifera, before, during and after the extinction events. These were the mixed layer dwellers *Morozovella crassata, Morozovella spinulosa*, *Acarinina praetopilensis* and *Globigerinatheka mexicana* and the thermocline dwellers *Turborotalia cocoaensis and Subbotina utilisindex*. This was to investigate the timing and origin of the extinction in response to palaeoceanographic history and climatic change. Other acarininids such as *A. rohri* were present within the samples at Site 1052, but these were too rare to be considered for isotopic and biostratigraphic examination.

6.3. Objectives

- Examine if biotic changes occur gradually or in a step-wise fashion through this interval.
- Document SST variation, palaeoceanographic state and sedimentation regimes during the decline and extinction of *Morozovella*, to assist its interpretation.

6.4. Isotopic results across the extinction events

6.4.1. Oxygen isotope results

The results of isotopic analyses are illustrated in figure 6.1. There is a large scatter in the *Morozovella spinulosa*, *M. crassata* and *Acarinina praetopilensis* oxygen isotope record close to the last occurrence of these species (figure 6.1a). *Morozovella* oxygen isotope values vary between –0.7 and –1.4‰, whilst *Acarinina* values are generally heavier and range from 0.0 to –1.7‰. The $\delta^{18}O$ values of *G. mexicana* are lighter than *A. praetopilensis* in most samples and range between –0.4 and –0.8‰. Oxygen isotope values of *Turborotalia cocoaensis* vary between –0.1 and –0.5‰ and *Subbotina* oxygen isotope values range from –0.4 to +0.4‰. There is a general increase in the *Subbotina* $\delta^{18}O$ values over time, although the time series here is not of great enough length to determine if this was a long-term climatic trend in the structure of thermocline. Bulk carbonate oxygen isotope values fluctuate between 0.5 and 0.9‰.

6.4.2. Carbon isotope results

Carbon isotope results from *Morozovella* and *Acarinina*, like those of oxygen, show a large variability (~1.2‰) close to the extinction event (figure 6.1b) and range from 2.2 to 3.4‰. *G. mexicana* $\delta^{13}C$ values are lighter than those of *Morozovella* and *Acarinina* but heavier than the thermocline dwellers and range from 1.9 to 2.4‰. The $\delta^{13}C$ values recorded by *Subbotina utilisindex* and *Turborotalia cocoaensis* are very similar to each other and vary between 1.0 and 1.7‰ PDB.

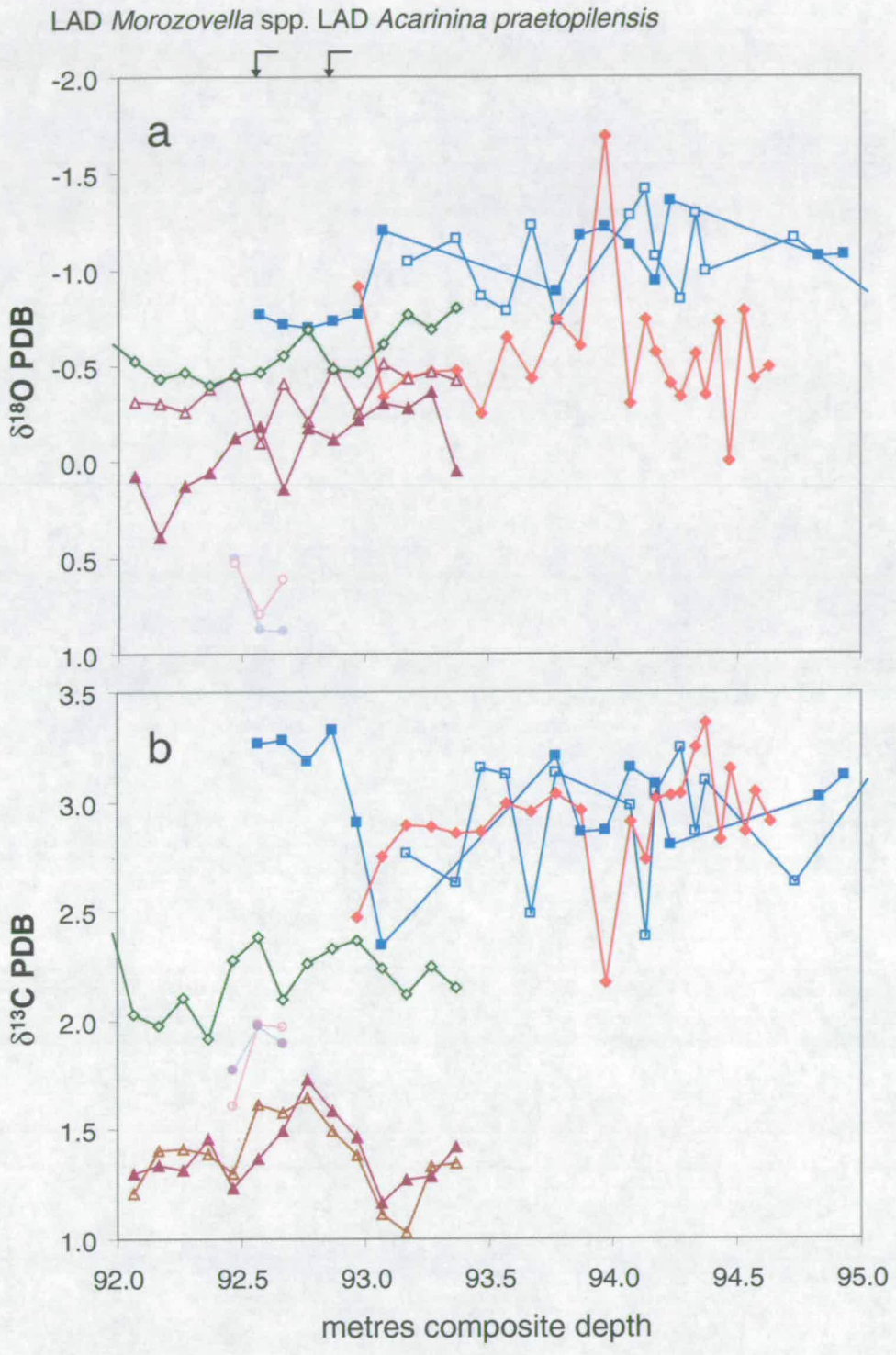

Figure 6.1. Stable isotope results of various species over the extinction of *Morozovella* and *Acarinina*. (a) Oxygen isotope results; (b) Carbon isotope results. ■ = *Morozovella crassata*; □ = *Morozovella spinulosa*; ♦ = *Acarinina praetopilensis*; ◇ = *Globigerinatheka mexicana*; ▲ = *Subbotina utilisindex*; △ = *Turborotalia cocoaensis*; open and filled circles = bulk carbonate results. LAD = last appearance datum.

6.5. Origin of the extinction events

6.5.1. Timing of events and qualitative observations

The timing of the extinction events is listed in table 2.5 (chapter 2). *Acarinina praetopilensis* does not terminate at the same horizon as *Morozovella* spp. The temporal difference between the last occurrence (LO) of *A. praetopilensis* (37.810 Ma) and *Morozovella* spp. (37.802 Ma) is only 8 kyr (30 cms), therefore only localities with a high sedimentation rate and high sampling intervals will exhibit this elsewhere.

The extinction of *Acarinina praetopilensis* does not represent the LO of the acarininid genera. Qualitative observations also reveal dwarfing of *Acarinina* spp. and small acarininid forms (Plate 4) continue in the <125 μm size fraction to the top of the studied interval (77.18 mcd). This process of dwarfing, referred to as terminal progenesis (*sensu* Glenister and Furnish, 1988), is probably related to environmental stress and was also documented with the extinction of *M. velascoensis* (Kelly *et al.*, 2000) in the late Palaeocene. Large acarininids were not seen in the >250 μm size fraction beyond 92.87 mcd. The LO of the large *A. praetopilensis* therefore represents a significant change in the biota that should be correlative elsewhere. There are two types of acarininid present in the 63 – 125 μm size fraction beyond 92.87 mcd, those with four and those with five chambers. Further work could investigate if these forms propagated in middle Eocene sediments before the extinction events at 92.87 mcd.

Qualitative observations indicated a decline in the abundance of *Morozovella* spp. from 110 mcd (38.30 Ma), 500 kyr before the extinction at 37.802 Ma. This suggests a period of increased ecological stress for the morozovellids. However, qualitative observations did not indicate a decline in the abundance of *Acarinina* spp. suggesting that the extinction of the larger *Acarinina praetopilensis* was abrupt. Future quantitative analysis could examine this more fully.

Plate 4. Middle Eocene specimens of *Morozovella* and *Acarinina*. Specimens (a) – (e) are from the 250 – 355 μm size fraction and scale bar represents 100 μm; Specimens (f) – (h) are from the 63 – 125 μm size fraction and scale bar represents 50 μm.

(a) **(b)** and **(c)** *Morozovella spinulosa* umbilical views, from samples 171B, 1052B, 11H-4, 103 – 106 (92.67 mcd); 171B, 1052B, 13H-4, 103 – 106 (113.10 mcd) and 171B, 1052F, 14H-6, 103 – 106 (131.01 mcd) respectively.

(d) *Acarinina praetopilensis* umbilical view, from sample 171B, 1052B, 14H-4, 23 – 26 (121.30 mcd).

(e) *Acarinina praetopilensis* spiral view, from sample 171B, 1052B, 14H-4, 23 – 26 (121.30 mcd).

(f) Dwarfed acarininid umbilical view, from sample 171B, 1052F, 10H-4, 73 – 76 (88.01 mcd).

(g) Dwarfed acarininid umbilical view, from sample 171B, 1052F, 10H-4, 73 – 76 (88.01 mcd).

(h) Dwarfed acarininid spiral view, from sample 171B, 1052F, 10H-4, 73 – 76 (88.01 mcd).

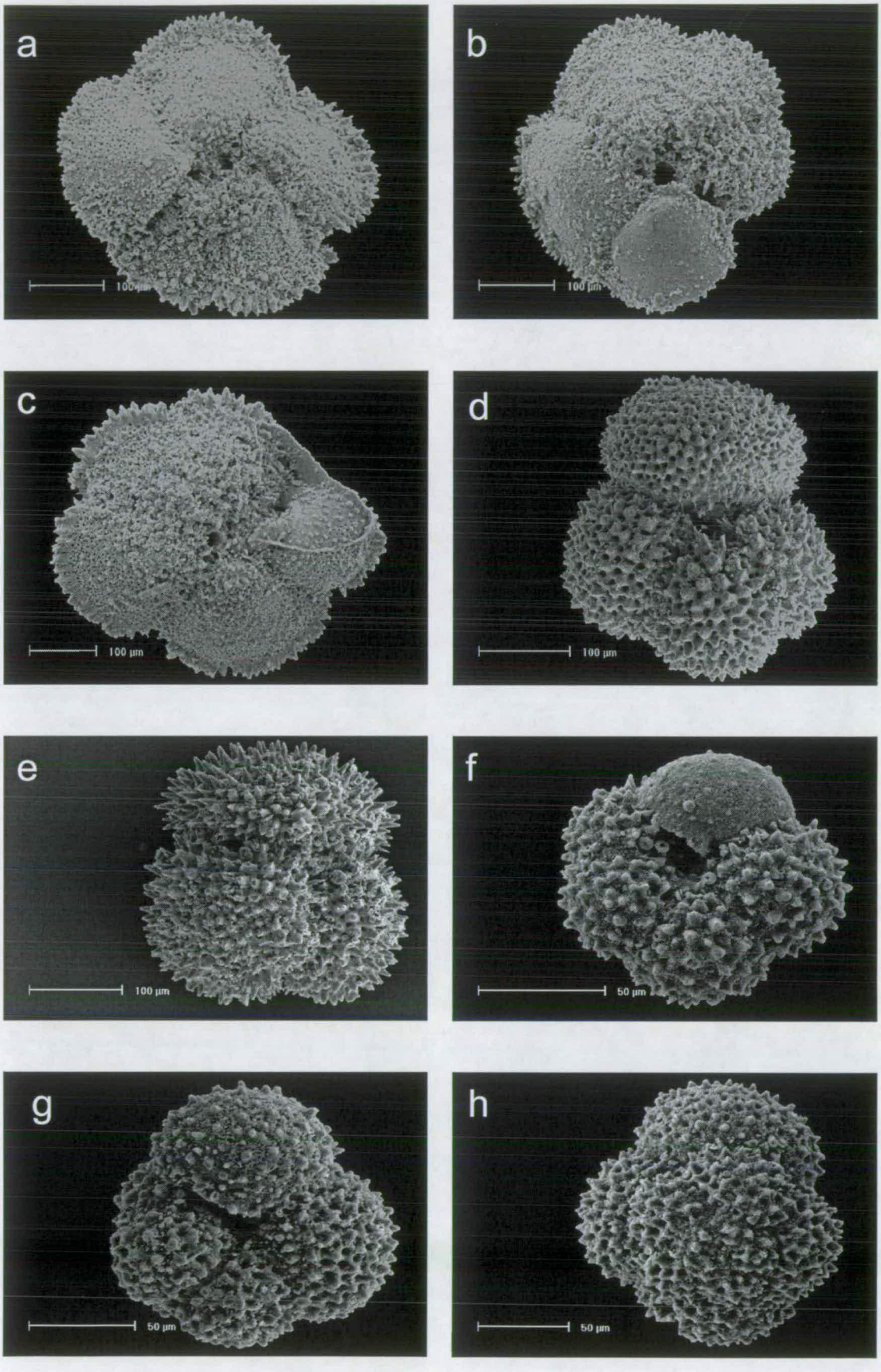
a
100 µm
b
100 µm
c
100 µm
d
100 µm
e
100 µm
f
50 µm
g
50 µm
h
50 µm

6.5.2. Temperature

The morozovellids typically record the lightest $\delta^{18}O$ values and heaviest $\delta^{13}C$ values compared to other Eocene planktonic foraminifera (figure 3.5). Surface dwelling warm water adapted species were the primary ecological group that declined or terminated in the latest middle Eocene (Keller *et al.*, 1992). The extinction of the muricate genera has therefore often been linked with decreasing SSTs and global cooling (Keller, 1983; Boersma and Premoli Silva, 1991; Keller *et al.*, 1992; Pearson, 1996).

The extinction of the surface water group without a decline in forms that inhabited deeper waters does suggest that either surface water cooling or nutrification were a dominant forcing factor. The highly fluctuating $\delta^{18}O$ values of surface dwelling planktonic foraminifera indicates considerable variation in SSTs and middle Eocene subtropical climate. Although both *Morozovella* and *Acarinina* go extinct during a cooling trend and within an SST low (inferred from the increasingly heavy $\delta^{18}O$) (figure 3.3), there is no major cooling or climatic shift associated with the extinction events and the oxygen isotope values are not heavier than those 471 kyr earlier at 109 mcd (figure 3.3). This suggests that surface water cooling was not the primary forcing factor for the extinction of these species. The data here do not support ideas that decreases in SST caused the extinction events and surface water cooling alone therefore cannot account for the extinction of the morozovellids and the demise of the acarininids.

The extinction of the morozovellids may have been due to the reduced thermal stratification, as suggested by Cifelli (1969). The extinction of *Morozovella* and the large acarininids at Blake Nose corresponds with an interval of reduced SSTs and thermal gradient related to the 400 kyr cycle (figures 5.4 and 5.6). The periodic reduction of the vertical thermal gradient will have caused the repeated disturbance of marine habitats. Perhaps heightened upwelling attributed to the 400 kyr eccentricity cycle resulted in disruption of the water column that removed the niche occupied by the morozovellids. However, this reduction in SSTs was no more severe than former SST minima at 110, 115 and 130 mcd (figure 5.4) and the question still

remains of why morozovellids did not go extinct earlier during the inferred strong upwelling events at 38.3, 39.1 and 39.5 Ma (figure 5.6). It is also difficult to apply this hypothesis on a global scale. Further detailed work investigating stratification in the Pacific Ocean is required.

The restriction of marine habitats may have been a contributing / causal factor to the extinction events. The decrease in water column stratification is primarily caused through the reduction in surface water temperatures. This will have diminished planktonic habitats in the depth domain. At 83 mcd a period thought to reflect strong stratification, the isotopic gradient between *G. mexicana* and *S. utilisindex* is ~1.4‰ (figure 3.3). However, the upwelling of deep water to the surface ocean causes the entire fauna to occupy the same cooled water mass (Kroon and Ganssen, 1989) and the isotopic gradient is compacted to 0.5‰ at 93 mcd, a period thought to have experienced intense upwelling. The increased environmental stress caused by the periodic reduction of habitat may have led to their demise. Future work on these specimens may involve the reconstruction of a thermocline record to investigate this further. Global cooling also decreased morozovellids habitat by the reduction of tropical and subtropical biogeographical provinces. High-resolution data from tropical regions of the Atlantic may reveal that morozovellids migrated to low-latitudes and continued beyond 37.8 Ma.

Like modern day *Globigerinoides ruber*, *Morozovella* spp. may have lived all year round. There is growing evidence of increased seasonality during the Eocene (e.g. Kobashi *et al.*, 2001). The greater mean annual temperature range would create a harsher climatic environment with greater extremes between summer and winter. Evidence of extreme seasonality, with seasonal temperature variations of up to 11.7°C, have been recorded in isotopic and palaeobotanical data from the Bighorn Basin (early Eocene) by Wing *et al.* (2000) and in the Gulf of Mexico by Kobashi *et al.* (2001). If seasonality were enhanced at this time it would require species to be more tolerant of temperature extremes and this may have contributed to the extinction events.

6.5.3. Habitat destruction, productivity and nutrification

The termination of the *Morozovella* lineage may have been in response to habitat destruction (Hallock *et al.*, 1991; Keller *et al.*, 1992), interspecies competition or environmental modifications (Pearson, 1996). This could have been due to upwelling or changes in the latitudinal thermal gradients. Allmon (2001) concluded that nutrient conditions were a prominent forcing factor in patterns of extinction in the western North Atlantic during the late Cenozoic. There is evidence of eutrophication of surface waters in the latest middle and late Eocene, with a greater range of upwelling provinces (Boersma *et al.*, 1987) and abundant biosiliceous sediments throughout the Gulf of Mexico and equatorial and subtropical Atlantic (Berger and Von Rad, 1972; McCoy and Zimmerman, 1977; Tucholke and Vogt, 1979; Premoli Silva and Boersma, 1986; Ehrmann and Thiede, 1986). If upwelling occurred at Blake Nose, this would require species to have adapted to varying temperatures and nutrient levels. Both *Morozovella* and *Acarinina* probably possessed algal symbionts (Pearson *et al.*, 1993; D'Hondt *et al.*, 1994; Norris, 1998) and were therefore more likely to thrive in oligotrophic conditions. Their demise may have been in response to increased nutrification that allowed other asymbiotic taxa, such as *Subbotina* and *Hantkenina* to occupy the mixed layer and thrive (Coxall *et al.*, 2000), and possibly outcompete *Morozovella*. Long-term variations in trophic resources caused by the initiation of the cryosphere may be a strong contributing factor. The loss of oligotrophic habitats will have affected competition and trophic resources for many marine organisms.

The reason for the extinction of these species therefore remains enigmatic. It is probably the result of a number of environmental and genetic factors and it is not possible to identify the driving force for the extinction events from isotopic data alone. Previous work (e.g. Cifelli, 1969; Lipps, 1970, 1986; Keller *et al.*, 1992) has suggested that the biotic turnover was attributed to global cooling and habitat destruction. The data obtained from Site 1052 indicate that habitat destruction caused by increased upwelling and surface water eutrophication may have been a primary forcing factor. Further work could involve the examination of the photosymbiotic relationships in *Morozovella* and *Acarinina* spp. to see if this changed over time or

deteriorated towards the extinction events. Quantitative abundance variations, particularly during the 400 kyr prior to the extinction, will enhance the understanding of diversity changes associated with ecological stress. A longer record of the thermocline or other mixed layer species is required to determine whether the structure of the water column changed significantly at this time. The examination of the extinction events at one location cannot explain the global extinction of *Morozovella* and the large acarininids. Further high-resolution work is required to constrain the timing of extinction events elsewhere (e.g. high-latitudes and the equatorial Pacific) and to investigate oceanic stratification at this time.

6.6. Summary

1) Stable isotopic examination was conducted on six species of planktonic foraminifera around the extinction events.
2) *Morozovella crassata* and *Morozovella spinulosa* terminate at the same horizon whilst *Acarinina praetopilensis* terminates 8 kyr before *Morozovella* spp.
3) Qualitative observations indicated a decline in the abundance of *Morozovella* spp. from 500 kyr before the extinction.
4) Dwarfed acarininid forms are present in the smaller size fractions after the extinction events.
5) Isotopic investigations could not reveal the cause of the extinction events but environmental stress caused by increased nutrification, habitat destruction and / or upwelling are suspected.

7. IMPLICATIONS AND MECHANISMS OF EOCENE CLIMATE CHANGE

7.1. Eocene climate instability

High-resolution (3 kyr) stable isotopic records were generated for a 2.3 myr interval spanning the latest middle Eocene from Site 1052. This data is necessary to understand the character and dynamics of the Eocene climate system and its response to orbital forcing. Most Palaeogene records do not have the required resolution to fully determine the short-term climatic signals and events. The consequence of inadequate sampling resolutions is that little is known about climatic variations in the Eocene and the stability of the climate system during intervals significantly different from the present day.

This study provides the first detailed chronology of climatic and oceanographic change during the latest middle Eocene. The main findings are the high amplitude shifts seen in $\delta^{18}O$ and $\delta^{13}C$ records of middle Eocene surface waters. The amplitude of isotopic variation is massive, suggesting a highly changeable and unstable climatic – oceanographic system. This variability is greater than that seen in open ocean Pleistocene records and has significant implications for climate system of the middle Eocene.

The forcing mechanisms behind these large and rapid shifts in $\delta^{18}O$ in a greenhouse world are not presently understood. Recent work by Lear *et al.* (2000) has constrained long-term ice volume changes in the Eocene, but this cannot account for the large variations seen in the planktonic foraminifera $\delta^{18}O$ record. As ice volume effects in the middle Eocene are generally believed to be modest, the changes in $\delta^{18}O$ in the tests of planktonic foraminifera are thought to primarily reflect temperature variations with some salinity effects on the ambient seawater ($\delta^{18}O_{sw}$). Feedback effects and threshold boundaries in the oceanic-atmosphere system that can abruptly shift ocean temperature or circulation are suggested by the large and rapid shifts in $\delta^{18}O$. There are several

hypotheses that could account of large amplitude temperature shifts at Blake Nose. These include changes in oceanic circulation, atmospheric transport, upwelling intensity and nonlinear responses to orbital insolation (discussed below).

7.2. Mechanisms to induce the high amplitude isotopic variations

7.2.1. Atmospheric transport

There is strong evidence that atmospheric and oceanic circulation were quite different during the Eocene from today (Rea *et al.*, 2000) and that the inter-tropical convergence zone may have been more than 20° north of the equator (Rea, 1994). General circulation model (GCM) experiments (e.g. Sloan and Morrill, 1998; Bice *et al.*, 2000b; Sloan and Huber, 2001b) predict large changes in atmospheric transport over Blake Nose and indicate that during the early and middle Eocene, Northern Hemisphere atmospheric thermal transport may have been more vigorous than today (if tropical SSTs were high). This may have caused large changes in wind-driven upwelling due to wind stress curl. The location and strength of the Atlantic storm track and the Hadley cell may also have implications at this site. The increased role of atmospheric heat transport would also supply heat to the high latitudes and provide a mechanism for Eocene high-latitude warming and the reduced meridonial thermal gradient. Figure 7.1 shows the possible changes in Eocene atmospheric transport. There are large variations in both the strength and direction of wind vectors in the Blake Nose region.

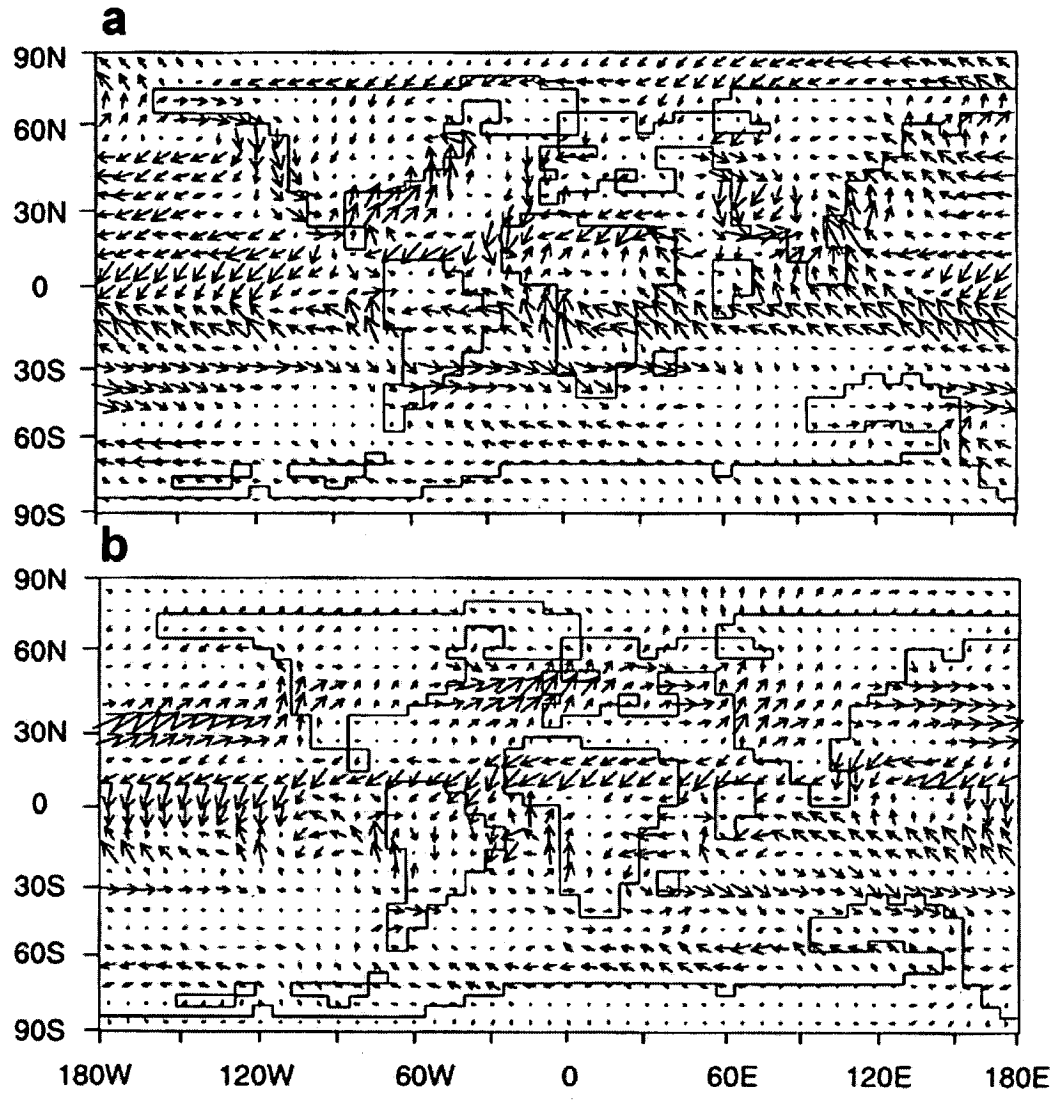

Figure 7.1. Changes in the strength and direction of atmospheric transport during the Eocene as predicted by Sloan and Morrill (1998). (a) summer; (b) winter. Orbital parameters were set to maximum Northern Hemisphere summer solar radiation.

7.2.2. Monsoonal climate variability

There is increasing evidence of the importance of heat and vapour transport in climate fluctuations. Modeling results by Crowley *et al.* (1992) suggested that the origin of eccentricity fluctuations in pre-Pleistocene sediments may be due to low-latitude monsoonal fluctuations. Monsoonal climatic variability could cause the large temperature changes in the Eocene ocean. This is invoked by variations in the location and distribution of maximum solar heating and wind convergence. Sloan and Morrill (1998) showed that seasonal insolation forcing had a large thermal response on the North American continent during the early Eocene. If large temperature variations took place on the North American continent in response to orbital forcing, in combination with increased zonal wind stress, this may have given rise to a more monsoonal type of climatic regime and thus enhanced upwelling events on the eastern American margin. The modulation of this monsoonal system by precessional and eccentricity forced variations in solar insolation could have given rise to the fluctuations recorded in $\delta^{18}O$ and $\delta^{13}C$ at Blake Nose. The orbitally controlled monsoonal wind systems may have altered the upwelling patterns and/or freshwater input, which are recorded in the marine record.

7.2.3. The hydrological cycle and continental runoff

It is possible that the importance of changes in the hydrological cycle have previously been downplayed. During a greenhouse period, such as the Eocene the higher sea level would have given rise to a greater availability of moisture supply (Barron *et al.*, 1989). This, combined with greater latent heat transport via the atmosphere, could effectively change $\delta^{18}O_{sw}$. The hydrological cycle is likely to be influenced by orbital variations in solar insolation, perhaps particularly so during ice-free periods. Water vapour is an important greenhouse gas that is sensitive to variations in SSTs and could enhance orbitally forced temperature changes (Herbert, 1997). The Eocene climatic simulation of Sloan and Huber (2001b) indicates a large (32%) change in precessionally forced

continental runoff from the eastern North American coast. The large changes in the magnitude of runoff variability may have influenced the isotopic records by providing periodically large amounts of freshwater and nutrient flux into the marine environment.

7.2.4. Fluctuations in oceanic circulation

Another possible cause of the isotopic shifts is orbital changes in gyre circulation. If there were large variations in the $\delta^{18}O_{sw}$ of differing water masses, then periodic shifts in the dominant water mass over Blake Nose could account for the variations in foraminifera $\delta^{18}O$. Figure 7.2 indicates possible surface water circulation patterns in the western North Atlantic. It is the specific salinities and temperatures of these surface currents that could give rise to the fluctuations recorded by the planktonic foraminifera at Blake Nose. Periodic shifts in the dominant surface current over Site 1052 would therefore be reflected in the $\delta^{18}O$ signatures of planktonic foraminifera. This hypothesis would also help to explain the differing signals in $\delta^{18}O$ and $\delta^{13}C$. The reason that $\delta^{13}C$ does not indicate the 400 kyr long period eccentricity signal, which strongly controls the $\delta^{18}O$ record (chapter 4), could be due to differing water masses which although having distinct $\delta^{18}O$ signals, having similar $\delta^{13}C$ signatures.

However, for this mechanism to achieve the large variations recorded in $\delta^{18}O$, significant differences are required between the properties of these surface currents. The magnitude of variation required is large and one current would either need to be some 6°C cooler, or have a salinity difference of 4‰. This variation is large and within an open ocean setting it is therefore difficult to account for isotopic variations by this means.

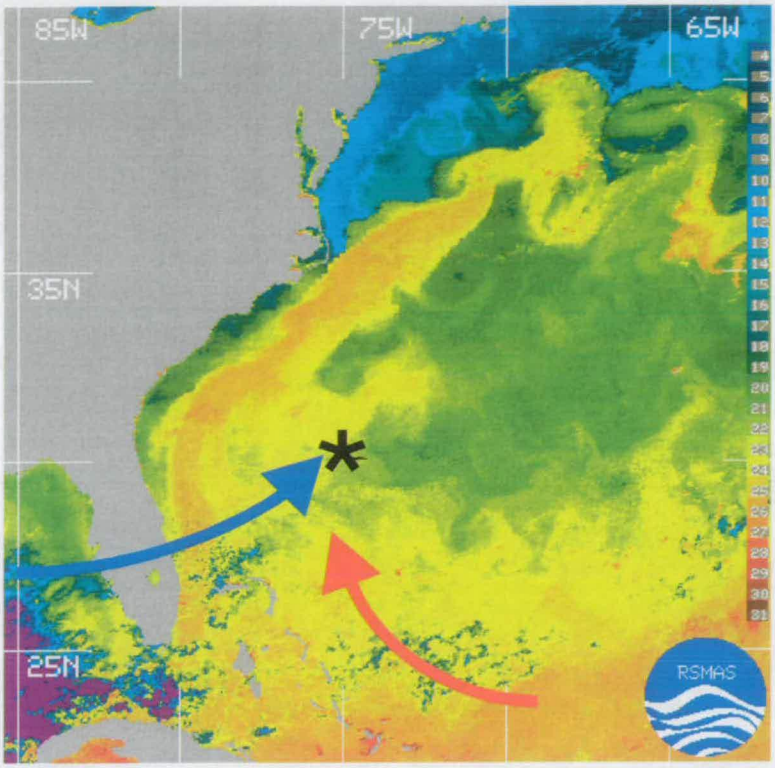

Figure 7.2. Modern SSTs in the western North Atlantic – May 2001 (modified from Rosenstiel School of Marine and Atmospheric Sciences). ✶ = location of Blake Nose. Arrows indicate the possible positions of palaeocurrents that influenced Site 1052. → = Gulf Steam; → = gyre current. Note, this is present day geography, not Eocene palaeogeography.

7.2.5. Upwelling

A shift in the location and intensity of the mid latitude atmospheric pressure system with a strong south-westerly airflow could have resulted in Ekman driven or monsoonal upwelling and induced stratification break down. Climatic modeling results for the early Eocene (e.g. Bice *et al.*, 2000b; Huber and Sloan, 2000; Sloan and Huber, 2001a, 2001b) predict intense Ekman driven upwelling along the eastern North American margin, which was highly sensitive to precessional forcing of solar insolation (figure 7.3). The eccentricity cycles may then modulate and periodically intensify this upwelling system. If the $\delta^{18}O$ profile of planktonic foraminifera reflects temperature alone, then the orbital variations in stable isotopic data may be the result of upwelling variability. Dramatic

intensification of this upwelling every 400 kyr causes complete water column stratification breakdown and the advection of deep water to the surface ocean. Less upwelling would have occurred when wind directions were north-easterly (like today) resulting in prominent stratification. The upwelling hypothesis is supported by periodic decreases in the thermal gradient (figure 5.5), which was also seen at Site 1051A (Wade *et al.*, 2000). Future climatic modeling work could investigate the eccentricity modulation and its effects on atmospheric and oceanic circulation.

Several other lines of evidence also point to large changes in temperature and/or nutrient levels in the Eocene Blake Nose region. The high abundance of radiolarians at this site is characteristic of a productive environment. The coccolith assemblage data (Mita, 2001; Belcher pers. comm.) are also indicative of a eutrophic and rapidly fluctuating environment. Oscillations in the percentage of the coccolith genus *Discoaster* (a warm and oligotrophic genus) and *Reticulofenestra* (a cold and eutrophic genus) confirm the large variability in SSTs and/or nutrient levels (figure 7.4).

Oceanic overturning is also a means by which surface waters could be cooled. However, to induce large scale overturning, density changes in the surface waters by either cooling or salinity are required. Although the density of surface and deep waters is unknown, the magnitude of temperature and salinity variation required was probably large. It is more likely that upwelling caused stratification to break down and resulted in overturning, rather than overturning being a causal mechanism.

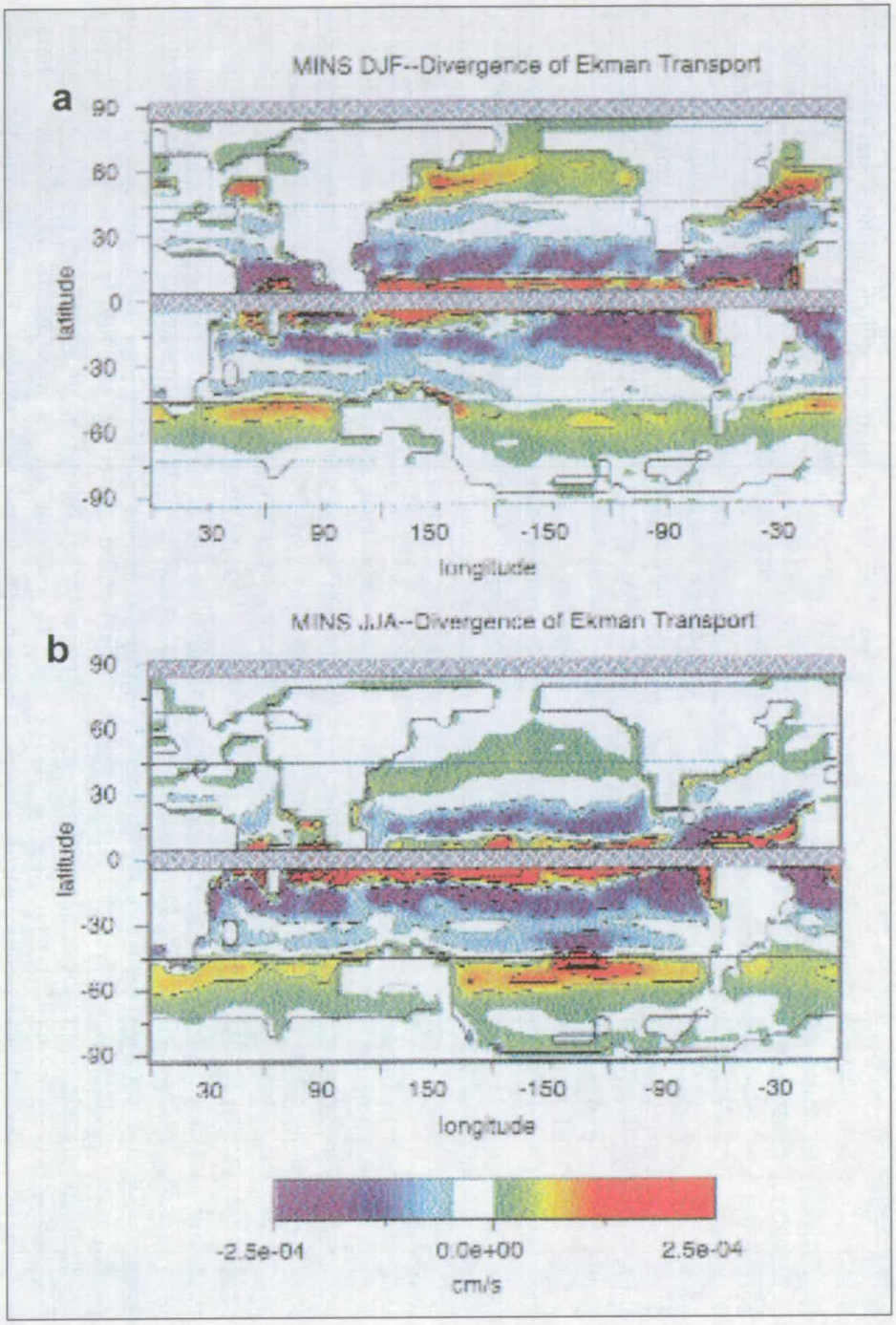

Figure 7.3. Areas of wind-driven upwelling as predicted by climatic modeling studies of the Eocene. (a) Winter simulation (b) Summer simulation (Sloan and Huber, 2001b).

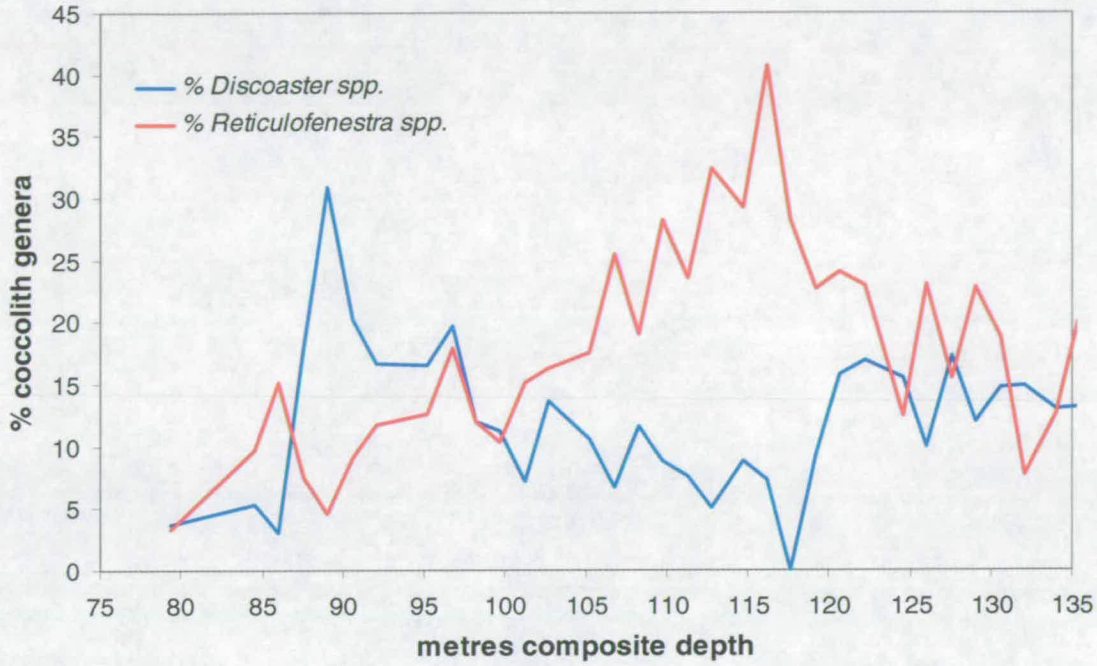

Figure 7.4. Percentage of the coccolith genera *Discoaster* and *Reticulofenestra* at Site 1052. Data from Mita, 2001.

7.3. Orbitally forced climate dynamics

Fourier analysis shows the presence of Milankovitch frequencies in the stable isotopic and Munsell hue records from Blake Nose. Power is concentrated in the eccentricity (~400 and 100 kyr) bands within the stable isotope records (chapter 4), whilst the precessional period (19-23 kyr) dominates the Munsell hue record (chapter 2). The results suggest that orbital variations in solar insolation are a large part of climatic variability during the Eocene transition period.

7.3.1. Precessional forcing of the sedimentary record

Precessional forcing of the colour record indicates that variations in low-latitude solar insolation were particularly important in the middle Eocene subtropical Atlantic. Sloan and Huber (2001b) indicated that SSTs, upwelling, marine productivity, continental

runoff and moisture balance were all sensitive to precessional variations in solar insolation in the western North Atlantic. The precessional frequencies in the colour record at Site 1051 (Wade *et al.*, 2001) and Site 1052 (chapter 2; Pälike *et al.* 2001), may be related to precessionally forced variations in carbonate productivity, continental runoff or atmospheric transport.

7.3.2. Eccentricity forced climate variations

The long-period eccentricity signal governs the large-scale fluctuations in middle Eocene SSTs and facilitates significant changes oceanic stability (chapter 5). The water column appears to have an increased response to the long-term modulation of insolation by the Earth's orbit at this time. The 400 kyr cycle is not common in Pliocene and Pleistocene records but has been recognised in many proxy records from the geological record, ranging from Triassic to Miocene age (e.g. Pisias *et al.*, 1985; Woodruff and Savin, 1991; Flower and Kennett, 1993; Zahn and Diester-Haass, 1995; Olsen and Kent, 1996; Zachos *et al.*, 1996; Shackleton and Crowhurst, 1997; Shackleton and Hall, 1997; Paul *et al.*, 2000; Zachos *et al.*, 2001b). This indicates that the long-term eccentricity cycle has been very pervasive in modulating the climatic system of the past. Why is this long-term eccentricity signal so common in older sediments but not in more recent records? Paul *et al.* (2000) have suggested that oceanic gateways at high and low latitudes may have been responsible. The lack of association between $\delta^{18}O$ and $\delta^{13}C$ at this periodicity (discussed in section 7.3.3) suggests that the enhanced 400 kyr signal in older sediments is not a response to high levels of atmospheric CO_2, as suggested by Zachos *et al.* (2001b).

The modulation of the climate system by eccentricity is significant. The cause of the prominent 100 kyr cycle in Pleistocene records is unknown and most theories involve internal feedbacks to ice volume (e.g. Imbrie *et al.*, 1993), which cannot be applied to the greenhouse conditions of the Eocene. The changes in solar insolation caused by the

eccentricity of the Earth's orbit are small (Berger *et al.*, 1992). However, eccentricity modulates the precessional variations in insolation and through this means can produce significant impacts on the climate system. These effects are probably generated from nonlinearities within the climatic system to precessional forcing, which amplify the eccentricity signal, rather than directly from eccentricity variations in solar insolation.

7.3.3. The uncoupled climate and carbon systems

Whilst the $\delta^{18}O$ record has significant 400 kyr oscillations, the long period eccentricity cycle was not evident in the planktonic foraminifera carbon isotopic record. The differences in the cyclicity of the $\delta^{18}O$ and $\delta^{13}C$ records are illustrated in figure 7.5. Here, oxygen and carbon isotopic results are plotted against the astronomical time-scale. As in figure 5.6, the horizontal shaded areas indicate the periodically heavy $\delta^{18}O$ values. Whilst the shifts in $\delta^{18}O$ are dramatic during these events, no obvious changes occur within the $\delta^{13}C$ record.

These findings are in contrast to results from the Oligocene / Miocene (Zachos *et al.*, 1997, 2001b; Paul *et al.*, 2000) where the long-term eccentricity cycle was found in both $\delta^{18}O$ and $\delta^{13}C$ deep sea signatures. The lack of the 400 kyr signal in the carbon isotopic record suggests that the climatic and carbon systems were uncoupled during the middle Eocene. The forcing mechanisms and feedback effects that dominate the climatic signal were not influencing carbon cycling and indicate that it is not simple atmospheric warming and cooling that caused the variations in SSTs.

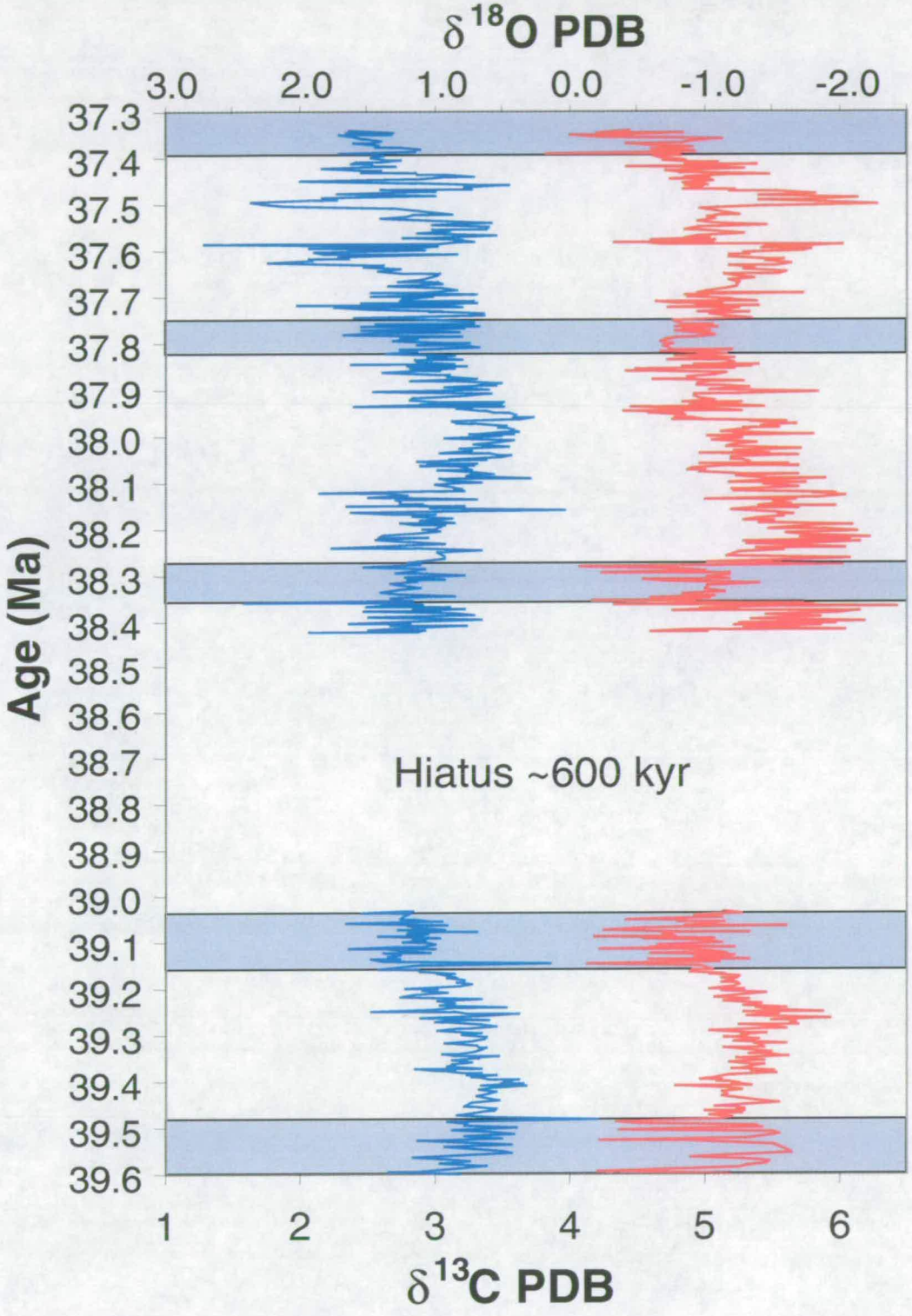

Figure 7.5. Oxygen (right) and carbon (left) isotopic results. The blue shaded areas indicate the 400 kyr cycles within the $\delta^{18}O$ record.

The $\delta^{18}O$ record is dominated by the 400 kyr cycle, whilst the $\delta^{13}C$ record indicates a short-term eccentricity (100 kyr) influence. It is the modulation of the precessional cycles by eccentricity that results in the different signals within the climate and carbon systems. The cause of this disparity and the lack of coherence between $\delta^{18}O$ and $\delta^{13}C$ may result from the way in which the signal is amplified in the climate record and from local versus global influences on the isotopic signals. The abrupt variations within the $\delta^{18}O$ record are probably a locally derived signal caused by variations in the wind systems, monsoonal activity and induced upwelling intensity. The long-term eccentricity cycle then modulates this variation to cause periodically intense upwelling events. The $\delta^{13}C$ record like the $\delta^{18}O$ signal is also influenced by short-term variations in wind-systems and associated productivity changes. However, the long-term variations in $\delta^{13}C$ are probably caused by global changes in the carbon reservoir, such as the flux and composition of organic and inorganic carbon within the oceanic / atmospheric system. This may be influenced by tectonic events and river systems, which do not have an orbital control. The $\delta^{13}C$ signal may also be affected by water masses, as suggested in section 7.2.4. Vital effects produced by the planktonic foraminifera also complicate the carbon isotopic record.

7.4. Carbon dioxide and feedbacks effects within the Eocene climate system

Whilst the orbital changes within the climate system were not related to the carbon cycle, increased CO_2 levels may have been responsible for higher global temperatures during the Eocene. Climatic models (e.g. Manabe and Bryan, 1985; Saravanan and McWilliams, 1995; Bush and Philander, 1997) suggest that tropical and subtropical SSTs should have been at least 2°C greater than modern if global warming was caused by elevated CO_2. Previous $\delta^{18}O$ data from surface dwelling foraminifera (e.g. Zachos *et al.*, 1994; Bralower *et al.*, 1995) indicate that Eocene tropical SSTs were significantly

lower than present. The difficulties in estimating palaeoseawater $\delta^{18}O$ and the ±2°C error in palaeotemperature equations prevent actual SSTs being calculated. Assuming the record reflects mean annual temperatures, the results from Blake Nose indicate that there were intervals when SSTs were 4 to 5°C greater than today.

The effects of insolation forcing alone cannot account for SSTs higher than modern therefore warmer intervals must have been forced by increases in atmospheric greenhouse gases. Results from Pearson and Palmer (2000) showed Eocene CO_2 levels to be greater than today, though highly variable. Amplified atmospheric CO_2 was probably the cause of SSTs greater than modern. Intense upwelling and the collapse of the water column then periodically lowered SSTs and prevented true subtropical SST maxima being calculated. Increased upwelling in the middle Eocene was probably due to the reorganisation of the oceanic system as the cryosphere developed. The enhanced aerial range of oceanic upwelling, providing cold, nutrient rich water to the ocean surface may have been a major mechanism in the eutrophication and cooling of tropical and subtropical surface waters. Eocene climatic warmth could have been caused by increased atmospheric CO_2 and that feedback effects within the ocean-climatic system were important in modulating subtropical temperatures. The postulation of greater thermal transport by the ocean to explain the cool tropical SSTs is probably incorrect.

Other possible feedback mechanisms include increased tropical and subtropical cloud cover which caused notable negative cloud feedback in this area and brought about cooler subtropical SSTs (Crowley and Zachos, 2000). Modern day climatic events in the North Atlantic may be linked to increased SSTs in the Pacific and Indian Oceans (e.g. Hoerling *et al.*, 2001). Whilst present day global temperatures have increased over the last fifty years, a slow cooling (0.1°C/10 years) appears to be occurring on the eastern North American continent. Climatic modeling by Robinson *et al.* (2001) suggests that this could be due to greater cloud cover, preventing maximum solar insolation reaching and heating the western North Atlantic. Periodic variations in latent heat fluxes and

cloud cover may act to moderate SSTs and vice versa, when the omission of cloud cover gives rise to clear skies and maximum SSTs (e.g. Hoerling *et al.*, 2001). This process may also have been important in the Eocene and acted to moderate tropical and subtropical SSTs.

7.5. Future work

7.5.1. Secondary SST proxies and refining palaeotemperature equations

Future work will include generation of secondary temperature proxies for Eocene climate. Palaeo SSTs can also be derived from magnesium – calcium ratios (Mg/Ca) in planktonic foraminifera, as laboratory studies indicate that the uptake of magnesium in marine biogenic calcite is temperature dependent (Dwyer *et al.*, 1995; Mitsuguchi *et al.*, 1996; Nürnberg *et al.*, 1996). Palaeotemperatures could be derived from planktonic foraminiferal Mg/Ca data from the same samples as those already measured for stable isotopes. In conjunction with benthic foraminiferal $\delta^{18}O$ this will allow the $\delta^{18}O_{sw}$ component to be separated from the isotopic temperature signal and thus be used to refine existing palaeotemperature equations. This will provide significant insights into the climatic forcing mechanisms responsible for increased polar temperatures in the Eocene and into what is controlling the planktonic foraminifera $\delta^{18}O$ in the middle Eocene. These results will contribute to the debate on mechanisms of climate change by establishing an independent record of SSTs, which are essential to constrain Eocene ocean and climate models.

7.5.2. Late Eocene climate variability

Whilst the large shifts in planktonic foraminifera $\delta^{18}O$ in the middle Eocene are a very significant finding, much remains to be understood about the nature and wider implications of the forcing mechanisms and their development through the late Eocene. It now appears that during the middle Eocene, which was previously accepted to be a

comparatively stable warm period, complex climatic variability took place that forced the climate at Milankovitch cyclicities. Although this study was extensive, covering 2.3 million years with an average sampling resolution of ~ 3, 000 years between samples, many questions remain unanswered. The upper 75 metres at Site 1052 are available, and a stable isotope record from this interval is necessary to document the climate stability in the late Eocene. This longer-term record is required to examine the nature of orbital forcing as the climate cools and the cryosphere develops.

7.5.3. Regional vs. global record

Future ODP Legs may also allow the direct comparison between Pacific and Atlantic sites. A coeval sequence from the Pacific would allow the separation of global and regional differences on the marine stable isotope record. This would provide insights into ocean and atmospheric dynamics and allow further examination of the biotic response to the Eocene climatic and oceanic changes. This could include the abundance and diversity of certain key taxa, as well as an examination of the depth of the thermocline, mixing intensity, productivity and upwelling. This will enable insights into the extent of such climatic changes and their effects on other parts of the oceanic-climatic system. The Pacific equatorial results from upcoming ODP Leg 198 (Shatsky Rise) and Leg 199 (Palaeogene Equatorial Pacific) will allow direct comparison between the Atlantic and Pacific and be used to separate regional and global influences on surface water $\delta^{18}O$.

7.5.4. Latitudinal thermal gradients

It would also be useful to compare these results with those attained at a high latitude site. This would allow the latitudinal temperature gradient to be examined through time. This may provide an indication of the controlling climatic factors. Cooling may not occur simultaneously at low and high latitudes, therefore the timing of events may be critical in

determining forcing mechanisms. At present the temporal resolution of high-latitude sites hinders this idea.

7.6. Summary

The orbital frequencies within the Munsell hue and planktonic foraminifera stable isotopic data indicates that Milankovitch forcing was a significant component of climate change during the Eocene. There are several possible hypotheses to explain the high amplitude $\delta^{18}O$ and $\delta^{13}C$ variability recorded in Eocene planktonic foraminifera at Blake Nose. The eccentricity forced variations in $\delta^{18}O$ are interpreted as variations in the intensity of Ekman driven upwelling of deep water to the ocean surface. The upwelling hypothesis is favoured here as it can account for the periodically cool SSTs and the reduction of the surface to benthos thermal gradient. These results are consistent with climatic modeling studies (e.g. Bice *et al.*, 2000b; Huber and Sloan, 2000; Sloan and Huber, 2001a, 2001b), which indicate an increased magnitude of temperature, runoff and upwelling variations in the Eocene western Atlantic. The large fluctuations in $\delta^{18}O$ are probably produced by indirect feedback to solar insolation changes, possibly via atmospheric transport, which induced intense upwelling events. Future work will investigate the upwelling hypothesis further and examine climate variability in the late Eocene. High-resolution coeval sections are required to better understand the feedback effects within the climate system and to separate regional and global influences on the stable isotopic records.

8. CONCLUSIONS

The middle Eocene represents a transitional climatic interval between hot-house and ice-house states. Stable isotopic examinations conducted on planktonic foraminifera of late middle Eocene age from Blake Nose indicate large variability in SSTs of up to 12°C. Evidence that upwelling occurred at Blake Nose during the late middle Eocene comes from the large oscillations in subtropical SSTs, with surface water temperatures periodically approaching deep water temperatures and the high abundance of radiolarians. It is concluded that the oscillation in the stable isotopic profiles at Site 1052 is due to climatic control on the intensity of upwelling of deep water to the surface ocean.

Warm climatic intervals were previously thought to be times of relative stability. However, the stable isotopic results suggest a highly unstable climate with variability comparable to that seen in the Plio-Pleistocene. There are intervals where recorded SSTs are up to 5°C greater than modern. These temperatures are similar to those recorded in the early Eocene suggesting increased CO_2 or other greenhouse gases may have forced warm intervals.

Spectral analyses of the composite isotopic records of the middle Eocene reveal Milankovitch cyclicity consistent with the wavelengths of both long- and short-term eccentricity in the planktonic foraminiferal stable isotope records. There is a prominent 400 kyr variability recorded in the middle Eocene $\delta^{18}O$ record. This is attributed to the long-term eccentricity cycle, which caused periodic reduction of SSTs and thermal stratification. These fluctuations cannot be caused by solar insolation alone and therefore feedback effects within the oceanic – climate system, possibly related to atmospheric transport and induced upwelling intensity must have had an important influence. The prominence of Milankovitch frequencies in middle Eocene climate and sedimentary records indicates that orbital forcing of solar insolation was an important parameter of climatic change at this time.

REFERENCES

Abreu, V. S. and Anderson, J. B. 1998. Glacial eustasy during the Cenozoic; sequence stratigraphic implications. *American Association of Petroleum Geologists Bulletin*, **82**, 1385 – 1400.

Adams, C. G., Lee, D. E. and Rosen, B. R. 1990. Conflicting isotopic and biotic evidence for tropical sea-surface temperatures during the Tertiary. *Palaeogeography, Palaeoclimatology and Palaeoecology*, **77**, 289 - 313.

Allmon, W. D. 2001. Nutrients, temperature, disturbance, and evolution: a model for the late Cenozoic marine record of the western Atlantic. *Palaeogeography, Palaeoclimatology and Palaeoecology*, **166**, 9 - 26.

Andreasson, F. P. and Schmitz, B. 1996. Winter and summer temperatures of the early middle Eocene of France from *Turritella* $\delta^{18}O$ profiles, *Geology*, **24**, 1067 – 1070.

Andreasson, F. P. and Schmitz, B. 1998. Tropical Atlantic seasonal dynamics in the early middle Eocene from stable oxygen and carbon isotope profiles of mollusk shells. *Paleoceaography*, **13**, 183 - 192.

Andreasson, F. P. and Schmitz, B. 2000. Temperature seasonality in the early middle Eocene North Atlantic region; evidence from stable isotope profiles of marine gatropod shells. *Geological Society of America Bulletin*, **112**, 628 – 640.

Aubry, M.-P. 1983. Late Eocene to early Oligocene calcareous nannoplankton biostratigraphy and biogeography. *American Association of Petroleum Geologists Bulletin*, **67**, 415.

Banner, F. T., 1982. A classification and introduction to the Globigerinacea. In: Banner, F. T. and Lord, A. R. (Eds.), *Aspects of micropalaeontology*. George Allen and Unwin, 142 - 239.

Barrera, E. and Huber, B. T. 1991. Paleogene and early Neogene oceanography of the southern Indian Ocean: Leg 119 foraminifer stable isotope results. In: Barron, J., Larsen, B. *et al. Proceedings of the Ocean Drilling Program, Scientific Results*, **119**, College Station, TX (Ocean Drilling Program), 693 - 717.

Barron, E. J. 1985. Explanations for the Tertiary global cooling trend. *Palaeogeography, Palaeoclimatology and Palaeoecology*, **50**, 729 - 739.

Barron, E. J. 1987. Eocene equator-to-pole surface ocean temperatures: a significant climate problem? *Paleoceanography*, **2**, 729 - 739.

Barron, E. J. and Washington, W. M. 1984. The role of geographic variables in explaining paleoclimates, results from Cretaceous climate model sensitivity studies. *Journal of Geophysical Research*, **89**, 1267 – 1279.

Barron, E. J. and Peterson, W. H. 1991. The Cenozoic ocean circulation based on ocean General Circulation Model results. *Palaeogeography, Palaeoclimatology, Palaeoecology*, **83**, 1 - 28

Barron, E. J., Sloan, L. C., Krujis, E., Peterson, W. H., Shinn, R. and Sloan, J. L. 1989. Cretaceous climate sedimentary relationships. *International Geological Congress, Abstracts*, **28**, 92.

Barron, E. J., Peterson, W. H., Pollard, D. and Thompson, S. L. 1993. Past climate and the role of ocean heat transport: model simulations for the Cretaceous. *Paleoceanography*, **8**, 785 - 798.

Belanger, P. E., Curry, W. B. and Matthews, R. K. 1981. Core-top evaluation of benthic foraminiferal isotopic ratios for paleo-oceanographic interpretations. *Palaeogeography, Palaeoclimatology and Palaeoecology*, **33**, 205 - 220.

Benjamini, C. 1980. Stratigraphy and Foraminifera of the Qezi'ot and Har 'Aqrav Formations (Latest Middle to Late Eocene) of the Western Negev, Israel. *Israel Journal of Earth Sciences*, **29**, 227 - 244.

Benson, R. H. 1975. The origin of the psychrosphere as recorded in changes of deep sea ostracode assemblages. *Lethaia*, **8**, 69 – 83.

Berger, A. 1978. Long-term variations of daily insolation and Quaternary climatic changes. *Journal of Atmospheric Sciences*, **35**, 2362 – 2367.

Berger, A., Loutre, M. F. and Laskar, J. 1992. Stability of the astronomical frequencies over Earth's history for paleoclimate studies. *Science*, **255**, 560 – 566.

Berger, W. H. 1979. Stable isotopes in foraminifera. In: *Foraminiferal Ecology and Paleoecology*. SEPM Short Course No. 6, Society of Economic Paleontolgists and Mineralogists. Houton, Texas, 156 – 198.

Berger, W. H. and Gardner, J. V. 1975. On the determination of Pleistocene temperatures from planktonic foraminifera. *Journal of Foraminiferal Research*, **5**, 102 – 113.

Berger, W. H. and von Rad, U. 1992. Cretaceous and Cenozoic sediments from the Atlantic Ocean. *Initial Reports of the Deep Sea Drilling Project*, **14**, U.S. Government printing Office, Washington, D. C., 787 – 886.

Berger, W. H., Vincent, E. and Thierstein, H. R. 1981. The Deep-Sea Record: major steps in Cenozoic Ocean Evolution. In: Emiliani, C. (Ed). *The Sea, ideas and observations on progress in the study of the seas,* **7**, The oceanic lithosphere. John Wiley and Sons, New York.

Berggren, W. A. 1982. Role of ocean gateways in climatic change. In: Berger, W. H. and Crowell, J. C. (Eds.). *Climate in Earth History*, National Academy Press, Washington, DC, 118 - 125.

Berggren, W. A. and Hollister, C. D. 1977. Plate tectonics and paleocirculation - commotion in the ocean. *Tectonophysics*, **11**, 11- 48.

Berggren, W. A. and Prothero, D. R. 1992. Eocene – Oligocene climatic and biotic evolution: An overview. In: Prothero, D. R. and Berggren, W. A. (Eds.). *Eocene - Oligocene Climatic and Biotic Evolution*. Princeton University Press, New Jersey, 1 - 28.

Berggren W. A. and Norris R. D. 1997. Biostratigraphy, phylogeny and systematics of Paleocene trochospiral planktic foraminifera. *Micropaleontology*, **43** Supplement 1, 116

Berggren, W. A., Kent, D. V., Swisher, C. C. III and Aubry, M.-P. 1995. A revised Cenozoic geochronology and chronostratigraphy. In: Berggren, W. A. Berggren, Kent, D. V., Aubry, M.-P. and Hardenbol, J. (Eds.) *Geochronology, Time Scales and Global Stratigraphic Correlation: A Unified Temporal Framework for an Historical Geology*, Society of Economic Paleontologists and Mineralogists Special Publication, **54**, 129 - 212.

Berner, R. A. 1991. A model for atmospheric CO_2 over Phanerozoic time. *American Journal of Science*, **291**, 339 - 376.

Berner, R. A. 1994. GEOCARB II: a revised model of atmospheric CO2 over Phanerozoic time. *American Journal of Science*, **294**, 56 – 91.

Bice, K. L. and Marotzke, J. 2000. Warm Climate Dynamics. *GFF* (Geological Society of Sweden), **122**, 29 – 30.

Bice, K. L., Scotese, C. R., Seidov, D. and Barron, E. J. 2000a. Quantifying the role of geographic change in Cenozoic ocean heat transport using uncoupled atmosphere and ocean models. *Palaeogeography, Palaeoclimatology and Palaeoecology*, **161**, 295 - 310.

Bice, K. L., Sloan, L. C. and Barron, E. J. 2000b. Comparison of early Eocene isotopic paleotemperatures and the three-dimensional OGCM temperature field: The potential for use of model-derived surface water $\delta^{18}O$. In: Huber, B. T., MacLoed, K. G and Wing, S. L. (Eds.). *Warm Climates in Earth History*. Cambridge University Press, 79 - 131.

Blow, W. H. 1979. The Cainozoic Globigerinida. Brill, 3 volumes.

Boersma, A. and Premoli Silva, I. 1986. Terminal Eocene events: planktonic Foraminifera and isotopic evidence. In: Pomerol, C and Premoli Silva, I. (Eds.). *Terminal Eocene Events*. Developments in Palaeontology and Stratigraphy, **9**. Elsevier, Amsterdam, 213 – 224.

Boersma, A. and Premoli Silva, I. 1991. Distribution of Paleogene planktonic foraminifera – analogies with the Recent? *Palaeogeography, Palaeoclimatology and Palaeoecology*, **83**, 29 - 48.

Boersma, A., Shackleton, N. J., Hall, M. and Given, Q. 1979. Carbon and oxygen isotope records at DSDP Site 384 (North Atlantic) and some Paleocene paleotemperatures and carbon isotope variations in the Atlantic Ocean. In: Tucholke, B. E., Vogt, P. R., Murdmaa, I. O. *et al. Initial Report of the Deep Sea Drilling Project*, **43**, Washington, D. C. U.S. Government Printing Office, 695 - 717.

Boersma, A., Premoli Silva, I. and Shackleton, N. J. 1987. Atlantic Eocene planktonic foraminiferal paleohydrographic indicators and stable isotope paleoceanography. *Paleoceanography*, **2**, 287 - 331.

Bottomley, M., Folland, C. K., Hsiling, J., Newell, R. E. and Parker, D. E. 1990. *Global Ocean Surface Temperature Atlas*. A Joint Project of the

Meteorological Office and Massachusetts Institute of Technology. Bracknell, United Kingdom, Meteorological Office, 333 pp.

Bradley, W. H. 1929. Algae reefs and oolites of the Green River Formation. *U. S. Geological Survey Professional Paper*, 154–G, 203 – 223.

Bralower, T. J., Zachos, J. C., Thomas, E., Parrow, M., Paull, C. K., Kelly, D. C., Premoli Silva, I., Sliter, W. V. and Lohmann, K. C. 1995. Late Paleocene to Eocene paleoceanography of the equatorial Pacific Ocean: Stable isotopes recorded at Ocean Drilling Program Site 865, Allison Guyot. *Paleoceanography*, **10**, 841 - 865.

Broecker, W. S. 1989. The salinity contrast between the Atlantic and Pacific Oceans during glacial time. *Paleoceanography*, **4**, 207 - 212.

Browning, J. V., Miller, K. G. and Pak, D. K. 1996. Global implications of Lower to Middle Eocene sequence boundaries on the New Jersey coastal plain: the icehouse cometh. *Geology*, **24**, 639 - 642.

Bush, A. B. G. and Philander, S. G. H. 1997. The Late Cretaceous; simulation with a coupled atmosphere-ocean general circulation model. *Paleoceanography*, **12**, 495 - 516

Cande, S. C. and Kent, D. V. 1992. A new geomagnetic polarity time scale for the Late Cretaceous and Cenozoic. *Journal of Geophysical Research*, **97**, 13917 – 13951.

Cande, S. C. and Kent, D. V. 1995. Revised calibration of the geomagnetic polarity timescale for the Late Cretaceous and Cenozoic. *Journal of Geophysical Research*, **100**, 6093 – 6095.

Chappell, J. and Shackleton, N. J. 1986. Oxygen isotopes and sea-level. *Nature*, **324**, 137 – 140.

Cifelli, R. 1969. Radiation of Cenozoic planktonic Foraminifera. *Systematic Zoology*, **18**, 154 – 168.

Corfield, R. M. and Cartlidge, J. E. 1991. Isotopic evidence for the depth stratification of fossil and Recent *Globigerinina*: a review. *Historical Biology*, **5**, 37 - 63.

Corfield, R. M. and Norris, R. D. 1996. Deep water circulation in the Paleocene Ocean. *In*: Knox, R. W., Corfield, R. M. and Dunay, R. E. (Eds.) *Correlation*

of the early Paleogene in Northwest Europe. Geological Society Special Publication No. **101**, 443 - 456.

Corfield, R. M. and Norris, R. D. 1998. The oxygen and carbon isotopic context of the Paleocene-Eocene Epoch boundary. *In*: Aubry, M-P., Lucas, S., Berggren, W. A., (Eds.) *Late Paleocene-early Eocene climatic and biotic events in the marine and terrestrial records.* Colombia University Press, New York, 124 - 137.

Corliss, B. H. 1979. Response of deep-sea benthonic foraminifera to development of the psychrosphere near the Eocene / Oligocene boundary. *Nature*, **282**, 63 – 65.

Cortijo, E., Lehman, S. J., Keigwin, L. D., Chapman, M., Paillard, D. and Labeyrie, L. 1999. Changes in meridional temperature and salinity gradients in the North Atlantic (30 – 72°N) during the last interglacial period. *Paleoceanography*, **14**, 23 – 33.

Covey, C. and Barron, E. J. 1988. The role of ocean heat transport in climate change. *Earth Science Reviews*, **24**, 429 – 445.

Covey, C. and Thompson, S. L. 1989. Testing the effects of ocean heat transport on climate. *Global Planetary Change*, **1**, 331 - 341.

Coxall, H . K., Pearson, P. N., Shackleton, N. J. and Hall, M. A. 2000. Hantkeninid depth adaptation: An evolving life strategy in a changing ocean. *Geology*, **28,** 87 – 90.

Craig, H. 1957. Isotopic standards for carbon and oxygen correction factors for mass spectrometric analysis of CO_2. *Geochimica et Cosmochimica Acta*, **12**, 133 - 149.

Craig, H. 1965. The measurement of oxygen isotope palaeotemperatures: *Consigl. Naz. Ric.,* Pisa, Italy.

Craig, H. and Gordon, L. I. 1965. Deuterium and oxygen 18 variations in the ocean and the marine atmosphere. *Symposium on marine geochemistry*, **3**, 277 – 374.

Crowley, T. J. 1991. Past CO_2 changes and tropical sea surface temperatures. *Paleoceanography*, **6**, 387 - 394.

Crowley, T. J. 1993. Climate change on tectonic time scales. *Tectonophysics*, **222**, 277 – 294.

Crowley, T. J. and Zachos, J. C. 2000. Comparison of zonal temperature profiles for past warm time periods. In: Huber, B. T., MacLoed, K. G and Wing, S. L. (Eds.). *Warm Climates in Earth History*. Cambridge University Press, 79 - 131.

Crowley, T. J., Kim, K.-Y., Mengel, J. and Short, D. 1992. Modeling 100, 000-year climate fluctuations in pre-Pleistocene time series. *Science*, **255**, 705 – 707.

Cubasch, U., Waszkewitz, J., Hegerl, G. ; and Perlwitz, J. 1995. Regional climate changes as simulated in time-slice experiments. *Climatic Change*, **31**, 273 – 304.

Deuser, W. G. 1987. Seasonal variations in isotopic composition and deep-water fluxes of the tests of perennially abundant planktonic foraminifera of the Sargasso Sea: Results from sediment trap collections and their paleoceanogrphic significance. *Journal of Foraminiferal Research*, **17**, 14 - 27.

Deuser, W. G. and Ross, E. H. 1989. Seasonally abundant planktonic foraminifera of the Sargasso Sea: Succession, deep-water fluxes, isotopic composition, and palaeoceanographic interpretation. *Journal of Foraminiferal Research*, **19**, 268 – 293.

Deuser, W. G., Ross, E. H., Hembleben, C. and Spindler, M. 1981. Seasonal changes in species composition, numbers, mass, size, and isotopic composition of planktonic foraminifera settling into the deep Sargasso Sea. *Palaeogeography, Palaeoclimatology and Palaeoecology*, **33**, 103 - 127.

D'Hondt, S., Zachos, J. C. and Schultz, G. 1994. Stable isotopic signals and photosymbiosis in Late Paleocene planktic foraminifera. *Paleobiology*, **20**, 391.

Duplessy, J.C., Lalou, C. and Vinot, A. C. 1970. Differential isotopic fractionation in benthic foraminifera and palaeotemperatures reassessed. *Science*, **168**, 250 - 251.

Dwyer, G. S., Cronin, T.M., Baker P.A., Raymo M.E., Buzas J.S. and Correge T. 1995. North Atlantic deepwater temperature change during late Pliocene and late Quaternary climatic cycles. *Science*, **270**, 1347 – 1350.

Ehrmann, W. U. and Thiede, J. 1986. Correlation of terrigenous and biogenic sediment fluxes in the North-Atlantic Ocean during the past 150 my. *Geologische Rundschau*, **75**, 43 – 55.

Elliott, J. R., Jewson, S. P. and Sutton, R. T. 2001. The impact of the 1997/98 El Nino event on the Atlantic Ocean. *Journal of Climate*, **14**, 1069 – 1077.

Elsom, D. 1992. *Earth: the making, shaping and workings of a planet.* Simon and Schuster Limited, London.

Emiliani, C. 1954. Depth habitats of some species of pelagic Foraminifera as indicated by oxygen isotope ratios. *American Journal of Science*, **252**, 149 - 158.

Emiliani, C. 1955. Pleistocene temperatures. *Journal of Geology*, **63**, 538 -578.

Epstein, S., Buchsbaum, R., Lowenstam, H. A. and Urey, H. C. 1953. Revised carbonate-water isotopic scale. *Geological Society of America Bulletin*, **64**, 1315 – 1325.

Erez, J. and Honjo, S. 1981. Comparison of isotopic composition of planktonic foraminifera in plankton tows, sediment traps and sediments. *Palaeogeography, Palaeoclimatology and Palaeoecology*, **33**, 129 - 156.

Erez, J. and Luz, B. 1983. Experimental paleotemperature equation for planktonic foraminifera. *Geocheica et Cosmochemica Acta,* **47**, 1025 - 1031.

Fairbanks, R. G. 1989. A 17,000 – year glacio-eustatic sea level record; influence of glacial melting rates on the younger Dryas event and deep-ocean circulation. *Nature*, **342**, 637 – 642.

Fairbanks, R. G., Charles, C. D. and Wright, J. D. 1992. Origin of global meltwater pulses. In: Taylor, R. E., Long, A and Kra, R. S. (Eds.). *Radiocarbon after four decades; an interdisciplinary perspective*, Springer-Verlag, New York, 473 – 500.

Fawcett, P. J. and Barron, E. J. 1998. The role of geography and atmospheric CO2 in long term climate change: results from model simulations for the late Permian

to the present. In: Crowley, T. and Burke, K. (Eds.), *Tectonic Boundary Conditions for Climate Reconstructions*. Oxford University Press, 21 – 36.

Fischer, A. G. and Roberts, L. T. 1991. Cyclicity in the Green River Formation (lacustrine Eocene) of Wyoming. *Journal of Sedimentary Petrology*, **61**, 1146 – 1154.

Flower, B. P. and Kennett, J. P. 1993. Middle Miocene ocean-climate transition; high-resolution oxygen and carbon isotopic records from Deep Sea Drilling Project Site 588A, Southwest Pacific. *Paleoceanography*, **8**, 811 – 843.

Flower, B. P., Zachos, J. C. and Paul, H. 1997. Milankovitch-scale climate variability recorded near the Oligocene/Miocene boundary. In: Shackleton, N. J., Curry, W. B., Richter, C. and Bralower, T. J. (Eds.), *Proceeding of the Ocean Drilling Program, Scientific Results*, **154**, 433 - 440.

Ganssen, G. M. and Kroon, D. 2000. The isotopic signature of planktic foraminifera from Northeast Atlantic surface sediments: implications for the reconstruction of past oceanic conditions. *Journal of the Geological Society of London*, **157**, 693 – 699.

Genthon, C., Barnola, J. M., Raynaud, D., Lourius, C., Jouzel, J., Barkov, N. I., Korotkevich, Y. and Kotlyakov, V. M. 1987. Vostok ice core: climatic response to CO2 and orbital forcing changes over the last climatic cycle. *Nature*, **329**, 414 – 418.

Gilbert, P. S., Lee, T. N. and Podesta, G. P. 1996. Transport of anomalous low-salinity waters from the Mississippi River flood of 1993 to the Straits of Florida. *Continental Shelf Research*, **16**, 1065 - 1085

Glenister, B. F. and Furnish, W. M. 1988. Terminal progenesis in Late Paleozoic ammonoid families. In: Wiedmann, J. and Kullmann, J. (Eds.). *Cephalopods – present and past*. Schweizerbart'sche Verlagsbuchhandlung, 51 – 66.

Graham, A. 1994. Neotropical Eocene coastal floras and $^{18}O/^{16}O$-estimated warmer vs. cooler equatorial waters. *American Journal of Botany*, **81**, 301 - 306.

Graham, A. 2000. Palynofloras and terrestrial environments in the Eocene of the Caribbean Basin. *GFF*, **122**, 64.

Graham, D. W., Corliss, B. H., Bender, M. L. and Keigwin, L. D., Jr. 1981. Carbon and oxygen isotopic disequilibria of recent deep-sea benthic foraminifera. *Marine Micropaleontology*, **6**, 483 - 497.

Guilderson, T. P., Fairbanks, R. G. and Rubenstone, J. L. 1994. Tropical temperature variations since 20,000 years ago; modulating interhemispheric climate change. *Science*, **263**, 663 – 665.

Hagelberg, T. K., Bond, G. and deMenocal, P. 1994. Milankovitch band forcing of sub-Milankovitch climate variability during the Pleistocene. *Paleoceanography*, **9**, 545 - 558.

Hallock, P., Premoli Silva, I. and Boersma, A. 1991. Similarities between planktonic and larger foraminiferal evolutionary trends through Paleogene paleoceanographic changes. *Palaeogeography, Palaeoclimatology and Palaeoecology*, **83**, 49 - 64.

Hambrey, M. J., Ehrmann, W. U. and Larsen B. 1991. Cenozoic glacial record of the Prydz Bay continental shelf, East Antarctica. In: Barron, J., Larsen, B. *et al. Proceedings of the Ocean Drilling Program, Scientific Results*, **119**, College Station, TX (Ocean Drilling Program), 77 - 132.

Haq, B. U. 1981. Paleogene paleoceanography, Early Cenozoic oceans. *Oceanologica Acta*, **4**, 71 - 82.

Hayes, D. E., Frakes, L. A. *et al.* 1975. *Initial Reports of the Deep Sea Drilling Project*, **28**, U.S. Government printing Office, Washington, D. C.

Herbert, T. D. 1997. A long marine history of carbon cycle modulation by orbital-climatic changes. *Proceedings of the National Academy of Sciences USA*, **94**, 8362 – 8369.

Herbert, T. D. and D'Hondt, S. L. 1990. Precessional climate cyclicity in Late Cretaceous – Early Tertiary marine sediments: a high resolution chronometer of Cretaceous – Tertiary boundary events. *Earth and Planetary Science Letters*, **99**, 263 – 275.

Hoerling, M. P., Hurrell, J. W. and Xu, T. 2001. Tropical origins for recent North Atlantic climate change. *Science*, **292**, 90 – 92.

Horrell, M. A. 1990. Energy balance constraints on ^{18}O based paleo-sea surface temperature estimates. *Paleoceanography*, **5**, 339 - 348.

Huber, M. and Sloan, L. C. 2000. Modelling the Paleogene, Part II: Paleogene wind-driven ocean circulation changes predicted from climate modeling studies. *GFF* (Geological Society of Sweden), **122**, 80 – 81.

Imbrie, J., Shackleton, N. J., Pisias, N. G., Morley, J. J., Prell, W. L., Martinson, D. G., Hays, J. D., McIntyre, A. and Mix, A. C. 1984. In: Berger, A., Imbrie, J., Hays, J., Kukla, G., Saltzman, B. (Eds.). *Milankovitch and Climate.* D. Reidel Publishing Company, Dordrecht, 269 - 306.

Imbrie, J., Boyle, E. A., Clemens, S. C., Duffy, A., Howard, W. R., Kukla, G., Kutzbach, J., Martinson, D. G., McIntyre, A., Mix, A. C., Molfino, B., Morley, J. J., Peterson, L. C., Pisias, N. G., Prell, W. L., Raymo, M. E., Shackleton, N. J. and Toggweiler, J. 1992. On the structure and origin of major glaciation cycles, 1.Linear responses to Milankovitch forcing. *Paleoceanography*, **7**, 701 – 738.

Imbrie, J., Berger, A., Boyle, E. A., Clemens, S. C., Duffy, A., Howard, W. R., Kukla, G., Kutzbach, J., Martinson, D. G., McIntyre, A., Mix, A. C., Molfino, B., Morley, J. J., Peterson, L. C., Pisias, N. G., Prell, W. L., Raymo, M. E., Shackleton, N. J. and Toggweiler, J. 1993. On the structure and origin of major glaciation cycles, 2. The 100,000-year cycle. *Paleoceanography*, **8**, 699 – 735.

Jenkins, D. G. 1971. The reliability of some Cenozoic planktonic foraminiferal "datum-planes" used in biostratigraphic correlation. *Journal of Foraminiferal Research*, **1**, 82 – 86.

Keigwin, L. D. and Corliss, B. H. 1986. Stable isotopes in late middle Eocene to Oligocene foraminifera. *Geological Society of America Bulletin*, **97**, 335 - 345.

Keigwin, L. D. and Boyle, E. A. 1999. Surface and deep ocean variability in the northern Sargasso Sea during marine isotope stage 3. *Paleoceanography*, **14**, 164 – 170.

Keller, G. 1983. Paleoclimatic analyses of middle Eocene through Oligocene planktic foraminiferal faunas. *Palaeogeography, Palaeoclimatology and Palaeoecology*, **43**, 73 - 94.

Keller, G., MacLeod, N. and Barrera, E. 1992. Eocene-Oligocene faunal turnover in planktic foraminifera, and Antarctic glaciation. In: Prothero, D. R. and Berggren, W. A. (Eds.). *Eocene - Oligocene Climatic and Biotic Evolution.* Princeton University Press, New Jersey, 218 - 244.

Kelly, D. C., Bralower, T. J. and Zachos, J. C. 2000. On the demise of the early Paleogene *Morozovella velascoensis* lineage: Terminal progenesis in the planktic foraminifera? *GFF* (Geological Society of Sweden), **122**, 86 – 87.

Kennett, J. P. 1977. Cenozoic evolution of Antarctic glaciation, the circum-Antarctic Ocean/their impact on global paleoceanography. *Journal of Geophysical Research,* **82**, 3843 - 3860.

Kennett, J. P. 1982. *Marine Geology.* Prentice-Hall, inc., Englewood Cliffs, N. J.

Kennett, J. P. and Shackleton, N. J. 1976. Oxygen isotopic evidence for the development of the psychrosphere 38 m.y. ago. *Nature*, **260**, 513 – 515.

Kennett, J. P. and Stott, L. D. 1990. Proteus and proto-oceanus: ancestral Paleogene oceans as revealed from Antarctic stable isotopic results: ODP Leg 113. In: Barker, P. F., Kennett, J. P., *et al. Proceedings of the Ocean Drilling Program, Scientific Results*, **113**, College Station, TX (Ocean Drilling Program), 865 – 880.

Kennett, J. P., Houtz, R. E. *et al.* 1975. Cenozoic paleoceanography in the Southwest Pacific Ocean, Antarctic Glaciation and the development of the Circum-Antarctic Current. In: Kennett, J. P., Houtz, R. E. *et al.* (Eds). *Initial Reports of the Deep Sea Drilling Project*, **29**. U.S. Government printing Office, Washington, D. C, 1155 – 1169.

Killingley, J. S. 1983. Effects of diagenetic recrystalization on $^{18}O/^{16}O$ values of deep-sea sediments. *Nature*, **301**, 594 - 597.

Kobashi, T., Yancey, T. E., Grossman, E. L. and Dockery, D. 2001. Records of seasonal temperature variation from Eocene – Oligocene shallow marine molluscs of the Gulf of Mexico: reconciliation of proxies for open ocean, coastal ocean, and continental Eocene paleotemperatures. In: Ash, A. W. and Wing, S. L. (Eds.). *Climate and biota of the early Paleogene*, International Meeting, July 3-8, 2001, p. 52.

Kroon, D. and Ganssen, G. 1989. Northern Indian Ocean upwelling cells and the stable isotope composition of living planktonic foraminifers. *Deep Sea Research*, **36**, 1219 – 1236.

Kroon, D., Reijmer, J. J. G. and Rendle, R. 2000. Mid- to late-Quaternary variations in the oxygen isotope signature of *Globigerinoides ruber* at Site 1006 in the western subtropical Atlantic. *Proceedings of the Ocean Drilling Program, Scientific Results*, **166**: College Station, TX (Ocean Drilling Program), 13 - 22.

Kroopnick, P. 1974. The dissolved O_2-CO_2-^{13}C system in the eastern equatorial Pacific. *Deep Sea Research*, **21**, 211 – 227.

Kroopnick, P. 1985. The distribution of ^{13}C of TCO_2 in the world oceans. *Deep Sea Research*, **32**, 57-84.

Laskar, J. 1990. The chaotic motion of the solar system: a numerical estimate of the size of the chaotic zones. *Icarus*, **88**, 266 – 291.

Laskar, J. 1999. The limits of Earth orbital calculations for geological time-scale use. *Philosophical Transactions of the Royal Society of London Series A,* **357**, 1735 – 1760.

Laskar, J., Joutel, F. and Robutel, P. 1993. Stabilization of the Earth's obliquity by the Moon. *Nature*, **361**, 615 – 617.

Lawver, L. A. and Gahagan, L. M. 1998. Opening of Drake Passage and its impact on Cenozoic ocean circulation. In: Crowley, T. J. and Burke, K. C. (Eds.). *Tectonic boundary conditions for climate reconstructions*. Oxford Monographs on Geology and Geophysics, **39**, Oxford University Press, Oxford, United Kingdom, 212 - 223

Lear, C. H., Elderfield, H. and Wilson, P. A. 2000. Cenozoic deep-sea temperatures and global ice volumes from Mg/Ca in benthic foraminiferal calcite. *Science*, **287**, 269 – 272.

Levitus, S., Burgett, R. and Boyer, T. P. 1994. Salinity, NOAA Atlas NESDIS 3. *World Ocean Atlas* 1994 volume **3**. U.S. Government Printing Office, Washington, DC. 99 pp.

Lipps, J. H. 1970. Plankton evolution. *Evolution*, **24**, 1 – 22.

Lipps, J. H. 1986. Extinction dynamics in pelagic ecosystems. In: Elliot, D. K. (Ed.). *Dynamics of Extinction*. John Wiley and Sons, New York, 89 – 103.

Lourens, L. J., Wehausen, R. and Brumsack, H. J. 2001. Geological constraints on tidal dissipation and dynamical ellipticity of the Earth over the past three million years. *Nature*, **409**, 1029 – 1033.

Mackensen, A. and Ehrmann, W. U. 1992. Middle Eocene through Early Oligocene climate history and paleoceanography in the Southern Ocean: Stable oxygen and carbon isotopes from ODP Sites on Maud Rise and Kerguelen Plateau. *Marine Geology*, **108**, 1 - 27.

Manabe, S. and Bryan, K. 1985. CO2-induced change in a coupled ocean-atmosphere model and its paleoclimatic implications. *Journal of Geophysical Research*, **90**, 11689 - 11708.

Manabe, S. and Stouffer R. J. 1994. Multiple-century response of a coupled ocean-atmosphere model to an increase of atmospheric carbon dioxide. *Journal of Climate*, **7**, 5 - 23

McCoy, F. and Zimmerman, H. 1977. A history of sediment lithofacies in the South Atlantic Ocean. In: Perch-Nielsen, K., Supko, P. *et al. Initial Reports of the Deep Sea Drilling Project,* **39**, Washington (U.S. Government Printing Office), 1047 - 1079.

Mikolajewicz, U. and Crowley, T. J. 1997. Response of a coupled ocean/energy balance model to restricted flow through the central American isthmus. *Paleoceanography*, **12**, 429 – 441.

Milankovitch, M. M. 1941. *Kanon der Erdbestrahlung und seine anwendung auf das eiszeitenproblem*. Academic Royale Serbe, Edition Speciale, **133**.

Miller, K. G., Fairbanks, R. G. and Mountain, G. S. 1987. Tertiary oxygen isotope synthesis, sea level history, and continental margin erosion. *Paleoceanography*, **2**, 1 – 19.

Miller, K. G., Wright, J. D. and Fairbanks, R. G. 1991. Unlocking the ice house – Oligocene-Miocene oxygen isotopes, eustasy and margin erosion. *Journal of Geophysical Research – Solid Earth and Planets*, **96** (B4), 6829 – 6848

Mita, I. 2001. Data Report: Early to Late Eocene calcareous nannofossil assemblages of Sites 1051 and 1052, Blake Nose, Northwestern Atlantic Ocean. In: Kroon,

D., Norris, R. D. and Klaus, A. (Eds.). *Proceedings of the Ocean Drilling Program, Scientific Results*, **171B**, [Online] Available from World Wide Web: <http://www-odp.tamu.edu/publications/171B_sr/171bsr.htm>.

Mitsuguchi, T., Matsumoto, E., Abe, O., Uchida, T. and Isdale, P. J. 1996. Mg/Ca thermometry in coral skeletons. *Science*, **274**, 961 - 963

Nocchi, M., Parisi, G., Monaco, P., Monechi, S., Madile, M., Napoleone, G., Ripepe, M., Orlando, M., Premoli Silva, I. And Bice, D. M. 1986. The Eocene – Oligocene boundary in the Umbrian pelagic sequences, Italy. In: Pomerol, C and Premoli Silva, I. (Eds.). *Terminal Eocene Events*. Developments in Palaeontology and Stratigraphy, **9**. Elsevier, Amsterdam, 24 – 40.

Norris, R. D. 1998. Recognition and macroevolutionary significance of photosymbiosis in molluscs, corals and foraminifera. *In*: Norris, R. D. and Corfield, R. M.(Eds.). Isotope Paleobiology and Paleoecology. *Paleontological Society Papers*, **4**, 68 - 100.

Norris, R. D. and Wilson, P. A. 1998. Low-latitude sea surface temperatures for the mid-Cretaceous and the evolution of planktonic foraminifera. *Geology*, **26**, 823 - 826.

Norris, R. D. and Röhl, U. 1999. Carbon cycling and chronology of climate warming during the Palaeocene/Eocene transition. *Nature*, **401**, 775 – 778.

Norris, R. D., Kroon, D., Klaus, A. *et al.* 1998. *Proceedings of the Ocean Drilling Program, Initial Results*, **171**: College Station, TX (Ocean Drilling Program).

Nürnberg D., Bijma J., Hemleben C. 1996. Assessing the reliability of magnesium in foraminiferal calcite as a proxy for water mass temperatures. *Geochimica et Cosmochimica Acta*, **60**, 803 – 814.

Ogg, J. G. and Bardot, L. 2001. Aptian through Eocene Magnetostratigraphic Correlation of the Blake Nose Transect (Leg 171B), Florida Continental Margin. In: Kroon, D., Norris, R. D. and Klaus, A. (Eds.). *Proceedings of the Ocean Drilling Program, Scientific Results*, **171B**, [Online] Available from World Wide Web: <http://www-odp.tamu.edu/publications/171B_sr/171bsr.htm>.

Olago, D. O., Ivanovich, M., Harkness, D. D., Odada, E. O., Street-Perrott, F. A. and Perrott, R. A. 2000. Long-term temporal characteristics of palaeomonsoon dynamics in equatorial Africa. *Global and Planetary Change*, **26**, 159 – 171.

Olsen, P. E. and Kent, D. V. 1996. Milankovitch climate forcing in the tropics of Pangaea during the Late Triassic. *Palaeogeography, Palaeoclimatology, Palaeoecology,* **122**, 1 - 26.

O'Neil, J. R., Clayton, R. N., Mayeda, T. K. 1969. Oxygen isotope fractionation in divalent metal carbonates. *Journal of Chemical Physics*, **51**, 5547 - 5558.

Owen, R. M and Rea, D. K. 1985. Sea floor hydrothermal activity links climate to tectonics, The Eocene greenhouse. *Science*, **227**, 166 - 169.

Paillard, D., Labeyrie, L. and Yiou, P. 1996. Macintosh program performs time-series analysis. *Eos Transactions, American Geophysical Union,* **77**, 379.

Pälike, H., Shackleton, N. J. and Röhl, U. 2001. Astronomical forcing in Late Eocene marine sediments. Earth and Planetary Science Letters, **193**, 589 - 602.

Park, J. and Oglesby, R. J. 1990. A comparison of precession and obliquity effects in a Cretaceous paleoclimate simulation. *Geophysical Research Letters*, **17**, 1929 – 1932.

Paul, H. A., Zachos, J. C., Flower, B. P. and Tripati, A. 2000. Orbitally induced climate and geochemical variability across the Oligocene/Miocene boundary. *Paleoceanography*, **15**, 471 – 485.

Paull, C. K., Hills, S. J. and Thierstein, H. R. 1988. Progressive dissolution of fine carbonate particles in pelagic sediments. *Marine Geology*, **81**, 27 - 40.

Pearson, P. N. 1996. Cladogenetic, extinction and survivorship patterns from a lineage phylogeny: the Paleogene planktonic foraminifera. *Micropaleontology*, **42**, 179 - 188.

Pearson, P. N. 1998. Stable isotopes and the study of evolution in planktonic foraminifera. In: Manger, W. L. and Meeks, L. K. (Eds.). Isotope paleobiology and paleoecology. *Paleontological Society Papers*, **4**, 138 – 178.

Pearson, P. N. and Shackleton, N. J. 1995. Neogene multispecies planktonic foraminifer stable isotope record, site 871, Limalok Guyot. In: Haggerty, J.

A., Premoli Silva, I., Rack, F. and McNutt, M. K. (Eds.), *Proceedings of the Ocean Drilling Program, Scientific Results*, **144**, 401 - 410.

Pearson, P. N. and Chaisson, W. P. 1997. Late Paleocene to Middle Miocene Planktonic Foraminifer Biostratigraphy of the Ceara Rise. In: Shackleton, N. J., Curry, W. B., Richter, C. and Bralower, T. J. (Eds.), *Proceeding of the Ocean Drilling Program, Scientific Results*, **154**, 33 - 68.

Pearson, P. N. and Palmer, M. R. 2000. Atmospheric carbon dioxide concentrations over the past 60 million years. *Nature*, **406**, 695 – 699.

Pearson, P. N., Shackleton, N. J. and Hall, M. A. 1993. Stable isotope paleoecology of middle Eocene planktonic foraminifera and multi-species isotope stratigraphy, DSDP Site 523, South Atlantic. *Journal of Foraminiferal Research*, **23**, 123 - 140.

Pearson, P. N., Shackleton, N. J., Weedon, G. P. and Hall, M. A. 1997. Multispecies planktonic foraminifer stable isotope stratigraphy through Oligocene/Miocene boundary climatic cycles, Site 926. In: Shackleton, N. J., Curry, W. B., Richter, C. and Bralower, T. J. (Eds.), *Proceeding of the Ocean Drilling Program, Scientific Results*, **154**, 33 - 68.

Pearson, P. N., Ditchfield, P. W., Singano, J., Harcourt-Brown, K. G., Nicholas, C. J., Olsson, R. N., Shackleton, N. J. and Hall, M. A. 2001. Warm tropical sea surface temperatures in the Late Cretaceous and Eocene epochs. *Nature*, **413**, 481 – 487.

Pelejero, C., Grimalt, J. O., Heilig, S., Kienast, M., Wang, L. J. 1999. High-resolution U-37(K) temperature reconstructions in the South China Sea over the past 220 kyr. *Paleoceanography*, **14**, 224 – 231.

Pinet, P. R. and Popenoe, P. 1985. A scenario of Mesozoic - Cenozoic ocean circulation over the Blake Plateau and its environs. *Geological Society of America Bulletin*, **96**, 618 - 626.

Pisias, N. G., Shackleton, N. J. and Hall, M. A. 1985. Stable isotope and calcium carbonate records from hydraulic piston cored Hole 574A: high-resolution records from the middle Miocene. In: Mayer, L., Theyer, F. *et al. Initial Reports of the Deep Sea Drilling Project,* **85**, Washington (U.S. Government Printing Office), 735 – 748.

Pisias, N. G., Mix, A. C. and Zahn, R. 1990. Nonlinear response in the global climate system: Evidence from benthic oxygen isotopic record in core RC13-110. *Paleoceanography*, **5**, 147 - 160.

Premoli Silva, I. and Boersma, A. 1986. Paleogene biofacies in the western North Atlantic Ocean. In: Vogt, P. and Tucholke, B. (Eds.). *The Geology of North America*, volume **M**, *The Western North Atlantic Region*. Geological Society of America, 527 – 546.

Prothero, D. R. 1994. The late Eocene – Oligocene extinctions. *Annual Review of Earth and Planetary Sciences*, **22**, 145 – 165.

Ramanathan, V., Cess, R. D., Harrison, E. F., Minnis, P., Barkstrom, B. R., Ahmad, E. and Hartmann, D. 1989. Cloud-radiative forcing and climate: Results from the Earth Radiation Budget Experiment. *Science*, **243**, 57 - 63.

Rea, D. K. 1994. The paleoclimatic record provided by eolian deposition in the deep sea: the geologic history of wind. *Reviews of Geophysics*, **32**, 159 – 195.

Rea, D. K., Zachos, J. C., Owen, R. M. and Gingerich, P. D. 1990. Global change at the Paleocene/Eocene boundary, Climatic and evolutionary consequences of tectonic events. *Palaeogeography, Palaeoclimatology and Palaeoecology*, **79**, 117 - 128.

Rea, D. K., Moore, T. C. and Lyle, M. 2000. Atmospheric and oceanic circulation dynamics in the equatorial Pacific in the Paleogene world. *GFF* (Geological Society of Sweden), **122**, 135 – 136.

Rind, D. 1986. The dynamics of warm and cold climates. *Journal of the Atmospheric Sciences*, **43**, 3 – 24.

Rind, D. and Chandler, M. 1991. Increased ocean heat transports and warmer climate. *Journal of Geophysical Research*, **96**, 7437 - 7461.

Robin, G. D. 1988. The Antarctic ice-sheet, its history and response to sea-level and climatic changes over the past 100 million years. *Palaeogeography, Palaeoclimatology and Palaeoecology*, **67**, 31 - 50.

Robinson, W. A., Hansen, J. E. and Reudy, R. 2001. Where's the heat? Insights from GCM experiments into the lack of eastern US warming. Twelfth symposium on global change and climate variations. American Meteorological Society, 5 – 6.

Röhl, U., Ogg, J. G., Geib, T. L. and Wefer, G. 2001. Astronomical calibration of the Danian time scale. In: Kroon, D., Norris, R. D. and Klaus, A. (Eds.). Western North Atlantic Palaeogene and Cretaceous Palaeoceanography. *Geological Society, London, Special Publications*, **183**, 163 – 184.

Rosenstiel School of Marine and Atmospheric Science, University of Miami. http://www.rsmas.miami.edu/images.html.

Ruddiman, W. F. and McIntyre, A. 1981. Oceanic mechanisms for amplification of the 23,000-year ice-volume cycle. *Science*, **212**, 617 – 627.

Ruddiman, W. F., Prell, W. L. and Raymo, M. E. 1989. Late Cenozoic uplift in southern Asia and the American West – Rationale for general-circulation modeling experiments. *Journal of Geophysical Research – Atmospheres*, **94**, 18379-18391.

Saravanan, R.and McWilliams, J. C. 1995. Multiple equilibria, natural variability, and climate transitions in an idealized ocean-atmosphere model. *Journal of Climate,* **8**, 2296 – 2323.

Schmidt, R. R and Raju, D. S. N. 1973. *Globorotalia palmerae* Cushman and Bermudez and closely related species from the lower Eocene, Cauvery Basin, south India. *Proceedings of the Koninklijke Nederlandse Akademie van Wetenschappen, Series B: Palaeontology, Geology, Physics and Chemistry*, **76**, 167 – 184.

Schrag, D. P., DePaolo, D. J. and Richter, F. M. 1995. Reconstructing past sea surface temperatures: Correcting for diagenesis of bulk marine carbonate: *Geochimica et Cosmochimica Acta*, **59**, 2265 - 2278.

Shackleton, N. J. 1974. Attainment of isotopic equilibrium between ocean water and benthonic foraminifera genus *Uvigerina*: isotopic changes in the ocean during the last glacial. *Cololoques Internationaux du C.N.R.S.*, **219**, 203 – 209.

Shackleton, N. J. and Opdyke, N. 1973. Oxygen isotope and palaeomagnetic stratigraphy of Pacific core V28-238. *Quaternary Research*, **3**, 39 – 55.

Shackleton, N. J. and Kennett, J. P. 1975. Paleotemperature history of the Cenozoic and the initiation of Antarctic glaciation: oxygen and carbon isotope analyses in DSDP Sites 277, 279, and 281. In: Kennett, J. P., Houltz, R. E. *et al.*

Initial Reports of the Deep Sea Drilling Project, **29**, Washington (U.S. Government Printing Office), 743 - 755.

Shackleton, N. J. and Boersma, A. 1981. The climate of the Eocene ocean. *Journal of the Geological Society London,* **138**, 153 - 157.

Shackleton, N. J. and Crowhurst, S. 1997. Sediment fluxes based on an orbitally tuned time scale 5 Ma to 14 Ma, Site 926. In: Shackleton, N. J., Curry, W. B., Richter, C. and Bralower, T. J. (Eds.). *Proceeding of the Ocean Drilling Program, Scientific Results*, **154**, 69 - 82.

Shackleton, N. J. and Hall, M. A. 1997. The late Miocene stable isotope record, Site 926. In: Shackleton, N. J., Curry, W. B., Richter, C. and Bralower, T. J. (Eds.). *Proceeding of the Ocean Drilling Program, Scientific Results*, **154**, 367 - 375.

Shackleton, N. J., Wiseman, J. D. H. and Buckeley, H. A. 1973. Non-equilibrium isotope fractionation between seawater and planktonic foraminiferal tests. *Nature*, **242**, 177 - 179.

Shackleton, N. J., Hall, M. A. and Boersma, A. 1984. Oxygen and carbon isotope data from Leg 74 foraminifers. *In:* Moore, T. C. Jr., Rabinowitz, P. D. *et al.* (Eds.). *Initial Reports of the Deep Sea Drilling Project,* **74**, Washington, D. C. (U.S. Government Printing Office), 599 - 612.

Shackleton, N. J., Corfield, R. M. and Hall, M. A. 1985. Stable isotope data and the ontogeny of Palaeocene planktonic foraminifera. *Journal of Foraminiferal Research*, **15**, 321 - 336.

Shackleton, N. J., Crowhurst, S. J., Weedon, G. P and Laskar, J. 1999. Astronomical calibration of Oligocene – Miocene time. *Philosophical Transactions of the Royal Society of London Series A,* **357**, 1907 – 1929.

Shackleton, N. J., Hall, M. A., Raffi, I., Tauxe, L. and Zachos, J. 2000. Astronomical calibration age for the Oligocene – Miocene boundary. *Geology*, **28**, 447 – 450.

Shipboard Scientific Party. 1998. Site 1052. In: Norris, R. D., Kroon, D., Klaus, A. *et al.* 1998. *Proceedings of the Ocean Drilling Program, Initial Results*, **171**: College Station, TX (Ocean Drilling Program), 241 – 319.

Sloan, L. C. and Barron, E. J. 1990. Equable climates during Earth history? *Geology*, **18**, 489 - 492.

Sloan, L. C. and Rea, D. K. 1995. Atmospheric carbon dioxide and early Eocene climate: A general circulation modeling sensitivity study. *Palaeogeography, Palaeoclimatology and Palaeoecology*, **119**, 275 - 292.

Sloan, L. C. and Morrill, C. 1998. Orbital forcing and Eocene continental temperatures. *Palaeogeography, Palaeoclimatology, Palaeoecology,* **144**, 21 - 35.

Sloan, L. C. and Huber, M. 2001a. North Atlantic Climate Variability in the early Palaeogene: A Climate Modeling Sensitivity Study. In: Kroon, D., Norris, R. D. and Klaus, A. (Eds.). Western North Atlantic Palaeogene and Cretaceous Palaeoceanography. *Geological Society, London, Special Publications*, **183**, 253 - 272.

Sloan, L. C. and Huber, M. 2001b. Eocene Oceanic Responses to Orbital Forcing on Precessional Time Scales. *Paleoceanography*, **16**, 101 - 111.

Sloan, L. C., Walker, J. C. G., Moore, T. C., Rea, D. K. and Zachos, J. C. 1992. Possible methane-induced polar warming in the early Eocene. *Nature*, **357**, 320 - 322.

Sloan, L. C., Walker, J. C. G. and Moore, T. C. 1995. Possible role of ocean heat transport in early Eocene climate. *Paleoceanography*, **10**, 347 - 356.

Spero, H. J. 1998. Life history and stable isotope geochemistry of planktonic foraminifera. In: Manger, W. L. and Meeks, L. K. (Eds.). Isotope paleobiology and paleoecology. *Paleontological Society Papers*, **4**, 7 – 36.

Spero, H. J., Lerche, I and Williams, D. F. 1991. Opening the carbon isotope "vital effect" black box; 2. Quantitative model for interpreting foraminiferal carbon isotope data. *Paleoceanography*, **6**, 639 - 655.

Stott, L. D. and Zachos, J. C. 1991. *Paleogene Paleoceanography Workshop Report, JOI-USSAC.*

Stott, L. D., Kennett, J. P., Shackleton, N. J. and Corfield, R. M. 1990. The evolution of Antarctic surface waters during the Paleogene: inferences from the stable isotopic composition of planktonic foraminifers, ODP Leg 113. In: Barker, P. F., Kennett, J. P. *et al. Proceedings of the Ocean Drilling Program,*

Scientific Results, **113**, College Station, TX (Ocean Drilling Program), 849 – 863.

Toumarkine, M. and Luterbacher, H. 1985. Paleocene and Eocene planktic foraminifera. In: Bolli, H. M., Saunders, J. B. and Perch-Nielsen, K. (Eds.), *Plankton Stratigraphy*, Volume 1, Cambridge University Press, Cambridge, 87 - 154.

Tripati, A. and Zachos, J. C. 2000. Paleocene and Eocene coastal ocean temperatures. *GFF* (Geological Society of Sweden), **122**, 171 – 172.

Tucholke, B. and Vogt, P. 1979. Western North Atlantic sedimentary evolution and aspects of the tectonic history. *Initial Reports of the Deep Sea Drilling Project*, **43**, U.S. Government printing Office, Washington, D. C., 795 – 863.

Urey, H. C. 1947. The thermodynamic properties of isotopic substances: *Journal of the Chemical Society*, 1947, 562 - 581.

van Andel, T. H., Heath, G. R. and Moore, T. C. Jr. 1975. Cenozoic history and paleoceanography of the central equatorial Pacific Ocean: a regional synthesis of Deep Sea Drilling Project data. *Memoir - Geological Society of America*, **143**, 127-134.

van Mourik, C. A., Brinkhuis, H and Williams, G. L. 2001. Middle to Late Eocene organic-walled dinoflagellate cysts from ODP Leg 171B, offshore Florida. In: Kroon, D., Norris, R. D. and Klaus, A. (Eds.). Western North Atlantic Palaeogene and Cretaceous Palaeoceanography. *Geological Society, London, Special Publications*, **183**, 225 – 252.

Wade, B. S., Kroon, D. and Norris, R. D. 2000. Upwelling in the late Middle Eocene at Blake Nose? *GFF* (Geological Society of Sweden), **122**, 174 – 175.

Wade, B. S., Kroon, D. and Norris, R. D. 2001. Orbitally forced climate change in the late middle Eocene at Blake Nose (Leg 171B): Evidence from stable isotopes in foraminifera. In: Kroon, D., Norris, R. D. and Klaus, A. (Eds.). Western North Atlantic Palaeogene and Cretaceous Palaeoceanography. *Geological Society, London, Special Publications*, **183**, 273 – 291.

Weedon, G. P. 1989. The detection and illustration of regular sedimentary cycles using Walsh power spectra and filtering, with examples from the Lias of Switzerland. *Journal of the Geological Society of London*, **146**, 133 – 144.

Weedon, G. P., Shackleton, N. J. and Pearson, P. N. 1997. The Oligocene time scale and cyclostratigraphy on the Ceara Rise, western equatorial Atlantic. In: Shackleton, N. J., Curry, W. B., Richter, C. and Bralower, T. J. (Eds.), *Proceeding of the Ocean Drilling Program, Scientific Results*, **154**, 101 - 116.

Williams, D. F., Be, A. W. H. and Fairbanks, R. G. 1981. Seasonal stable isotopic variations in living planktonic foraminifera from Bermuda plankton tows. *Palaeogeography, Palaeoclimatology and Palaeoecology*, **33**, 71 - 102.

Wilson, P. A. and Norris, R. D. 2001. Warm tropical ocean surface and global anoxia during the mid-Cretaceous period. *Nature*, **412**, 425 – 429.

Wing, S. L., Bao, H. and Koch, P. L. 2000. An early Eocene cool period? Evidence for continental cooling during the warmest part of the Cenozoic. In: Huber, B. T., MacLoed, K. G and Wing, S. L. (Eds.). *Warm Climates in Earth History*. Cambridge University Press, 197 – 237.

Wise, S. W. Jr., Breza, J. R., Harwood, D. M. and Wei, W. 1991. Paleogene glacial history of Antarctica. In: Mueller, D. W., McKenzie, J. A and Weissert, H. *Controversies in Modern Geology*. Academic, San Diego, 133 - 171.

Woodruff, F. and Savin, S. M. 1991. Mid-Miocene isotope stratigraphy in the deep sea: high-resolution correlations, paleoclimatic cycles, and sediment preservation. *Paleoceanography*, **6**, 755 – 806.

Woodruff, F. Savin, S. M. and Douglas, R. G. 1980. Biological fractionation of oxygen and carbon isotopes by Recent benthic foraminifera. *Marine Micropaleontology*, **5**, 3 – 11.

Wu, G., Herguera, C. and Berger, W. H. 1990. Differential dissolution, Modification of late Pleistocene oxygen isotope records in the western equatorial Pacific. *Paleoceanography*, **5**, 581 - 594.

Zachos , J. C., Rea, D. K., Seto, K., Nomura, R. and Niitsuma, N. 1992. Paleogene and Early Neogene deep water paleoceanography of the Indian Ocean as determined from benthic foraminifer stable carbon and oxygen isotope records. In: Duncan, R. A., Rea, D. K., *et al.* (Eds.) *Synthesis of Results of Scientific Drilling in the Indian Ocean*, Geophysical Monograph **70**, American Geophysical Union, 351 - 385.

Zachos, J. C., Lohmann, K. C., Walker, J. C. G. and Wise, S. W. 1993, Abrupt Climate Change and Transient Climates in the Paleogene: A Marine Perspective. *Journal of Geology*, **100**, 191 - 213.

Zachos, J. C., Stott, L. D. and Lohmann, K. C. 1994. Evolution of early Cenozoic marine temperatures. *Paleoceanography*, **9**, 353 - 387.

Zachos, J. C., Quinn, T. M. and Salamy, K. A., 1996. High-resolution (10^4 years) deep-sea foraminiferal stable isotope records of the Eocene-Oligocene climate transition. *Paleoceanography*, **11**, 251 - 266.

Zachos, J. C., Flower, B. P. and Paul, H. 1997. Orbitally paced climate oscillations across the Oligocene/Miocene boundary. *Nature*, **388**, 567 – 570.

Zachos, J. C., Opdyke, B. N., Quinn, T. M., Jones, C. E. and Halliday, A. N. 1999. Eocene-Oligocene Climate and Seawater $^{87}Sr/^{86}Sr$: Is There A Link? In: Veizer, J. (Ed.). The Chemical Evolution of the Oceans. *Chemical Geology*, special volume, **161**, 165 - 180.

Zachos, J.C., Pagani, M., Sloan, L., Thomas, E. and Billups, K. 2001a. Trends, Rhythms, and Aberrations in Global Climate 65 Ma to present. *Science*, **292**, 686 – 693.

Zachos, J. C., Shackleton, N. J., Revenaugh, J. S., Pälike, H. and Flower, B. P. 2001b. Climate Response to Orbital Forcing Across the Oligocene – Miocene Boundary. *Science*, **292**, 274 – 278.

Zahn, R. and Diester-Haass, L. 1995. Orbital forcing of Eocene-Oligocene climate: High resolution records of benthic isotopes from ODP Site 689, Maud Rise. *ICP V Progromme Abstracts, 5th International Conference on Paleoceanography*, Halifax, 177.

APPENDICES

The following pages list the stable isotopic results from Site 1052. The right hand column (*n*) in Appendix 1 lists the number of specimens of foraminifera analysed for each sample. Duplicate samples were occasionally analysed for further details on analytical precision and the initial "D" indicates these. A number of values shown in the Appendix 1 have been rejected and thus removed from the figures in this thesis. These results are highlighted in grey. This was because the recorded values were significantly different from the surrounding results. Many of these samples were re-analysed using alternative species (e.g. *Morozovella spinulosa* or *Acarinina praetopilensis*) and are indicated by the initial "R". The anomalous values are probably the result of low sample weights.

To reconstruct the composite stable isotopic time series (Appendix 2) the corrected planktonic foraminifera values were used, as discussed in section 3.5. When *Morozovella crassata* values were unavailable for a particular sample (normally due to low species abundance) alternative species were used in the composite record. *Morozovella spinulosa* was normally selected, however when this species was also unavailable stable isotopic values from *Acarinina praetopilensis* were utilised.

There are a number of intervals within the carbon isotope record (e.g. 91, 86 and 83 mcd) where negative $\delta^{13}C$ values are recorded (Appendix 1). These results are unusual and have been removed from the figures in this thesis. Raw results from the mass spectrometer did not suggest instrumentation or calibration problems although these cannot be ruled out. These results were investigated further by the additional analysis of thermocline, benthic foraminifera and bulk carbonate over these intervals. These light $\delta^{13}C$ values were not recorded in bulk carbonate, benthic (*Nuttalides truempyi*) or thermocline (*Subbotina utilisindex*) foraminiferal results, and are therefore only seen in the mixed layer.

A probable causal mechanism for these changes could be periodic influxes of freshwater. However, the amount of freshwater required would demand substantial changes in the hydrological cycle (discussed in section 5.2). If the decrease in $\delta^{13}C$ of

G. mexicana reflected changes in seawater chemistry or productivity, then the light values should also be recorded in the $\delta^{13}C$ of the thermocline dwelling *S. utilisindex*. These shifts cannot therefore be explained at present, although it is unlikely that they reflect large changes in global carbon cycling.

There were other intervals when unusually light or heavy isotopic values were recorded. However, when sample weights were high (>15 specimens) and no problems occurred with the mass spectrometer, there was no reason to believe that these results did not reflect a true record of Eocene climate variability and these were therefore not rejected from the data set.

Appendix 1. Stable Isotope Results at Site 1052

Hole	Core	Section	Interval (cm)	Depth (mbsf)	MCD	$\delta^{18}O$	$\delta^{13}C$	*n*
Globigerinatheka mexicana								
1052B	10H	1	73-76	72.75	77.18	-0.17	1.58	15
1052B	10H	1	83-86	72.85	77.28	0.07	1.92	15
1052B	10H	1	93-96	72.95	77.38	-0.57	1.58	15
1052B	10H	1	103-106	73.05	77.48	-0.12	1.91	15
1052B	10H	1	113-116	73.15	77.58	0.27	1.51	15
1052B	10H	1	123-126	73.25	77.68	0.05	1.63	15
1052B	10H	1	133-136	73.35	77.78	-0.85	1.68	15
1052B	10H	1	143-146	73.45	77.88	-0.80	1.70	15
1052B	10H	2	3-6	73.55	77.98	-0.62	1.83	15
1052B	10H	2	13-16	73.65	78.08	-0.57	1.75	15
1052B	10H	2	23-26	73.75	78.18	-0.14	1.62	15
1052B	10H	2	33-36	73.85	78.28	-0.33	1.81	15
1052B	10H	2	43-46	73.95	78.38	-0.64	1.79	15
1052B	10H	2	53-56	74.05	78.48	-0.46	1.96	15
1052B	10H	2	63-66	74.15	78.58	-0.33	2.12	15
1052B	10H	2	73-76	74.25	78.68	-0.54	2.08	15
1052B	10H	2	83-86	74.35	78.78	-0.66	2.08	15
1052B	10H	2	93-96	74.45	78.88	0.46	1.52	15
1052B	10H	2	103-106	74.55	78.98	-0.52	1.73	15
1052B	10H	2	113-116	74.65	79.08	-0.55	1.81	15
1052B	10H	2	123-126	74.75	79.18	-0.35	1.85	15
1052B	10H	2	133-136	74.85	79.28	-0.40	1.75	15
1052B	10H	2	143-146	74.95	79.38	-0.59	1.86	15
1052B	10H	3	3-6	75.05	79.48	-0.42	1.97	15
1052B	10H	3	13-16	75.15	79.58	-0.61	1.82	15
1052B	10H	3	23-26	75.25	79.68	-0.82	1.65	15
1052B	10H	3	33-36	75.35	79.78	-0.59	1.62	15
1052B	10H	3	43-46	75.45	79.88	-1.12	1.75	15
1052B	10H	3	53-56	75.55	79.98	-0.78	1.68	D 15
1052B	10H	3	53-56	75.55	79.98	-0.71	1.88	D 15
1052B	10H	3	63-66	75.65	80.08	-0.14	1.94	15
1052B	10H	3	73-76	75.75	80.18	-1.02	1.40	15
1052B	10H	3	83-86	75.85	80.28	-0.54	1.69	15
1052B	10H	3	93-96	75.95	80.38	-0.43	1.83	15
1052B	10H	3	103-106	76.05	80.48	-0.56	1.68	15
1052B	10H	3	113-116	76.15	80.58	-0.54	2.09	15
1052B	10H	3	123-126	76.25	80.68	-1.20	2.10	15
1052B	10H	3	133-136	76.35	80.78	-0.91	2.31	15
1052B	10H	3	143-146	76.45	80.88	-0.58	2.52	15
1052B	10H	4	3-6	76.55	80.98	-0.76	2.32	15
1052B	10H	4	13-16	76.65	81.08	-0.47	2.13	15
1052B	10H	4	23-26	76.75	81.18	-0.72	2.08	15
1052B	10H	4	33-36	76.85	81.28	-0.78	1.23	15
1052B	10H	4	43-46	76.95	81.38	-0.56	1.97	15
1052B	10H	4	53-56	77.05	81.48	-0.69	2.08	15
1052B	10H	4	63-66	77.15	81.58	-0.74	2.60	15
1052B	10H	4	73-76	77.25	81.68	-0.58	2.77	15
1052B	10H	4	83-86	77.35	81.78	-0.70	2.45	15
1052B	10H	4	93-96	77.45	81.88	-0.56	2.51	15
1052B	10H	4	103-106	77.55	81.98	-0.95	1.83	15
1052B	10H	4	113-116	77.65	82.08	-0.92	2.14	15

Appendix 1. Stable Isotope Results at Site 1052

Hole	Core	Section	Interval (cm)	Depth (mbsf)	MCD	$\delta^{18}O$	$\delta^{13}C$	*n*
***Globigerinatheka mexicana* (continued)**								
1052B	10H	4	123-126	77.75	82.18	-1.26	2.24	15
1052B	10H	4	133-136	77.85	82.28	-1.55	1.51	15
1052B	10H	4	143-146	77.95	82.38	-1.13	2.23	15
1052B	10H	5	3-6	78.05	82.48	-1.86	1.39	15
1052B	10H	5	13-16	78.15	82.58	-1.46	1.51	15
1052B	10H	5	23-26	78.25	82.68	-1.12	1.34	15
1052B	10H	5	33-36	78.35	82.78	-1.63	0.86	15
1052B	10H	5	43-46	78.45	82.88	-2.00	0.95	15
1052B	10H	5	53-56	78.55	82.98	-1.14	1.09	15
1052B	10H	5	63-66	78.65	83.08	-0.69	1.93	15
1052B	10H	5	73-76	78.75	83.18	-1.45	-0.05	15
1052B	10H	5	83-86	78.85	83.28	-1.46	-0.23	15
1052B	10H	5	93-96	78.95	83.38	-0.98	2.36	15
1052B	10H	5	103-106	79.05	83.48	-0.85	2.08	15
1052B	10H	5	113-116	79.15	83.58	-0.74	2.04	15
1052B	10H	5	123-126	79.25	83.68	-0.80	1.82	15
1052B	10H	5	133-136	79.35	83.78	-0.67	2.29	15
1052B	10H	5	143-146	79.45	83.88	-0.79	2.66	15
1052B	10H	6	3-6	79.55	83.98	-1.18	2.22	15
1052B	10H	6	13-16	79.65	84.08	-0.67	2.63	15
1052B	10H	6	23-26	79.75	84.18	-0.57	2.62	15
1052B	10H	6	33-36	79.85	84.28	-0.64	2.22	15
1052B	10H	6	43-46	79.95	84.38	-0.83	2.34	15
1052B	10H	6	53-56	80.05	84.48	-1.02	2.10	15
1052B	10H	6	63-66	80.15	84.58	-0.66	2.69	15
1052B	10H	6	73-76	80.25	84.68	-0.58	2.24	15
1052B	10H	6	83-86	80.35	84.78	-0.76	2.00	15
1052B	10H	6	93-96	80.45	84.88	-0.33	2.43	15
1052B	10H	6	103-106	80.55	84.98	-0.78	2.51	15
1052B	10H	6	113-116	80.65	85.08	-0.44	2.38	15
1052B	10H	6	123-126	80.75	85.18	-0.80	2.26	15
1052F	10H	2	83-86	83.35	85.11	-0.40	2.37	15
1052F	10H	2	93-96	83.45	85.21	-0.05	2.37	15
1052F	10H	2	103-106	83.55	85.31	-0.27	2.43	15
1052F	10H	2	113-116	83.65	85.41	-1.75	0.52	15
1052F	10H	2	123-126	83.75	85.51	-1.38	1.78	15
1052F	10H	2	133-136	83.85	85.61	-1.19	2.25	15
1052F	10H	2	143-146	83.95	85.71	-1.14	2.10	15
1052F	10H	3	3-6	84.05	85.81	-1.50	1.29	15
1052F	10H	3	13-16	84.15	85.91	-1.45	2.16	15
1052F	10H	3	23-26	84.25	86.01	-1.33	-0.07	15
1052F	10H	3	33-36	84.35	86.11	-1.02	1.34	15
1052F	10H	3	43-46	84.45	86.21	-1.06	1.42	15
1052F	10H	3	53-56	84.55	86.31	-0.90	2.39	15
1052F	10H	3	63-66	84.65	86.41	-0.91	1.51	15
1052F	10H	3	73-76	84.75	86.51	-1.16	1.59	15
1052F	10H	3	83-86	84.85	86.61	-1.30	1.30	15
1052F	10H	3	93-96	84.95	86.71	-1.18	1.32	15
1052F	10H	3	103-106	85.05	86.81	-1.37	1.00	15
1052F	10H	3	113-116	85.15	86.91	-1.25	1.73	15
1052F	10H	3	123-126	85.25	87.01	-0.91	1.84	15

Appendix 1. Stable Isotope Results at Site 1052

Hole	Core	Section	Interval (cm)	Depth (mbsf)	MCD	$\delta^{18}O$	$\delta^{13}C$	*n*
***Globigerinatheka mexicana* (continued)**								
1052F	10H	3	133-136	85.35	87.11	-1.09	1.71	15
1052F	10H	3	143-146	85.45	87.21	-1.02	1.98	15
1052F	10H	4	3-6	85.55	87.31	-1.33	1.81	15
1052F	10H	4	13-16	85.65	87.41	-1.28	1.98	15
1052F	10H	4	23-26	85.75	87.51	-0.87	2.26	15
1052F	10H	4	33-36	85.85	87.61	-0.94	2.25	15
1052F	10H	4	43-46	85.95	87.71	-1.09	2.20	15
1052F	10H	4	53-56	86.05	87.81	-0.91	2.14	15
1052F	10H	4	63-66	86.15	87.91	-0.98	1.96	15
1052F	10H	4	73-76	86.25	88.01	-0.98	2.25	15
1052F	10H	4	83-86	86.35	88.11	-0.97	2.29	15
1052F	10H	4	93-96	86.45	88.21	-0.96	1.88	15
1052F	10H	4	103-106	86.55	88.31	-0.89	2.28	15
1052F	10H	4	113-116	86.65	88.41	-0.74	2.40	15
1052F	10H	4	123-126	86.75	88.51	-0.68	2.15	15
1052F	10H	4	133-136	86.85	88.61	-1.45	1.75	15
1052F	10H	4	143-146	86.95	88.71	-0.58	2.53	15
1052F	10H	5	3-6	87.05	88.81	-0.62	2.50	15
1052F	10H	5	13-16	87.15	88.91	-0.74	1.75	15
1052F	10H	5	23-26	87.25	89.01	-0.60	2.21	15
1052F	10H	5	33-36	87.35	89.11	-0.93	2.05	15
1052F	10H	5	43-46	87.45	89.21	-0.84	1.99	15
1052F	10H	5	53-56	87.55	89.31	-1.10	1.98	15
1052B	11H	2	73-76	83.75	89.37	-0.37	2.52	15
1052F	10H	5	63-66	87.65	89.41	-0.51	2.30	15
1052B	11H	2	83-86	83.85	89.47	-0.86	1.69	15
1052F	10H	5	73-76	87.75	89.51	-0.67	2.53	15
1052B	11H	2	93-96	83.95	89.57	-0.64	2.49	15
1052F	10H	5	83-86	87.85	89.61	-0.70	2.29	15
1052B	11H	2	103-106	84.05	89.67	-1.13	1.22	15
1052B	11H	2	113-116	84.15	89.77	-0.45	2.44	15
1052B	11H	2	123-126	84.25	89.87	-0.97	1.49	15
1052B	11H	2	133-136	84.35	89.97	-0.92	1.73	15
1052B	11H	2	143-146	84.45	90.07	-0.67	2.29	15
1052B	11H	3	3-6	84.55	90.17	-1.05	2.20	15
1052B	11H	3	13-16	84.65	90.27	-0.77	2.59	15
1052B	11H	3	23-26	84.75	90.37	-0.87	2.60	15
1052B	11H	3	43-46	84.95	90.57	-1.07	1.63	15
1052B	11H	3	53-56	85.05	90.67	-0.49	2.27	15
1052B	11H	3	63-66	85.15	90.77	-0.54	2.53	15
1052B	11H	3	73-76	85.25	90.87	-0.57	2.47	D 15
1052B	11H	3	73-76	85.25	90.87	-0.61	2.52	D 15
1052B	11H	3	83-86	85.35	90.97	-0.77	1.79	15
1052B	11H	3	93-96	85.45	91.07	-0.51	2.56	15
1052B	11H	3	103-106	85.55	91.17	-0.81	1.68	15
1052B	11H	3	113-116	85.65	91.27	-0.56	2.45	15
1052B	11H	3	123-126	85.75	91.37	-1.14	0.08	15
1052B	11H	3	133-136	85.85	91.47	-0.77	1.69	15
1052B	11H	3	143-146	85.95	91.57	-0.50	2.08	15
1052B	11H	4	3-6	86.05	91.67	-0.66	2.41	15
1052B	11H	4	13-16	86.15	91.77	-0.76	1.87	15

Appendix 1. Stable Isotope Results at Site 1052

Hole	Core	Section	Interval (cm)	Depth (mbsf)	MCD	$\delta^{18}O$	$\delta^{13}C$	*n*
***Globigerinatheka mexicana* (continued)**								
1052B	11H	4	23-26	86.25	91.87	-0.79	1.56	15
1052B	11H	4	33-36	86.35	91.97	-0.62	2.43	15
1052B	11H	4	43-46	86.45	92.07	-0.53	2.03	15
1052B	11H	4	53-56	86.55	92.17	-0.44	1.97	15
1052B	11H	4	63-66	86.65	92.27	-0.47	2.10	15
1052B	11H	4	73-76	86.75	92.37	-0.40	1.92	15
1052B	11H	4	83-86	86.85	92.47	-0.45	2.28	15
1052B	11H	4	93-96	86.95	92.57	-0.46	2.38	15
1052B	11H	4	103-106	87.05	92.67	-0.56	2.10	15
1052B	11H	4	113-116	87.15	92.77	-0.69	2.26	15
1052B	11H	4	123-126	87.25	92.87	-0.48	2.33	15
1052B	11H	4	133-136	87.35	92.97	-0.47	2.37	15
1052B	11H	4	143-146	87.45	93.07	-0.61	2.24	15
1052B	11H	5	3-6	87.55	93.17	-0.77	2.12	15
1052B	11H	5	13-16	87.65	93.27	-0.69	2.25	15
1052B	11H	5	23-26	87.75	93.37	-0.80	2.15	15
1052F	14H	6	93-96	127.55	130.91	-0.20	2.13	20
Morozovella crassata								
1052B	11H	4	93-96	86.95	92.57	-0.76	3.27	20
1052B	11H	4	103-106	87.05	92.67	-0.71	3.28	20
1052B	11H	4	113-116	87.15	92.77	-0.70	3.19	20
1052B	11H	4	123-126	87.25	92.87	-0.73	3.33	20
1052B	11H	4	133-136	87.35	92.97	-0.77	2.91	16
1052B	11H	4	143-146	87.45	93.07	-1.21	2.35	10
1052B	11H	5	63-66	88.15	93.77	-0.88	3.21	17
1052B	11H	5	73-76	88.25	93.87	-1.18	2.86	19
1052B	11H	5	83-86	88.35	93.97	-1.22	2.87	19
1052B	11H	5	93-96	88.45	94.07	-1.12	3.15	19
1052F	11H	1	113-116	91.65	94.13	-2.23	0.95	5
1052B	11H	5	103-106	88.55	94.17	-0.94	3.08	19
1052F	11H	1	123-126	91.75	94.23	-1.36	2.80	15
1052F	11H	1	143-146	91.95	94.43	-2.17	2.03	4
1052F	11H	2	33-36	92.35	94.83	-1.06	3.02	20
1052F	11H	2	43-46	92.45	94.93	-1.07	3.12	16
1052F	11H	2	73-76	92.75	95.23	-0.63	3.26	15
1052F	11H	2	83-86	92.85	95.33	-2.63	1.93	6
1052F	11H	2	93-96	92.95	95.43	-1.07	3.13	18
1052F	11H	2	103-106	93.05	95.53	-0.96	3.49	20
1052F	11H	2	113-116	93.15	95.63	-0.96	3.34	20
1052F	11H	2	123-126	93.25	95.73	-1.09	3.45	20
1052F	11H	2	133-136	93.35	95.83	-1.33	3.07	20
1052F	11H	2	143-146	93.45	95.93	-1.04	3.40	20
1052F	11H	3	3-6	93.55	96.03	-1.85	2.55	20
1052F	11H	3	13-16	93.65	96.13	-1.24	3.43	20
1052F	11H	3	23-26	93.75	96.23	-0.94	3.41	20
1052F	11H	3	63-66	94.15	96.63	-0.84	3.03	15
1052F	11H	3	93-96	94.45	96.93	-2.11	2.51	5
1052F	11H	3	103-106	94.55	97.03	-1.96	1.65	5
1052F	11H	3	113-116	94.65	97.13	-1.24	2.89	20

Appendix 1. Stable Isotope Results at Site 1052

Hole	Core	Section	Interval (cm)	Depth (mbsf)	MCD	$\delta^{18}O$	$\delta^{13}C$	*n*
Morozovella crassata **(continued)**								
1052F	11H	3	123-126	94.75	97.23	-0.91	3.49	20
1052F	11H	3	133-136	94.85	97.33	-1.04	3.18	20
1052F	11H	3	143-146	94.95	97.43	-1.45	2.39	15
1052F	11H	4	3-6	95.05	97.53	-0.60	3.52	19
1052F	11H	4	33-36	95.35	97.83	-0.99	3.16	15
1052F	11H	4	43-46	95.45	97.93	-1.28	3.33	18
1052F	11H	4	53-56	95.55	98.03	-0.40	3.39	20
1052F	11H	4	63-66	95.65	98.13	-0.84	3.45	20
1052F	11H	4	73-76	95.75	98.23	-0.58	3.56	20
1052F	11H	4	83-86	95.85	98.33	-0.85	3.61	20
1052F	11H	4	93-96	95.95	98.43	-0.79	3.59	20
1052F	11H	4	113-116	96.15	98.63	-0.98	3.63	21
1052F	11H	4	123-126	96.25	98.73	-0.76	3.63	20
1052F	11H	4	133-136	96.35	98.83	-1.60	3.15	20
1052F	11H	4	143-146	96.45	98.93	-1.35	3.14	15
1052F	11H	5	3-6	96.55	99.03	-1.56	3.17	18
1052F	11H	5	13-16	96.65	99.13	-1.68	3.28	17
1052F	11H	5	23-26	96.75	99.23	-1.43	3.49	18
1052F	11H	5	33-36	96.85	99.33	-1.49	3.54	20
1052F	11H	5	43-46	96.95	99.43	-1.55	3.48	20
1052F	11H	5	53-56	97.05	99.53	-1.30	3.54	19
1052F	11H	5	63-66	97.15	99.63	-1.34	3.59	20
1052F	11H	5	73-76	97.25	99.73	-1.26	3.56	20
1052F	11H	5	83-86	97.35	99.83	-1.14	3.63	18
1052F	11H	5	93-96	97.45	99.93	-1.13	3.53	20
1052F	11H	5	103-106	97.55	100.03	-1.61	3.33	20
1052F	11H	5	113-116	97.65	100.13	-1.23	3.58	15
1052F	11H	5	123-126	97.75	100.23	-1.80	3.26	18
1052F	11H	5	133-136	97.85	100.33	-1.02	3.49	19
1052F	11H	5	143-146	97.95	100.43	-1.28	3.07	16
1052F	11H	6	3-6	98.05	100.53	-1.05	3.58	20
1052F	11H	6	13-16	98.15	100.63	-1.40	3.45	20
1052F	11H	6	23-26	98.25	100.73	-1.22	3.29	15
1052F	11H	6	33-36	98.35	100.83	-2.14	1.90	7
1052F	11H	6	53-56	98.55	101.03	-1.72	2.51	18
1052F	11H	6	63-66	98.65	101.13	-1.23	3.28	15
1052F	11H	6	73-76	98.75	101.23	-1.48	3.04	18
1052F	11H	6	83-86	98.85	101.33	-0.97	3.40	17
1052F	11H	6	93-96	98.95	101.43	-1.70	2.83	15
1052F	11H	6	103-106	99.05	101.53	-1.61	2.16	19
1052F	11H	6	113-116	99.15	101.63	-1.09	0.76	5
1052F	11H	6	123-126	99.25	101.73	-1.21	3.11	18
1052F	11H	6	133-136	99.35	101.83	-2.33	1.99	6
1052F	11H	6	143-146	99.45	101.93	-1.34	2.87	19
1052F	11H	7	3-6	99.55	102.03	-1.35	3.08	19
1052B	12H	3	133-136	95.35	102.05	-1.55	3.04	15
1052F	11H	7	13-16	99.65	102.13	-0.97	3.32	15
1052B	12H	3	143-146	95.45	102.15	-1.62	2.95	20
1052F	11H	7	23-26	99.75	102.23	-1.09	3.31	18
1052B	12H	4	3-6	95.55	102.25	-1.70	2.90	20

Appendix 1. Stable Isotope Results at Site 1052

Hole	Core	Section	Interval (cm)	Depth (mbsf)	MCD	$\delta^{18}O$	$\delta^{13}C$	*n*
Morozovella crassata **(continued)**								
1052B	12H	4	13-16	95.65	102.35	-1.21	3.15	15
1052B	12H	4	73-76	96.25	102.95	-1.69	3.27	15
1052B	12H	4	103-106	96.55	103.25	-1.90	3.04	19
1052B	12H	4	123-126	96.75	103.45	-2.73	1.96	8
1052B	12H	4	133-136	96.85	103.55	-1.75	3.25	15
1052B	12H	4	143-146	96.95	103.65	-1.44	3.01	15
1052B	12H	5	3-6	97.05	103.75	-1.70	3.13	15
1052B	12H	5	13-16	97.15	103.85	-1.35	3.21	18
1052B	12H	5	23-26	97.25	103.95	-1.20	3.14	19
1052B	12H	5	33-36	97.35	104.05	-3.72	2.08	4
1052B	12H	5	43-46	97.45	104.15	-4.41	0.44	4
1052B	12H	5	53-56	97.55	104.25	-1.97	2.15	16
1052B	12H	5	63-66	97.65	104.35	-1.81	2.62	19
1052B	12H	5	73-76	97.75	104.45	-2.04	2.81	20
1052B	12H	5	83-86	97.85	104.55	-1.86	2.51	17
1052B	12H	5	93-96	97.95	104.65	-1.82	2.67	20
1052B	12H	5	103-106	98.05	104.75	-1.01	3.30	20
1052B	12H	5	113-116	98.15	104.85	-1.68	2.71	20
1052B	12H	5	123-126	98.25	104.95	-1.52	2.75	20
1052B	12H	5	133-136	98.35	105.05	-1.64	2.75	16
1052B	12H	5	143-146	98.45	105.15	-1.53	2.91	20
1052F	12H	2	73-76	102.25	105.16	-1.56	2.88	19
1052B	12H	6	3-6	98.55	105.25	-4.22	-0.14	4
1052B	12H	6	13-16	98.65	105.35	-1.57	3.22	15
1052F	12H	2	93-96	102.45	105.36	-1.63	3.17	18
1052B	12H	6	23-26	98.75	105.45	-1.68	3.09	20
1052F	12H	2	103-106	102.55	105.46	-1.70	3.04	20
1052F	12H	2	113-116	102.65	105.56	-1.37	2.97	18
1052F	12H	2	123-126	102.75	105.66	-1.20	3.97	20
1052F	12H	2	133-136	102.85	105.76	-1.51	2.39	18
1052F	12H	2	143-146	102.95	105.86	-2.34	1.86	9
1052F	12H	3	3-6	103.05	105.96	-1.66	2.69	15
1052F	12H	3	13-16	103.15	106.06	-1.56	3.01	18
1052F	12H	3	23-26	103.25	106.16	-1.59	2.85	14
1052F	12H	3	33-36	103.35	106.26	-1.40	3.13	20
1052F	12H	3	43-46	103.45	106.36	-1.29	2.90	17
1052F	12H	3	53-56	103.55	106.46	-1.53	2.94	15
1052F	12H	3	63-66	103.65	106.56	-1.51	3.14	15
1052F	12H	3	73-76	103.75	106.66	-1.41	2.74	15
1052F	12H	3	103-106	104.05	106.96	-2.56	2.48	4
1052F	12H	3	113-116	104.15	107.06	-1.48	3.00	15
1052F	12H	4	33-36	104.85	107.76	-2.61	2.28	4
1052F	12H	4	63-66	105.15	108.06	-1.78	3.08	15
1052F	12H	4	83-86	105.35	108.26	-2.00	-0.08	9
1052F	12H	4	93-96	105.45	108.36	-2.05	2.23	15
1052F	12H	4	113-116	105.65	108.56	1.06	1.99	6
1052F	12H	5	3-6	106.05	108.96	0.81	2.56	6
1052F	12H	5	13-16	106.15	109.06	-1.03	2.80	20
1052F	12H	5	23-26	106.25	109.16	0.05	2.71	5
1052F	12H	5	33-36	106.35	109.26	0.63	2.58	7

Appendix 1. Stable Isotope Results at Site 1052

Hole	Core	Section	Interval (cm)	Depth (mbsf)	MCD	$\delta^{18}O$	$\delta^{13}C$	*n*
***Morozovella crassata* (continued)**								
1052F	12H	5	43-46	106.45	109.36	-0.07	2.47	15
1052F	12H	5	53-56	106.55	109.46	-0.77	2.92	17
1052F	12H	5	63-66	106.65	109.56	-0.77	2.89	20
1052F	12H	5	73-76	106.75	109.66	-1.01	2.87	20
1052F	12H	5	83-86	106.85	109.76	-0.24	2.71	15
1052F	12H	5	93-96	106.95	109.86	-1.20	2.85	15
1052F	12H	5	103-106	107.05	109.96	0.80	2.14	4
1052F	12H	5	113-116	107.15	110.06	-1.02	2.79	20
1052F	12H	5	123-126	107.25	110.16	-1.20	3.07	20
1052F	12H	5	133-136	107.35	110.26	-0.56	2.81	20
1052F	12H	5	143-146	107.45	110.36	-0.71	2.88	20
1052F	12H	6	3-6	107.55	110.46	-1.41	2.67	20
1052F	12H	6	13-16	107.65	110.56	-1.02	2.78	20
1052F	12H	6	23-26	107.75	110.66	-1.02	2.90	20
1052F	12H	6	33-36	107.85	110.76	-1.01	2.73	20
1052F	12H	6	43-46	107.95	110.86	-1.16	2.61	20
1052F	12H	6	53-56	108.05	110.96	-0.84	2.74	20
1052F	12H	6	63-66	108.15	111.06	-0.88	2.75	20
1052F	12H	6	73-76	108.25	111.16	-0.94	3.15	20
1052F	12H	6	83-86	108.35	111.26	-1.08	3.01	20
1052F	12H	6	93-96	108.45	111.36	-0.61	2.68	20
1052F	12H	6	113-116	108.65	111.56	-0.89	2.76	15
1052F	12H	6	123-126	108.75	111.66	-0.17	2.83	18
1052F	12H	6	133-136	108.85	111.76	-1.27	1.59	18
1052B	13H	3	123-126	104.75	111.80	-7.07	-2.68	2
1052F	12H	6	143-146	108.95	111.86	-1.26	2.84	19
1052B	13H	3	133-136	104.85	111.90	-1.74	2.54	15
1052F	12H	7	3-6	109.05	111.96	-0.78	2.92	20
1052B	13H	3	143-146	104.95	112.00	-1.81	2.80	15
1052F	12H	7	13-16	109.15	112.06	-0.34	2.73	15
1052B	13H	4	3-6	105.05	112.10	-2.42	2.50	15
1052F	12H	7	23-26	109.25	112.16	1.13	2.23	5
1052B	13H	4	13-16	105.15	112.20	-2.92	1.61	20
1052F	12H	7	33-36	109.35	112.26	2.44	2.39	4
1052B	13H	4	23-26	105.25	112.30	-5.08	-0.78	3
1052F	12H	7	43-46	109.45	112.36	-0.77	2.93	15
1052B	13H	4	33-36	105.35	112.40	-2.15	2.47	20
1052B	13H	4	43-46	105.45	112.50	-1.98	3.15	20
1052B	13H	4	53-56	105.55	112.60	-1.46	3.30	20
1052B	13H	4	63-66	105.65	112.70	-1.86	2.51	15
1052B	13H	4	73-76	105.75	112.80	-1.35	3.34	20
1052B	13H	4	83-86	105.85	112.90	-2.20	2.79	15
1052F	13H	1	53-56	110.05	112.96	-1.26	2.36	20
1052B	13H	4	93-96	105.95	113.00	-1.98	2.82	16
1052F	13H	1	63-66	110.15	113.06	-1.23	2.68	20
1052B	13H	4	103-106	106.05	113.10	-1.87	3.24	19
1052F	13H	1	73-76	110.25	113.16	-1.30	2.76	20
1052B	13H	4	113-116	106.15	113.20	-2.04	2.52	15
1052F	13H	1	83-86	110.35	113.26	-1.12	2.78	20
1052F	13H	1	93-96	110.45	113.36	-0.90	2.93	20

Appendix 1. Stable Isotope Results at Site 1052

Hole	Core	Section	Interval (cm)	Depth (mbsf)	MCD	$\delta^{18}O$	$\delta^{13}C$	*n*
Morozovella crassata **(continued)**								
1052F	13H	1	103-106	110.55	113.46	-0.60	2.88	20
1052F	13H	1	113-116	110.65	113.56	-1.02	2.08	20
1052F	13H	1	123-126	110.75	113.66	-0.35	2.85	20
1052F	13H	1	133-136	110.85	113.76	-1.15	2.84	20
1052F	13H	1	143-146	110.95	113.86	-1.27	2.45	20
1052F	13H	2	3-6	111.05	113.96	-1.26	2.82	20
1052F	13H	2	13-16	111.15	114.06	-1.00	2.80	20
1052F	13H	2	23-26	111.25	114.16	-0.94	2.79	20
1052F	13H	2	33-36	111.35	114.26	-1.13	2.76	20
1052F	13H	2	43-46	111.45	114.36	-0.43	2.75	20
1052F	13H	2	53-56	111.55	114.46	-0.87	2.86	20
1052F	13H	2	63-66	111.65	114.56	-0.81	2.95	20
1052F	13H	2	73-76	111.75	114.66	-1.16	3.05	20
1052F	13H	2	83-86	111.85	114.76	-1.05	2.34	20
1052F	13H	2	93-96	111.95	114.86	-0.87	3.10	18
1052F	13H	2	103-106	112.05	114.96	-1.60	2.81	18
1052F	13H	2	113-116	112.15	115.06	-0.54	2.85	20
1052F	13H	2	123-126	112.25	115.16	-0.27	3.08	20
1052F	13H	2	133-136	112.35	115.26	-0.27	2.74	20
1052F	13H	2	143-146	112.45	115.36	-0.83	3.03	20
1052F	13H	3	3-6	112.55	115.46	-1.34	3.32	20
1052F	13H	3	13-16	112.65	115.56	-0.82	2.81	20
1052F	13H	3	23-26	112.75	115.66	-0.69	2.80	20
1052F	13H	3	33-36	112.85	115.76	-0.73	2.94	20
1052F	13H	3	43-46	112.95	115.86	-0.78	2.88	20
1052F	13H	3	53-56	113.05	115.96	-0.19	2.59	20
1052F	13H	3	63-66	113.15	116.06	-1.07	3.04	20
1052F	13H	3	73-76	113.25	116.16	-0.56	2.90	15
1052F	13H	3	83-86	113.35	116.26	-1.05	2.84	20
1052F	13H	3	93-96	113.45	116.36	-1.05	2.93	20
1052F	13H	3	103-106	113.55	116.46	-1.12	2.77	20
1052F	13H	3	113-116	113.65	116.56	-1.14	2.93	20
1052F	13H	3	123-126	113.75	116.66	-0.66	3.00	20
1052F	13H	3	133-136	113.85	116.76	-1.08	2.92	20
1052F	13H	3	143-146	113.95	116.86	-0.61	2.73	20
1052F	13H	4	3-6	114.05	116.96	-1.22	2.73	15
1052F	13H	4	13-16	114.15	117.06	-0.22	2.36	15
1052F	13H	4	23-26	114.25	117.16	-0.73	2.37	18
1052F	13H	4	33-36	114.35	117.26	-0.73	2.63	20
1052F	13H	4	43-46	114.45	117.36	-1.05	2.74	20
1052F	13H	4	53-56	114.55	117.46	-1.17	2.96	20
1052F	13H	4	63-66	114.65	117.56	-0.61	2.62	20
1052F	13H	4	73-76	114.75	117.66	-1.22	2.75	20
1052F	13H	4	83-86	114.85	117.76	-0.93	2.66	20
1052F	13H	4	93-96	114.95	117.86	-1.34	2.75	20
1052F	13H	4	103-106	115.05	117.96	-0.58	2.52	20
1052F	13H	4	113-116	115.15	118.06	-1.12	2.62	20
1052F	13H	4	123-126	115.25	118.16	-0.13	3.85	20
1052F	13H	4	133-136	115.35	118.26	-0.97	2.88	20
1052F	13H	4	143-146	115.45	118.36	-1.06	2.58	20

Appendix 1. Stable Isotope Results at Site 1052

Hole	Core	Section	Interval (cm)	Depth (mbsf)	MCD	$\delta^{18}O$	$\delta^{13}C$	*n*
***Morozovella crassata* (continued)**								
1052F	13H	5	3-6	115.55	118.46	-0.92	2.88	20
1052F	13H	5	13-16	115.65	118.56	-0.89	2.89	20
1052F	13H	5	23-26	115.75	118.66	-1.15	3.14	20
1052F	13H	5	33-36	115.85	118.76	-1.05	3.02	20
1052F	13H	5	43-46	115.95	118.86	-1.27	3.11	20
1052F	13H	5	53-56	116.05	118.96	-1.25	3.17	20
1052F	13H	5	63-66	116.15	119.06	-1.13	3.09	20
1052F	13H	5	73-76	116.25	119.16	-1.23	3.23	20
1052F	13H	5	83-86	116.35	119.26	-1.14	3.22	20
1052F	13H	5	93-96	116.45	119.36	-1.25	3.17	20
1052F	13H	5	103-106	116.55	119.46	-1.26	3.27	15
1052F	13H	5	113-116	116.65	119.56	-1.22	3.18	20
1052F	13H	5	123-126	116.75	119.66	-1.04	2.78	20
1052F	13H	5	133-136	116.85	119.76	-1.30	3.02	20
1052F	13H	5	143-146	116.95	119.86	-1.13	2.91	20
1052F	13H	6	3-6	117.05	119.96	-1.46	3.09	16
1052F	13H	6	13-16	117.15	120.06	-1.29	2.85	20
1052F	13H	6	23-26	117.25	120.16	-1.08	2.75	20
1052F	13H	6	33-36	117.35	120.26	-1.33	3.34	20
1052F	13H	6	43-46	117.45	120.36	-1.15	3.02	20
1052F	13H	6	53-56	117.55	120.46	-1.42	3.15	20
1052B	14H	3	93-96	113.95	120.50	-1.61	3.53	16
1052F	13H	6	63-66	117.65	120.56	-1.29	3.04	21
1052B	14H	3	103-106	114.05	120.60	-1.46	2.98	19
1052F	13H	6	73-76	117.75	120.66	-1.39	3.16	15
1052B	14H	3	113-116	114.15	120.70	-1.88	2.53	19
1052B	14H	3	123-126	114.25	120.80	-1.29	3.15	20
1052B	14H	3	133-136	114.35	120.90	-1.53	3.24	20
1052B	14H	3	143-146	114.45	121.00	-1.55	3.62	20
1052B	14H	4	3-6	114.55	121.10	-1.32	3.38	20
1052B	14H	4	13-16	114.65	121.20	-2.04	2.88	D 15
1052B	14H	4	13-16	114.65	121.20	-1.94	2.90	D 16
1052B	14H	4	23-26	114.75	121.30	-1.90	2.98	20
1052B	14H	4	33-36	114.85	121.40	-1.50	3.41	20
1052B	14H	4	43-46	114.95	121.50	-1.68	3.13	20
1052B	14H	4	53-56	115.05	121.60	-1.68	3.00	20
1052B	14H	4	63-66	115.15	121.70	-1.68	2.98	15
1052B	14H	4	63-66	115.15	121.70	-1.65	3.17	22
1052B	14H	4	73-76	115.25	121.80	-1.70	3.35	21
1052B	14H	4	83-86	115.35	121.90	-1.26	3.35	20
1052B	14H	4	93-96	115.45	122.00	-1.44	3.38	20
1052B	14H	4	93-96	115.45	122.00	-1.52	3.54	15
1052B	14H	4	103-106	115.55	122.10	-1.61	3.26	20
1052B	14H	4	113-116	115.65	122.20	-1.52	3.19	20
1052B	14H	4	123-126	115.75	122.30	-1.05	3.02	20
1052B	14H	4	133-136	115.85	122.40	-1.33	3.29	20
1052B	14H	4	143-146	115.95	122.50	-1.46	3.34	20
1052B	14H	5	3-6	116.05	122.60	-1.29	3.21	20
1052B	14H	5	13-16	116.15	122.70	-1.31	3.37	20
1052B	14H	5	23-26	116.25	122.80	-1.14	3.37	D 20

Appendix 1. Stable Isotope Results at Site 1052

Hole	Core	Section	Interval (cm)	Depth (mbsf)	MCD	$\delta^{18}O$	$\delta^{13}C$	*n*
Morozovella crassata **(continued)**								
1052B	14H	5	23-26	116.25	122.80	-1.17	3.39	D 20
1052B	14H	5	33-36	116.35	122.90	-1.40	3.37	20
1052B	14H	5	43-46	116.45	123.00	-1.22	3.28	15
1052B	14H	5	53-56	116.55	123.10	-1.62	3.07	20
1052B	14H	5	63-66	116.65	123.20	-1.37	3.12	20
1052B	14H	5	73-76	116.75	123.30	-1.42	3.32	20
1052B	14H	5	83-86	116.85	123.40	-1.45	3.34	20
1052B	14H	5	93-96	116.95	123.50	-1.16	3.38	20
1052B	14H	5	103-106	117.05	123.60	-1.31	3.35	20
1052B	14H	5	113-116	117.15	123.70	-1.50	3.30	20
1052B	14H	5	123-126	117.25	123.80	-1.33	3.19	20
1052B	14H	5	133-136	117.35	123.90	-1.48	3.07	20
1052B	14H	5	143-146	117.45	124.00	-1.56	3.15	20
1052B	14H	6	3-6	117.55	124.10	-1.62	3.48	20
1052B	14H	6	13-16	117.65	124.20	-1.34	3.26	20
1052B	14H	6	23-26	117.75	124.30	-1.24	3.34	20
1052B	14H	6	33-36	117.85	124.40	-1.41	3.12	20
1052B	14H	6	43-46	117.95	124.50	-1.45	3.16	20
1052B	14H	6	53-56	118.05	124.60	-1.18	3.28	21
1052B	14H	6	63-66	118.15	124.70	-1.36	3.12	16
1052B	14H	6	73-76	118.25	124.80	-1.44	3.15	20
1052B	14H	6	83-86	118.35	124.90	-1.35	3.10	20
1052B	14H	6	93-96	118.45	125.00	-1.28	3.35	20
1052F	14H	2	103-106	121.55	125.01	-1.21	3.26	20
1052B	14H	6	103-106	118.55	125.10	-1.35	3.28	20
1052F	14H	2	113-116	121.65	125.11	-1.26	2.86	20
1052B	14H	6	113-116	118.65	125.20	-1.52	3.00	20
1052F	14H	2	123-126	121.75	125.21	-1.36	3.15	20
1052B	14H	6	123-126	118.75	125.30	-2.35	2.94	5
1052F	14H	2	133-136	121.85	125.31	-1.40	3.05	20
1052F	14H	2	143-146	121.95	125.41	-1.39	3.21	20
1052F	14H	3	3-6	122.05	125.51	-1.54	3.34	20
1052F	14H	3	13-16	122.15	125.61	-1.21	3.35	20
1052F	14H	3	23-26	122.25	125.71	-1.23	3.24	20
1052F	14H	3	33-36	122.35	125.81	-1.18	3.45	20
1052F	14H	3	43-46	122.45	125.91	-1.10	3.27	20
1052F	14H	3	53-56	122.55	126.01	-1.11	3.33	20
1052F	14H	3	63-66	122.65	126.11	-0.96	3.41	20
1052F	14H	3	73-76	122.75	126.21	-1.08	3.45	20
1052F	14H	3	83-86	122.85	126.31	0.20	3.12	5
1052F	14H	3	93-96	122.95	126.41	-1.14	3.62	20
1052F	14H	3	103-106	123.05	126.51	-1.09	3.52	20
1052F	14H	3	113-116	123.15	126.61	-1.18	3.58	20
1052F	14H	3	123-126	123.25	126.71	-1.25	3.50	20
1052F	14H	3	133-136	123.35	126.81	-1.20	3.65	20
1052F	14H	4	3-6	123.55	127.01	-0.79	3.67	19
1052F	14H	4	13-16	123.65	127.11	-1.17	3.42	19
1052F	14H	4	23-26	123.75	127.21	-1.27	3.34	20
1052F	14H	4	33-36	123.85	127.31	-1.14	3.47	20
1052F	14H	4	43-46	123.95	127.41	-1.17	3.39	19

Appendix 1. Stable Isotope Results at Site 1052

Hole	Core	Section	Interval (cm)	Depth (mbsf)	MCD	$\delta^{18}O$	$\delta^{13}C$	*n*
Morozovella crassata **(continued)**								
1052F	14H	4	53-56	124.05	127.51	-1.13	3.32	17
1052F	14H	4	63-66	124.15	127.61	-1.38	3.47	16
1052F	14H	4	83-86	124.35	127.81	-1.08	3.21	19
1052F	14H	4	93-96	124.45	127.91	-1.20	3.28	15
1052F	14H	4	103-106	124.55	128.01	-1.29	3.47	18
1052F	14H	4	113-116	124.65	128.11	-1.24	3.46	21
1052F	14H	4	123-126	124.75	128.21	-1.29	3.45	20
1052F	14H	4	133-136	124.85	128.31	-1.00	3.41	21
1052F	14H	4	143-146	124.95	128.41	-1.18	3.30	21
1052F	14H	5	3-6	125.05	128.51	-1.27	3.30	20
1052F	14H	5	13-16	125.15	128.61	-1.03	3.17	20
1052F	14H	5	23-26	125.25	128.71	-1.21	3.43	20
1052F	14H	5	33-36	125.35	128.81	-1.12	4.21	20
1052F	14H	5	43-46	125.45	128.91	-0.36	3.10	20
1052F	14H	5	53-56	125.55	129.01	0.58	3.08	5
1052F	14H	5	63-66	125.65	129.11	-1.39	3.22	20
1052F	14H	5	73-76	125.75	129.21	-1.23	3.60	21
1052F	14H	5	83-86	125.85	129.31	-1.43	3.60	20
1052F	14H	5	93-96	125.95	129.41	-0.37	3.13	20
1052F	14H	5	103-106	126.05	129.51	-1.52	3.43	19
1052F	14H	5	113-116	126.15	129.61	-1.54	3.58	15
1052F	14H	5	123-126	126.25	129.71	-1.44	3.22	15
1052F	14H	5	133-136	126.35	129.81	-1.31	3.49	16
1052F	14H	5	143-146	126.45	129.91	-0.22	3.02	20
1052F	14H	6	3-6	126.55	130.01	-0.81	2.88	20
1052F	14H	6	13-16	126.65	130.11	-1.52	3.57	16
1052F	14H	6	23-26	126.75	130.21	0.42	2.93	5
1052F	14H	6	53-56	127.05	130.51	-0.89	2.85	20
1052F	14H	6	63-66	127.25	130.61	0.38	2.57	3
1052F	14H	6	73-76	127.35	130.71	-1.48	3.26	20
1052F	14H	6	83-86	127.45	130.81	0.19	2.91	5
1052F	14H	6	93-96	127.55	130.91	-1.32	3.33	22
1052F	14H	6	103-106	127.65	131.01	-1.32	3.38	20
1052F	14H	6	113-116	127.75	131.11	-1.05	3.24	D 20
1052F	14H	6	113-116	127.85	131.11	-1.26	3.20	D 20
1052F	14H	6	123-126	127.95	131.21	-0.20	2.88	19
1052F	14H	6	133-136	128.05	131.31	-0.31	2.66	22
1052F	14H	6	143-146	128.15	131.41	-1.19	3.49	18
Hantkenina alabamensis								
1052B	10H	3	113-116	76.15	80.58	-0.36	1.32	15
1052F	14H	6	13-16	126.65	130.11	0.05	1.35	15
Chiloguembelina cubensis								
1052F	14H	4	63-66	124.15	127.61	0.60	2.14	20

Appendix 1. Stable Isotope Results at Site 1052

Hole	Core	Section	Interval (cm)	Depth (mbsf)	MCD	$\delta^{18}O$	$\delta^{13}C$	*n*
Morozovella spinulosa								
1052B	11H	5	3-6	87.55	93.17	-1.04	2.77	22
1052B	11H	5	23-26	87.75	93.37	-1.16	2.63	19
1052B	11H	5	33-36	87.85	93.47	-0.86	3.15	20
1052B	11H	5	43-46	87.95	93.57	-0.78	3.13	18
1052B	11H	5	53-56	88.05	93.67	-1.23	2.49	22
1052B	11H	5	63-66	88.15	93.77	-0.73	3.13	17
1052B	11H	5	93-96	88.45	94.07	-1.28	2.98	21
1052F	11H	1	113-116	91.65	94.13	-1.41	2.38	R 22
1052B	11H	5	103-106	88.55	94.17	-1.07	3.04	22
1052B	11H	5	113-116	88.65	94.27	-0.84	3.25	15
1052F	11H	1	133-136	91.85	94.33	-1.29	2.86	16
1052B	11H	5	123-126	88.75	94.37	-0.99	3.09	15
1052F	11H	2	23-26	92.25	94.73	-1.16	2.63	20
1052F	11H	2	53-56	92.55	95.03	-0.88	3.09	20
1052F	11H	2	63-66	92.65	95.13	-0.94	3.31	20
1052F	11H	3	33-36	93.85	96.33	-0.94	3.23	20
1052F	11H	3	43-46	93.95	96.43	-0.97	2.85	19
1052F	11H	3	63-66	94.15	96.63	-0.49	3.03	22
1052F	11H	3	83-86	94.35	96.83	-0.73	3.51	20
1052F	11H	4	3-6	95.05	97.53	-1.32	3.14	19
1052F	11H	4	83-86	95.85	98.33	-0.78	3.51	20
1052F	11H	4	103-106	96.05	98.53	-0.90	3.74	20
1052F	11H	4	143-146	96.45	98.93	-0.93	3.57	20
1052F	11H	5	123-126	97.75	100.23	-1.84	2.92	20
1052F	11H	5	133-136	97.85	100.33	-1.16	3.62	20
1052F	11H	5	143-146	97.95	100.43	-1.40	3.33	20
1052F	11H	6	3-6	98.05	100.53	-1.22	3.45	20
1052F	11H	6	23-26	98.25	100.73	-1.13	3.49	20
1052F	11H	6	33-36	98.35	100.83	-1.17	3.54	R 20
1052F	11H	6	43-46	98.45	100.93	-1.57	3.18	20
1052F	11H	6	53-56	98.55	101.03	-1.17	3.27	20
1052F	11H	6	63-66	98.65	101.13	-1.14	3.51	20
1052F	11H	6	73-76	98.75	101.23	-1.10	3.53	20
1052F	11H	6	83-86	98.85	101.33	-0.98	3.31	20
1052F	11H	6	93-96	98.95	101.43	-1.19	3.48	20
1052F	11H	6	103-106	99.05	101.53	-1.06	3.57	20
1052F	11H	6	113-116	99.15	101.63	-1.21	3.49	R 20
1052F	11H	6	123-126	99.25	101.73	-1.09	3.21	20
1052F	11H	6	133-136	99.35	101.83	-1.28	3.39	R 20
1052F	11H	6	143-146	99.45	101.93	-1.09	3.33	20
1052F	11H	7	3-6	99.55	102.03	-1.11	3.47	20
1052F	11H	7	13-16	99.65	102.13	-1.22	3.41	20
1052B	12H	3	143-146	95.45	102.15	-1.40	3.27	20
1052F	11H	7	23-26	99.75	102.23	-1.21	3.30	20
1052B	12H	4	13-16	95.65	102.35	-1.49	3.27	20
1052B	12H	4	83-86	96.35	103.05	-1.24	3.23	19
1052B	12H	4	103-106	96.55	103.25	-1.57	3.18	20
1052B	12H	4	123-126	96.75	103.45	-1.18	3.34	R 20
1052B	12H	4	143-146	96.95	103.65	-1.30	3.37	20
1052B	12H	5	13-16	97.15	103.85	-1.26	3.51	20

Appendix 1. Stable Isotope Results at Site 1052

Hole	Core	Section	Interval (cm)	Depth (mbsf)	MCD	$\delta^{18}O$	$\delta^{13}C$	*n*
***Morozovella spinulosa* (continued)**								
1052F	12H	2	83-86	102.35	105.26	-1.98	2.34	15
1052F	12H	3	13-16	103.15	106.06	-1.49	2.97	20
1052F	12H	3	23-26	103.25	106.16	-1.50	2.94	20
1052F	12H	3	53-56	103.55	106.46	-1.50	2.80	20
1052F	12H	3	83-86	103.85	106.76	-2.09	2.86	15
1052F	12H	3	93-96	103.95	106.86	-1.91	3.08	16
1052F	12H	3	113-116	104.15	107.06	-1.57	2.78	20
1052F	12H	4	33-36	104.85	107.76	-2.09	2.56	R 20
1052F	12H	5	103-106	107.05	109.96	0.80	2.20	R 4
1052F	14H	3	83-86	122.85	126.31	0.20	3.13	R 4
1052F	14H	5	53-56	125.55	129.01	-0.52	3.24	R 15
1052F	14H	5	73-76	125.75	129.21	-1.21	3.49	20
Acarinina praetopilensis								
1052B	11H	4	133-136	87.35	92.97	-0.91	2.47	20
1052B	11H	4	143-146	87.45	93.07	-0.34	2.75	20
1052B	11H	5	3-6	87.55	93.17	-0.44	2.89	20
1052B	11H	5	13-16	87.65	93.27	-0.47	2.88	19
1052B	11H	5	23-26	87.75	93.37	-0.47	2.86	20
1052B	11H	5	33-36	87.85	93.47	-0.25	2.86	20
1052B	11H	5	43-46	87.95	93.57	-0.65	2.99	20
1052B	11H	5	53-56	88.05	93.67	-0.43	2.95	20
1052B	11H	5	63-66	88.15	93.77	-0.74	3.03	20
1052B	11H	5	73-76	88.25	93.87	-0.60	2.96	20
1052B	11H	5	83-86	88.35	93.97	-1.69	2.17	20
1052B	11H	5	93-96	88.45	94.07	-0.30	2.91	20
1052F	11H	1	113-116	91.65	94.13	-0.74	2.74	R 20
1052B	11H	5	103-106	88.55	94.17	-0.57	3.01	20
1052F	11H	1	123-126	91.75	94.23	-0.40	3.03	20
1052B	11H	5	113-116	88.65	94.27	-0.34	3.03	20
1052F	11H	1	133-136	91.85	94.33	-0.56	3.24	20
1052B	11H	5	123-126	88.75	94.37	-0.35	3.36	20
1052F	11H	1	143-146	91.95	94.43	-0.72	2.83	R 20
1052B	11H	5	133-136	88.85	94.47	0.00	3.15	20
1052F	11H	2	3-6	92.05	94.53	-0.79	2.86	20
1052B	11H	5	143-146	88.95	94.57	-0.43	3.05	20
1052F	11H	2	13-16	92.15	94.63	-0.50	2.91	20
1052F	11H	2	83-86	92.85	95.33	-0.80	2.82	R 20
1052F	11H	3	53-56	94.05	96.53	-1.08	2.83	20
1052F	11H	3	73-76	94.25	96.73	-1.33	1.35	10
1052F	11H	3	83-86	94.35	96.83	-1.27	2.86	21
1052F	11H	3	93-96	94.45	96.93	-0.47	3.40	R 20
1052F	11H	4	13-16	95.15	97.63	-0.46	3.15	20
1052F	11H	4	23-26	95.25	97.73	-0.72	3.27	20
1052B	12H	3	143-146	95.45	102.15	-1.31	2.93	20
1052B	12H	4	13-16	95.65	102.35	-1.03	3.16	20
1052B	12H	4	23-26	95.75	102.45	-0.92	3.25	20
1052B	12H	4	33-36	95.85	102.55	-0.88	3.28	20
1052B	12H	4	43-46	95.95	102.65	-1.00	3.24	20
1052B	12H	4	53-56	96.05	102.75	-0.97	3.28	20
1052B	12H	4	63-66	96.15	102.85	-1.29	3.44	20

Appendix 1. Stable Isotope Results at Site 1052

Hole	Core	Section	Interval (cm)	Depth (mbsf)	MCD	$\delta^{18}O$	$\delta^{13}C$	*n*
***Acarinina praetopilensis* (continued)**								
1052B	12H	4	73-76	96.25	102.95	-1.11	3.39	20
1052B	12H	4	83-86	96.35	103.05	-0.66	3.74	20
1052B	12H	4	93-96	96.45	103.15	-0.96	3.71	20
1052B	12H	4	103-106	96.55	103.25	-1.22	3.41	20
1052B	12H	4	113-116	96.65	103.35	-1.14	3.14	20
1052B	12H	5	33-36	97.35	104.05	-0.73	3.23	R 20
1052B	12H	5	43-46	97.45	104.15	-0.74	3.01	R 20
1052B	12H	6	3-6	98.55	105.25	-0.91	2.94	R 20
1052F	12H	3	133-136	104.35	107.26	-1.64	3.05	20
1052F	12H	3	143-146	104.45	107.36	-1.33	2.97	20
1052F	12H	4	3-6	104.55	107.46	-1.68	2.90	20
1052F	12H	4	13-16	104.65	107.56	-1.25	3.14	20
1052F	12H	4	33-36	104.85	107.76	-1.85	2.66	R 20
1052F	12H	4	53-56	105.05	107.96	-1.55	2.98	20
1052F	12H	4	73-76	105.25	108.16	-1.32	3.03	20
1052F	12H	4	103-106	105.55	108.46	-0.89	2.86	20
1052F	12H	4	113-116	105.65	108.56	-1.09	3.35	R 20
1052F	12H	4	123-126	105.75	108.66	-0.76	3.02	20
1052F	12H	4	133-136	105.85	108.76	-0.67	3.08	20
1052F	12H	4	143-146	105.95	108.86	-1.58	3.07	20
1052F	12H	5	23-26	106.25	109.16	-0.82	2.90	R 20
1052F	12H	5	33-36	106.35	109.26	-1.52	2.89	R 20
1052F	12H	5	103-106	107.05	109.96	-0.69	3.22	R 20
1052F	12H	6	103-106	108.55	111.46	-0.54	2.74	20
1052F	12H	7	23-26	109.25	112.16	-1.11	3.12	R 20
1052F	12H	7	33-36	109.35	112.26	-0.48	2.84	R 20
1052B	13H	4	23-26	105.25	112.30	-0.75	3.23	R 20
1052F	14H	3	143-146	123.45	126.91	-0.86	3.34	20
1052F	14H	4	63-66	124.15	127.61	-1.03	3.38	20
1052F	14H	4	73-76	124.25	127.71	-1.06	3.29	20
1052F	14H	6	13-16	126.65	130.11	-0.60	3.39	20
1052F	14H	6	23-26	126.75	130.21	-1.55	3.07	R 20
1052F	14H	6	33-36	126.85	130.31	-1.13	3.50	20
1052F	14H	6	43-46	126.95	130.41	-1.15	3.57	20
1052F	14H	6	63-66	127.15	130.61	-0.79	3.10	R 20
1052F	14H	6	83-86	127.45	130.81	-0.96	3.04	R 20
1052F	14H	6	133-136	128.05	131.31	-1.16	3.50	20
1052F	14H	6	143-146	128.15	131.41	-1.62	3.18	20
Nuttalides truempyi								
1052B	10H	5	63-66	78.65	83.08	0.20	1.01	15
1052B	10H	5	73-76	78.75	83.18	0.51	0.96	15
1052B	10H	5	83-86	78.85	83.28	0.60	0.85	D 15
1052B	10H	5	83-86	78.85	83.28	0.45	0.99	D 15
1052B	10H	5	93-96	78.95	83.38	0.59	0.95	15
1052B	11H	3	113-116	85.65	91.27	0.35	0.90	15
1052B	11H	3	123-126	85.75	91.37	0.51	0.95	15
1052B	11H	3	133-136	85.85	91.47	0.46	0.95	15

Appendix 1. Stable Isotope Results at Site 1052

Hole	Core	Section	Interval (cm)	Depth (mbsf)	MCD	$\delta^{18}O$	$\delta^{13}C$	*n*
Mixed morozovellids								
1052B	12H	4	43-46	95.95	102.65	-1.65	2.95	19
1052B	12H	4	113-116	96.65	103.35	-1.46	3.10	18
1052F	12H	3	123-126	104.25	107.16	-1.87	2.91	19
1052F	12H	3	143-146	104.45	107.36	-1.62	2.87	16
1052F	12H	4	3-6	104.55	107.46	-1.78	2.62	16
1052F	12H	4	13-16	104.65	107.56	-2.23	2.58	16
1052F	12H	4	23-26	104.75	107.66	-1.71	2.95	18
1052F	12H	4	43-46	104.95	107.86	-1.31	2.76	23
1052F	12H	4	53-56	105.05	107.96	-2.16	2.82	15
1052F	12H	4	73-76	105.25	108.16	-1.32	3.06	21
1052F	12H	4	133-136	105.85	108.76	1.21	2.12	5
1052F	12H	4	143-146	105.95	108.86	-1.71	2.97	17
1052F	12H	6	103-106	108.55	111.46	-0.28	2.54	20
Turborotalia cocoaensis								
1052B	11H	4	43-46	86.45	92.07	-0.31	1.21	15
1052B	11H	4	53-56	86.55	92.17	-0.30	1.41	15
1052B	11H	4	63-66	86.65	92.27	-0.26	1.42	15
1052B	11H	4	73-76	86.75	92.37	-0.38	1.39	15
1052B	11H	4	83-86	86.85	92.47	-0.46	1.30	15
1052B	11H	4	93-96	86.95	92.57	-0.10	1.62	15
1052B	11H	4	103-106	87.05	92.67	-0.41	1.58	15
1052B	11H	4	113-116	87.15	92.77	-0.21	1.65	15
1052B	11H	4	123-126	87.25	92.87	-0.49	1.50	15
1052B	11H	4	133-136	87.35	92.97	-0.25	1.38	15
1052B	11H	4	143-146	87.45	93.07	-0.51	1.11	15
1052B	11H	5	3-6	87.55	93.17	-0.43	1.03	15
1052B	11H	5	13-16	87.65	93.27	-0.47	1.33	15
1052B	11H	5	23-26	87.75	93.37	-0.42	1.34	15
Mixed benthic foraminifer								
1052B	10H	5	63-66	78.65	83.08	0.78	0.45	15
Bulk carbonate								
1052B	10H	1	73-76	72.75	77.18	0.74	1.66	D
1052B	10H	1	73-76	72.75	77.18	0.82	1.79	D
1052B	10H	1	83-86	72.85	77.28	0.90	1.83	D
1052B	10H	1	83-86	72.85	77.28	0.97	1.91	D
1052B	10H	1	93-96	72.95	77.38	0.98	1.82	
1052B	10H	1	103-106	73.05	77.48	0.40	1.48	D
1052B	10H	1	103-106	73.05	77.48	0.94	1.84	D
1052B	10H	1	113-116	73.15	77.58	0.72	1.61	
1052B	10H	1	123-126	73.25	77.68	0.58	1.51	D
1052B	10H	1	123-126	73.25	77.68	0.50	1.46	
1052B	10H	1	133-136	73.35	77.78	0.87	1.60	D
1052B	10H	1	133-136	73.35	77.78	1.20	1.88	D
1052B	10H	1	143-146	73.45	77.88	0.57	1.46	D
1052B	10H	5	63-66	78.65	83.08	0.64	1.86	D
1052B	10H	5	63-66	78.65	83.08	0.49	1.79	D
1052B	10H	5	73-76	78.75	83.18	0.60	1.87	D

Appendix 1. Stable Isotope Results at Site 1052

Hole	Core	Section	Interval (cm)	Depth (mbsf)	MCD	$\delta^{18}O$	$\delta^{13}C$	*n*
Bulk carbonate (continued)								
1052B	10H	5	73-76	78.75	83.18	0.71	1.99	D
1052B	10H	5	83-86	78.85	83.28	0.62	1.89	D
1052B	10H	5	83-86	78.85	83.28	0.58	1.85	D
1052B	10H	5	93-96	78.95	83.38	0.72	1.91	D
1052B	10H	5	93-96	78.95	83.38	0.67	1.86	D
1052B	11H	4	83-86	86.85	92.47	0.50	1.61	D
1052B	11H	4	83-86	86.85	92.47	0.53	1.77	D
1052B	11H	4	93-96	86.95	92.57	0.88	1.98	D
1052B	11H	4	93-96	86.95	92.57	0.80	1.98	D
1052B	11H	4	103-106	87.05	92.67	0.88	1.97	D
1052B	11H	4	103-106	87.05	92.67	0.62	1.89	D
1052B	13H	4	3-6	105.05	112.10	0.50	1.69	D
1052B	13H	4	3-6	105.05	112.10	0.48	1.71	D
1052F	12H	7	23-26	109.25	112.16	0.72	1.83	D
1052F	12H	7	23-26	109.25	112.16	0.42	1.60	D
1052B	13H	4	13-16	105.15	112.20	0.54	1.68	D
1052B	13H	4	13-16	105.15	112.20	0.50	1.74	D
1052F	12H	7	33-36	109.35	112.26	0.60	1.67	D
1052F	12H	7	33-36	109.35	112.26	0.51	1.81	D
1052B	13H	4	23-26	105.25	112.30	0.51	1.72	D
1052B	13H	4	23-26	105.25	112.30	0.60	1.75	D
Subbotina utilisindex								
1052B	10H	5	63-66	78.65	83.08	-0.15	1.51	15
1052B	10H	5	73-76	78.75	83.18	-0.10	1.35	15
1052B	10H	5	83-86	78.85	83.28	-0.03	1.47	15
1052B	10H	5	93-96	78.95	83.38	-0.08	1.38	15
1052B	11H	3	113-116	85.65	91.27	-0.20	1.41	15
1052B	11H	3	123-126	85.75	91.37	-0.33	1.32	15
1052B	11H	3	133-136	85.85	91.47	-0.34	1.28	15
1052B	11H	4	43-46	86.45	92.07	0.08	1.30	15
1052B	11H	4	53-56	86.55	92.17	0.39	1.34	15
1052B	11H	4	63-66	86.65	92.27	0.13	1.31	15
1052B	11H	4	73-76	86.75	92.37	0.06	1.46	15
1052B	11H	4	83-86	86.85	92.47	-0.12	1.23	15
1052B	11H	4	93-96	86.95	92.57	-0.18	1.37	15
1052B	11H	4	103-106	87.05	92.67	0.15	1.50	15
1052B	11H	4	113-116	87.15	92.77	-0.17	1.73	15
1052B	11H	4	123-126	87.25	92.87	-0.12	1.59	15
1052B	11H	4	133-136	87.35	92.97	-0.22	1.46	15
1052B	11H	4	143-146	87.45	93.07	-0.31	1.17	15
1052B	11H	5	3-6	87.55	93.17	-0.28	1.27	15
1052B	11H	5	13-16	87.65	93.27	-0.37	1.28	15
1052B	11H	5	23-26	87.75	93.37	0.05	1.42	15

Appendix 2. Continuous stable isotopic time series

Hole	Core	Section	Interval (cm)	MCD	Age (Ma)	Oxygen	Carbon
1052B	10H	1	73-76	77.18	37.341	-0.45	2.36
1052B	10H	1	83-86	77.28	37.344	-0.21	2.69
1052B	10H	1	93-96	77.38	37.346	-0.85	2.35
1052B	10H	1	103-106	77.48	37.349	-0.40	2.68
1052B	10H	1	113-116	77.58	37.352	-0.01	2.29
1052B	10H	1	123-126	77.68	37.355	-0.23	2.40
1052B	10H	1	133-136	77.78	37.358	-1.13	2.45
1052B	10H	1	143-146	77.88	37.361	-1.08	2.47
1052B	10H	2	3-6	77.98	37.364	-0.90	2.60
1052B	10H	2	13-16	78.08	37.367	-0.85	2.53
1052B	10H	2	23-26	78.18	37.370	-0.42	2.40
1052B	10H	2	33-36	78.28	37.373	-0.61	2.59
1052B	10H	2	43-46	78.38	37.376	-0.92	2.56
1052B	10H	2	53-56	78.48	37.379	-0.74	2.74
1052B	10H	2	63-66	78.58	37.381	-0.61	2.90
1052B	10H	2	73-76	78.68	37.384	-0.82	2.86
1052B	10H	2	83-86	78.78	37.387	-0.94	2.85
1052B	10H	2	93-96	78.88	37.390	0.18	2.30
1052B	10H	2	103-106	78.98	37.392	-0.80	2.51
1052B	10H	2	113-116	79.08	37.395	-0.83	2.58
1052B	10H	2	123-126	79.18	37.398	-0.63	2.63
1052B	10H	2	133-136	79.28	37.400	-0.68	2.52
1052B	10H	2	143-146	79.38	37.403	-0.87	2.64
1052B	10H	3	3-6	79.48	37.405	-0.70	2.74
1052B	10H	3	13-16	79.58	37.408	-0.89	2.60
1052B	10H	3	23-26	79.68	37.411	-1.10	2.42
1052B	10H	3	33-36	79.78	37.413	-0.87	2.39
1052B	10H	3	43-46	79.88	37.415	-1.40	2.52
1052B	10H	3	53-56	79.98	37.418	-1.06	2.56
1052B	10H	3	63-66	80.08	37.420	-0.42	2.72
1052B	10H	3	73-76	80.18	37.423	-1.30	2.17
1052B	10H	3	83-86	80.28	37.425	-0.82	2.46
1052B	10H	3	93-96	80.38	37.428	-0.71	2.60
1052B	10H	3	103-106	80.48	37.430	-0.84	2.45
1052B	10H	3	113-116	80.58	37.433	-0.82	2.87
1052B	10H	3	123-126	80.68	37.435	-1.48	2.88
1052B	10H	3	133-136	80.78	37.438	-1.19	3.09
1052B	10H	3	143-146	80.88	37.440	-0.86	3.30
1052B	10H	4	3-6	80.98	37.443	-1.04	3.09
1052B	10H	4	13-16	81.08	37.445	-0.75	2.90
1052B	10H	4	23-26	81.18	37.447	-1.00	2.85
1052B	10H	4	33-36	81.28	37.450	-1.06	2.00
1052B	10H	4	43-46	81.38	37.453	-0.84	2.74
1052B	10H	4	53-56	81.48	37.455	-0.97	2.85
1052B	10H	4	63-66	81.58	37.458	-1.02	3.38
1052B	10H	4	73-76	81.68	37.461	-0.86	3.55
1052B	10H	4	83-86	81.78	37.464	-0.98	3.23
1052B	10H	4	93-96	81.88	37.467	-0.84	3.28
1052B	10H	4	103-106	81.98	37.470	-1.23	2.61
1052B	10H	4	113-116	82.08	37.472	-1.20	2.92
1052B	10H	4	123-126	82.18	37.475	-1.54	3.01
1052B	10H	4	133-136	82.28	37.478	-1.83	2.28

Appendix 2. Continuous stable isotopic time series

Hole	Core	Section	Interval (cm)	MCD	Age (Ma)	Oxygen	Carbon
1052B	10H	4	143-146	82.38	37.481	-1.41	3.00
1052B	10H	5	3-6	82.48	37.485	-2.14	2.16
1052B	10H	5	13-16	82.58	37.489	-1.74	2.28
1052B	10H	5	23-26	82.68	37.493	-1.40	2.11
1052B	10H	5	33-36	82.78	37.497	-1.91	1.63
1052B	10H	5	43-46	82.88	37.501	-2.28	1.73
1052B	10H	5	53-56	82.98	37.505	-1.42	1.87
1052B	10H	5	63-66	83.08	37.509	-0.97	2.70
1052B	10H	5	73-76	83.18	37.513	-1.73	-0.05
1052B	10H	5	83-86	83.28	37.517	-1.74	-0.23
1052B	10H	5	93-96	83.38	37.521	-1.26	3.13
1052B	10H	5	103-106	83.48	37.525	-1.13	2.85
1052B	10H	5	113-116	83.58	37.529	-1.02	2.81
1052B	10H	5	123-126	83.68	37.533	-1.08	2.60
1052B	10H	5	133-136	83.78	37.537	-0.95	3.06
1052B	10H	5	143-146	83.88	37.541	-1.07	3.43
1052B	10H	6	3-6	83.98	37.545	-1.46	2.99
1052B	10H	6	13-16	84.08	37.549	-0.95	3.40
1052B	10H	6	23-26	84.18	37.553	-0.85	3.39
1052B	10H	6	33-36	84.28	37.557	-0.92	2.99
1052B	10H	6	43-46	84.38	37.561	-1.11	3.11
1052B	10H	6	53-56	84.48	37.565	-1.30	2.87
1052B	10H	6	63-66	84.58	37.568	-0.94	3.46
1052B	10H	6	73-76	84.68	37.571	-0.86	3.01
1052B	10H	6	83-86	84.78	37.574	-1.04	2.77
1052B	10H	6	93-96	84.88	37.577	-0.61	3.21
1052B	10H	6	103-106	84.98	37.579	-1.08	3.14
1052B	10H	6	113-116	85.08	37.580	-1.06	3.29
1052F	10H	2	83-86	85.11	37.582	-0.72	3.15
1052B	10H	6	123-126	85.18	37.583	-0.33	3.15
1052F	10H	2	93-96	85.21	37.585	-0.55	3.21
1052F	10H	2	103-106	85.31	37.587	-0.68	3.04
1052F	10H	2	113-116	85.41	37.587	-2.03	1.30
1052F	10H	2	123-126	85.51	37.590	-1.66	2.55
1052F	10H	2	133-136	85.61	37.592	-1.47	3.03
1052F	10H	2	143-146	85.71	37.595	-1.42	2.88
1052F	10H	3	3-6	85.81	37.598	-1.78	2.07
1052F	10H	3	13-16	85.91	37.600	-1.73	2.93
1052F	10H	3	23-26	86.01	37.603	-1.61	-0.07
1052F	10H	3	33-36	86.11	37.606	-1.30	2.12
1052F	10H	3	43-46	86.21	37.608	-1.34	2.19
1052F	10H	3	53-56	86.31	37.611	-1.18	3.17
1052F	10H	3	63-66	86.41	37.614	-1.19	2.29
1052F	10H	3	73-76	86.51	37.617	-1.44	2.36
1052F	10H	3	83-86	86.61	37.619	-1.58	2.08
1052F	10H	3	93-96	86.71	37.623	-1.46	2.10
1052F	10H	3	103-106	86.81	37.627	-1.65	1.77
1052F	10H	3	113-116	86.91	37.631	-1.53	2.51
1052F	10H	3	123-126	87.01	37.634	-1.19	2.62
1052F	10H	3	133-136	87.11	37.638	-1.37	2.48
1052F	10H	3	143-146	87.21	37.642	-1.30	2.76
1052F	10H	4	3-6	87.31	37.646	-1.61	2.58

Appendix 2. Continuous stable isotopic time series

Hole	Core	Section	Interval (cm)	MCD	Age (Ma)	Oxygen	Carbon
1052F	10H	4	13-16	87.41	37.649	-1.56	2.76
1052F	10H	4	23-26	87.51	37.653	-1.15	3.04
1052F	10H	4	33-36	87.61	37.656	-1.22	3.03
1052F	10H	4	43-46	87.71	37.660	-1.37	2.97
1052F	10H	4	53-56	87.81	37.663	-1.19	2.91
1052F	10H	4	63-66	87.91	37.667	-1.26	2.74
1052F	10H	4	73-76	88.01	37.671	-1.26	3.03
1052F	10H	4	83-86	88.11	37.675	-1.25	3.06
1052F	10H	4	93-96	88.21	37.679	-1.24	2.66
1052F	10H	4	103-106	88.31	37.683	-1.17	3.05
1052F	10H	4	113-116	88.41	37.687	-1.02	3.17
1052F	10H	4	123-126	88.51	37.690	-0.96	2.93
1052F	10H	4	133-136	88.61	37.693	-1.73	2.52
1052F	10H	4	143-146	88.71	37.695	-0.86	3.31
1052F	10H	5	3-6	88.81	37.698	-0.90	3.28
1052F	10H	5	13-16	88.91	37.700	-1.02	2.52
1052F	10H	5	23-26	89.01	37.703	-0.88	2.98
1052F	10H	5	33-36	89.11	37.705	-1.21	2.82
1052F	10H	5	43-46	89.21	37.707	-1.12	2.77
1052F	10H	5	53-56	89.31	37.710	-1.38	2.76
1052B	11H	2	73-76	89.37	37.711	-0.65	3.30
1052F	10H	5	63-66	89.41	37.712	-0.79	3.08
1052B	11H	2	83-86	89.47	37.713	-1.14	2.47
1052F	10H	5	73-76	89.51	37.715	-0.95	3.31
1052B	11H	2	93-96	89.57	37.716	-0.92	3.26
1052F	10H	5	83-86	89.61	37.719	-0.98	3.06
1052B	11H	2	103-106	89.67	37.719	-1.41	1.99
1052B	11H	2	113-116	89.77	37.722	-0.73	3.21
1052B	11H	2	123-126	89.87	37.726	-1.25	2.26
1052B	11H	2	133-136	89.97	37.729	-1.20	2.50
1052B	11H	2	143-146	90.07	37.732	-0.95	3.07
1052B	11H	3	3-6	90.17	37.735	-1.33	2.97
1052B	11H	3	13-16	90.27	37.738	-1.05	3.37
1052B	11H	3	23-26	90.37	37.741	-1.15	3.37
1052B	11H	3	43-46	90.57	37.748	-1.35	2.40
1052B	11H	3	53-56	90.67	37.751	-0.77	3.04
1052B	11H	3	63-66	90.77	37.755	-0.82	3.30
1052B	11H	3	73-76	90.87	37.758	-0.85	3.30
1052B	11H	3	83-86	90.97	37.761	-1.05	2.56
1052B	11H	3	93-96	91.07	37.764	-0.79	3.33
1052B	11H	3	103-106	91.17	37.766	-1.09	2.46
1052B	11H	3	113-116	91.27	37.768	-0.84	3.23
1052B	11H	3	133-136	91.47	37.773	-1.05	2.46
1052B	11H	3	143-146	91.57	37.775	-0.78	2.85
1052B	11H	4	3-6	91.67	37.778	-0.94	3.19
1052B	11H	4	13-16	91.77	37.780	-1.04	2.64
1052B	11H	4	23-26	91.87	37.783	-1.07	2.33
1052B	11H	4	33-36	91.97	37.786	-0.90	3.21
1052B	11H	4	43-46	92.07	37.789	-0.81	2.80
1052B	11H	4	53-56	92.17	37.791	-0.72	2.75
1052B	11H	4	63-66	92.27	37.794	-0.75	2.88
1052B	11H	4	73-76	92.37	37.797	-0.68	2.69

Appendix 2. Continuous stable isotopic time series

Hole	Core	Section	Interval (cm)	MCD	Age (Ma)	Oxygen	Carbon
1052B	11H	4	83-86	92.47	37.799	-0.73	3.05
1052B	11H	4	93-96	92.57	37.802	-0.76	3.27
1052B	11H	4	103-106	92.67	37.805	-0.71	2.87
1052B	11H	4	113-116	92.77	37.807	-0.70	3.19
1052B	11H	4	123-126	92.87	37.810	-0.73	3.33
1052B	11H	4	133-136	92.97	37.813	-0.77	2.91
1052B	11H	4	143-146	93.07	37.815	-1.21	2.75
1052B	11H	5	3-6	93.17	37.818	-1.04	2.77
1052B	11H	5	13-16	93.27	37.821	-0.69	2.88
1052B	11H	5	23-26	93.37	37.824	-1.16	2.63
1052B	11H	5	33-36	93.47	37.827	-0.86	3.15
1052B	11H	5	43-46	93.57	37.830	-0.78	3.13
1052B	11H	5	53-56	93.67	37.833	-1.23	2.95
1052B	11H	5	63-66	93.77	37.836	-0.73	3.21
1052B	11H	5	73-76	93.87	37.839	-1.18	2.86
1052B	11H	5	83-86	93.97	37.842	-1.22	2.87
1052B	11H	5	93-96	94.07	37.845	-1.12	3.15
1052F	11H	1	113-116	94.13	37.846	-1.41	2.38
1052B	11H	5	103-106	94.17	37.847	-0.94	3.08
1052F	11H	1	123-126	94.23	37.849	-1.36	2.80
1052B	11H	5	113-116	94.27	37.850	-0.84	3.25
1052F	11H	1	133-136	94.33	37.852	-1.29	2.86
1052B	11H	5	123-126	94.37	37.853	-0.99	3.09
1052F	11H	1	143-146	94.43	37.856	-1.22	2.83
1052B	11H	5	133-136	94.47	37.856	-0.50	3.15
1052F	11H	2	3-6	94.53	37.859	-0.79	2.86
1052B	11H	5	143-146	94.57	37.859	-0.43	3.05
1052F	11H	2	13-16	94.63	37.862	-0.50	2.91
1052F	11H	2	23-26	94.73	37.865	-1.16	2.63
1052F	11H	2	33-36	94.83	37.868	-1.06	3.02
1052F	11H	2	43-46	94.93	37.870	-1.07	3.12
1052F	11H	2	53-56	95.03	37.873	-0.88	3.09
1052F	11H	2	63-66	95.13	37.876	-0.94	3.31
1052F	11H	2	73-76	95.23	37.879	-0.63	3.26
1052F	11H	2	83-86	95.33	37.882	-1.30	2.82
1052F	11H	2	93-96	95.43	37.885	-1.07	3.13
1052F	11H	2	103-106	95.53	37.888	-0.96	3.49
1052F	11H	2	113-116	95.63	37.891	-0.96	3.34
1052F	11H	2	123-126	95.73	37.894	-1.09	3.45
1052F	11H	2	133-136	95.83	37.897	-1.33	3.07
1052F	11H	2	143-146	95.93	37.901	-1.04	3.40
1052F	11H	3	3-6	96.03	37.905	-1.85	2.55
1052F	11H	3	13-16	96.13	37.908	-1.24	3.43
1052F	11H	3	23-26	96.23	37.912	-0.94	3.41
1052F	11H	3	33-36	96.33	37.917	-0.94	3.23
1052F	11H	3	43-46	96.43	37.921	-0.97	2.85
1052F	11H	3	53-56	96.53	37.925	-1.08	2.83
1052F	11H	3	63-66	96.63	37.927	-0.84	3.03
1052F	11H	3	83-86	96.83	37.930	-1.27	3.51
1052F	11H	3	93-96	96.93	37.931	-0.97	3.40
1052F	11H	3	113-116	97.13	37.933	-1.24	2.89
1052F	11H	3	123-126	97.23	37.934	-0.91	3.49

Appendix 2. Continuous stable isotopic time series

Hole	Core	Section	Interval (cm)	MCD	Age (Ma)	Oxygen	Carbon
1052F	11H	3	133-136	97.33	37.935	-1.04	3.18
1052F	11H	3	143-146	97.43	37.936	-1.45	2.39
1052F	11H	4	3-6	97.53	37.937	-0.60	3.52
1052F	11H	4	13-16	97.63	37.939	-0.46	3.15
1052F	11H	4	23-26	97.73	37.942	-0.72	3.27
1052F	11H	4	33-36	97.83	37.944	-0.99	3.16
1052F	11H	4	43-46	97.93	37.946	-1.28	3.33
1052F	11H	4	53-56	98.03	37.949	-0.40	3.39
1052F	11H	4	63-66	98.13	37.951	-0.84	3.45
1052F	11H	4	73-76	98.23	37.954	-0.58	3.56
1052F	11H	4	83-86	98.33	37.956	-0.85	3.61
1052F	11H	4	93-96	98.43	37.958	-0.79	3.59
1052F	11H	4	103-106	98.53	37.961	-0.90	3.74
1052F	11H	4	113-116	98.63	37.963	-0.98	3.63
1052F	11H	4	123-126	98.73	37.966	-0.76	3.63
1052F	11H	4	133-136	98.83	37.968	-1.60	3.15
1052F	11H	4	143-146	98.93	37.970	-1.35	3.14
1052F	11H	5	3-6	99.03	37.973	-1.56	3.17
1052F	11H	5	13-16	99.13	37.975	-1.68	3.28
1052F	11H	5	23-26	99.23	37.977	-1.43	3.49
1052F	11H	5	33-36	99.33	37.980	-1.49	3.54
1052F	11H	5	43-46	99.43	37.982	-1.55	3.48
1052F	11H	5	53-56	99.53	37.984	-1.30	3.54
1052F	11H	5	63-66	99.63	37.986	-1.34	3.59
1052F	11H	5	73-76	99.73	37.988	-1.26	3.56
1052F	11H	5	83-86	99.83	37.991	-1.14	3.63
1052F	11H	5	93-96	99.93	37.993	-1.13	3.53
1052F	11H	5	103-106	100.03	37.995	-1.61	3.33
1052F	11H	5	113-116	100.13	37.997	-1.23	3.58
1052F	11H	5	123-126	100.23	37.999	-1.80	3.26
1052F	11H	5	133-136	100.33	38.002	-1.02	3.49
1052F	11H	5	143-146	100.43	38.006	-1.28	3.07
1052F	11H	6	3-6	100.53	38.010	-1.05	3.58
1052F	11H	6	13-16	100.63	38.014	-1.40	3.45
1052F	11H	6	23-26	100.73	38.018	-1.22	3.29
1052F	11H	6	33-36	100.83	38.022	-1.17	3.54
1052F	11H	6	43-46	100.93	38.027	-1.72	3.18
1052F	11H	6	53-56	101.03	38.031	-1.72	3.27
1052F	11H	6	63-66	101.13	38.033	-1.23	3.28
1052F	11H	6	73-76	101.23	38.036	-1.48	3.04
1052F	11H	6	83-86	101.33	38.039	-0.97	3.40
1052F	11H	6	93-96	101.43	38.041	-1.70	3.48
1052F	11H	6	103-106	101.53	38.044	-1.61	3.57
1052F	11H	6	113-116	101.63	38.047	-1.21	3.49
1052F	11H	6	123-126	101.73	38.050	-1.21	3.11
1052F	11H	6	133-136	101.83	38.053	-1.28	3.39
1052F	11H	6	143-146	101.93	38.057	-1.34	2.87
1052F	11H	7	3-6	102.03	38.058	-1.35	3.08
1052B	12H	3	133-136	102.05	38.060	-1.55	3.04
1052F	11H	7	13-16	102.13	38.061	-0.97	3.32
1052B	12H	3	143-146	102.15	38.062	-1.62	2.95
1052F	11H	7	23-26	102.23	38.064	-1.09	3.30

Appendix 2. Continuous stable isotopic time series

Hole	Core	Section	Interval (cm)	MCD	Age (Ma)	Oxygen	Carbon
1052B	12H	4	3-6	102.25	38.064	-1.70	2.90
1052B	12H	4	13-16	102.35	38.067	-1.21	3.15
1052B	12H	4	23-26	102.45	38.070	-0.92	3.25
1052B	12H	4	33-36	102.55	38.073	-0.88	3.28
1052B	12H	4	43-46	102.65	38.076	-1.00	3.03
1052B	12H	4	53-56	102.75	38.078	-0.97	3.28
1052B	12H	4	63-66	102.85	38.081	-1.29	3.44
1052B	12H	4	73-76	102.95	38.084	-1.69	3.27
1052B	12H	4	83-86	103.05	38.087	-1.24	3.23
1052B	12H	4	93-96	103.15	38.091	-1.46	3.71
1052B	12H	4	103-106	103.25	38.094	-1.90	3.04
1052B	12H	4	113-116	103.35	38.097	-1.46	3.10
1052B	12H	4	123-126	103.45	38.101	-1.18	3.34
1052B	12H	4	133-136	103.55	38.104	-1.75	3.25
1052B	12H	4	143-146	103.65	38.107	-1.44	3.01
1052B	12H	5	3-6	103.75	38.111	-1.70	3.13
1052B	12H	5	13-16	103.85	38.113	-1.35	3.21
1052B	12H	5	23-26	103.95	38.116	-1.20	3.14
1052B	12H	5	33-36	104.05	38.119	-1.23	3.23
1052B	12H	5	43-46	104.15	38.121	-1.24	3.01
1052B	12H	5	53-56	104.25	38.124	-1.97	2.15
1052B	12H	5	63-66	104.35	38.127	-1.81	2.62
1052B	12H	5	73-76	104.45	38.129	-2.04	2.81
1052B	12H	5	83-86	104.55	38.132	-1.86	2.51
1052B	12H	5	93-96	104.65	38.135	-1.82	2.67
1052B	12H	5	103-106	104.75	38.137	-1.01	3.30
1052B	12H	5	113-116	104.85	38.140	-1.68	2.71
1052B	12H	5	123-126	104.95	38.142	-1.52	2.75
1052B	12H	5	133-136	105.05	38.145	-1.64	2.75
1052B	12H	5	143-146	105.15	38.148	-1.53	2.91
1052F	12H	2	73-76	105.16	38.148	-1.56	2.88
1052B	12H	6	3-6	105.25	38.150	-1.41	2.94
1052F	12H	2	83-86	105.26	38.150	-1.98	2.34
1052B	12H	6	13-16	105.35	38.153	-1.57	3.22
1052F	12H	2	93-96	105.36	38.153	-1.63	3.17
1052B	12H	6	23-26	105.45	38.156	-1.70	3.04
1052F	12H	2	103-106	105.46	38.156	-1.68	3.09
1052F	12H	2	113-116	105.56	38.158	-1.37	2.97
1052F	12H	2	123-126	105.66	38.161	-1.20	3.97
1052F	12H	2	133-136	105.76	38.164	-1.51	2.39
1052F	12H	3	3-6	105.96	38.169	-1.66	2.69
1052F	12H	3	13-16	106.06	38.172	-1.56	3.01
1052F	12H	3	23-26	106.16	38.175	-1.59	2.85
1052F	12H	3	33-36	106.26	38.178	-1.40	3.13
1052F	12H	3	43-46	106.36	38.181	-1.29	2.90
1052F	12H	3	53-56	106.46	38.184	-1.53	2.94
1052F	12H	3	63-66	106.56	38.187	-1.51	3.14
1052F	12H	3	73-76	106.66	38.190	-1.41	2.74
1052F	12H	3	83-86	106.76	38.192	-2.09	2.86
1052F	12H	3	93-96	106.86	38.195	-1.91	3.08
1052F	12H	3	113-116	107.06	38.200	-1.48	3.00
1052F	12H	3	123-126	107.16	38.204	-1.87	2.91

Appendix 2. Continuous stable isotopic time series

Hole	Core	Section	Interval (cm)	MCD	Age (Ma)	Oxygen	Carbon
1052F	12H	3	133-136	107.26	38.207	-2.14	3.05
1052F	12H	3	143-146	107.36	38.211	-1.62	2.87
1052F	12H	4	3-6	107.46	38.215	-1.78	2.62
1052F	12H	4	13-16	107.56	38.218	-2.23	2.58
1052F	12H	4	23-26	107.66	38.221	-1.71	2.95
1052F	12H	4	33-36	107.76	38.224	-2.09	2.56
1052F	12H	4	43-46	107.86	38.227	-1.31	2.76
1052F	12H	4	53-56	107.96	38.230	-2.16	2.82
1052F	12H	4	63-66	108.06	38.233	-1.78	3.08
1052F	12H	4	73-76	108.16	38.236	-1.32	3.06
1052F	12H	4	93-96	108.36	38.242	-2.05	2.23
1052F	12H	4	103-106	108.46	38.245	-1.39	2.86
1052F	12H	4	113-116	108.56	38.248	-1.59	3.35
1052F	12H	4	123-126	108.66	38.253	-1.26	3.02
1052F	12H	4	133-136	108.76	38.259	-1.17	3.08
1052F	12H	4	143-146	108.86	38.265	-2.08	3.07
1052F	12H	5	13-16	109.06	38.273	-1.03	2.80
1052F	12H	5	23-26	109.16	38.277	-1.32	2.90
1052F	12H	5	33-36	109.26	38.280	-2.02	2.89
1052F	12H	5	43-46	109.36	38.283	-0.07	2.47
1052F	12H	5	53-56	109.46	38.286	-0.77	2.92
1052F	12H	5	63-66	109.56	38.290	-0.77	2.89
1052F	12H	5	73-76	109.66	38.293	-1.01	2.87
1052F	12H	5	83-86	109.76	38.296	-0.24	2.71
1052F	12H	5	93-96	109.86	38.300	-1.20	2.85
1052F	12H	5	103-106	109.96	38.303	-1.19	3.22
1052F	12H	5	113-116	110.06	38.306	-1.02	2.79
1052F	12H	5	123-126	110.16	38.309	-1.20	3.07
1052F	12H	5	133-136	110.26	38.313	-0.56	2.81
1052F	12H	5	143-146	110.36	38.316	-0.71	2.88
1052F	12H	6	3-6	110.46	38.319	-1.41	2.67
1052F	12H	6	13-16	110.56	38.324	-1.02	2.78
1052F	12H	6	23-26	110.66	38.330	-1.02	2.90
1052F	12H	6	33-36	110.76	38.335	-1.01	2.73
1052F	12H	6	43-46	110.86	38.339	-1.16	2.61
1052F	12H	6	53-56	110.96	38.341	-0.84	2.74
1052F	12H	6	63-66	111.06	38.343	-0.88	2.75
1052F	12H	6	73-76	111.16	38.346	-0.94	3.15
1052F	12H	6	83-86	111.26	38.348	-1.08	3.01
1052F	12H	6	93-96	111.36	38.351	-0.61	2.68
1052F	12H	6	103-106	111.46	38.353	-1.04	2.74
1052F	12H	6	113-116	111.56	38.355	-0.89	2.76
1052F	12H	6	123-126	111.66	38.358	-0.17	2.83
1052F	12H	6	133-136	111.76	38.360	-1.27	1.59
1052F	12H	6	143-146	111.86	38.362	-1.26	2.84
1052B	13H	3	133-136	111.90	38.363	-1.74	2.54
1052F	12H	7	3-6	111.96	38.365	-0.78	2.92
1052B	13H	3	143-146	112.00	38.366	-1.81	2.80
1052F	12H	7	13-16	112.06	38.368	-0.34	2.73
1052B	13H	4	3-6	112.10	38.369	-2.42	2.50
1052F	12H	7	23-26	112.16	38.371	-1.61	3.12
1052F	12H	7	33-36	112.26	38.374	-0.98	2.84

Appendix 2. Continuous stable isotopic time series

Hole	Core	Section	Interval (cm)	MCD	Age (Ma)	Oxygen	Carbon
1052B	13H	4	23-26	112.30	38.375	-1.25	3.23
1052F	12H	7	43-46	112.36	38.377	-0.77	2.93
1052B	13H	4	33-36	112.40	38.379	-2.15	2.47
1052B	13H	4	43-46	112.50	38.383	-1.98	3.15
1052B	13H	4	53-56	112.60	38.388	-1.46	3.30
1052B	13H	4	63-66	112.70	38.393	-1.86	2.51
1052B	13H	4	73-76	112.80	38.398	-1.35	3.34
1052B	13H	4	83-86	112.90	38.403	-2.20	2.79
1052F	13H	1	53-56	112.96	38.408	-1.26	2.36
1052B	13H	4	93-96	113.00	38.408	-1.98	2.82
1052F	13H	1	63-66	113.06	38.412	-1.23	2.68
1052B	13H	4	103-106	113.10	38.414	-1.87	3.24
1052F	13H	1	73-76	113.16	38.416	-1.30	2.76
1052B	13H	4	113-116	113.20	38.419	-2.04	2.52
1052F	13H	1	83-86	113.26	38.419	-1.12	2.78
1052F	13H	1	93-96	113.36	38.422	-0.90	2.93
1052F	13H	1	103-106	113.46	38.424	-0.60	2.88
1052F	13H	1	113-116	113.56	38.426	-1.02	2.08
1052F	13H	1	123-126	113.66	38.868	-0.35	2.85
1052F	13H	1	133-136	113.76	39.032	-1.15	2.84
1052F	13H	1	143-146	113.86	39.034	-1.27	2.45
1052F	13H	2	3-6	113.96	39.036	-1.26	2.82
1052F	13H	2	13-16	114.06	39.039	-1.00	2.80
1052F	13H	2	23-26	114.16	39.041	-0.94	2.79
1052F	13H	2	33-36	114.26	39.044	-1.13	2.76
1052F	13H	2	43-46	114.36	39.047	-0.43	2.75
1052F	13H	2	53-56	114.46	39.049	-0.87	2.86
1052F	13H	2	63-66	114.56	39.052	-0.81	2.95
1052F	13H	2	73-76	114.66	39.055	-1.16	3.05
1052F	13H	2	83-86	114.76	39.058	-1.05	2.34
1052F	13H	2	93-96	114.86	39.061	-0.87	3.10
1052F	13H	2	103-106	114.96	39.064	-1.60	2.81
1052F	13H	2	113-116	115.06	39.067	-0.54	2.85
1052F	13H	2	123-126	115.16	39.070	-0.27	3.08
1052F	13H	2	133-136	115.26	39.072	-0.27	2.74
1052F	13H	2	143-146	115.36	39.074	-0.83	3.03
1052F	13H	3	3-6	115.46	39.076	-1.34	3.32
1052F	13H	3	13-16	115.56	39.077	-0.82	2.81
1052F	13H	3	23-26	115.66	39.079	-0.69	2.80
1052F	13H	3	33-36	115.76	39.082	-0.73	2.94
1052F	13H	3	43-46	115.86	39.084	-0.78	2.88
1052F	13H	3	53-56	115.96	39.087	-0.19	2.59
1052F	13H	3	63-66	116.06	39.089	-1.07	3.04
1052F	13H	3	73-76	116.16	39.092	-0.56	2.90
1052F	13H	3	83-86	116.26	39.094	-1.05	2.84
1052F	13H	3	93-96	116.36	39.096	-1.05	2.93
1052F	13H	3	103-106	116.46	39.099	-1.12	2.77
1052F	13H	3	113-116	116.56	39.101	-1.14	2.93
1052F	13H	3	123-126	116.66	39.104	-0.66	3.00
1052F	13H	3	133-136	116.76	39.106	-1.08	2.92
1052F	13H	3	143-146	116.86	39.108	-0.61	2.73
1052F	13H	4	3-6	116.96	39.109	-1.22	2.73

Appendix 2. Continuous stable isotopic time series

Hole	Core	Section	Interval (cm)	MCD	Age (Ma)	Oxygen	Carbon
1052F	13H	4	13-16	117.06	39.111	-0.22	2.36
1052F	13H	4	23-26	117.16	39.112	-0.73	3.00
1052F	13H	4	33-36	117.26	39.115	-0.73	2.63
1052F	13H	4	43-46	117.36	39.118	-1.05	2.74
1052F	13H	4	53-56	117.46	39.121	-1.17	2.96
1052F	13H	4	63-66	117.56	39.124	-0.61	2.62
1052F	13H	4	73-76	117.66	39.127	-1.22	2.75
1052F	13H	4	83-86	117.76	39.130	-0.93	2.66
1052F	13H	4	93-96	117.86	39.133	-1.34	2.75
1052F	13H	4	103-106	117.96	39.137	-0.58	2.52
1052F	13H	4	113-116	118.06	39.141	-1.12	2.62
1052F	13H	4	123-126	118.16	39.146	-0.13	3.85
1052F	13H	4	133-136	118.26	39.151	-0.97	2.88
1052F	13H	4	143-146	118.36	39.156	-1.06	2.58
1052F	13H	5	3-6	118.46	39.159	-0.92	2.88
1052F	13H	5	13-16	118.56	39.163	-0.89	2.89
1052F	13H	5	23-26	118.66	39.166	-1.15	3.14
1052F	13H	5	33-36	118.76	39.169	-1.05	3.02
1052F	13H	5	43-46	118.86	39.172	-1.27	3.11
1052F	13H	5	53-56	118.96	39.175	-1.25	3.17
1052F	13H	5	63-66	119.06	39.178	-1.13	3.09
1052F	13H	5	73-76	119.16	39.182	-1.23	3.23
1052F	13H	5	83-86	119.26	39.185	-1.14	3.22
1052F	13H	5	93-96	119.36	39.188	-1.25	3.17
1052F	13H	5	103-106	119.46	39.191	-1.26	3.27
1052F	13H	5	113-116	119.56	39.194	-1.22	3.18
1052F	13H	5	123-126	119.66	39.197	-1.04	2.78
1052F	13H	5	133-136	119.76	39.200	-1.30	3.02
1052F	13H	5	143-146	119.86	39.204	-1.13	2.91
1052F	13H	6	3-6	119.96	39.207	-1.46	3.09
1052F	13H	6	13-16	120.06	39.211	-1.29	2.85
1052F	13H	6	23-26	120.16	39.216	-1.08	2.75
1052F	13H	6	33-36	120.26	39.221	-1.33	3.34
1052F	13H	6	43-46	120.36	39.226	-1.15	3.02
1052F	13H	6	53-56	120.46	39.232	-1.42	3.15
1052B	14H	3	93-96	120.50	39.237	-1.29	3.04
1052F	13H	6	63-66	120.56	39.238	-1.61	3.53
1052B	14H	3	103-106	120.60	39.242	-1.39	3.16
1052F	13H	6	73-76	120.66	39.243	-1.46	2.98
1052B	14H	3	113-116	120.70	39.248	-1.88	2.53
1052B	14H	3	123-126	120.80	39.250	-1.29	3.15
1052B	14H	3	133-136	120.90	39.253	-1.53	3.24
1052B	14H	3	143-146	121.00	39.256	-1.55	3.62
1052B	14H	4	3-6	121.10	39.258	-1.32	3.38
1052B	14H	4	13-16	121.20	39.261	-1.94	2.89
1052B	14H	4	23-26	121.30	39.263	-1.90	2.98
1052B	14H	4	33-36	121.40	39.266	-1.50	3.41
1052B	14H	4	43-46	121.50	39.269	-1.68	3.13
1052B	14H	4	53-56	121.60	39.271	-1.68	3.00
1052B	14H	4	63-66	121.70	39.274	-1.65	3.08
1052B	14H	4	73-76	121.80	39.276	-1.70	3.35
1052B	14H	4	83-86	121.90	39.279	-1.26	3.35

Appendix 2. Continuous stable isotopic time series

Hole	Core	Section	Interval (cm)	MCD	Age (Ma)	Oxygen	Carbon
1052B	14H	4	93-96	122.00	39.281	-1.52	3.46
1052B	14H	4	103-106	122.10	39.284	-1.61	3.26
1052B	14H	4	113-116	122.20	39.287	-1.52	3.19
1052B	14H	4	123-126	122.30	39.290	-1.05	3.02
1052B	14H	4	133-136	122.40	39.293	-1.33	3.29
1052B	14H	4	143-146	122.50	39.296	-1.46	3.34
1052B	14H	5	3-6	122.60	39.299	-1.29	3.21
1052B	14H	5	13-16	122.70	39.303	-1.31	3.37
1052B	14H	5	23-26	122.80	39.306	-1.14	3.38
1052B	14H	5	33-36	122.90	39.309	-1.40	3.37
1052B	14H	5	43-46	123.00	39.312	-1.22	3.28
1052B	14H	5	53-56	123.10	39.316	-1.62	3.07
1052B	14H	5	63-66	123.20	39.319	-1.37	3.12
1052B	14H	5	73-76	123.30	39.322	-1.42	3.32
1052B	14H	5	83-86	123.40	39.325	-1.45	3.34
1052B	14H	5	93-96	123.50	39.329	-1.16	3.38
1052B	14H	5	103-106	123.60	39.332	-1.31	3.35
1052B	14H	5	113-116	123.70	39.335	-1.50	3.30
1052B	14H	5	123-126	123.80	39.338	-1.33	3.19
1052B	14H	5	133-136	123.90	39.341	-1.48	3.07
1052B	14H	5	143-146	124.00	39.343	-1.56	3.15
1052B	14H	6	3-6	124.10	39.346	-1.62	3.48
1052B	14H	6	13-16	124.20	39.349	-1.34	3.26
1052B	14H	6	23-26	124.30	39.351	-1.24	3.34
1052B	14H	6	33-36	124.40	39.354	-1.41	3.12
1052B	14H	6	43-46	124.50	39.356	-1.45	3.16
1052B	14H	6	53-56	124.60	39.359	-1.18	3.28
1052B	14H	6	63-66	124.70	39.362	-1.36	3.12
1052B	14H	6	73-76	124.80	39.365	-1.44	3.15
1052B	14H	6	83-86	124.90	39.367	-1.35	3.10
1052B	14H	6	93-96	125.00	39.371	-1.28	3.35
1052F	14H	2	103-106	125.01	39.371	-1.21	3.26
1052B	14H	6	103-106	125.10	39.374	-1.35	3.28
1052F	14H	2	113-116	125.11	39.374	-1.26	2.86
1052B	14H	6	113-116	125.20	39.377	-1.52	3.00
1052F	14H	2	123-126	125.21	39.377	-1.36	3.15
1052F	14H	2	133-136	125.31	39.379	-1.40	3.05
1052F	14H	2	143-146	125.41	39.381	-1.39	3.21
1052F	14H	3	3-6	125.51	39.382	-1.54	3.34
1052F	14H	3	13-16	125.61	39.384	-1.21	3.35
1052F	14H	3	23-26	125.71	39.386	-1.23	3.24
1052F	14H	3	33-36	125.81	39.388	-1.18	3.45
1052F	14H	3	43-46	125.91	39.390	-1.10	3.27
1052F	14H	3	53-56	126.01	39.391	-1.11	3.33
1052F	14H	3	63-66	126.11	39.393	-0.96	3.41
1052F	14H	3	73-76	126.21	39.394	-1.08	3.45
1052F	14H	3	93-96	126.41	39.397	-1.14	3.62
1052F	14H	3	103-106	126.51	39.398	-1.09	3.52
1052F	14H	3	113-116	126.61	39.399	-1.18	3.58
1052F	14H	3	123-126	126.71	39.402	-1.25	3.50
1052F	14H	3	133-136	126.81	39.405	-1.20	3.65
1052F	14H	3	143-146	126.91	39.408	-1.36	3.34

Appendix 2. Continuous stable isotopic time series

Hole	Core	Section	Interval (cm)	MCD	Age (Ma)	Oxygen	Carbon
1052F	14H	4	3-6	127.01	39.411	-0.79	3.67
1052F	14H	4	13-16	127.11	39.414	-1.17	3.42
1052F	14H	4	23-26	127.21	39.417	-1.27	3.34
1052F	14H	4	33-36	127.31	39.421	-1.14	3.47
1052F	14H	4	43-46	127.41	39.427	-1.17	3.39
1052F	14H	4	53-56	127.51	39.434	-1.13	3.32
1052F	14H	4	63-66	127.61	39.440	-1.38	3.47
1052F	14H	4	73-76	127.71	39.447	-1.56	3.29
1052F	14H	4	83-86	127.81	39.453	-1.08	3.21
1052F	14H	4	93-96	127.91	39.456	-1.20	3.28
1052F	14H	4	103-106	128.01	39.458	-1.29	3.47
1052F	14H	4	113-116	128.11	39.460	-1.24	3.46
1052F	14H	4	123-126	128.21	39.463	-1.29	3.45
1052F	14H	4	133-136	128.31	39.465	-1.00	3.41
1052F	14H	4	143-146	128.41	39.468	-1.18	3.30
1052F	14H	5	3-6	128.51	39.470	-1.27	3.30
1052F	14H	5	13-16	128.61	39.474	-1.03	3.17
1052F	14H	5	23-26	128.71	39.478	-1.21	3.43
1052F	14H	5	33-36	128.81	39.482	-1.12	4.21
1052F	14H	5	43-46	128.91	39.486	-0.36	3.10
1052F	14H	5	53-56	129.01	39.490	-0.52	3.24
1052F	14H	5	63-66	129.11	39.494	-1.39	3.22
1052F	14H	5	73-76	129.21	39.498	-1.23	3.60
1052F	14H	5	83-86	129.31	39.502	-1.43	3.60
1052F	14H	5	93-96	129.41	39.506	-0.37	3.13
1052F	14H	5	103-106	129.51	39.509	-1.52	3.43
1052F	14H	5	113-116	129.61	39.513	-1.54	3.58
1052F	14H	5	123-126	129.71	39.517	-1.44	3.22
1052F	14H	5	133-136	129.81	39.521	-1.31	3.49
1052F	14H	5	143-146	129.91	39.525	-0.22	3.02
1052F	14H	6	3-6	130.01	39.529	-0.81	2.88
1052F	14H	6	13-16	130.11	39.535	-1.52	3.57
1052F	14H	6	23-26	130.21	39.542	-1.55	3.07
1052F	14H	6	33-36	130.31	39.548	-1.63	3.50
1052F	14H	6	43-46	130.41	39.555	-1.65	3.57
1052F	14H	6	53-56	130.51	39.561	-0.89	2.85
1052F	14H	6	63-66	130.61	39.568	-1.29	3.10
1052F	14H	6	73-76	130.71	39.574	-1.48	3.26
1052F	14H	6	83-86	130.81	39.577	-1.46	3.04
1052F	14H	6	93-96	130.91	39.580	-1.32	3.33
1052F	14H	6	103-106	131.01	39.584	-1.32	3.38
1052F	14H	6	113-116	131.11	39.588	-1.26	3.24
1052F	14H	6	123-126	131.21	39.593	-0.20	2.88
1052F	14H	6	133-136	131.31	39.596	-0.31	2.66
1052F	14H	6	143-146	131.41	39.598	-1.19	3.18